Selected Topics on Mathematical Models in Immunology and Medicine

R. Mohler and A. Asachenkov
Editors

CP-90-007
September 1990

**Proceedings of the International Workshop
Mathematical Modelling in Immunology and
Medicine Kiev, 29 August – 7 September 1989**

Preface

In 1988 the new IIASA project on System Immunology was inaugurated. The new activity focusses theoretical and experimental research in immunology and system mathematics to experimental planning and prediction for relevant disease applications and systematic understanding of immunology. IIASA analysis and simulation should lead to an effective plan of successive experiments to identify and to quantify particularly sensitive parameters in this most complex system of information processing, decision and control. The integration of such diverse disciplines is extremely difficult but some basis has already been established.

For several years IIASA has sponsored international workshops dealing with dynamical systems and their applications to biology. These include: (1) The conference on "Dynamics of Macrosystems", Laxenburg, Austria, 1984, (2) The Working Conference on "Theoretical Immunology", Mogilany, Poland, 1985, (3) The Workshop on "Selected Topics in Biomathematics", Laxenburg, Austria, 1987. The proceedings of the last meeting are published by Kluwer as a special issue of the Journal Acta Applicandae Mathematicae ("Evolution and Control in Biological Systems", vol. 14, no. 1 & 2, January/February 1989).

The present volume contains the proceedings of the latest Workshop "Mathematical Modelling in Immunology and Medicine", held at Kiev, USSR in September 1989.

Part 1 deals with the mathematical models of autoimmune, infectious diseases and AIDS. The models are studied with the intent to establish a basis for more effective treatment. In Part 2, questions of computer simulation and data analysis in cancer research are analyzed. Part 3 is devoted to the models for antibody binding, immunoassay dynamics and immunogenetic systems. The problems of system analysis and medical decision making are discussed in Part 4. This volume has been edited by Dr. Alexander Asachenkov, System and Decision Sciences Program of the International Institute for Applied Systems Analysis, Laxenburg, Austria, and Ron Mohler, Oregon State University, Corvallis, USA.

Alexander B. Kurzhanski
Chairman
System and Decision Sciences Program
International Institute for Applied Systems Analysis
Laxenburg, Austria

Contents

Selected Topics on Mathematical Models in Immunology and Medicine

R. Mohler and A. Asachenkov

Editors

Part I

Models of Disease

Chapter 1

Mathematical Modeling of Autoimmune Disease and its Therapy

Jacek Waniewski
Institute of Biocybernetics and Biomedical Engineering
Warsaw, Poland

Daniela Přikrylová
Institute of Microbiology
Prague, Czechoslovakia

1.1 Introduction

There can be two main aims of mathematical modeling in biology and medicine: 1) quantitative description of particular experiments and 2) formalization and refinement of the hypotheses about structure and internal and external regulation mechanisms of a modeled system [1-2]. Such general "model-theories" may be particularly useful if the system is a complicated part of the living organism. Then, usually only a few direct quantitative data about the entire system are available, but a lot of partial knowledge can be obtained from experiments related to a part of the systems or experiments in vitro.

In this situation one can try to formulate general hypotheses concerning the system and ask if the applied assumptions are able to explain the collected partial data. A mathematical model can help in 1) examination of the consistency of the hypotheses, 2) evaluation of the values of those parameters that are not known or are variable in different individuals or species or under different conditions, 3) qualitative analysis of the behavior of the system under various influences, external conditions or in different individual and generic representations of the system, 4) studies of the role of a part of the system in the behavior of the whole system, 5) looking for the ways of system control, 6) interpretation of experimental data, 7) design of new experiments, 8) formulation of new hypotheses if the model yields incorrect predictions and 9) explanation and teaching of the ideas.

The consequence of mathematical models can be studied analytically or they can be evaluated in the course of numerical simulations. However, it should not be forgotten that these consequences are related to general hypotheses, particular details taken into account in the model, values of the unknown or uncertain parameters and mathematical approximations used.

An example of this approach to mathematical modeling is the model of the humoral immune response and its regulation by interleukins designed by Přikrylová [3-6]. In the present paper a new version of this model including memory helper cells is presented. The field of the applications

of the model is also extended to include clinical problems related to autoimmune disorders and their therapy [7–8].

1.2 Model

The model describes kinetics of different cell populations and soluble factors produced during the immune response after antigenic stimulus [3–6]. The populations differ in their functional properties and the kind of receptors expressed on the surface of cells. Binding of the respective soluble factors to their receptors can become a signal for a cell to transform their properties, that means to turn from one population into another. The rate of the transformation depends on the amount of the signal particles per one cell—only after binding of a threshold amount of particles the cell can start to transform. However, the further increase of the signal intensity does not lead to a higher transformation rate—a saturation phenomenon can be observed.

In principle, the rate of transformation could be described by a step function, but for practical reasons it is approximated in the model by the following function:

$$f(r) = \frac{r^n}{1 + r^n} \tag{1.1}$$

$$r = \frac{\text{signal intensity}}{\left(\begin{array}{c}\text{sensitivity}\\\text{to signal}\end{array}\right) \times \left(\begin{array}{c}\text{amount of cells}\\\text{susceptable to signal}\end{array}\right)} \tag{1.2}$$

After many simulations of the immune response with various values of n used, the value $n = 2$ was chosen (Přikrylová, not published). For $n > 2$ no significant changes were found in the simulated course of the immune response and $n = 1$ was also acceptable. Therefore, it can be stated that a switch of the transformation rate from zero to its maximal value when r approaches 1 is important in the model, but not a particular shape of the function f.

The schematic representation of cell transformations after an antigenic stimulus as well as humoral factors that stimulate the respective transformation are shown in Figure 1. The differential equations describing the kinetics of cell populations and soluble factors are as follows (compare [3–6]):

$$
\begin{aligned}
IL1' &= l_1 f_s - (f_1 H_a + m_1) IL1 \\
H_x' &= l_{Hx} - (f_x + m_x) H_x \\
H_a' &= f_x H_x - (f_a + m_a) H_a \\
H_y' &= f_g f_a H_a + (1_y f_p - 1_z(1 - f_p)) H_y \\
H_z' &= (1 - f_g) f_a H_a + f_y(1 - f_p) 1_z H_y + f_m H_m - m_z H_z \\
H_m' &= 1_z(1 - f_p)(1 - f_y) H_y + (1_y f_p - f_m - m_m) H_m \\
IL2' &= l_2 H_z - [k_{2h}(H_a + H_y + Y + H_m + M) + m_2] IL2 \\
B_x' &= 1_{Bx} - (f_x + m_x) B_x \\
B_y' &= f_x B_x + f_p f_m B_m + (1_y f_p - 1_z(1 - f_p)) B_y \\
B_z' &= (1 - f_p)(1_z f_y B_y + f_m B_m) - m_z B_z \\
B_m' &= 1_z(1 - f_p)(1 - f_y) B_y - (f_m + m_m) B_m \\
Ab' &= l_{ab} B_z - (m_{ab} + k_{abag} Ag) Ab \\
Ag' &= l_{ag} - (m_{ag} + kk_{abag} Ab) Ag
\end{aligned}
$$

The rate functions f are chosen according to (1) with $n = 2$ for the following r:

$$
\begin{aligned}
f_{x,y,m,s} : r &= \frac{Ag}{q_{x,y,m,s}(H_x + H_a + H_y + H_m + B_x + B_y + B_m)} \\
f_a : r &= \frac{IL1 + IL2}{q_i H_a + q_a(H_a + H_y + H_m + B_y + B_m)} \\
f_g : r &= \frac{IL2}{q_g IL1} \\
f_p : r &= \frac{IL2 \cdot \max(0, 1 - pAg^r)}{q_p(H_a + H_y + H_m + B_y + B_m)}
\end{aligned}
$$

The values of the parameters in the differential equations were chosen according to the literature [3–8]:

generation rates: $1_{Bx} = 1_{Hx} = 0.001$, $1_{Ab} = 0.002$, $1_{IL1} = 0.09$, $1_{IL2} = 0.1$;
death of cells and catabolic rates of solutes: $m_x = 0.001$, $m_z = 0.02$, $m_m = 0.0002$, $m_{IL1} = m_{IL2} = 0.007$, $m_{Ab} = 0.005$, $m_{Ag} = 0.05$;
proliferation rate: $1_y = 0.05$;
binding coefficients: $k_{IK1} = k_{IL2} = 0.07$, $k_{AbAg} = 0.9$, $k = 2$.

The sensitivity parameters in the switching functions were determined during many simulations to get a good qualitative course of primary and secondary responses under various initial conditions and the values of kinetic parameters of the system. As the result of this procedure the following parameters were chosen [3–8]:

$$q_x = q_y = q_m = q_p = 0.001, \quad q_a = q_g = q_s = q_f = 0.01, \quad q_i = 0.1, \quad p = 0.2, \quad r = 0.5.$$

The model was used to simulate primary and secondary responses for antigen considered as a chemical compound ($1_{Ag} = 0$) and as a proliferating species ($1_{Ag} = \tilde{1}_{Ag}Ag$, $m_{Ag} = 0$). The results were analogous to those presented in [3–8].

1.3 Autotolerance and Autoimmunity

Autoantigens are usually persistent because they can be produced by the body even if the produced quantities are quickly destroyed or inactivated. Fortunately, autoantigens are as a rule well tolerated by the immune system. The first theory of this phenomenon stated that autoreactive clones are deleted from the total repertoire of immunocompetent cells (clonal deletion theory [9]). Later investigations proved that T cells can be made tolerant much easier than B cells (partial clonal deletion theory [10]).

Therefore, to simulate autotolerance the rate of the supply of helper T cells was diminished (Figure 2). At the beginning there was an antigen but T and B cells were absent. They started to come into being (as in ontogeny), but the rate of the input of helper precursors was assumed as being 20 times less than for non-autoreactive clones. The steady state of autotolerance raised with the level of the antigen slightly decreased, a few plasma cells, no T cells and almost no free antibody, because all the produced antibody was bound to the antigen. This phenomenon was referred to in the literature as a "tread mill" effect [11].

Sometimes a spontaneous breaking up of autotolerance can occur and then an autoimmune disease can develop. Autoimmune disorders are very difficult to treat and are often fatal. The suggested reasons for the termination of autotolerance are both genetic and environmental [11]. In our simulations we described the rise of autoimmunity as the increase of the supply rate of helper T cells (diminished in the autotolerant state) to its normal value (Figure 2). The immune system switched from the state of autotolerance to the state of developed autoimmunity with the high levels of autoantibody, plasma cells and memory cells. However, the amount of helper cells was less than the amount of B cells (Figure 2).

In fact, autoimmune diseases are very difficult to treat and total remissions are rare. To keep patients alive two main treatments are usually performed.

- The autoimmune response can be weakened by immunosuppression. Most of the immunosuppressive drugs are cytotoxic or cytostatic [12]. Therefore in our simulations we described immunosuppression as a diminished rate of the proliferation of cells [7–8]. However, sometimes immunosuppression does not yield the total remission of the disease, but only transient and partial improvement of the patient's state. In Figure 3 an impact of immunosuppression on the antibody level for three different values of the diminished proliferation rate is shown.

- The removal of autoantibodies results in the increase of the level of autoantigen. It can be done in several ways: exchange of whole plasma or a fraction of plasma, lymph removal or specific immunosorption performed in an extracorporeal circuit [13]. The simulation of extracorporeal antibody removal showed the same mechanism of quick rebound of antibody level to its previous value as it was described previously: the diminished amount of antibodies led to the increase of the autoantigen level followed by the rise of autoantigen stimulated memory cells which turned into plasma cells and started to produce the antibody in large amounts [7-8]. But in the version of the model presented in this study memory helper cells were also stimulated to produce $IL2$. Therefore more cells proliferated and thus the amount of plasma cells was higher. This yielded a much quicker rebound of antibody (and even a slight overshoot of its initial level) than in the version of the model without memory T cells (Figure 4).

The further comparisons of the two versions of the model showed that the system including helper memory cells is more resistant to immunosuppression than the system without these cells. For example, the 2.5 times diminished proliferation rate yielded only partial improvement (Figure 3) while in the previous simulations this same decreased proliferation rate resulted in the state of tolerance [7-8].

A significant difference between the two versions of the model can be demonstrated if the supply of B and T precursors is stopped during the autoimmune response. Then, if memory helper cells are not taken into account the model predicts the cease of the response. In contrast, the model with memory helper cells proves that the steady state of autoimmunity would not be changed in any significant way (Figure 5).

1.4   Discussion

The topic of steady states of the immune system is a more general problem than the states of autotolerance and autoimmunity discussed in this paper. Namely, the stabilization of the immune response can also be observed (and mathematically described) in chronic infectious diseases [14] and in cancer development [15]. Medical therapies in these cases are aimed at the strengthening of the immune system and the elimination of antigenic factors. In contrast, therapeutic treatments of autoimmune disorders try to stop or weaken the immune response and keep the amount of autoantigens high enough for the normal function of the body. Similar problems arise also in the prevention of graft rejections.

Medical therapies of autoimmune disorders perturb the immune system: either the extracorporeal antibody removal or the immunosuppression. However, the immune system seems to be largely resistant to these perturbations: the effects last as long as the treatment is performed. Total remissions of the disease are rare.

A widely discussed problem is the possible role of suppressor cells anti-idiotypic interactions in autoimmune disorders. It has been argued that those factors cannot be decisive in the maintenance of autotolerance and therefore also in the loss of its control [16]. Even the existence of suppressor cells as an independent population has been questioned [17]. On the other hand, anti-idiotypic antibodies specific to self-reacting anti-acetylcholine receptor antibodies were found in myasthenia gravis [18]. In our model, antigen is the main regulatory factor of the immune response and no additional cell populations are needed to control the system: if antigen is eliminated, then the response ends. In particular, a steady state can be reached by the system during autoimmune response. However, because of the long lasting high autoantibody level a significant anti-idiotypic response can develop or putative suppressors can originate. The impact of those possible factors on the effects of therapy needs an independent study.

The mathematical model presented in this paper proved itself to be able to describe the phenomena of autotolerance and autoimmunity according to the current knowledge about their origin [19]. Moreover, it revealed the strong resistance to perturbations that can be interpreted

as medical treatments. Such resistance is in agreement with the observed effects of the therapy of autoimmune disorders. Unfortunately up to now, no experimental data are available that could help to choose between the new version of the model (with helper memory cells) and the previous one [3–8]. Nevertheless, the model seems to be useful for the discussion of the modifications of the system (new cell population) as well as of a new range of phenomena which had not been taken into account during the model's formulation (autotolerance and autoimmunity). This supports a view that the model is a "model-theory" correctly describing the basic structures and features of the modeled system.

1.5 References

[1] Jilek, M. and D. Přikrylová. (1985) *Some notes on mathematical modeling of the immune response.* In: *Immunology and Epidemiology.* G.W. Hoffman and T. Hraba (Eds). Springer-Verlag, Berlin. p. 8–14.

[2] Jilek, M. and D. Přikrylová. (1985) *The X-Y-Z scheme after 23 years.* Folia Microbiol. **30**, p. 302–311.

[3] Přikrylová, D. (1985) *Mathematical modeling of the immune response: a model of the proliferation control.* In: *Immunology and Epidemiology.* G.W. Hoffman and T. Hraba (Eds). Springer-Verlag, Berlin. p. 44–52.

[4] Přikrylová, D., M. Jilek and J. Doležal. (1986) *A new mathematical model of proliferation control during immune response.* Immun. Letters **18**, p. 317 - 321.

[5] Přikrylová, D. (1987) *Úloha interleukinu 2 v regulaci immuni odprovědi.* Kandidátská disertační práce. Prague.

[6] Přikrylová, D. (1989) *Interleukin 2 and immune response control. Mathematical Model.* Acta. Appl. Math. **14**, p. 179–189.

[7] Waniewski, J. and D. Přikrylová. (1989) *Autoimmunity and its therapy: mathematical modeling.* Immun. Letters **18**, p. 77–80.

[8] Waniewski, J. and D. Přikrylová. (1989) *A mathematical model of extracorporeal antibody removal in autoimmune disease.* Int. J. Artif. Organs. **12**, p. 471–478.

[9] Burnet, F.M. (1959) *The clonal selection theory of acquired immunity.* Cambridge Univ. Press, London.

[10] Weigle, W.O. (1980) *Analysis of autoimmunity through experimental models of thyroiditis and allergic encephalomyelitis.* Advances in Immunology **30**, p. 159–273.

[11] Talal, N. (1980) *Tolerance and autoimmunity.* In: *Clinical Immunology.* Volume 1. Ch.W. Parker (Ed). Saunders, Philadelphia.

[12] Webb, D.R. and A. Winkelstein. (1982) *Immunosuppression, immunopotentation and anti-inflamantory drugs.* In: *Basic and clinical immunology.* D.P. Stites, J.D. Stobo, H.H. Fundenberg, and J.V. Wells (Eds). Lange Medical Publications, Los Altos.

[13] Nose, Y., P.S. Malchesky, and J.W. Smith (Eds). (1984) *Therapeutic apheresis: a critical look.* ISAO Press, Cleveland.

[14] Marchuk, G.I. (1985) *Mathematical models in immunology.* Science Press, Moscow (in Russian).

[15] Mohler, R.R. (1987) *Foundations of immune control and cancer.* In: *Recent Advances in System Science.* A.V. Balakrishnan (Ed). Optimization Software, Publishing Div., New York.

[16] Langman, R.E. (1987) *The self - nonself discrimination is not regulated by suppression.* Cellular Immun. **108**, p. 214–219.

[17] Sanders, M.E., M.W. Makgoba, and S. Shaw. (1988) *Human naive and memory cells: reinterpretation of helper-inducer and suppressor-inducer subsets.* Immunol. Today. **9**, p. 195–199.

[18] Lefvert, A.K. (1986) *Evidence for the existence of an idiotype-anti-idiotype network in human myasthenia gravis.* Plasma Ther. Transfus. Technol. **7**, p. 187–196.

[19] Melchers, F. (1989) *Introduction.* In: *Basel Institute for Immunology Annual Report 1988.* F. Hoffman–La Roche, Basel.

(a)

(b)
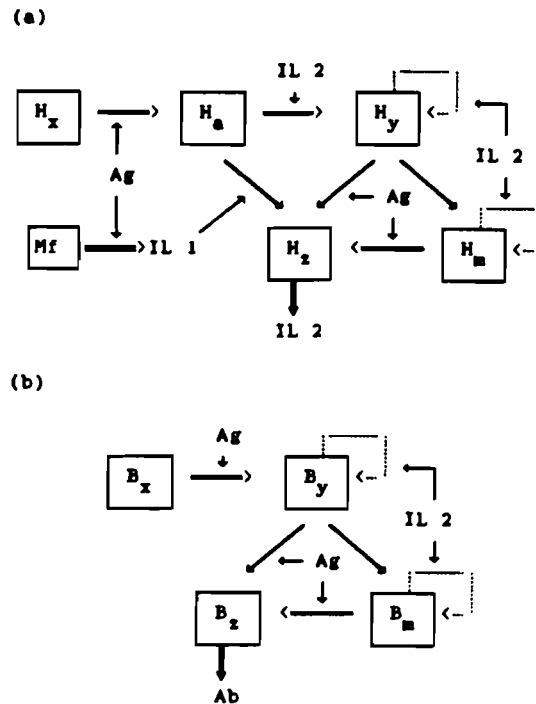
Figure 1.1. Scheme of helper cells (a) and B cells (b) development after antigenic stimulation. H-helper T cells, B-B cells, Mf-macrophages, Ag-antigen, Ab-antibody, $IL1$-interleukin 1, $IL2$-interleukin 2. Indices: x-precursors, a-activated cells, y-proliferating cells, z-producers, m-memory cells. $\longrightarrow$ - cell transformation, $\Longrightarrow$ - secretion, $\longrightarrow$ - influence of signal particles on cell transformation, $\cdots >$ - proliferation.
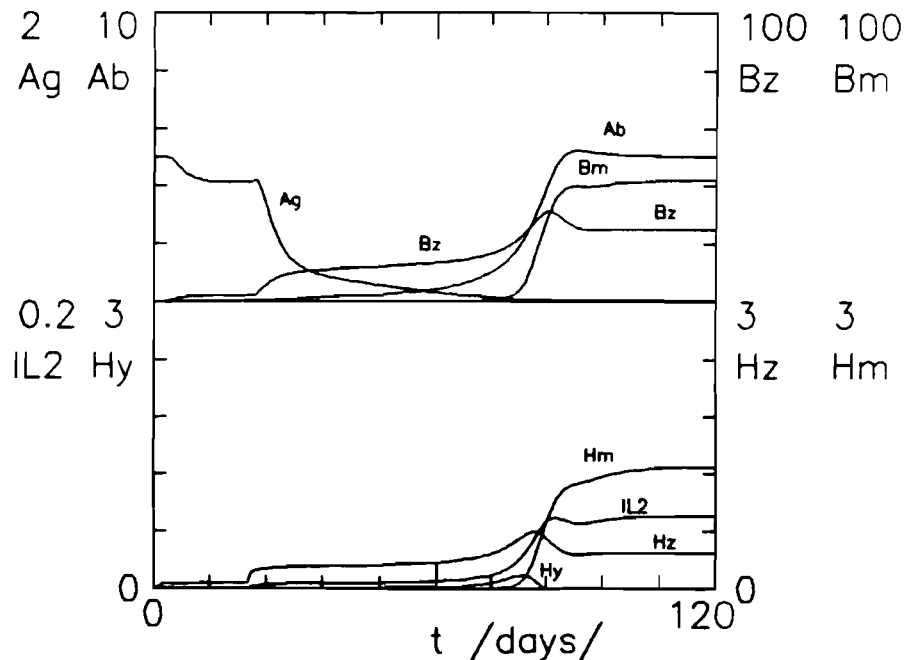
Figure 1.2. Autotolerance (0-20 days) and autoimmunity (20-120 days). Initial values: $Ag = 1$, other variables $= 0$. Parameters: $1_{Ag} - 0.05$, $1_{Hx} = 0.00005$ for $0 \leq t \leq 20$ and $1_{Hx} = 0.001$ for $20 \leq t \leq 120$, other parameters as described in Chapter 2.
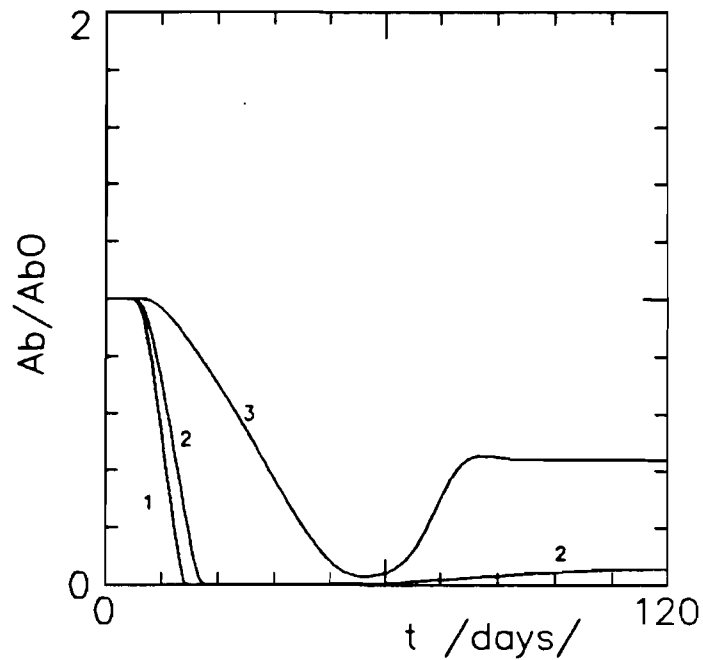
Figure 1.3. The impact of immunosuppression on antibody level. The initial values are the final values from Figure 2. Parameters: (1) $1_y = 0$, (2) $l_y = 0.01$, (3) $l_y = 0.02$, other parameters as in Figure 2.
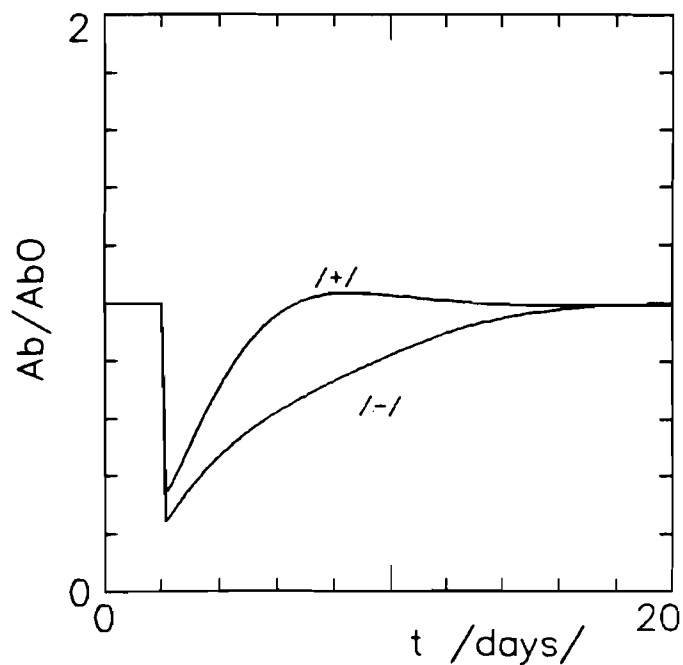
Figure 1.4. The impact of extracorporeal antibody removal on antibody level. The inital values are the final values from Figure 2. (+) - the model with memory helper cells (Chapter 2), (−) - the model without memory helper cells [7].
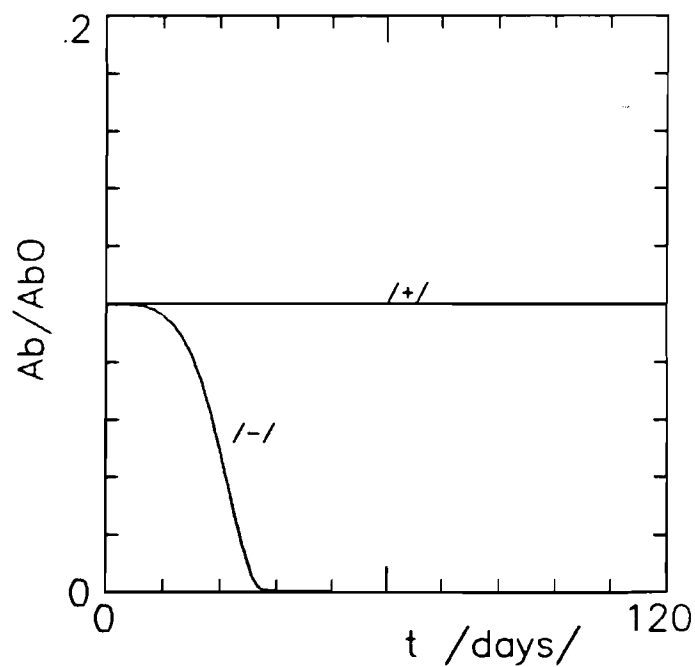
Figure 1.5. The impact of the stopping of T and B precursors supply on the autoimmune response. The inital values are the final values from Figure 2. *At* $t = 1$ 1_{Bx} and 1_{Hx} were changes to 0. (+) - the model with memory helper cells (Chapter 2), (−) - the model with memory helper cells [7].

Chapter 2

Lymphocyte Population Dynamics: Model-based Qualitative Analysis

S. Čelikovský, J. Doležal
Institute of Information Theory and Automation
Czechoslovak Academy of Sciences
182 08 Prague, Czechoslovakia

T. Hraba
Institute of Molecular Genetics
Czechoslovak Academy of Sciences
142 20 Prague, Czechoslovakia

2.1   Introduction

The experimental basis of our mathematical model of immunological tolerance [1] were findings on the mechanisms of tolerance induced by human serum albumin in hatched chickens. Suppressor cells were not found to play a significant role in this experimental model. Therefore, the elimination or irreversible functional inactivation of lymphocytes by the tolerance inducing antigen seems to be the mechanism underlying inhibition of immune response in tolerant birds. The affected clones of lymphocytes are those reacting with the tolerated antigen.

Tolerance to heterogeneous proteins was observed to be temporary and followed by gradual recovery of immune reactivity. Because the duration of tolerance to protein can be prolonged by additional administration of tolerated antigen, it was assumed that the escape from tolerance is caused by differentiation of new lymphocytes when the concentration of the tolerated antigen drops by non-immune elimination below the level necessary for induction of tolerance in these newly differentiating cells. New lymphocytes mature continually by an antigen-independent process from precursors which do not possess antigen specificity. When they encounter their specific antigen during maturation they are eliminated or functionally inactivated, i.e. tolerance is induced. The dose of antigen necessary for antigen induction is lower in the case of differentiating cells than the mature ones.

The mathematical model of tolerance was based on the above experimental conclusions. Originally, it was formulated for B cell tolerance and it was extended later to T cell tolerance. Essentially, it can be applied to recovery of any deletion of some lymphocyte population, where the deleting stimulus ceases to act. Thus it was used to model the dynamics of idiotype or isotype suppression caused in neonatal mice by antibodies to the respective immunoglobulin markers, and polyclonal tolerance induced by mitogen stimulation followed by application of cyclophosphamide. Depletion of $CD4^+$ lymphocytes in HIV infection seems to be effected by viral products. Because the dynamics of concentration of these products are inverse to those

of non-replicating antigen inducing tolerance, the model could be alternatively used to describe the dynamics of $CD4^+$ lymphocyte depletion in HIV infected persons.

This paper presents analysis of this class of models, which is based on the representation of a solution of the corresponding nonautonomous system of linear differential equations. Alternatively, if the amount of antigen is assumed to be an input, the so-called bilinear system is obtained and the existing methodology is also applicable. The aim is to investigate both qualitatively and quantitatively the available range of applications of such a model, especially its limits. Analytic representation of the recovery solution curves are derived, and the limit cases of model parameters (antigen elimination rate, lifespans of lymphocytes) are discussed. Also the recently introduced feedback mechanism is analyzed in detail and it is shown that the originally nonlinear form of this mechanism is fully approximated by the classical linear feedback, which in fact, substantially simplifies analysis of this model and is also of considerable biological impact. Such analysis contributes to further understanding of the model, mainly from the point of view of its further applications.

2.2 Mathematical Models of Recovery from Inhibition

Let us briefly survey the development of the original simple mathematical model of immunological tolerance to its present form and its various modifications. The leading motivation there was the aim to have a satisfactory description of the recovery from the inhibition phenomenon in immunology representing the *qualitative* form of the immune response, i.e. restoration of the immune system responsiveness. According to the available experimental data concerning the immunological tolerance to human serum albumin in chickens, the first version of the model was suggested [1] assuming only B cell tolerance.

The model is based on two assumptions: (i) antigen induces tolerance by irreversible inactivation of B lymphocytes specifically reactive to it; (ii) the escape from tolerance is effected by differentiation of lymphocytes reactive to the tolerated antigen after its disappearance from the organism. Two developmental compartments of B lymphocytes (see Figure 1) are anticipated in the model: the immature cell compartment — $\bar{P}$ cells; the mature cell compartment — P cells. The immature antigen-reactive lymphocytes $\bar{P}$ arise by an antigen-independent differentiation process from their precursors, and they mature, independently of antigen, too, into mature antigen-reactive lymphocytes P. The immature $\bar{P}$ cells arise from their precursors with the rate $\bar{\tau}_P \bar{P}_E$ (index E denotes steady-state values).

Sizes of $\bar{P}$ and P cell compartments are described by the following differential equations with the given initial values:

$$\frac{d\bar{P}(t)}{dt} = \bar{\tau}_P[\bar{P}_E - \bar{P}(t)] - \bar{c}_P\, a(t)\bar{P}(t), \quad \bar{P}(0) = \bar{P}_0, \tag{1}$$

$$\frac{dP(t)}{dt} = \bar{\tau}_P \bar{P}(t) - \tau_P P(t) - c_P\, a(t)P(t), \quad P(0) = P_0, \tag{2}$$

where $P(t)$ and $\bar{P}(t)$ are the numbers of P and $\bar{P}$ cells at time t, $\bar{\tau}_P$ and τ_P are the rates (all rates are in days^{-1}) of maturation of $\bar{P}$ cells into P cells death of P cells respectively. The quantity $\bar{c}_P a(t)$ is the rate of irreversible inactivation of $\bar{P}$ cells by the tolerizing dose of antigen, and analogously, $c_P a(t)$ that of P cells. It is assumed that $\bar{c}_P > c_P > 0$ reflecting the fact that immature cells are assumed to be more susceptible to the tolerance induction in comparison with the mature ones; the effect of antigen $a(t) = a_0 \exp(-\beta(t - t_1))$, where a_0 depends on the amount of antigen injected, β is the rate of its nonimmune elimination, and t_1 is the day of antigen administration. From the steady-state considerations in the absence of antibody, i.e. $a(t) \equiv 0$, it simply follows that it must hold $\bar{\tau}_P \bar{P}_E = \tau_P P_E$. Clearly, $\bar{\tau}_P \bar{P}_E$ is the influx of the immature cell precursors.

Denote $P_c(t)$ the number of P cells in the controls at time t, which is equal to the solution of the model equations (1) - (2) with $a(t) \equiv 0$. Then the value

$$r_0(t) = 100\,[P(t)/P_c] \tag{3}$$

is the percent measure of P cell recovery from tolerance (responsiveness).

Applications details of such a model to study the tolerance in chickens can be found in [1]. In [2] this model was also tested on experimental data reported by other authors dealing with B cell tolerance in mice. As T helper cell tolerance plays an important role in tolerance to proteins, the model was appropriately modified [3]. It was assumed that T helper lymphocytes undergo the same inhibition process as B cells, i.e. after denoting $\bar{Q}$ and Q the respective numbers of immature and mature T helper lymphocytes, the analogical system of equations to (1) - (2) is obtained

$$\frac{d\bar{Q}(t)}{dt} = \bar{\tau}_Q[\bar{Q}_E - \bar{Q}(t)] - \bar{c}_Q\,a(t)\bar{Q}(t), \quad \bar{Q}(0) = \bar{Q}_0, \tag{4}$$

$$\frac{dQ(t)}{dt} = \bar{\tau}_Q\bar{Q}(t) - \tau_Q Q(t) - c_Q\,a(t)Q(t), \quad Q(0) = Q_0, \tag{5}$$

where the meaning of the introduced symbols is fully analogical as above. As a rule, the lifespan of τ_Q of mature T helper cells is substantially longer, the superposition of their recovery with that of B cells contributed to more exact simulation results [3] using as a measure of recovery from tolerance the value

$$r_1(t) = 100\,[P(t)/P_c]\,[Q(t)/Q_c], \tag{6}$$

where the meaning of Q_c is the same as in (3). From hypothetical reason also the possibility of necessary cooperation of two T helper lymphocyte populations, denoted Q and R, was investigated [3] for the value

$$r_2(t) = 100\,[P(t)/P_c]\,[Q(t)/Q_c]\,[R(t)/R_c], \tag{7}$$

Another attempt was performed in [4], where always two populations (short-lived and long-lived) of B and T helper lymphocytes were assumed, each of them described by the respective system of equations of the type (1) - (2) and recovery function of the type (3). Various combinations of the respective recovery functions provide working alternatives used to explain tolerance phenomenon [4].

Because of the analogous mechanism of B cell tolerance and idiotype and isotype suppression of short duration caused by the respective antibodies, the original model was applied also to the recovery from this inhibition phenomenon [5]. Model equations (1) - (3) were used together with the effect of antibodies assumed in the form

$$a(t) = \begin{cases} 0, & 0 \le t < t_1 \\ a_0, & t_1 \le t \le t_2 \\ a_0\exp(-\beta(t - t_2)), & t \ge t_2, \end{cases} \tag{8}$$

where a_0 depends on the amount of monoclonal antibody injected, β is the rate of its non-immune elimination, t_1 is the day of monoclonal antibody administration (the day of birth), and t_2 is the day when the antibody concentration starts to decrease below the full suppression level a_0. In fact, the time course of $a(t)$ for $t_1 \le t \le t_2$ does not influence the recovery from suppression, as long as $a(t) \ge a_0$. It serves only to simulate the retarded recovery from the suppression, and the sake of simplicity a constant value $a(t) = a_0$, $t_1 < t < t_2$, was chosen for simulation runs. Based on the extensive comparison with experimental data the hypothesis of the *virtual* age-dependent antibody elimination rate β was postulated [5].

During experimentation with the model the following fundamental observation was made. Namely, for β substantially smaller than $\bar{\tau}_P$ and τ_P, i.e. much faster antigen elimination with

respect to the lifespans of B lymphocytes, the recovery curve τ_0 is determined almost fully by the values of these lifespans. In fact this means that system (1) - (2) without antigen returns freely to its steady-state from the state $\bar{P}_0 = 0$, $P_0 = 0$, where it was brought by the tolerizing dose of antigen. On the other hand, when β is substantially larger than $\bar{\tau}_P$ and τ_P, i.e. the antigen persists for a long time in the organism, the recovery curve is fully dependent on the current β value as the fast system dynamics cause the quasi-steady-state at each time instant. This rough analysis can be supported by the respective analytic solution of system (1) - (2) for the assumed exponential input. Such straightforward computations would confirm this conclusion as the mentioned rates appear in the solution as negative exponents of exponential function multiples, which fact it is was not very difficult to envisage. Then it is possible to determine the model bounds taking into account the realistic range of the involved rates. The corresponding explicit solution formulas for these cases are included in the next section - see (16) - (17) for slow antigen elimination and (18l) - (19) for fast antigen elimination.

When an attempt was made to apply this model to the phenomenon of polyclonal tolerance [6], the just mentioned contradictory situation became more apparent. There did not exist any immunologically acceptable combination of the respective rate constants to fit the experimental data collected on mice after the treatment with bacterial lypopolysaccharide followed by the application of cyclophosphamide [7]. Otherwise speaking, the model was too *slow* to fit this phenomenon. Therefore, a feedback mechanism from mature B cell compartment was suggested [6] to amplify the influx of immature B cells, when the number of mature B cells decreases. The following modification of the original equations was used

$$\frac{d\bar{P}(t)}{dt} = \bar{\tau}_P[\bar{P}_E\left(\frac{P_E}{P(t)}\right)^{\nu} - \bar{P}(t)] - \bar{c}_P\, a(t)\bar{P}(t), \quad \bar{P}(0) = \bar{P}_0, \tag{9}$$

$$\frac{dP(t)}{dt} = \bar{\tau}_P\bar{P}(t) - \tau_P P(t) - c_P\, a(t)P(t), \quad P(0) = P_0, \tag{10}$$

where time varying influx $\bar{\tau}_P\bar{P}_E$ of immature $\bar{P}$ cells depends on the relative deficit of mature P cells, i.e. on $\frac{P_E}{P(t)}$. Exponent ν is a parmeter of fine tuning of the recovery as used also by other authors. With this modification it was possible to adjust the model to fit the experimental data [7].

The growing importance of AIDS etiopathology investigation resulted in the exploitation of the previous experience with the mathematical model of immunological tolerance to HIV infection being also a kind of very dangerous inhibition phenomenon. To recapitulate, the original model assumes that lymphocytes reacting with the tolerated antigen are eliminated or irreversibly inactivated by the tolerogenic dose of antigen. The $CD4^+$ lymphocyte depletion in individuals infected with HIV seems to be also effected by HIV products, although by a mechanism which differs from that of tolerance induction. As the dynamics of these products are inverse to those of tolerance inducing antigen, the existing mathematical model is capable of describing the $CD4^+$ lymphocyte depletion.

Preliminary results of this respect can be found in [8] assuming ad hoc HIV products increase in time. More appropriate simulation results are obtained when limitation of HIV growth by specific cytotoxic cells, which receive the helper effect of mature $CD4^+$ cells in the form of certain feedback, is included in the model [9]. Then the model is able to manifest all three major phases of the $CD4^+$ lymphocyte depletion: (i) rapid initial decline, (ii) stabilized intermediate level; (iii) final accelerated decline. As the substantial decrease of $CD4^+$ lymphocytes during HIV infection could activate a feedback mechanism, in order to increase their production, several ways of incorporation of such a feedback mechanism in the model were investigated further [10]. Promising simulation results were achieved provided that the nonlinear feedback mechanism was activated by the decrease in the total number of T cells. Such a feedback mechanism then increases not only the production of $CD4^+$ lymphocytes, but also of $CD8^+$ lymphocytes. Under such an assumption it is possible to simulate simultaneously both $CD4^+$ lymphocyte depletion and the observed increase $CD8^+$ lymphocytes in HIV infection.

2.3 Model with Linear Feedback

As concluded above, the simple original model of immunological tolerance (1) - (2) is not always capable to explain some available experimental or clinical data. One way to overcome this difficulty was the introduction of a generally nonlinear feedback influence of the number of mature cells on the influx of the immature ones. Although the indicated decrease reciprocal amplification can be one of the available alternatives (signal transmission), it unfortunately substantially complicates the original model by the added nonlinear term $\frac{P_E}{P(t)}$. Moreover, this term tends to infinity when the number of mature cells tends to zero, resulting in a somewhat paradox limit situation with the missing immunological interpretation.

Therefore the alternative possibility of *linear* feedback was investigated. Recall that all above introduced feedback mechanisms should compensate a fairly steep phase of the restoration of number of mature cells P, for which purpose the above singularity was a possible tool. The linear feedback can provide a faster return to the steady-state value of mature cell number. As the subsequent analysis will show, these two ideas, seemingly near the same at first glance, possess fairly different interpretations.

Preserving the above notation, the linear feedback in (9) - (10) has the following form

$$\frac{d\bar{P}(t)}{dt} = f[P_E - P(t)] + \bar{\tau}_P[\bar{P}_E - \bar{P}(t)] - \bar{c}_P\, a(t)\bar{P}(t), \quad \bar{P}(0) = \bar{P}_0, \tag{11}$$

$$\frac{dP(t)}{dt} = \bar{\tau}_P\bar{P}(t) - \tau_P P(t) - c_P\, a(t)P(t), \quad P(0) = P_0, \tag{12}$$

where f denotes the feedback coefficient (amplification). Observe that in this case additive influx amplification is obtained in comparison with the multiplicative one in (9) - (10). In comparison with the original simple model (1) - (2) the additional feedback term

$$F(P(t)) = f[P_E - P(t)],$$

i.e. this additional influx is proportional to the difference between the steady-state and current values of mature cells P. Coefficient f is analogously as ν in (9) a free parameter and can be used to obtain better coincidence the experimental data.

Let us compare the models (11) - (12) and (9) - (10). The influx in (9) can be written as

$$F(P(t)) = \bar{\tau}_P\bar{P}_E\left(\frac{P_E}{P(t)}\right)^\nu.$$

Straightforward computations reveal that

$$\bar{\tau}_P\bar{P}_E\left(\frac{P_E}{P(t)}\right)^\nu = \bar{\tau}_P\bar{P}_E + \nu\tau_P[P_E - P(t)] + O(P_E - P(t)),$$

where

$$\frac{O(P_E - P(t)}{|P_E - P(t)|} \to 0 \text{ for } |P_E - P(t)| \to 0.$$

This implies that as long as $P(t)$ is near to P_E, the nonlinear feedback with parameter ν is nearly the same as the linear one with parameter $\nu\tau_P$. In spite of the fact that the linear feedback model was constructed independently, it was shown that this model is the linearization of the former nonlinear feedback model in the steady-state of the pertinent system.

To simplify further presented analysis of certain qualitative properties of the model (11) - (12), let us introduce the more convenient coordinate system. Denote $x = (x_1, x_2)^T$ and let

$$x_1(t) = \bar{P}(t) - \bar{P}_E, \quad x_1(0) = x_1^0 = \bar{P}_0 - \bar{P}_E,$$

$$x_2(t) = P(t) - P_E, \quad x_2(0) = x_2^0 = P_0 - P_E.$$

Then the system (11) - (12) is equivalent to the following one

$$\dot{x} = Ax + (Bx + c)u, \tag{13}$$

where

$$A = \begin{pmatrix} -\bar{\tau}_P & -f \\ \bar{\tau}_P & -\tau_P \end{pmatrix}, \quad B = \begin{pmatrix} -\bar{c}_P & 0 \\ 0 & -c_P \end{pmatrix}, \quad c = \begin{pmatrix} -\bar{c}_P\bar{P}_E \\ -c_P P_E \end{pmatrix}, \quad u(t) = a(t).$$

Such a system is usually denoted as a bilinear one from the point of view of control theory with antigen being the input. The principal difficulty in analysis of system (13) is the product term $Bx(t)u(t)$. That the reason why it is not a simple task to find the exact explicit formula for the solution $x(t)$ of (13) for general $u(t)$ and to analyze the character of dependence of response $x(t)$ on the input $u(t)$ – see [11] and [12]. To obtain some simple representation of $x(t)$, some additional assumptions concerning the system (13) are necessary, e.g. that both A and B are upper (or lower) triangular matrices (this is the case if $f = 0$.)

The model (1) - (2) will have the form (13) for $f = 0$. Therefore the principal advantage of considering the model (1) - (2) is the existence of an explicit formula for the solution $x(t)$ of (13) with an arbitrary input $u(t)$ and initial state $x(0) = x^0$.

Theorem 1. Consider the system (13) with $f = 0$. Then its solution $x(t)$ has the form

$$x_1(t) = e^{-\bar{\tau}_P - \bar{c}_P w(t)}(x_1^0 - \bar{c}_P \bar{P}_E \int_0^t e^{\bar{\tau}_P s + \bar{c}_P w(s)} u(s) ds), \tag{14}$$

$$\begin{aligned} x_2(t) = \quad & e^{-\tau_P - c_P w(t)}(x_2^0 - \bar{\tau}_P x_1^0 \int_0^t e^{-\bar{\tau}_P s - \bar{c}_P w(s)} e^{\tau_P s + c_P w(s)} ds \\ & -\bar{\tau}_P \bar{c}_P \bar{P}_E \int_0^t e^{-\bar{\tau}_P s - \bar{c}_P w(s)} e^{\tau_P s + c_P w(s)} \int_0^s e^{\bar{\tau}_P \alpha + \bar{c}_P w(\alpha)} u(\alpha) d\alpha \, ds \,, \\ & -c_P P_E \int_0^t e^{\tau_P s + c_P w(s)} u(s) \, ds), \end{aligned} \tag{15}$$

where $w(t) = \int_0^t u(\alpha) d\alpha$. Validity of these formulas can be checked by a direct differentiation with respect to t.

Corollary 1. Let $u(t) \equiv u_0$ for any $t \geq 0$ and $x_1(0) = x_1^0$, $x_2(0) = x_2^0$. Then

$$x_1(t) = e^{-(\bar{\tau}_P + \bar{c}_P u_0)t}(x_1^0 - \hat{x}_1(u_0)) + \hat{x}_1(u_0),$$

$$x_2(t) = \begin{cases} e^{-(\tau_P + c_P u_0)t} \left(x_2^0 - \hat{x}_2(u_0) - \bar{\tau}_P \dfrac{x_1^0 - \hat{x}_1(u_0)}{\tau_P + c_P u_0 - \bar{\tau}_P - \bar{c}_P u_0} \right) \\ \qquad\qquad + e^{-(\bar{\tau}_P + \bar{c}_P u_0)t} \bar{\tau}_P \dfrac{x_1^0 - \hat{x}_1(u_0)}{\tau_P + c_P u_0 - \bar{\tau}_P - \bar{c}_P u_0} + \hat{x}_2(u_0), \quad \text{if } \bar{\tau}_P \neq \tau_P, \\[4pt] e^{-(\tau_P + c_P u_0)t} \left(x_2^0 - \hat{x}(u_0) + t\tau_P(x_1^0 - \hat{x}_1(u_0)) \right) + \hat{x}_2(u_0), \quad \text{if } \bar{\tau}_P = \tau_P \end{cases}$$

where $(\hat{x}_1(u_0), \hat{x}_2(u_0))^T$ is the steady-state for $u(t) \equiv u_0$

$$\hat{x}_1(u_0) = -\frac{\bar{c}_P \bar{P}_E u_0}{\bar{\tau}_P + \bar{c}_P u_0)} \quad \text{and} \quad \hat{x}_2(u_0) = -\left(\frac{\bar{\tau}_P \bar{c}_P \bar{P}_E u_0}{(\bar{\tau}_P + \bar{c}_P u_0)(\tau_P + c_P u_0)} - \frac{c_P P_E u_0}{\tau_P + c_P u_0} \right).$$

One can see, that if $\bar{\tau}_P$ and τ_P are large enough, after a short time period it approximately holds that $x_1(t) = \hat{x}_1(u_0)$, $x_2(t) = \hat{x}_2(u_0)$. If the elimination of antigen is so small that changes of its concentration are negligible during this time period, the approximate solution for such antigen $u(t)$, $t \in [0, T]$ is written as

$$x_1(t) = -\frac{\bar{c}_P \bar{P}_E u(t)}{\bar{\tau}_P + \bar{c}_P u(t)}, \tag{16}$$

$$x_2(t) = -\left(\frac{\bar{\tau}_P \bar{c}_P \bar{P}_E u(t)}{(\bar{\tau}_P + \bar{c}_P u(t))(\tau_P + c_P u(t))} - \frac{c_P P_E u(t)}{\tau_P + c_P u(t)} \right). \tag{17}$$

Corollary 2. Let $u(t) = 0$ for any $t \geq 0$ and

$$x_1^0 = -\bar{P}_E, \quad \text{i.e.} \quad \bar{P}(0) = 0,$$

$$x_2^0 = -\bar{P}_E, \quad \text{i.e.} \quad P(0) = 0.$$

Then

$$x_1(t) = -e^{-\bar{\tau}_P t} \bar{P}_E, \tag{18}$$

$$x_2(t) = \begin{cases} \frac{\bar{\tau}_P}{\tau_P - \bar{\tau}_P}(e^{-\tau_P t} P_E - e^{-\bar{\tau}_P t} \bar{P}_E), & \text{if } \tau_P \neq \bar{\tau}_P, \\ e^{-\tau_P t} P_E(1 + \tau_P t), & \text{if } \tau_P = \bar{\tau}_P(\text{and } P_E = \bar{P}_E) \end{cases} \tag{19}$$

Solutions (18) - (19) describe the hypothetic situation when the numbers of both, immature and mature cells are zero and no antigen is present. Such a solution represents, in fact, the fastest possible recovery from suppression. However, there exist experimental data, e.g. concerning the polyclonal suppression [6], which relate to the still faster recovery than (18) - (19) can produce. Therefore, some kind of feedback has to be admitted. Moreover, some cases of recovery with P values above P_E were observed. Also this phenomenon can be explained applying the linear feedback. Unfortunately in this case ($f \neq 0$) there is no possibility for simple and explicit representation of solution (13) for some nonconstant input and other methods are to be used to investigate such a model.

Proposition 1. Let us consider a model with the linear feedback (11) - (12) and let $f = \nu \tau_P$, $\nu \neq 0$, and $x_2(0) < 0$. If

$$(1 - \frac{\bar{\tau}_P}{\tau_P})^2 < 4\nu \frac{\bar{\tau}_P}{\tau_P}, \tag{20}$$

then there exist some values of time t^*, t^{**}, $t^* < t^{**}$, such that for $t^* < t < t^{**}$ it holds

$$x_2(t) > 0. \text{ i.e. } P(t) > P_E. \tag{21}$$

Moreover, if (20) does not hold, then for each $t \geq 0$ one has

$$x_2(t) < 0. \text{ i.e. } P(t) < P_E.$$

Proof. Let us consider system (13) with $f = \nu \tau_P$ and let $x_2(0) < 0$. To prove the second part of this proposition let us neglect the antigen $u(t)$ in (13). Then $x_2(t)$ can be only increased, i.e. it is sufficient to prove this second part only for the case $u(t) \equiv 0$. From (13) resulting homogeneous system has clearly the following eigenvalues.

$$\lambda_{1,2} = -\frac{\tau_P + \bar{\tau}_P}{2} \pm \sqrt{(\frac{\tau_P + \bar{\tau}_P}{2})^2 - \tau_P(f + \tau_P)} \tag{22}$$

It can be easily shown, that if (20) is not true, both λ_1 and λ_2 are the real roots implying that $x_2(t)$, $t \geq 0$ must be a monotonous function. This proves the second part of the proposition. When proving the first part, realize that because $u(t)$ tends to zero, one can for some $\tilde{t} > 0$ approximately assume that $u(t) = 0$ for $t > \tilde{t}$. Now if (20) holds, then (22) implies that λ_1 and λ_2 are the conjugate complex roots with a negative real part. Then $x_2(t)$ is a product of exponential and trigonometric function, and this is the reason why (21) is valid.

Condition (20) shows that if τ_P and $\bar{\tau}_P$ are sufficiently close to each other and the feedback parameter ν (or $f = \nu \bar{\tau}_P$) is large enough, the case (21) occurs, i.e. the recovery is not

monotonous, but exhibits dampened oscillations about the steady-state value. For the sake of illustration let us consider the discussed case of polyclonal tolerance simulation [6], which resulted in such behaviour. Various parameters of (9) - (10) were selected as follows: $\bar{r}_P = r_P = 0.2$, $\bar{c}_P = c_P = 1.0$, $\bar{P}_0 = \bar{P}_E = 100.0$, $P_0 = P_E = 100.0$. Antigen was assumed in the form of (8) with $a_0 = 0.9$, $\beta = 3.0$, $t_1 = 2.0$, $t_2 = 15.0$, $\nu = 0.65$ to duplicate the case of [6] on Figure 2 – dashed line. For the case with linear feedback (11) - (12) the only change was to select the initial dose $a_0 = 0.62$ for the same lowest level of $r_0(t)$ and to adjust $f = 0.31$ to produce the solid line in Figure 2. This confirms the fact that the suggested linear feedback produce at least the same effect as the originally used nonlinear one.

2.4   Conclusions

The growing number of modifications and applications of the original mathematical model of tolerance demanded a deeper theoretical analysis of the involved system of differential equations. The provided analysis confirmed the importance of inclusion of feedback mechanisms in mathematical models for simulation of recovery from various inhibition phenomena in immunology. It was shown that in the suggested class of mathematical models the linear feedback mechanism is fully sufficient, which in fact, considerably simplifies the pertinent investigations. The augmented flexibility of the model can be used to study and simulate other related phenomena exhibiting also oscillatory character.

2.5   References

[1] Klein, P., T. Hraba, and J. Doležal. (1983) *The use of immunological tolerance to investigate B lymphocyte replacements in chickens.* J. Math. Biology. **16**, p. 131 - 140.

[2] Klein, P., T. Hraba, and J. Doležal. (1985) *Mathematical model of B lymphocytes replacement kinetics: its application to the recovery from tolerance in adult mice.* Math. Biosci. **73**, p. 227 - 238.

[3] Doležal, J. and T. Hraba. (1988) *A contribution to mathematical modelling of immunological tolerance.* Arch. Immunol. Ther. Exper. **36**, p. 23 - 30.

[4] Doležal, J. and T. Hraba. (1984) *T helper cell inclusion into the mathematical model of immunological tolerance.* Folia Biol. (Praha) **30**, p. 426 - 431.

[5] Doležal, J. and T. Hraba. (1988) *Simulation analysis of the escape from immunoglobulin suppression.* Folia Biol. (Praha) **34**, p. 331 - 337.

[6] Doležal, J. et al. (1989) *Recovery from polyclonal tolerance.* Folia Biol. (Praha) **35**, p. 164 - 170.

[7] Fontalin, L.N. et al. (1988) *Polyclonal B cell anergy induced by bacterial polysaccharide and cyclophosphamide.* Folia Biol. (Praha) **34**, p. 72 - 83.

[8] Doležal, J. and T. Hraba. (1988) *Application of the mathematical model of immunological tolerance to HIV infection.* Folia Biol. (Praha) **34**, p. 338 - 343.

[9] Hraba, T. and J. Doležal. (1989) *Mathematical model of $CD4^+$ lymphocyte depletion in HIV infection.* Folia Biol. (Praha) **35**, p. 159 - 163.

[10] Hraba, T. and J. Doležal. (1989) *Simulation analysis of $CD4^+$ lymphocyte dynamics in HIV infected persons.* In: *Mathematical Modelling in Immunology and Medicine.* Kiev, U.S.S.R. August 28 - September 7, 1989. This volume.

[11] Čelikovský, S. (1987) *On the representation of trajectories of bilinear systems and its applications.* Kybernetica **23**, p. 198 - 213.

[12] Čelikovský, S. (1988) *On the continuous dependence of trajectories of bilinear systems on controls and its applications.* Kybernetica **24**, p. 278 - 292.

$$\bar{\tau}_P a(t) \qquad\qquad c_P a(t)$$
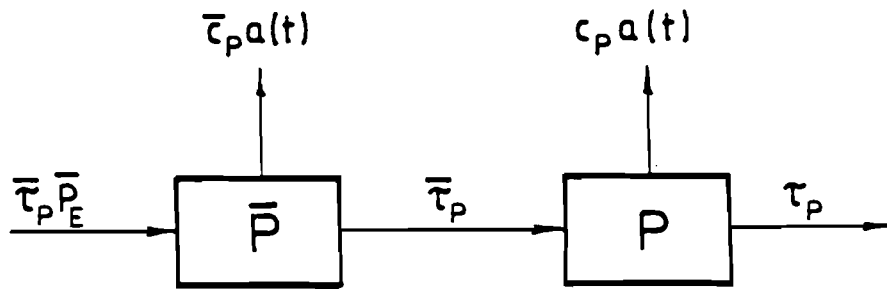
Figure 2.1. Block diagram of the compartmental model.
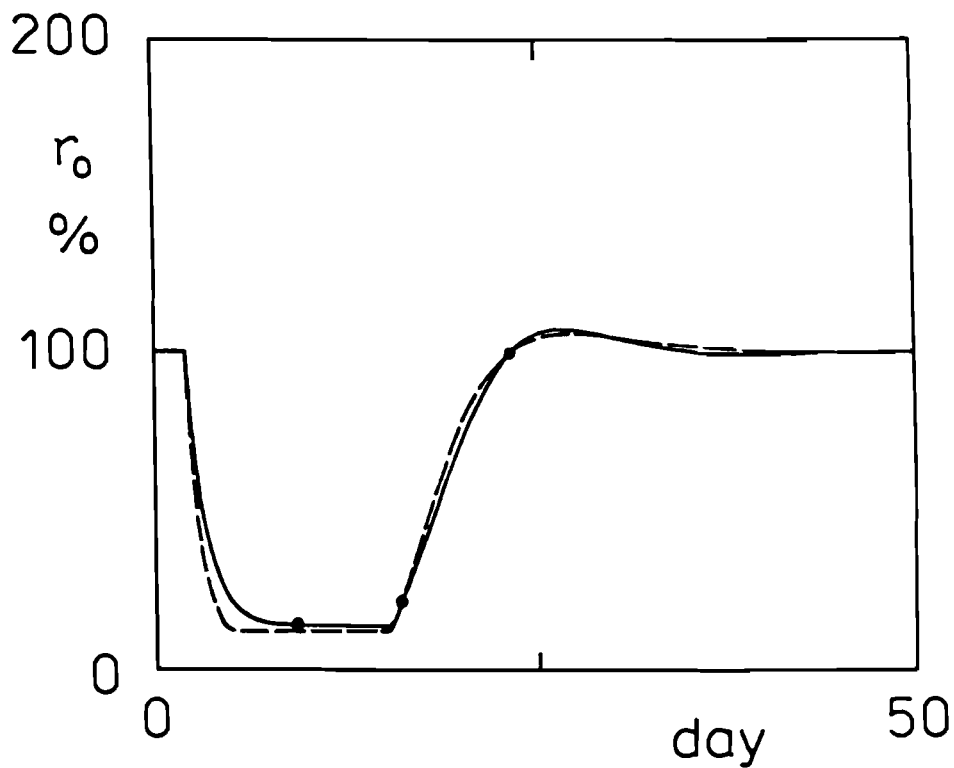
Figure 2.2. Comparison of nonlinear feedback (dashed line) and linear feedback (solid line) recovery simulation with experimental data (●).

Chapter 3

Simulation Analysis of $CD4^+$ Lymphocyte Dynamics in HIV Infected Persons

T. Hraba
Institute of Molecular Genetics
Czechoslovak Academy of Sciences
142 20 Prague, Czechoslovakia

J. Dolezal
Institute of Information Theory and Automation
Czechoslovak Academy of Sciences
182 08 Prague, Czechoslovakia

3.1 Introduction

The dominant immunologic abnormality in AIDS patients is the depletion of $CD4^+$ lymphocytes [1-3]. This depletion is probably not due to the cytopathogenic effect of HIV on this subset of lymphocytes, because the number of cells in peripheral blood and lymph nodes, that express HIV, is too low to explain the observed decrease of $CD4^+$ lymphocytes. Depletion of these cells in HIV infected individuals seems to be caused by HIV products either directly or by an immune reaction induced by them [1-2]. The increasing concentration of HIV products during the progression of the infection can be assumed to increase the CD_4^+ lymphocyte depletion.

The increase of HIV products during infection is inverse to the decreasing concentration of non-reproducing antigen used for the induction of immunological tolerance. If it is anticipated that tolerance is due to deletion or irreversible functional inactivation of the specific lymphocytes by antigen, the dynamics of the reappearance of lymphocytes reacting with the tolerated antigen during the recovery from tolerance are necessarily inverse to the depletion of $CD4^+$ lymphocytes in HIV infection. This observation led us to the suggestion that our mathematical model of immunological tolerance [4, 5], which is based on the assumption mentioned above, is applicable to CD_4^+ lymphocyte depletion in HIV infected individuals [6]. However, it does not imply that the same mechanism is operative in both cases.

According to clinical findings [7,8], there exists a substantial decrease in $CD4^+$ lymphocytes during the first year, and especially during the first six months, after seroconversion. However, after this initial drop of the T cell subset, the level of $CD4^+$ lymphocytes remains fairly stationary during the following period. When $CD4^+$ lymphocyte depletion was simulated under assumption of unrestricted HIV reproduction, the simulated $CD4^+$ lymphocyte depletion did not agree well with the clinical data [6]. The arrest of further depletion of $CD4^+$ lymphocytes in the initial stage of infection is probably caused by an immune reaction to the HIV. As it was

suggested that cytotoxic T cells could be the respective immunological mechanism retarding the progression of HIV infection [1, 9], we included this inactivation of HIV by specific cytotoxic T cells in our mathematical model [10]. By such modification of the model it was possible to simulate the observed three major phases of $CD4^+$ lymphocyte depletion:

(i) Initial rapid decline.
(ii) Stationary intermediate level.
(iii)Final accelerated decline.

In our model of immunological tolerance [4, 5] we assumed a constant influx of new B or T lymphocytes from stem cells. Assumption of this kind is justified, as even if the mechanism effecting tolerance is the deletion of clones reacting with the tolerated antigen, the total number of lymphocytes in the organism remains unaffected, because only a small fraction of lymphocytes is deleted.

A different situation was encountered in [11] dealing with the simulation of dynamics of polyclonal B cell tolerance induced in mice by treatment with bacterial lipopolychaccharide followed by application of cyclophosphamide [12]. The resulting suppression of antibody production is very probably caused by a substantial deletion of B cells. To obtain satisfactory simulation of the recovery from this type of tolerance, it was necessary to assume that the exhibited substantial decrease of B cells activates a feedback mechanism that increases, in turn, the influx of new B cells from stem cells. With such mechanism included in the mathematical model [11], the simulation results agreed well with the experimental data in [12].

It has to be expected that the depletion of $CD4^+$ lymphocytes even in the early stages of HIV infection is sufficient to activate a feedback mechanism increasing the influx of these cells. This paper presents several alternatives how feedback mechanisms of different structure affect the simulation of $CD4^+$ lymphocyte depletion in HIV infected individuals.

3.2   Mathematical Model

Two developmental compartments of $CD4^+$ lymphocytes are considered in the model:

(i) The immature cell compartment - $\bar{P}$ cells.
(ii) The mature cell compartment - P cells.

Sizes of $\bar{P}$ and P cell compartments are described by the following differential equations with the given initial values:

$$\frac{d\bar{P}(t)}{dt} = I_P(F_P(t))^\mu - \bar{\tau}_P \bar{P}(t) - \bar{c}_P\, a(t)\bar{P}(t), \quad \bar{P}(0) = \bar{P}_0, \tag{3.1}$$

$$\frac{dP(t)}{dt} = \bar{\tau}_P \bar{P}(t) - \tau_P P(t) - c_P\, a(t)P(t), \quad P(0) = P_0, \tag{3.2}$$

where $P(t)$ and $\bar{P}(t)$ are the numbers of P and $\bar{P}$ cells at time t, I_P is the influx of $\bar{P}$ cells, i.e. the rate (all rates are in days^{-1}) of differentiation of $\bar{P}$ cells from stem cells, $F_P(t)$ is the later specified feedback effect of P cells on the influx of $\bar{P}$ cells with intensity μ at time t, $\bar{\tau}_P$ is the rate of maturation of $\bar{P}$ cells into P cells, and τ_P is the rate of natural death of P cells. The quantity $\bar{c}_P a(t)$ is the rate of elimination of $\bar{P}$ cells due to HIV products, and analogously, $c_P a(t)$ that of P cells, where parameter $a(t)$ corresponds to the amount of HIV products at time T.

The dynamics of HIV products during the infection are described by the differential equation:

$$\frac{da(t)}{dt} = a(t)[\theta - \gamma C(t)], \quad a(0) = a_0, \tag{3.3}$$

where a_0 is the function of the infectious dose of HIV and θ characterizes the growth rate of HIV. $C(t)$ denotes the number of cytotoxic T cell specific for HIV (C cells) at time t and γ the rate of inactivation of HIV products due to the killing capacity of these cells.

The size of C cell compartment is described by the following equation:

$$\frac{dC(t)}{dt} = [\varepsilon I_C + \alpha C(t)]a(t)\left(\frac{P(t)}{P_0}\right)^{\nu} - \tau_C C(t), \; C(0) = C_0. \tag{3.4}$$

The maturation of C cells from their precursors is assumed to be dependent of the encounter with HIV products and the effect of HIV specific helper T cells. I_C is the influx of C cell precursors, ε their maturation rate, α the proliferation rate of C cells, and τ_C their natural death rate. It is assumed that the decrease of the number of HIV specific helper T cells is proportional to the total number of $CD4^+$ lymphocytes in HIV infected persons. In consequence, the helper T cell effect on maturation and proliferation of C cells can be expressed be the ratio $P(t)/P_0$; the coefficient ν is introduced to characterize the intensity of this helper effect.

In simulation runs, the various parameters were set as follows: $\bar{\tau}_P = 0.2, \tau_P = 0.01, \tau_C = 0.01, I_P = 1.0, I_C = 0.5, \bar{P}_0 = 5.0, P_0 = 100.0, C_0 = 0.0, a_0 = 0.0005, \theta = 0.02, \gamma = 0.7, \alpha = 0.1$. Note that for a required value of P_0 the corresponding value of $\bar{P}_0$ is determined from the steady-state considerations in absence of HIV products ($a(t) \equiv 0$) and feedback mechanism ($\mu = 0.0$), i.e. $\bar{\tau}_P \bar{P}_0 = \tau_P P_0$ - see [4, 5]. The remaining parameter ε was adjusted in each considered case to obtain satisfactory fit with clinical evidence. Insignificant differences in simulation results were observed when HIV products were assumed to affect both immature and mature $CD4^+$ lymphocytes ($\bar{P}$ and P cells) or the mature ones (P cells) only. Therefore, simulation results are presented, where only mature P cells are sensitive to HIV products, i.e. $\bar{c}_P = 0.0$. If not explicitly mentioned, the value $c_P = 1.0$ was used throughout the simulation.

3.3 Results

Now let us consider several different structures of inclusion of the feedback mechanism in the above described model illustrated by results of the respective simulation runs.

3.4 Model Without Feedback Effect

For the sake of comparison let us include an example of simulation results (Fig. 1) obtained without taking into account the activation of a feedback mechanism increasing the influx of $\bar{P}$ cells ($\mu = 0.0$). With $\nu = 1.0$, a constant decreased level of $CD4^+$ lymphocytes was obtained after the initial drop, and the curve did not exhibit the final decrease in a wide range of ε and also α parameters. The curve a was obtained for the values $\nu = 2.0$ and $\varepsilon = 0.205$. It manifested the three phases of the P cell dynamics, but the initial drop is somewhat higher than the clinical observed one. The curve b for $\nu = 3.0$ and $\varepsilon = 0.35$ gives then a very good approximation to the clinical observations. The value $\nu = 3.0$ was therefore used in subsequent analysis.

3.5 Feedback Mechanism Affecting the Influx into $\bar{P}$ Compartment

In this modification it was assumed that the decreased level of $CD4^+$ lymphocytes activates a feedback mechanism which increases the influx of I_P into the $\bar{P}$ cell compartment. For such case the value

$$F_P(t) = \frac{P_0}{P(t)}. \tag{3.5}$$

Figure 2 depicts the simulated dynamics of $CD4^+$ lymphocyte depletion for $\mu = 1.0$ and $\varepsilon = 0.135$. The value $\mu = 1.0$ was used also in the remaining investigated cases.
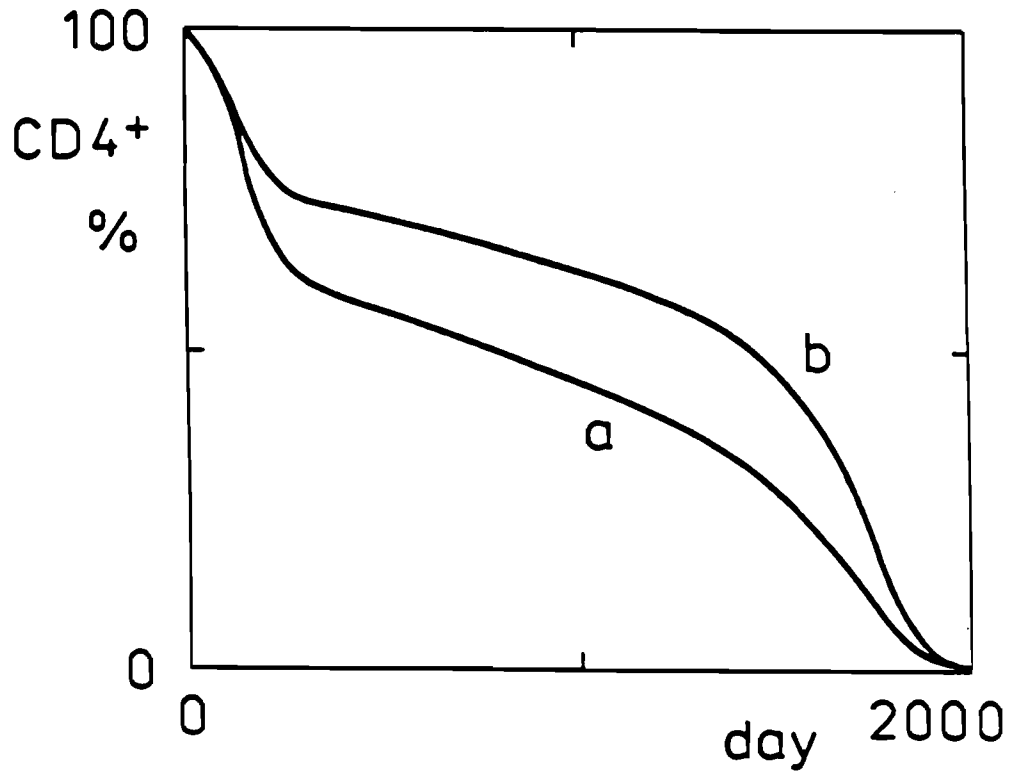
Figure 3.1. $CD4^+$ lymphocyte depletion curves without feedback effect; curve a for $\nu = 2.0$, curve b for $\nu = 3.0$.
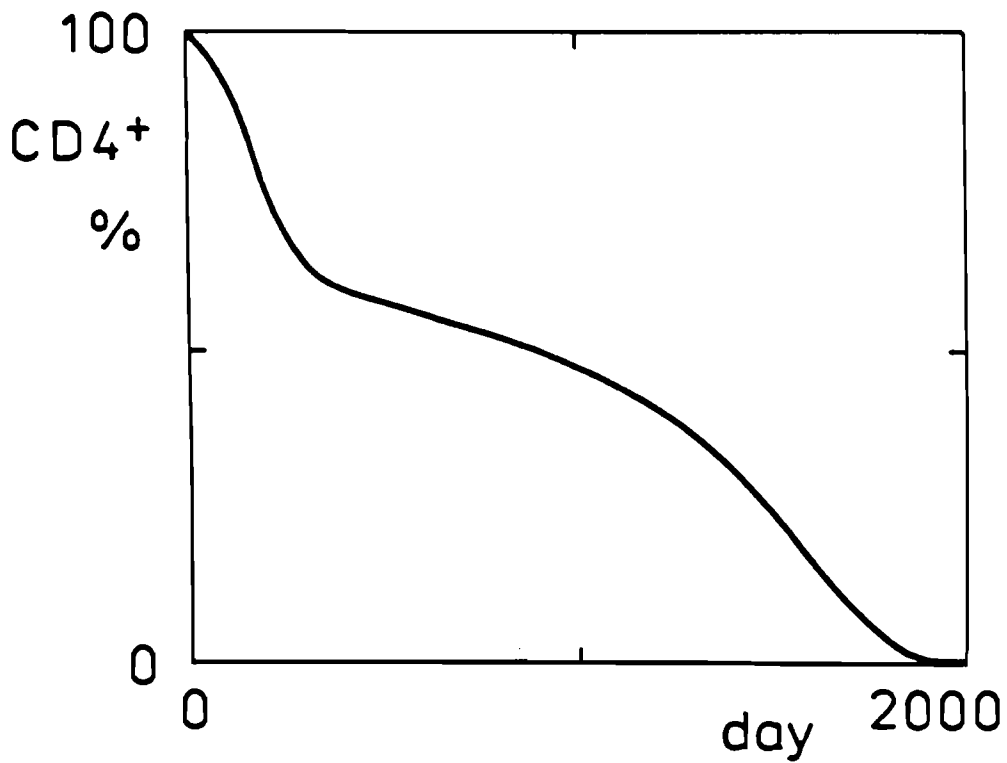
Figure 3.2. $CD4^+$ lymphocyte depletion curve with feedback mechanism according to Eq. 5.

3.6 Feedback Mechanism Affecting the Common Precursor of $CD4^+$ and $CD8^+$ Lymphocytes

Our attention was turned to the possibility that the feedback mechanism is activated by the decrease of the total number of T cells and acts on a common precursor of $CD4^+$ and $CD8^+$ lymphocytes by L.M. Adleman (Univ. of Southern California; manuscript). He based this hypothesis among other findings on the dynamics of $CD4^+$ and $CD8^+$ lymphocytes in individuals infected with HIV. Such a mechanism would increase the production of both types of T cells, even if only one of them is depleted. There are two possible ways, how the feedback mechanism is activated:

(i) By the decrease of the total number of T lymphocytes, i.e. the sum of $CD4^+$ and $CD8^+$ lymphocytes.

(ii) The change in the cell numbers of each T cell subset ($CD4^+$ or $CD8^+$) activates a separate feedback mechanism, but both of these mechanisms act on the same precursor.

For incorporation of the mechanism in the model, it was necessary to add the following differential equations describing the sized of immature ($\bar{R}$) and mature (R) $CD8^+$ lymphocyte compartments:

$$\frac{d\bar{R}(t)}{dt} = I_R(F_R(t))^\mu - \bar{\tau}_R \bar{R}(t), \quad \bar{R}(0) = \bar{R}_0, \tag{3.6}$$

$$\frac{dR(t)}{dt} = \bar{\tau}_R \bar{R}(t) - \tau_R R(T), \quad R(0) = R_0 \tag{3.7}$$

Here $R(t)$ and $\bar{R}(t)$ are the numbers of R and $\bar{R}$ cells at time t, I_R is the influx of $\bar{R}$ cells, $F_R(t)$ is the feedback effect of R cells on the influx of $\bar{R}$ cells with intensity μ at time t, $\bar{\tau}_R$ is the rate of maturation of $\bar{R}$ cells into R cells, and τ_R is the rate of natural death of R cells. The used notation is fully analogical to that used in the earlier relations.

In simulations runs the following values were used: $\bar{\tau}_R = \bar{\tau}_P = 0.2$, $\tau_R = \tau_P = 0.01$, $I_R = 0.666$, $\bar{R}_0 = 3.33$, $R_0 = 66.6$. These parameters correspond to those of $CD4^+$ lymphocytes and R_0 was selected in accordance with existing ratio of $CD4^+$ and $CD8^+$ lymphocytes in common pool. The $\bar{R}_0$ was again determined from the steady-state consideration as in Eqs. (1)–(2).

In the case (i) with feedback mechanism triggered by the total number of T lymphocytes, the effect is described as follows:

$$F_P(t) = F_R(t) = \frac{P_0 + R_0}{P(t) + R(t)}. \tag{3.8}$$

One of the acceptable simulation cases is depicted in Figure 3 for $\varepsilon = 0.238$. The curve a gives the number of $CD4^+$ lymphocytes, the curve b that of $CD8^+$ ones, and the curve c of their sum. The simulated total number of T lymphocytes is only slightly lower than the observed clinical values [7], otherwise a considerably good coincidence was achieved.

If the case (ii) having the feedback mechanism triggered separately by the respective numbers of $CD4^+$ and $CD8^+$ lymphocytes, is considered, then

$$F_P(t) = F_R(t) = \frac{P_0 R_0}{P(t) R(t)}. \tag{3.9}$$

This case is not documented here as the simulation results exhibit only insignificant differences with respect to those applying the feedback mechanism (8). Instead, Figure 4 depicts the simulated dynamics of the different T cell populations under the assumption that only immature $CD4^+$ lymphocytes ($\bar{P}$ cells) are affected by HIV products ($\bar{c}_P = 1.0$, $c_P = 0.0$) for parameter $\varepsilon = 0.0045$. The general character of the curves remains the same as in the preceeding situation, where only mature P cells were affected. The major difference is the later onset of $CD4^+$ lymphocyte depletion and somewhat larger increase in $CD8^+$ lymphocyte number.
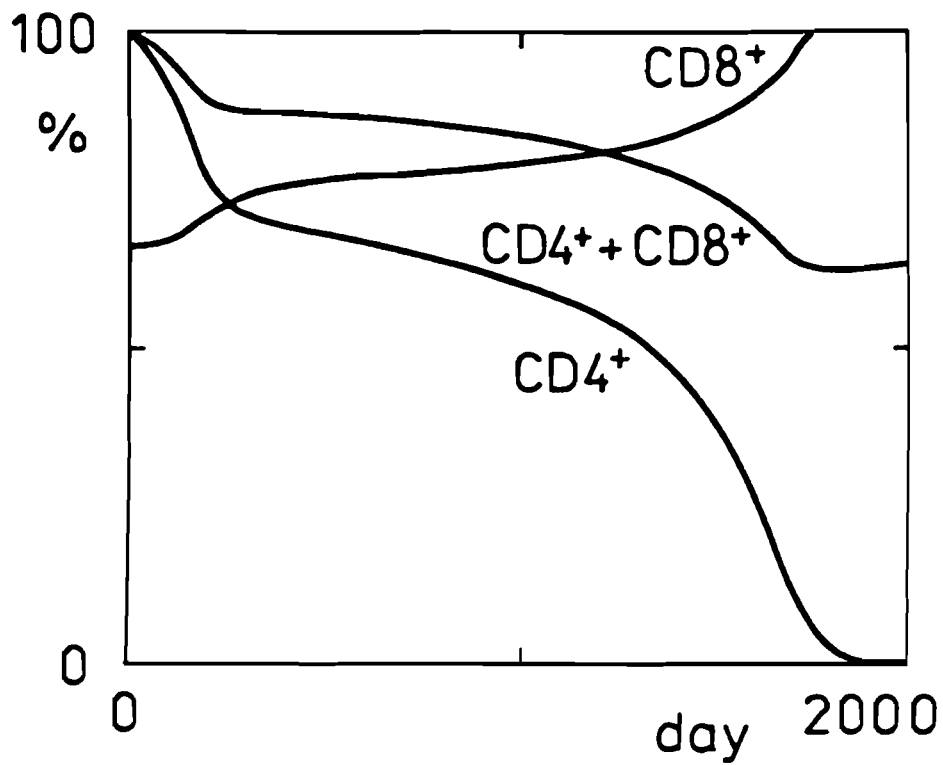
Figure 3.3. $CD4^+$ and $CD8^+$ lymphocytes development curves with feedback mechanism according to Eq. 8.
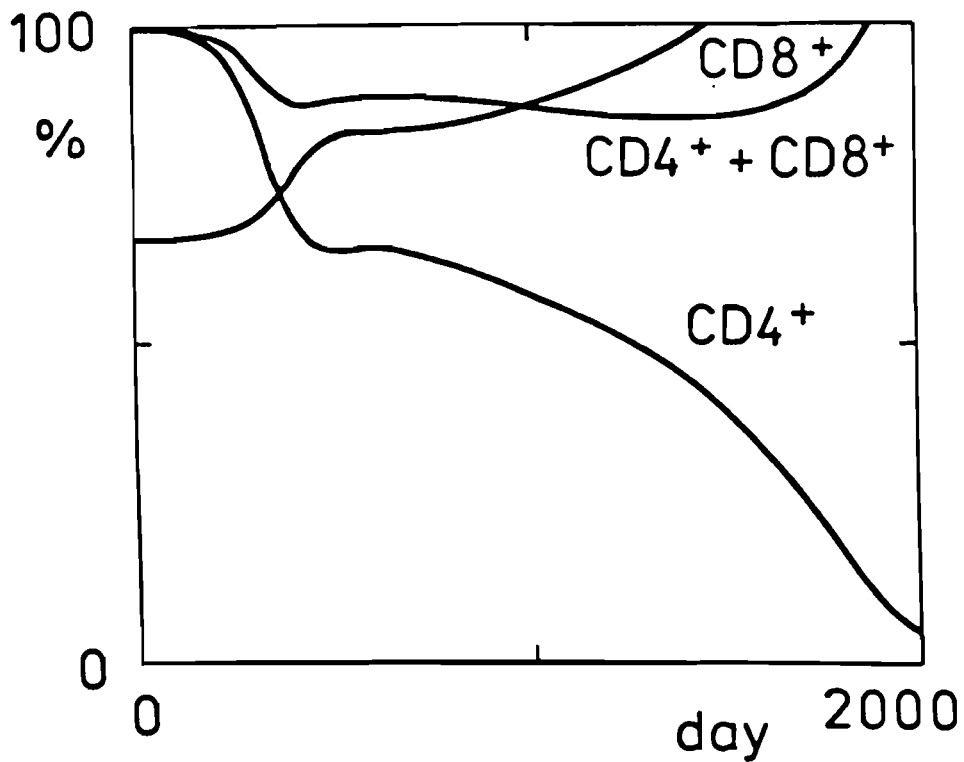
Figure 3.4. $CD4^+$ and $CD8^+$ lymphocytes development curves with feedback mechanism according to Eq. 9 with $\bar{c}_P = 1.0$ and $c_P = 0.0$.

3.7 Discussion

Satisfactory simulation of dynamics of $CD4^+$ lymphocyte depletion in HIV infection can be provided by the suggested model, if it is postulated that HIV reproduction is limited by the action of cytotoxic T cells [6]. These cytotoxic cells are assumed to mature and proliferate after contact with antigen under influence of specific helper T cells. This helper activity declines when the number of $CD4^+$ lymphocytes decreases during HIV infection. If it is assumed that the helper activity decreases linearly with the number of $CD4^+$ lymphocytes ($\nu = 0.0$), the simulated number of $CD4^+$ lymphocytes stabilizes at a lower level and does not exhibit the final decline. For the simulation of this terminal phase it is necessary to postulate that the depletion of $CD4^+$ lymphocytes causes a faster than linear decrease of the helper activity. Such an assumption is acceptable, because it was observed that the activity of $CD4^+$ lymphocytes in HIV infected individuals decreases faster than their numbers [1-3].

This model does not take into account that the decrease of $CD4^+$ lymphocytes will most probably activate a feedback mechanism effecting their increased production. The inclusion of such a mechanism regulating the influx into $\bar{P}$ cell compartment led to not fully satisfactory results. However, when the feedback mechanism was accepted to be activated by the decrease in the total number of T cells resulting in the increased production of both $CD4^+$ and $CD8^+$ lymphocytes, the simulation results were in good agreement with available clinical data. As double positive ($CD4^+$ and $CD8^+$) thymocytes are the precursors of the single positive, more mature, ones [13], this mechanism can be expected to exist.

It is worth mentioning that two modifications of the model – one assuming the feedback mechanism activated by the total number of T cells, the other by each T cell subset ($CD4^+$ and $CD8^+$) separately – allowed fully acceptable simulation analysis. The achieved coincidence was not only in $CD4^+$ lymphocyte depletion, but also in $CD8^+$ lymphocyte increase in HIV infected persons, as reported in [7, 8]. The simulated numbers of $CD8^+$ lymphocytes increased even more in the final stage of the disease in contrast to the decrease observed in AIDS patients [8]. The mathematical model can simulate satisfactorily the dynamics of $CD4^+$ lymphocytes during the whole course of the HIV infection. As far as the $CD8^+$ lymphocyte dynamics are concerned, it would be necessary to postulate that some additional mechanism starts to act at the final stage of disease.

It was suggested that the depletion of $CD4^+$ lymphocytes in HIV infected individuals could be due to the infection of their precursors leading to impaired production of mature cells (2). The model without feedback gave satisfactory results (6), when it was assumed that both immature and mature, or immature $CD4^+$ lymphocytes alone, are depleted by HIV products. With the model including feedback mechanism the approximation of clinical data was good, when simultaneous depletion of immature and mature $CD4^+$ lymphocytes by HIV was postulated. On the other hand, less acceptable fit was obtained when only immature $CD4^+$ lymphocytes were assumed to be depleted by HIV products. Eventual depletion of common precursors of $CD4^+$ and $CD8^+$ lymphocytes by HIV products should result in depletion of both T cell subsets, but this would contradict the clinical findings.

3.8 Conclusions

The $CD4^+$ lymphocyte depletion in HIV infected persons seems to be effected by HIV products. As the dynamics of the concentration of HIV products are inverse to those of non-replicating antigen used for tolerance induction, the mathematical model of immunological tolerance can be used to describe the dynamics of $CD4^+$ lymphocyte depletion. To simulate the clinically observed dynamics, it is necessary to include the limitation of HIV growth by the corresponding cytotoxic T cells and their dependence on the helper effect of $CD4^+$ lymphocytes.

The substantial decrease of $CD4^+$ lymphocytes in HIV infection can possible activate a feedback mechanism increasing their production. Several ways of incorporation of such feedback

mechanisms in the model are investigated. Very good simulation results are achieved provided that the nonlinear feedback mechanism is activated by the decrease in the total number of T cells. Under such assumption it is possible to simulate simultaneously both $CD4^+$ lymphocyte depletion and the observed increase of $CD8^+$ lymphocytes during the course of the HIV infection.

3.9 References

[1] Fauci, A.A. (1988) *The human immunodeficiency virus: Infectivity and mechanisms of pathogenesis.* Science **239**, p. 617–639.

[2] Seligmann, M. (1988) *Immunology of infection with the human immunodeficiency virus.* Rec. Prog Medicina. **79**, p. 330 -337.

[3] Spickelt, G.P. and A.G. Dalgleish. (1988) *Cellular immunology of HIV-infection.* Clin. Exp. Immunol. **70**, p. 1–7.

[4] Klein, P., T. Hraba, and J. Doležal. (1983) *The use of immunological tolerance to investigate B lymphocyte replacement kinetics in chickens.* J. Math. Biol. **16**, p. 131–140.

[5] Doležal, J. and T. Hraba. (1988) *A contribution to mathematical modelling of immunological tolerance.* Arch. Immunol. Ther. Exper. **36**, p. 23–30.

[6] Doležal, J. and T. Hraba. (1988) *Applications of the mathematical model of immunological tolerance to HIV infection.* Folia Biol. (Praha) **34**, p. 338–343.

[7] Fahey, J.L., et al. (1987) *Immune pathogenesis of AIDS and related syndromes.* In: *Acquired Immune Deficiency Syndrome.* J.C. Gluckman and E. Vilmer (Eds.). Elsevier, Paris. p. 107–114.

[8] Lang, W., et al. (1989) *Patterns of T lymphocyte changes with human immunodeficiency virus infection: From seroconversion to the development of AIDS.* J. AIDS **2**, p. 63–69.

[9] Levy, J.A. (1988) *Mysteries of HIV: challenges for therapy and prevention.* Nature (London), p. 519–523.

[10] Hraba, T. and J. Doležal. (1989) *Mathematical model of $CD4^+$ lymphocyte depletion in HIV infection.* Folia Biol. (Praha) **35**, p. 159–163.

[11] Doležal, J., et al. (1989) *Recovery from polyclonal tolerance.* Folia Biol. (Praha) **35**, p. 164–170.

[12] Foltalin, L.N., et al. (1988) *Polyclonal B cell energy induced by bacterial polysaccharide and cyclophosphamide.* Folia Biol. (Praha) **34**, p. 72–83.

[13] von Boehmer, H. (1988) *The development biology of T lymphocytes.* Ann. Rev. Immunol. **6**, p. 309–326.

Chapter 4

Modeling of the Blood Sugar System by Difference-Differential Equations

Donatas Shvitra and Eugenijus Janchys
Institute of Mathematics and Cybernetics
232600 Vilnius, U.S.S.R.

4.1 Introduction

There is a possibility to verify some hypotheses on the functioning of the physiological regulation system of the normal blood sugar level as well as pathologic, ensuing in the development of diabetes mellitus and hyperinsulinism with the help of mathematical modeling. It is most important to take into account the oscillatory nature of the considered physiological volume, appearing as a consequence of time delay in the blood sugar system, equal to the duration of production of insulin on β-cells of the pancreas. The simplest model of the blood sugar level regulation is constructed and investigated below with the help of a system of four nonlinear difference-differential equations. An extension of this model is also developed, namely, taking into account the fraction of proinsulin, of the functional connection of hormones of α-, β-, and δ-cells of the Islets of Langerhans. Furthermore, dietary regimen are taken into account. The problem of controlling the dynamics of the blood sugar level is investigated.

4.2 High-frequency and Low-frequency Oscillation of the Blood Sugar Level

Let us isolate by some trains two groups of studying the dynamics of the blood sugar level.

The works of the first group combine those whose authors defined the blood sugar level in a short time, within the scope of minutes. For example, Aleksentseva [1], studying the problem on dogs, took blood from the artery every three minutes and detected rather rhythmical oscillations in the blood sugar level with periodicities of 9 minutes. The presence of such oscillations which will be called high-frequency (hf) ones, were also confirmed by other researchers (see [2, 3]). From [2] it follows that apart from high-frequency (hf) oscillations in the blood sugar level with periodicities of $\sim 400 - 500$ seconds, there are oscillations of still higher frequencies at $\sim 30 - 40$ second intervals. It may be taken for certain [4] that the regulation, whose consequences are hf oscillations in the blood sugar level, is realized with the help of the central nervous system involved and, obviously, by neurohumoral means along the hypothalamus-hypophysis.

To the second group belong those works in which the blood sugar level was defined at different hours of day and night, and blood was taken several times during the day (and night) (see, for

example, [5, 6]). The level of immunoreactive insulin (IR) in blood plasma was measured in parallels. Analysis of the curves from [5, 6] shows the presence of diurnal oscillations in blood sugar and IRI levels with periodicities equal to 24 hours. Such oscillations will be called low frequency (lf) ones. There is no doubt that low-frequency (lf) oscillations in the blood sugar levels reflect the dynamics of the liver glycogenic function controlled by the endocrine system [4].

4.3   A Survey of Some Mathematical Models

The amount of works on mathematical modeling of the blood sugar level regulation, necessary for a better understanding of the problem on the whole, and perhaps, for the explanation of the functioning mechanism of the physiological system considered, is not great. Let us discuss some of these investigations.

The models of Bolie [7], Ackerman et al. [8], and Norwich [9], differ mainly by the amount of linear differential equations selected for modeling separate organs of the control system of the blood sugar level. Note that the above authors are interested not in the functioning of the dynamic system in normal physiological conditions, but in its behavior under the effect of extremal loading with glucose or insulin, i.e. the so-called transient process. The approach to the problem considered initiated in [7, 9] is considerably extended in [10]. Furthermore, the model in [11] describes in detail the interaction of numerous components of the physiological system under consideration. Its complexity, however, is presented to take nonlinearity in to account. The authors of paper [12] point to the nonlinear nature of the pancreas and, what is not important, they introduce and confirm the idea that the activity of the pancreas must depend on the prehistory of the given pancreas. Davis [13] interprets the problem on self-regulation of the blood sugar level at intercorrelations of the "predator-prey" type, where insulin is a predator and sugar is the prey. Paper [14] ought to be noted too, which described and realized a mathematical model of the functioning of the Islets of Langerhans as a system of α-, β-, and δ-cells by computer. Analysis of the model showed the presence of oscillatory conditions. The investigation results in [15] clinically confirmed the assumption that oscillatory conditions add to the efficiency of hormone secretion. It was shown that pulsative conditions of intravenous injection of insulin to the sick with diabetes mellitus has a greater hypoglycemic effect than continuous infusion of insulin at a constant rate.

4.4   The Simplest Mathematical Model of the Blood Sugar Level Regulation

As was already noted above, high-frequency (hf) oscillations are a consequence of neurohumoral regulation, and low-frequency (lf) oscillations in the blood sugar level are a consequence of humoral or local regulation and they are quickly and slowly transient processes. Selection of the slow range is stimulated by the following reasons. First, the mechanism of the neurohumoral blood sugar level regulation is not quite clear; second, contemporary medicine is not yet capable of "working" within the scope of minutes; third, the known disorder in the blood sugar level regulation becomes apparent as slowly transient processes within the scope of hours and days. It does not mean that the neural regulation is neglected. It is only averaged. While modeling it is displayed by that instead of hf oscillations in the blood sugar levels their average values will be taken.

Let $I(t)$ and $I_A(t)$ be the levels of joint and active insulin in plasma, correspondingly, at the same moment t, K_I and K_{IA} be their means, whereas h is the time, necessary for the production of insulin in β-cells of the pancreas. Furthermore, let $G(t)$ be the level of blood sugar and K_G be its mean. Following the general scheme of the blood level regulation, the interactions in the physiological system considered may be interpreted as in the problem "predator-predator-prey",

where $I(t)$ and $I_A(t)$ are "the predators" and $G(t)$ is "a prey". Thus, (see [16, 17]) we obtain a system of difference-differential equations.

$$\dot{I}(t) = z_I \left[\frac{G(t)}{K_G} + a\left(\frac{G(t)}{K_G} - \frac{I_A(t)}{K_{IA}} \right) - \frac{I(t-h)}{K_I} \right] I(t), \tag{4.1}$$

$$\dot{I}_A(t) = z_{IA} \left[\frac{G(t)}{K_G} + b\left(\frac{G(t)}{K_G} - \frac{I(t)}{K_I} \right) - \frac{I_A(t)}{K_I} \right] I_A(t), \tag{4.2}$$

$$\dot{G}(t) = z_G \left[1 + c\left(1 - \frac{I_A(t)}{K_{IA}} \right) - \frac{G(t)}{K_G} \right] G(t), \tag{4.3}$$

where the positive variable z_I characterizes the linear rate of insulin production, positive variables z_{IA} and z_G show the linear growth of concentrations of active insulin and the blood sugar, respectively, and with the help of parameters a, b and c, a feedback is realized. Parameter a controls the rate of insulin production, parameter b regulates the level of active insulin in the blood and parameter c regulates the blood sugar level. These parameters play the main role in the regulation of the system (1)–(3), and moreover they are positive in their biological sense.

The model (1)–(3) $I(t)$ denotes not only the fraction of connected insulin in blood plasma but all the insulin produced in β-cells. This inaccuracy does not play an important role in the analysis of functioning of the physiological system in normal and pathological cases. However it appears, as it turned out, in the analysis of the mechanism of elementary glycemia, i.e. the mechanism of the blood sugar level increase, connected with meals. Correction of model (1)–(3) by means of excretion of joint insulin $I_S(t)$ fraction in blood plasma separately is also important for practical purposes. At present there exist only the methods of determination of immunoreactive insulin (IRI) in blood plasma. An IRI fraction contains I_S and I_A. Thus, to the system of equations (1)–(3), should be added

$$\dot{I}_S(t) = z_{IS} \left[\frac{I(t)}{K_I} + d\left(\frac{I(t)}{K_I} - \frac{I_A(t)}{K_{IA}} \right) - \frac{I_S(t)}{K_{IS}} \right] I_S(t) \tag{4.4}$$

where $I_S(t)$ is the level of joint insulin in blood plasma at the instant of time t, K_{IS} is its mean, z_{IS} is the linear rate of growth in joint insulin concentration in the blood, and d is a parameter of feedback.

4.5 Investigation of the Simplest Mathematical Model

It is obvious that the solutions of the system of equations (1)–(3) also determines the dynamics of $I_S(t)$. While investigating system (1)–(4) we shall assume that [16, 17]

$$\frac{z_I}{K_I} = c_I, \quad \frac{z_{IA}}{K_{IAP}} = c_{IA}, \quad \frac{z_G}{K_G} = c_G, \quad \frac{z_{IS}}{K_{IS}} = c_{IS}, \quad z_G(1+c) = z_G^*, \tag{4.5}$$

where the variables c_I, c_{IA}, c_G, c_{IS} are positive constants and z_G^* is a Malthus coefficient of linear growth. The system of nonlinear differential equations (1)–(3) has five equilibrium states with non-negative coordinates, from which for $ac < 1$ and $ab < 1$, stable may be only the inner state of equilibrium

$$I(t) \equiv K_I, \quad I_A(t) \equiv K_{IA}, \quad G(t) \equiv K_G. \tag{4.6}$$

Let us consider further the stability of the state of equilibrium (6). In the initial system (1)–(3) let us substitute

$$I(t) = K_I[1 + x(t)], \quad I_A(t) = K_{IA}[1 + y(t)], \quad G(t) = K_G[1 + z(t)]. \tag{4.7}$$

As a result we shall obtain the system of differential equations, whose characteristic quasi-polynomial of the linear part is the function

$$P(\lambda) = [\lambda + z_I \exp(-\lambda h)][\lambda^2 + (z_{IA} + z_G)\lambda + \gamma z_{IA} z_G] - b z_I z_{IA}(a\lambda + \alpha z_G), \tag{4.8}$$

where $\alpha = a + c + ac$, $\gamma = 1 + c + bc$. The investigation of root location on a complex plane of a quasi-polynomial in a general case is a rather complicated problem (see [16]), therefore let us make some biological considerations.

A CASE OF DIABETES MELLITUS. In this case $z_G \gg z_{IA}, z_I$. (3) and the well-known Tichonov theorem yield the approximate equality

$$\frac{G(t)}{K_G} = 1 + c\left[1 - \frac{I_A(t)}{K_{IA}}\right]. \tag{4.9}$$

With respect to (9), after substitutions (7), it follows that

$$\dot{x}(t) + z_I[x(t - h) + \alpha y(t)]\,[1 + x(t)] = 0, \tag{4.10}$$

$$\dot{y}(t) + z_{IA}[bx(t) + \gamma y(t)]\,[1 + y(t)] = 0. \tag{4.11}$$

In a case of diabetes mellitus the normal regulation of the blood sugar level is disturbed, which leads to the reduction of feedback of the physiological system. Therefore, in this case we shall consider the parameters a and c to be small.

Consider the characteristic quasi-polynomial

$$P(\lambda) = [\lambda + z_I \exp(-\lambda h)]\,(\lambda + \gamma z_{IA}) - z_I z_{IA} \alpha b \tag{4.12}$$

of the linear part (10)–(11). It is easy to prove that when

$$z_I = \frac{\Pi}{2h} + \varepsilon, \ z_I \alpha = \alpha_0 \varepsilon \ (0 \le \varepsilon \ll 1) \tag{4.13}$$

quasi-polynomial (12) has simple roots $\tau(\varepsilon) \pm iG(\varepsilon)$ satisfying the conditions $G_0 = G(0) = \frac{\Pi}{2h}$, $\tau(0) = 0$,

$$\tau_0^1 = \frac{G_0 h}{1 + G_0^2 h^2}\left[1 - \frac{\alpha_0 b z_{IA} G_0}{\gamma^2 z_{IA}^2 + G_0^2}\left(1 - \frac{\gamma z_{IA}}{G_0^2 h}\right)\right], \tag{4.14}$$

$$G_0^1 = \frac{1}{1 + G_0^2 h^2}\left[1 - \frac{\alpha_0 b z_{IA} G}{\gamma^2 z_{IA}^2 + G_0^2}\left(1 + h\gamma z_{IA}\right)\right], \tag{4.15}$$

whereas its remaining roots are the left open complex halfplane. Hence and from [18] it follows

Theorem 1. Under the conditions (13) in a sufficiently small neighborhood of zero the system of differential equations (10)–(11) has a unique (accurate to time shifts) stable periodic solution, for which the presentation

$$x(t) = \xi \cos G_0 \tau + 0(\xi^2), \tag{4.16}$$

$$y(t) = \xi(A_{IS} \sin G_0 \tau + A_{IC} \cos G_0 \tau) + 0(\xi^2), \tag{4.17}$$

is valid, where

$$\tau\left[1 - \left(\frac{\tau_0' c_0}{d_0} + \frac{G_0}{G_0}\right)\varepsilon\right] = t, \ \xi = \sqrt{-\frac{\tau_0' \varepsilon}{d_0}}, \tag{4.18}$$

$$A_{IS} = -\frac{b z_{IA} G_0}{\gamma^2 z_{IA}^2 + G_0^2}, \ A_{IC} = -\frac{b\gamma z_{IA}^2}{\gamma^2 z_{IA}^2 + G_0^2}, \tag{4.19}$$

and c_0 and d_0 are defined by the formulas

$$c_0 = \frac{\Pi + G}{10(\Pi^2 + 4)}, \ d_0 = -\frac{G_0(3\Pi - 2)}{10(\Pi^2 + 4)}, \tag{4.20}$$

Thus, in a case of diabetes mellitus, the system of differential equations (1)–(4) has the stable periodic solution, which may be defined by the approximate formulas (7)–(9), and (13)–(20) and

$$I_S(t) = K_{IS}[1 + \xi(B_{IS} \sin G_0 \tau + B_{IS} \cos\left[G_0 \tau) + 0(\xi^2)\right], \tag{4.21}$$

where

$$B_{IS} = \frac{z_{IS}}{z_{IS}^2 + G_0}\left[G_0(1 + d - dA_{IC}) - z_{IS}dA_{IC}\right], \tag{4.22}$$

$$B_{IC} = \frac{z_{IS}}{z_{IS}^2 + G_0^2}\left[z_{IS}(1 + d - dA_{IC}) + G_0 dA_{IS}\right]. \tag{4.23}$$

The approximate formulas obtained together with equalities (5) will help us, with respect to the experimental data from [4, 19] to select the values of parameters of model (1)–(4). In a case of diabetes mellitus: $h = 4$ (hours), $z_I = 0.38$, $z_{IA} = 0.6$, $z_G = 21.6$, $z_{IS} = 0.35$, $a = 0.3$, $b = 1.18$, $c = 0.34$, $d = 0.05$, $K_I = 17.5$, $K_{IA} = 2.8$, $K_G = 168$, $K_{IS} = 17.5$. Hence, we obtain in addition that

$$c_I = 0.0217, \quad c_{IA} = 0.2143, \quad c_G = 0.129, \quad c_{IS} = 0.02, \quad z_G^* = 30. \tag{4.24}$$

The numerical solution $I_S(t) + I_A(t)$, $G(t)$ of system (1–4) in the above selected values of parameters is presented in Figure 1.

NORMAL CASE. In this case the parameter z_G is considerably smaller but the equality $z_G(1 + c) = z_G^*$ remains. The parameter c is considerably larger, whereas parameters a and b are significantly smaller and close to zero. Following the experimental data from [4, 19] and taking into consideration (24–25), say in a case of normal regulation: $h = 5$ (hours), $z_I = 0.325$, $z_{IA} = 1.5$, $z_G = 12$, $z_{IS} = 0.3$, $a = 0.1$, $b = 0.3$, $d = 0.4$, $K_I = 15$, $K_G = 93$, $K_{IS} = 15$. In Figure 2 the numerical solution $I_S(t) + I_A(t)$, $G(t)$ of model (1–4) is presented.

HYPERINSULINISM CASE. The equality $z_G(1 + c) = z_G^*$ is preserved, but the parameter z_G is even smaller. The regulation with the help of parameters a and b remains, i.e. a and b, in fact, are the same, though the parameter c is considerably larger. At a relatively normal regulation the sensitivity of organism to insulin considerably increases [19]. Following the experimental data from [4, 19] and taking into consideration (24) and (25), let us assume: $h = 5$ (hours), $z_I = 0.325$, $z_{IA} = 0.8$, $z_G = 5.88$, $z_{IS} = 0.55$, $a = 0.1$, $b = 0.22$, $c = 4.1$, $d = 0.15$, $K_I = 15$, $K_{IA} = 3.73$, $K_G = 4.6$, $K_{IS} = 27.5$. In Figure 3 the numerical solution $I_S(t) + I_A(t)$, $G(t)$ of model (1)–(4) is presented for a case of hyperinsulinism.

4.6 The Functional Relation of Hormones of the Islets of Langerhans

At present, there are a lot of proofs that endocrinic cells of the Islets of Langerhans function as a unit, regulating the utilization of nutritive matters by issues and their accumulation and preservation. Three types of endocrinic cells are part of the Islets of Langerhans, responsible for the deposition and preservation processes and mobilization of energy in organism: α-cells secrete glucagon, β-cells - insulin, and δ-cells - somatostatin [4]. A considerable increase of the glucagon level in blood plasma is observed among the people with hypoglycemia caused by insulin. On the contrary the level of glucagon decreases and the contents of insulin increases as a result of taking carbohydrate foods. An inverse dependence in respect to the contents of glucagon and the blood sugar level is also established in the tests with perfusion of the pancreas [4]. Thus, there exists a mechanism of insulin and glucagon interaction in an antiphase, when an increase of the level of one hormone corresponds to a decrease of the level of another. Note, that glucagon stimulates the production of insulin, while insulin suppresses the production of glucagon [4].

Somatostatin secreted in δ-cells is a peculiar regulator of the activity of α-cells and β-cells, i.e. it decreases glucagon and insulin secretion [4]. In its turn the somatostatin secretion is stimulated by an increase of the glucagon level in the blood [4]. Glucose also has a stimulating influence on somatostatin secretion [4].

Based on the above experimental data with respect to the functioning of the Islets of Langerhans endocrinic cells as a unit and on the simplest mathematical model of the system of blood

sugar (1)–(4), let us compose a mathematical model of the blood sugar system with regard to a functional relation of α-, β- and δ-cells hormones.

Let $\alpha(t)$ and $\delta(t)$ be the levels of glucagon and somatostatin in blood plasms, respectively, at the time t, K_α and K_δ be their mean levels. Furthermore, let z_α and z_δ reflect the linear growth of glucagon and somatostatin levels in the blood, respectively. Then in order to describe the functioning of the blood sugar system we may apply (see [17]) the system of difference-differential equations (2)–(4) and

$$\dot{I} = z_I \left[\frac{G}{K_G} + a\left(\frac{G}{K_G} - \frac{I_A}{K_{IA}} \right) + a_{\alpha\delta}\left(\frac{\alpha}{K_\alpha} - \frac{\delta}{K_\delta} \right) - \frac{I(t-h)}{K_I} \right] I, \qquad (4.25)$$

$$\dot{\alpha} = z_\alpha \left[1 + q_I\left(1 - \frac{I}{K_I} \right) + q_\delta\left(1 - \frac{\delta}{K_\delta} \right) - \frac{\alpha}{K_\alpha} \right] \alpha, \qquad (4.26)$$

$$\dot{\delta} = z_\delta \left[\Delta \frac{G}{K_G} + (1 - \Delta)\frac{\alpha}{K_\alpha} - \frac{\delta}{K_\delta} \right] \delta. \qquad (4.27)$$

In system (2)–(4), and in (25)–(27), additional feedbacks are realized by means of parameters $a_{\alpha\delta}$, q_I, q_δ and Δ. While investigating it, we shall assume equalities (5) and

$$\frac{z_\alpha}{K_\alpha} = c_\alpha, \quad \frac{z_\delta}{K_\delta} = c_\delta, \quad z_\alpha(1 + q_I + q_\delta) = z_\alpha^*, \qquad (4.28)$$

satisfied, where c_α, c_δ are positive constants and z_α^* is a Malthus coefficient of linear growth. The investigation has been made numerically in the neighborhood of the equilibrium state

$$I(t) \equiv K_I, \quad I_A(t) \equiv K_{IA}, \quad I_S(t) \equiv K_{IS}, \quad G(t) \equiv K_G, \quad \alpha(t) \equiv K_\alpha, \quad \delta(t) \equiv K_\delta.$$

The functional relation of hormones of the Islets of Langerhans in mathematical model allows us, the same as in [10], to make a conclusion that in a case of diabetes mellitus a tendency to hyperproduction of glucagon is observed.

4.7 The Insulin "Age Structure"

From the general scheme of the blood sugar level regulation, described in [16], it follows that there exists a certain "age structure" of insulin, where "younger" proinsulin by its activity yields considerably to "older" insulin. It is possible to calculate insulin "age structure" in mathematical model (1)–(4) by replacing differential equation (1) with the following:

$$\dot{I}(t) = z_I \left[\frac{G(t)}{K_G} + a\left(\frac{G(t)}{K_G} - \frac{I_A(t)}{K_{IA}} \right) - \frac{pI(t - h_p) + (1 - p)I(t - h)}{K_I} \right] I(t). \qquad (4.29)$$

In (29) h_p is the time necessary for proinsulin biosynthesis and the parameter $p \geq 0$ reflects a contribution of proinsulin fractions into a total amount of insulin produced in β-cells.

4.8 The Dietary Regime

It is known that glucose usually gets into organisms together with food. The mechanism of the blood sugar level increase connected with meals, i.e. the mechanism of elementary hyperglycemia, is not explained up to now. Furthermore, it is known that dietary regimen may synchronize the dynamics of the blood sugar level [17], thus concealing an individual biorhythm of the blood sugar level. An elementary hyperglycemia is a clearly sufficient expressed processes, appearing as an effect on the blood sugar system of some periodic external force. Therefore, taking into account the dietary regime in the blood sugar system is simply indispensable.

Let the function $g(t) \equiv g(t + 24)$ reflect in some way the dietary regime and γ_i ($i = 1, 2, 4$) be some parameters. Assume that in order to take into account the dietary regime in the

mathematical model (29), and (2)–(4), it is necessary to modify equations (2)–(4) in the following way:

$$\dot{I}_A = z_{IA}\left[\frac{G}{K_G} + \gamma_1\, g(t) + b\left(\frac{G}{K_G} - \frac{I}{K_I}\right) - \frac{I_A}{K_{IA}}\right] I_A, \tag{4.30}$$

$$\dot{G} = z_G\left[1 + \gamma_2\, g(t) + c\left(1 - \frac{I_A}{K_{IA}}\right) - \frac{G}{K_G}\right] G, \tag{4.31}$$

$$\dot{I}_S = z_{IS}\left[\frac{I}{K_I} + \gamma_4\, g(t) + d\left(\frac{I}{K_I} - \frac{I_A}{K_{IA}}\right) - \frac{I_S}{K_{IS}}\right] I_S. \tag{4.32}$$

Figure 4 illustrates the graph of the selected, by us, "meals" function $g(t)$.

The investigation of model (29)–(32) was carried out numerically which $h = 5$, $h_p = 3$, $z_I = 0.237$, $z_{IA} = 1.5$, $z_G = 11.58$, $z_{IS} = 0.3$, $a = 0.1$, $b = 0.67$, $c = 1.5$, $d = 0.4$, $K_I = 15$, $K_{IA} = 5$, $K_G = 88$, $t_1^1 = 8$, $t_1^2 = 12$, $t_1^3 = 18$, $K_{IS} = 5$, $h^1 = 0.6$, $h^2 = 0.64$, $h^3 = 0.82$, $\gamma_1 = 0.35$, $\gamma_2 = 1$, $\gamma_4 = 5$, $t_{11}^i = t_1^i + 1$, $t_{12}^i = t_1^I + 1.5$, $t_{13}^i = t_1^i + 5$, the solution $G(t)$ of model (29)–(32) corresponds to the experimental data from [22] rather well.

4.9 Control of the Blood Sugar Level

A necessity to develop the control methods of the blood sugar level in patients with diabetes mellitus is indisputable. Let $i(t)$ be a function, reflecting in some sense the effect injected insulin on the dynamics of the blood sugar level. It is proposed to introduce the control into the model in the following way:

$$\dot{G} = z_G\left[1 + g(t) - i(t) + c\left(1 - \frac{I_A}{K_{IA}}\right) - \frac{G}{K_G}\right] G. \tag{4.33}$$

The numerical investigation of model (29), 30)–(32) has been made. The investigation of model (29), (30), (32), (33) was carried out numerically in which $z_I = 0.495$, $b = 1.82$, $d = 0.05$, $K_I = 25$, $K_{IA} = 2$, $K_G = 400$, $K_{IS} = 5.8$, $\gamma_1 = 0.4$, $\gamma_2 = 1$, $\gamma_3 = 1$, $h^i = 0.3$ $(i = \overline{1,4})$, $t_1^1 = 8$, $t_1^2 = 14$, $t_1^3 = 20$, $t_1^4 = 2$, $\gamma_4 = 1$, $t_{11}^i = t_1^i + 1$, $t_{12}^i = t_1^i = 1.5$, $t_{13}^i - t_1^i + 6$ $(i = \overline{1,4}$, the solution $G(t)$ in Figure 6 model (29), (30), (32) corresponds to the experiment points of the 3rd patient from [23], who at 8 o'clock in the morning received 44 units of NPH insulin. Figure 7 illustrates the graph of the function $i(t)$ selected by us.

4.10 References

[1] Aleksentseva, E.S. (1939) *Sugar and lactic acid oscillations in the arterial blood.* Physicl. Journ. **27** (1), p. 132–138 (in Russian).

[2] Iberal, A. et al. (1968) *High frequency blood glucose oscillations in man.* Metabolism **12** 17, p. 119–1121.

[3] Anderson, G. et al. (1956) *Postabsorptive undulations and oscillations in blood glucose.* Amer. J. Clin. Nutr. **4**, p. 673.

[4] Baranov, V.G. (Ed.) (1979) *Physiology of Endocrinic Systems.* Leningrad: Nauka, p. 680 (in Russian).

[5] Malherbe, C. et al. (1969) *Circadian variations of blood sugar and plasma insulin levels in man.* Diabetologia **6** (5), p. 397–404.

[6] Nicolau, G.Y. et al. (1984) *Circadian variations in plasma immunoreactive insulin (IRI) and C-peptide concentrations in adult onset (type II) Diabetes Mellitus.* Rev. Roum. Med. (Rndocrinol) 1 (22), p. 3–16.

[7] Bolie, V.W. (1961) *Coefficients of normal blood glucose regulation.* J. Appl. Physiol. p. 783–788.

[8] Ackerman, E. et al. (1965) *Model studies of blood-glucose regulation.* Bull. Math. Biophys. **27**, p. 21–37.

[9] Norwich, K.H. (1969) *Mathematical models of the kinetics of glucose and insulin in plasma.* Bull. Math. Biophys. **31**, p. 105–121.

[10] Dreval, A.V. et al. (1983) *Check analysis of some hypothesis of diabetes mellitus pathogenesis by mathematical modeling.* Biophysics **28** (5), p. 866 - 872 (in Russian).

[11] Antomonov, J.G. et al. (1971) *Mathematical theory of the blood sugar system.* Kiev: Naukova dumka. p. 84 (in Russian).

[12] Bergman, R and R. Bewcolow. (1973) *Nonlinear dynamics of pancreatic glands and liver metabolism.* Dynamic System and Control **95** (3), p. 60 - 65.

[13] Davis, M.J. (1979) *Differential model of diabetes mellitus.* Mathematical Modelling. Moscow: Mir, p. 128 - 139 (in Russian).

[14] Atakisheva, M.K. et al. (1984) *Mathematical model of Langerhans insulae functioning.* Preprint of Sci. CBI of Ac. Sci. USSR (in Russian).

[15] Mathews, D.R. et al. (1983) *Pulsative insulin has greater hypoglycemic effect than continuous delivery.* Diabetes **32**, p. 617 - 621.

[16] Shvitra, D.J. (1985) *Mathematical modelling of the blood sugar level self-regulation.* Mathematical Models in Biology and Medicine **1**, p. 109 - 129 (in Russian).

[17] Shvitra, D.J. (1987) *The role of time-delay in mathematical models of physiological systems of the organism.* Lithuanian Math. Journ. **27** (3), (in Russian).

[18] Kolesov, J.S. and D.J. Shvitra. (1979) *Oscillations in the systems with time-delay.* Vilnius: Mokslas, p. 147 (in Russian).

[19] Genes, S.G. (1972) *Insulin formation and secretion.* Pathological physiology and experimental therapy **6**, p. 77 - 82 (in Russian).

[20] Kostiuk, E.P. (1985) *Somatostatin and glucagon secretion correlation in a case of diabetes mellitus.* Physiol. Journ. **31** (2), p. 195 - 201 (in Russian).

[21] Shvitra, D.J. and E.S. Janchys. (1986) *Mathematical theory of the thyroid functioning mechanism.* Lithuanian Math. Journ. **26** (3), p. 560 - 573 (in Russian).

[22] Tasaka, Y. et al. (1975) *Levels of pancreatic glucagon, insulin and glucose during twenty-four hours of the day in normal subjects.* Horm. Metab. Res. **7** (3), p. 205 - 206.

[23] Service, F.J. (1978) *Normalization of plasma glucose of nustable diabetes: studies under ambulatory, fed conditions with pumped intravenous insulin.* The J. of Lab. Clin. Med. **91** (3), p. 480 - 489.
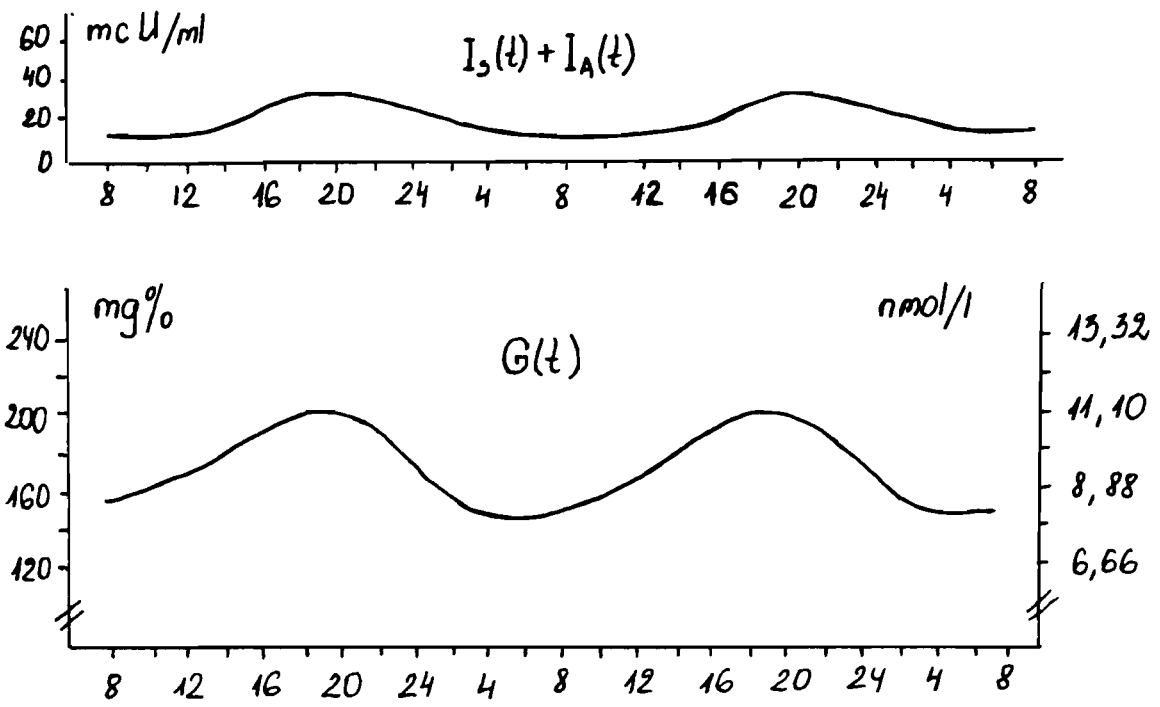
Figure 4.1. Normal Case – Time (clock hour)
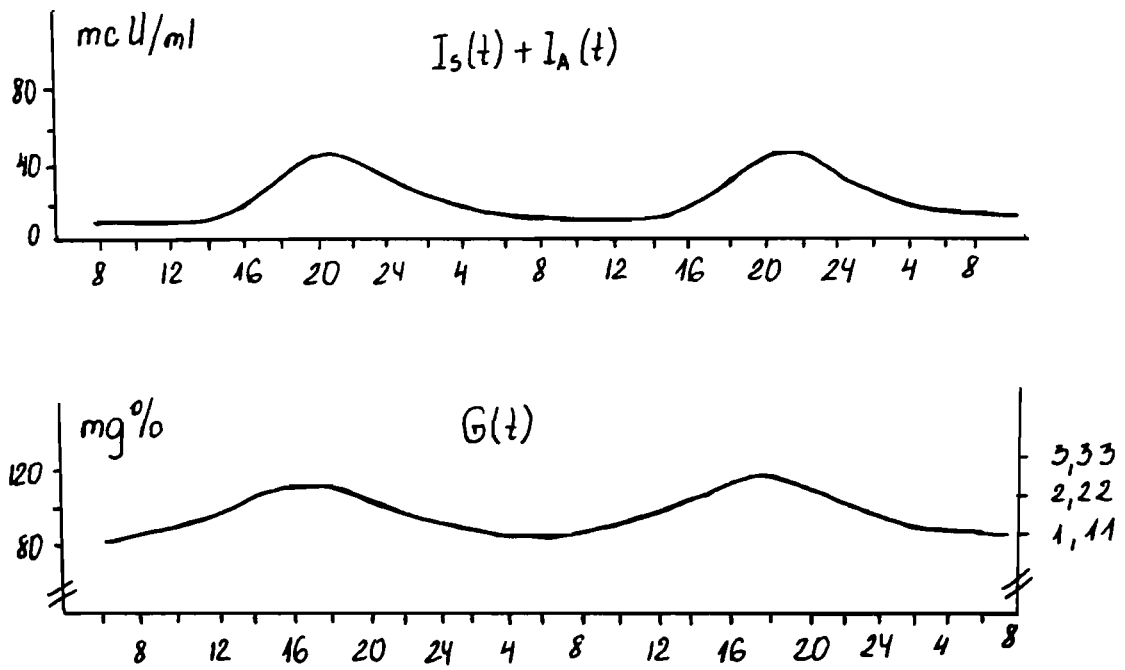
Figure 4.2. Diabetes mellitus – Time (clock hour)
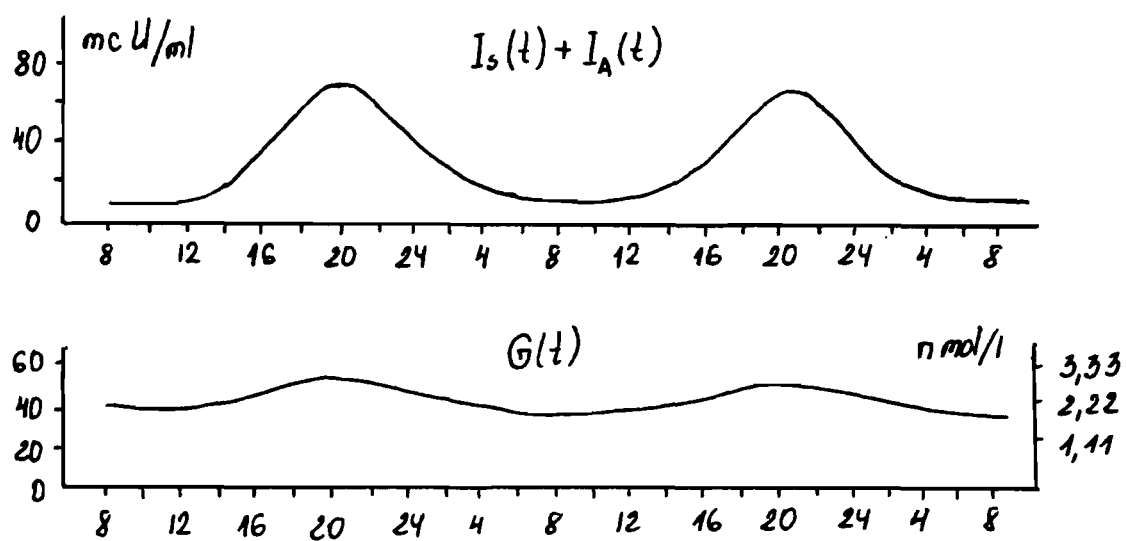
Figure 4.3. Time (clock hour)
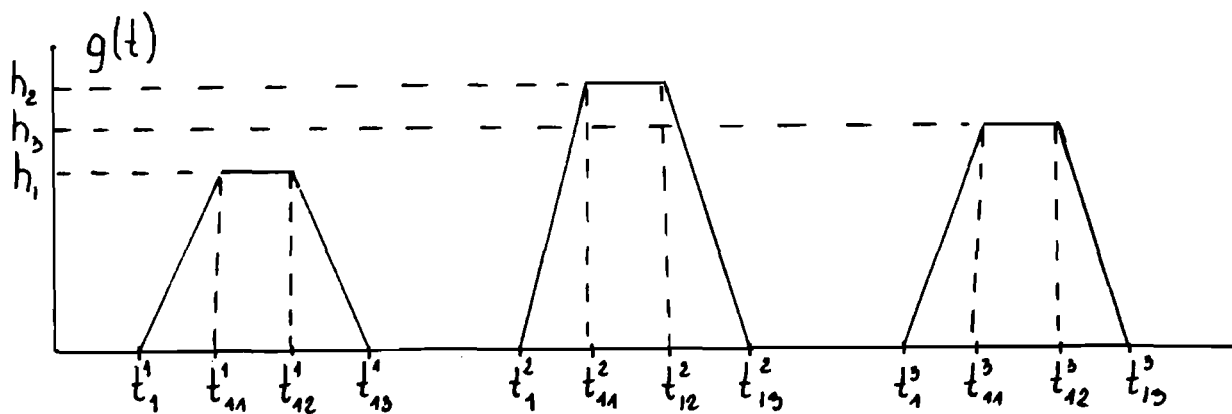
Figure 4.4. Text of caption.
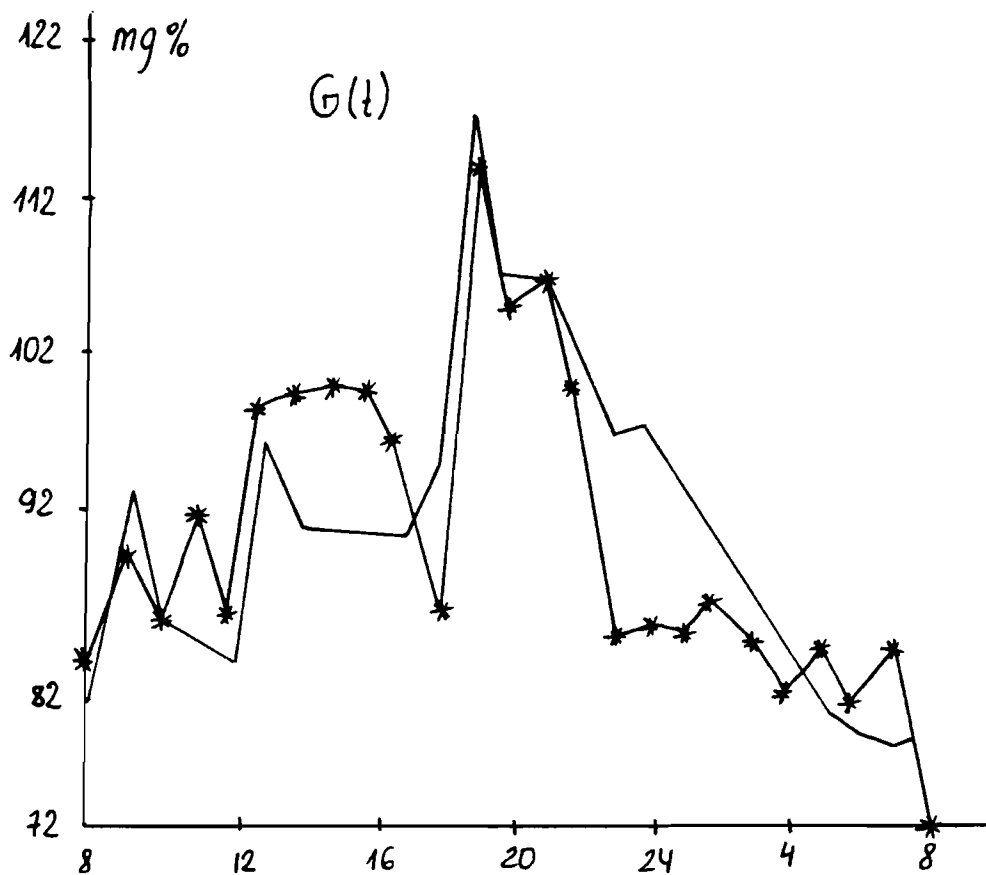
Figure 4.5. Time (clock hour)
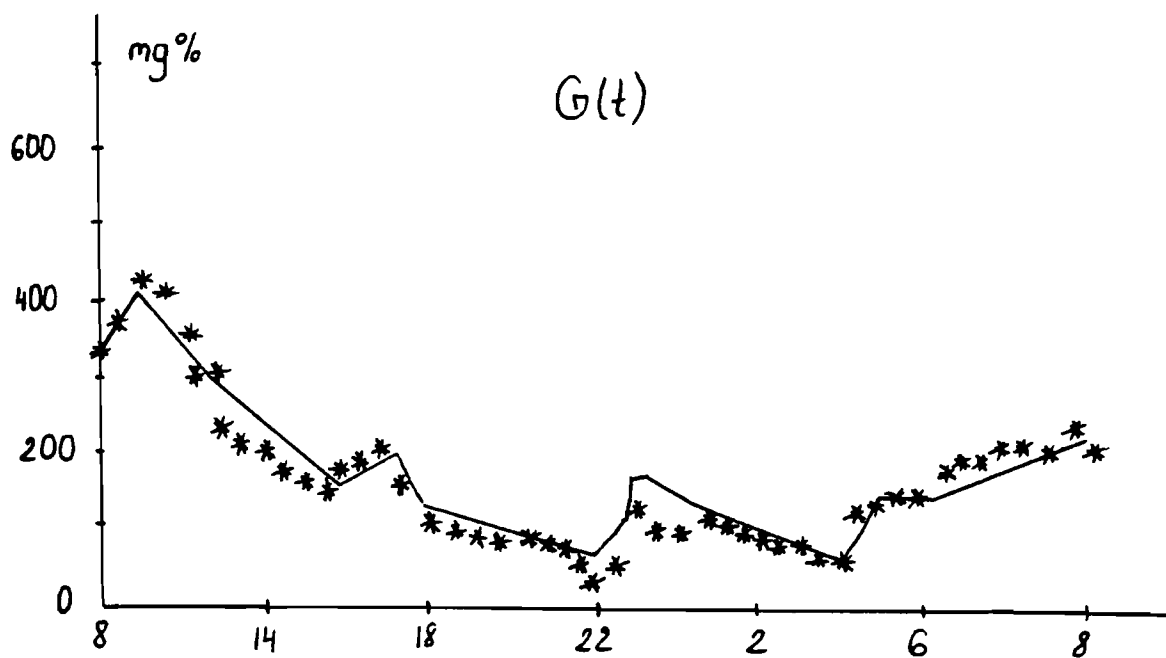
Figure 4.6. Time (clock hour)
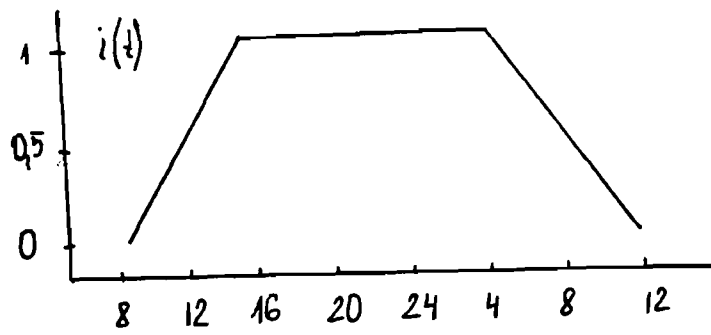
Figure 4.7. Time (clock hour)

Chapter 5

Model for Analysis of Drug Action During Experimental Influenza

R.Ya. Poljak, L.K. Chetverikova, T.Ya. Dubrovina
A.I. Dukhin, D.V. Kaljaev, T.A. Kramskaya
I.A. Ivanova, G.F. Leontieva, V.P. Lozitsky
L.F. Meringova, N.K. Shidlovskaya, B.L. Voitsechovsky
R.N. Usmanov, I.V. Yakovleva
Institute of Experimental
Medicine AMS USSR, Leningrad
The Department of the Computative
Mathematics AS USSR, Moscow
Mechnicov Institute of Virology
and Epidemiology, Odessa

Introduction

The analysis of main mechanisms of viral infection pathogenesis is important for the solution of the problems of fundamental science and practical health service. In order to interfere in the pathological process, it is necessary to have clear ideas of the strategy and tactics of drug use.

The aim of the present work uses the experimental and mathematical model of influenza [6, 11, 15] for the analysis of the drug action. The mechanisms of antiviral effects of chemical preparations in development of a prophylactic or therapeutic effects are studied.

The experimental influenza model aided to study prophylactic and therapeutic schemes of the use of the proteolysis inhibitor (ε-aminocapronic acid - ε-ACA) and the antioxydant ionol. The proteolysis inhibitors as antiviral means have been studied in detail in experiments [7, 8, 26] and widely used in clinical practices [2, 3, 7]. Natural or synthetic antioxydants have been extensively studied as antistress agents (see [18] and as correctors of interferon formation (9). Study of ionol enabled B.A. Frolov et al. [18] to reveal its new properties as a prophylactic drug in lethal forms of the influenza. One of its possible sites of action is the prophylaxis of lesion of the tissue barriers permeability. [13, 17, 19]

Materials and Methods

Experimental infection of mongrel or F1 line mice (CBA x C57 Black) was intranasal administration of 10_3 -10_4 embryonal infectious doses (EID_{50}) of influenza A/PR8/34 virus (H1N1). For control groups consisted of either intact animals or the mice who were given preparations ε-ACA according to prophylactic or therapeutic scheme and ionol according to prophylactic scheme (see details in text).

interferon or antibodies of IgG and IgM classes in the serum, the cytotoxic lysis induced with the spleen's natural killers (NK) in respect to the K-562 cells, and the complement- and antibody-dependent lysis (ADDC) in respect to the target-cells infected with the homologous virus within the "splenocyte against splenocyte" system. The modifications of used techniques of the immunoassay, or virological analysis as well as the mathematical techniques of their evaluation have been described elsewhere [4, 12, 15, 20, 21].

The general appearance of used mathematical model (11) represents an equation

$$dX/dt = \Phi(X, \alpha), X(0) = X0, t \in [0, T] \tag{5.1}$$

where $X \in \mathbf{R}^n$ - is a vector of state variables; $\alpha \in \mathbf{R}^l$ - R is a vector of coefficients.

The mathematical model describing the experimental influenza has the following (6, 11, 15):

$$V = \frac{\alpha_1 + \alpha_{10}}{1 + \alpha_{10}} V - \alpha_2 V3 - \alpha_3 V Le - \alpha_{10} V \tag{5.2}$$

$$Lp = Lpo(t - t^*) + \alpha_{11} Lp[1 - exp(-\alpha_{12} V)] \tag{5.3}$$

$$Le = \alpha_4 Lp[1 - exp(-\alpha_{12} V)] - \alpha_5 Le \tag{5.4}$$

$$F = \alpha_6 Le - \frac{\alpha_7 V F}{1 + \alpha_9 F} - \alpha_8 F \tag{5.5}$$

where $V\alpha_i$ - the number of infectious virus particles in population; t - the time after infecting in days; Lp - is a number of lymphocytes-precursors of a corresponding specificity; $Le(T)$ - is a number of specific lymphocytes-effectors; F - is the amount of specific immunoglobulins.

For the description of lymphocytes proliferation and differentiation processes the next scheme was used [15, 23-25]. The specific lympocytes were divided into precursors (Lp) and effectors (Le). We have supposed that the B-cells are the constant part of Lp and Le populations and the other part of these populations are T-cells (it is impossible to describe the relations of these parts of different groups of animals using the known methods). The nonactive precursors (Lpo) corresponds to the pools of specific cells which can be activated by the antigen and became the proliferating cell-effectors (Le). We had supposed that the numeric parameters of this process can be described by equations (3) and (4). So, in our model the variables Lp and Le are the main ones, they are including all the mechanisms of cellular defence of infected organism (NK, CTL, ADDC). The complete agrumentation of the accepted system has been given by Marchuk G.I. et al. (1988) [11].

Results and Discussions

On the model of influenza lethal infection with the A/PR8 virus (the infecting dose $10_{4.5}$ EID$_{50}$), it has been found that prophylactic subcutaneous administration of ε-ACA in the dose of 30 mg per mouse 2 days prior to infecting, or the therapeutic scheme of the ε-ACA adminstration during 5 days starting from the 1st day after infecting (the total dose 450 mg per mouse), or prophylactic administration of ionol daily intraperitoneally during 3 days prior to infecting (the total dose 1.5 mg per mouse) exerted an obvious favourable effect on the survival of the animals, having increased it by 30-50%. It has been found that, against the background of application of the preparations, the virus contents was always somewhat lower in the site of infections, although the curves were quite comparable. The curves of the interferon contents in serum differed from each other insignificantly. The contents of spleen NK and ADDC preserved their wave-form alterations. The NK activity was enhanced by the preparations, particularly during the second week. The change of the ADDC activity level was the most obvious. An increased level of IgM was also noted against the background of ionol application. The curves of the IgG contents altered insignificantly.

The description of the data obtained in result of a daily analysis of all the parameters of the process has revealed no most characteristic sign with it would be possible to associate

prophylactic or therapeutic effect. The using of the mathematical model made possible to receive the additional biological information.

A mathematical model has been developed on the basis of experimental (Fig.1).

The graphs of Fig.2 show the solution of the model's equations for prophylactic action of the ε-ACA and ionol. Table 1 shows the values of the model's coefficients (2)-(5) according to the experimental data. The details of this work were described in papers [6, 11].

The action of the preparations is most obvious at the initial stage of infection when the efficiency of tissue lesion at the initial moment and in the same dose of administered virus decreases by few orders (Fig.2, $Ln(V)$). The effectiveness of precursor's stimulation (Lp) was increased by both preparations, and the activity of effectors (Le) was increased by the action of ε-ACA. Throughout the process a lower level in virus accumulation preserves in those groups of animals who were given the preparations. However, a value of some model coefficients do not change. (Table 1).

Model's Coefficients Identification Using Experimental Data

	Values of Coefficient for infected mice		
Coefficient	Without Preparation	Ionol	ε - ACA
α_1	2.2	2.328	2.581
α_2	0.0	0.0	$4.316 \cdot 10^{-4}$
α_3	0.958	0.972	0.950
α_4	1.8	1.8	1.8
α_5	0.891	1.51	1.0
α_6	$1.530 \cdot 10^4$	$2.178 \cdot 10^4$	$1.411 \cdot 10^3$
α_7	$2.190 \cdot 10^{-2}$	$2.190 \cdot 10^{-2}$	$2.190 \cdot 10^{-2}$
α_8	0.0	1.834	0.0
α_9	$4.730 \cdot 10^{-6}$	$2.226 \cdot 10^{-5}$	0.0
α_{10}	7.0	7.0	7.0
α_{11}	0.201	0.332	0.294
α_{12}	$3.870 \cdot 10^{-3}$	$1.115 \cdot 10^{-2}$	$7.664 \cdot 10^{-2}$
t(days)	3	3	3
$V(0)$	$5.037 \cdot 10^{-2}$	-1.139	-1.139
$Lp0$	1	1	1

For example, α_1, α_3, α_4, α_7, α_{10}. On the contrary, the other coefficients undergo considerable changes.

The data obtained can be interpreted as follows: in normal infected mice and in application of ionol, the maximum of the virus accumulation and the subsequent inhibition of its proliferation are maintained, chiefly, by the action of cytotoxic mechanisms mediated by the lymphocyte effectors Le. One more mechanism is added in the group of mice defended by the ε-ACA, the mechanism being still unidentified. The results of the experiments based on usage of the model's equations (2)-(5) have shown that the main influence on the values of variable V (virus in the host organism) had the components ($\alpha 3$, V, Le) [2], corresponded to cytotoxic effect. The variable F had a lower significance. In the case of ε-ACA treatment the coefficient $\alpha_9 = 0$. The possible reason of this state is the masking of free specific antibody activity by more significant cytotoxic mechanisms ($\alpha 3$, V, Le) in the equation (2).

For the group of animals who were given the preparations $\alpha_1 2$ a few times less than for the untreated group. This seems to reflect a lowering of the threshold in the amount of virus at which point the processes of proliferation and differentiation start to proceed with the maximal intensity. The studies show these changes to be quite considerable. Desedes, in these groups,

the $\alpha_1 1$ increases by 1.5 times which suggest, probably, more intensive processes of proliferation, formation of the immunological memory in these groups which is very important, too. Just these very changes, probably, cause the antiviral effect of chemical preparations under study observed in experiment.

The data obtained corroborates the possibility of the approach used to investigate the effect and points of action of the chemical preparations (as well as other factors) upon the process of acute infection in the host organism. Besides, the use of the mathematical model enables one to obtain quantitative characteristics of internal processes by the data in vivo. A larger experimental material will provide the possibility to determine statistically significantly the changes in mechanisms under study induced by the chemical preparations, to single out the most important components of defence, i.e. to construct and check up the "scenarios" of development of infectious disease in the organism during prophylaxis and treatment.

Conclusions

The protective effects of proteolysis inhibitor ε-ACA and antioxydant ionol upon lethal and non-lethal forms of influenza infection have been studied in mice.

Use of experimental and mathematical models has revealed that the anti-influenza action of the preparations is actualized through several mechanisms. Three of them have been identified by means of the analysis of the model's coefficients:

- a lower efficacy of infecting of the target-organ's cells (with the same infecting dose);
- the threshold of effective antigenic stimulation of the immune response as measured by the amount of the necessary virus, is lowered;
- a higher intensity of proliferation of the immune system's cells-precursors.

This way can be effective addition to the traditional experimental or clinical analysis of infection process's characteristics.

Bibliography

[1] Dubrovina, T. Ya. In: "Strategy of parasite in host organism" Eds. A.A. Totolyan and R. Ya. Poljak, Leningrad, 1987, pp. 87-96.

[2] Bujko, V.P., Lozitsky, V.P., Pediatria, 1984, No. 9, pp. 23-26

[3] Bucrinskaya, A.G., Ketiladze, E.S. et al. Vopr.virusol., 1986, No.4, pp.400-404

[4] Voitsechovsky, B.L. In: "Solidphase Enzymeimmunoassay", Leningrad, 1988, pp.44-58

[5] Zuev, S.M. "Statistic analysis of parameters of disease's mathematical

[6] Kaljaev, D.V. In: "Strategy of parasite in host organism" Eds.: A. A. Totoljan and R. Ya. Poljak, Leningrad, 1987, pp. 26-40

[7] Lozitsky, V.P., Bujko, V.P. et al. Vopr.virusol., 1988, No. 3, pp. 75-81

[8] Lozitsky, V.P., Poljak, R. Ya., Uspehi sovr. biol. 1982, Vol. 93, No. 3, pp. 352-362

[9] Malinovskaya, V.V., Apanenko, A.A. et al. Vopr.virusol., 1983, No. 6, pp. 681-684

[10] Marchuk, G.I., Petrov, R.V., Vischisl. Processy i sistemy, 1985, Moscow, Nauka, No. 3, pp. 5-11

[11] Marchuk, G.I., Poljak, R. Ya. et al. Jurnal VHO im Mendeleeva, 1988, Vol. 33, No. 5, pp. 537-551

[12] Meringova, L.F. In: "Solidphase enzymeimmunoassay", Leningrad, 1988, pp. 114-119

[13] Micheneva, M.S., Chetverikova, L. K. et al. Molec. genetica, microbiol., virusol., 1988, No. 2, pp.45-48

[14] Pogozgev, I.B. In: "Mathematical modelling in immunology and medicine", Moscow, 1986, pp. 35-58

[15] Poljak, R. Ya., Belych, L.N. et al. In: "Strategy of parasite in host organism", Eds.: A. A. Totolyan, R. Ya. Poljak, Leningrad, 1987, pp. 10-26

[16] Poljak, R. Ya., Dubrovina, T. Ya. et al. In: "Itogy nauki i techniki, Ser. Immunologia", Moscow, 1986, Vol. 17, pp. 147-177

[17] Poljak, R. Ya., Dubrovina, T. Ya. et al. In: "Immunobiological preparations of new generation and methods of its control", Moscow, 1988, pp. 3-11.

[18] Frolov, B.A., Chetvericova, L.K. et al. In: "Antiviral drugs during experimental therapy of viral diseases", Minsk, 1986, pp. 68-72

[19] Chetvericova, L.K., Kildivatov, I. Yu. et al. Vestnik, AMN SSSR, 1989, No. 11, pp. 55-61

[20] Shidlovskaya, N.K., JMEI, 1989, No. 7, pp. 32-35

[21] Shidlovskaya, N.K., Leontieva, G.F., Vopr. virusol., 1987, No. 2, pp. 241-244

[22] Shidlovskaya, N.K., Masina, I.V. et al. JMEI, 1989, No. 8, pp. 79-84

[23] Ada, G.L., Jones, P.D. Curr. Top Microbiol. and Immunol. 1986, Vol. 88, pp. 1-54

[24] Jones, P.D., Ada, G.L., Cell Immunol. 1987, No. 109, pp. 53-64

[25] Fundamental. Immunol. Ed. W. E. Paul, New York, Raven Press, 1984.

[26] Tahiro, M., Klenk, H., Rott, R. J.gen. Virology, 1987, Vol. 67, pp. 2039-2041

Figure 1
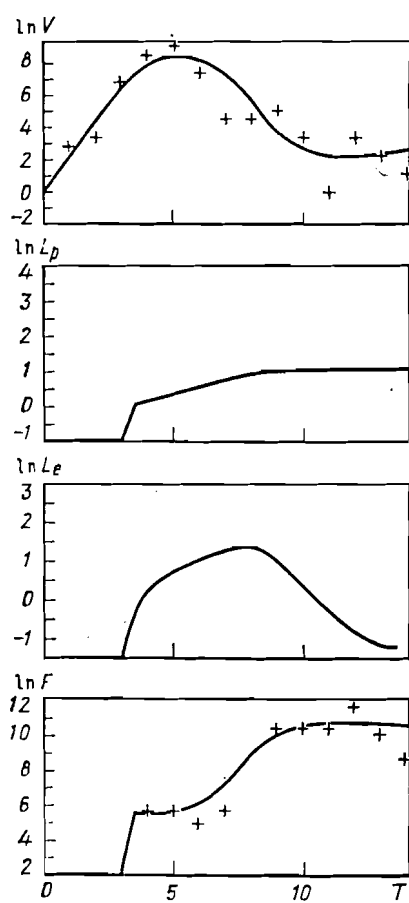
Figure 1

Figure 2
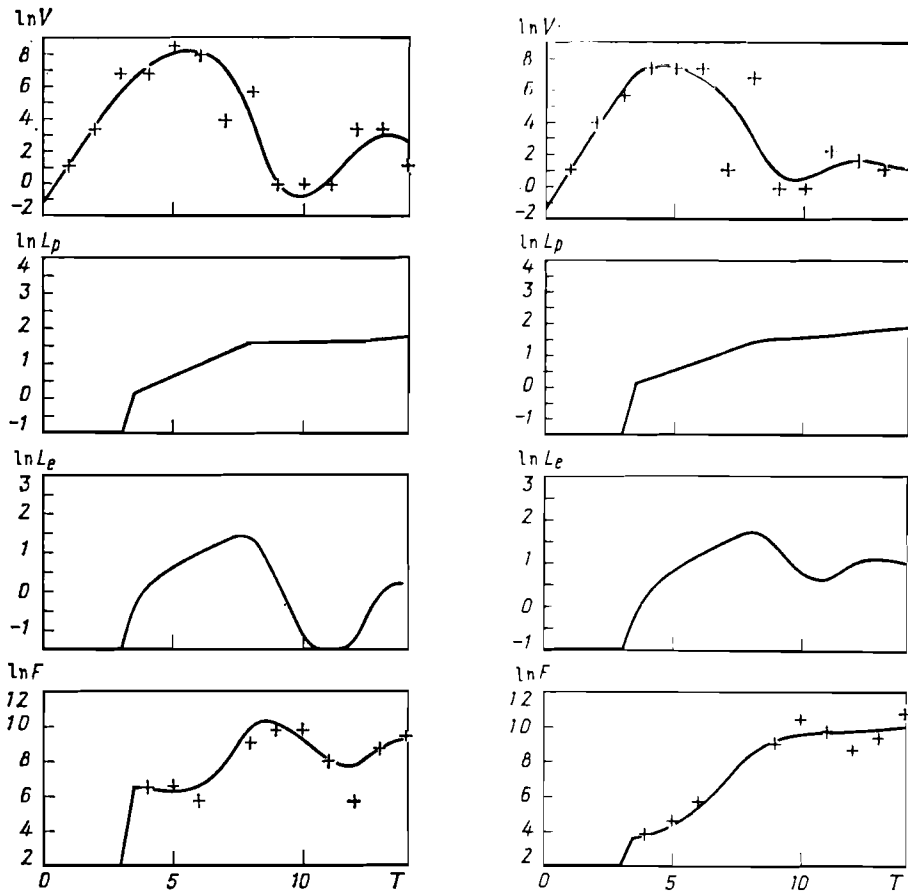
Figure 2
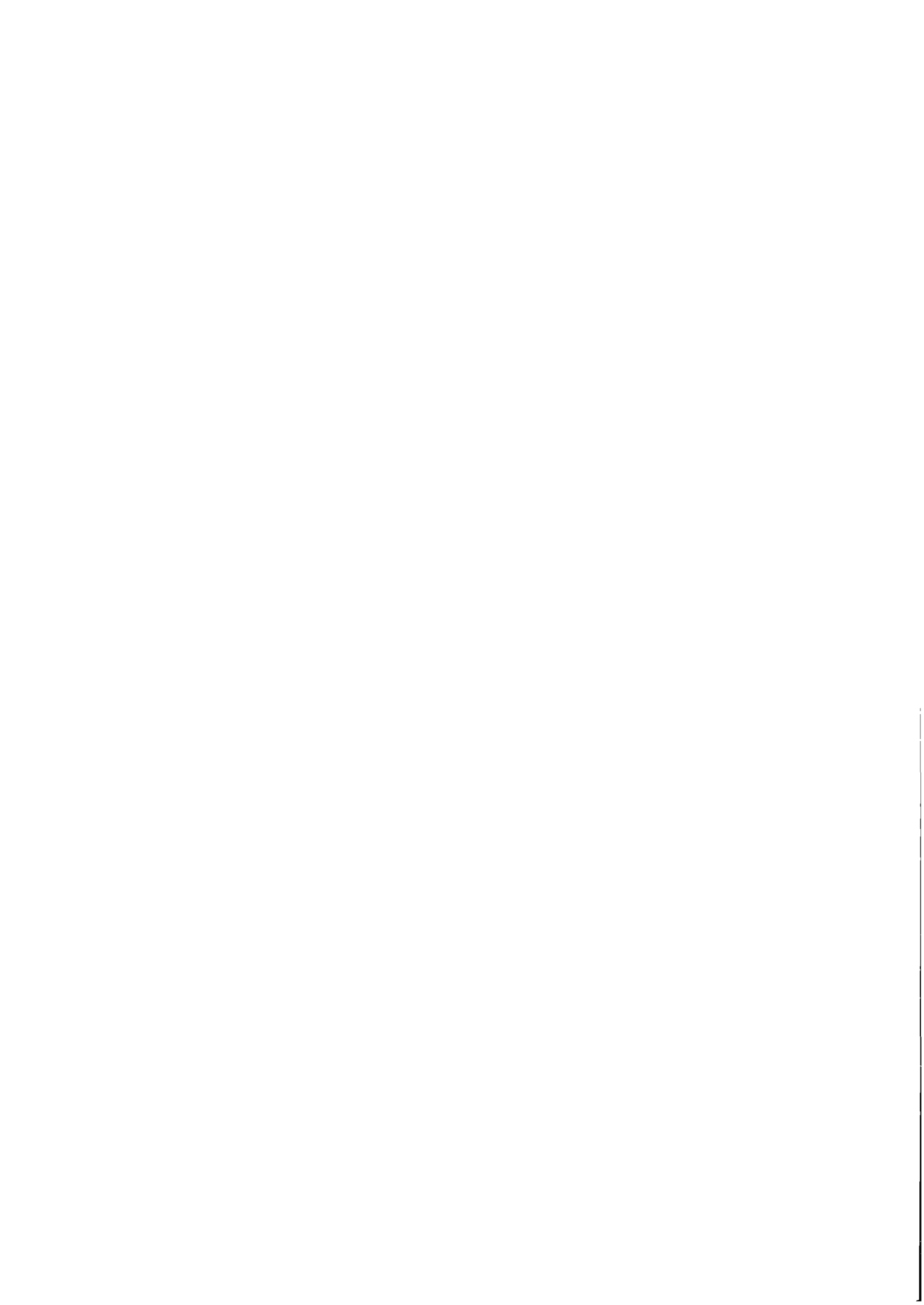
Part II

Models in Cancer Research

Chapter 6

Computer Simulation in Cancer Research With Applications in Radiooncology

W. Düchting, R. Lehrig, G. Radermacher
Department of Electrical Engineering
University of Siegen, Holderlinstr. 3, D-5900 Siegen, F.R.G.

W. Ulmer
Department of Radiology
St. Marienkrankenhaus, D-5900 Siegen, F.R.G.

Introduction

Cancer is the end of a multistage, multifactorial process. Characteristic features of malignancy are (i) uncontrolled proliferation, (ii) invasion in adjacent normal tissue, (iii) formation of metastases, (iv) the ability to evade immune survellance. In spite of enormous investments of time and money the central question how genes and the growth of normal and malignant cells are regulated still remains open. The cancer problem may be studied from different points of view (1). In our group we started in 1968 applying methods of systems analysis, control theory, automata theory and computer science to this problem (2). The key idea was to interpret tumor growth as an unstable closed-loop control circuit. Thus, step by step the dynamic behaviour of cell-growth control loops has been investigated. Furthermore, we extended this approach by modelling the spatial behaviour of tumor growth (3).

In the present paper we outline some strategies (i) to substitute in vitro experiments of spheroidal tumor growth by computer models, and (ii) to apply clinical irradiation schemes on in-vitro tumor spheroids for testing the result of standard and non-standard fractionations.

Modelling and simulation of in-vitro tumor growth

The multiplication of an individual tumor cell innoculated into a three-dimensional nutrient medium is described in (4). It is important to note that spheroidal growth stops at a dimeter of 3...4 mm, that means there is a maximum volume of the spheroid beyond which no further expansion occurs. Figure 1 illustrates the real growth of a MGH-U 1 tumor spheroid from (5). One can clearly recognize the existing steady state between the outside margin of the proliferating tumor cells and the inner necrotic center.

The construction of a model describing in-vitro tumor growth requires:

- a cytokinetic model (6) describing the division of a tumor cell (Figure 2)

- experimentally gained data of the cell-cycle phase durations (Table 1)
- cell production and interaction rules describing the cell-to-cell communication. For instance some rules of the catalogue may say:

  (1) The multiplication of a tumor cell is possible only if the distance between a dividing tumor cell and the nutrient medium is less than three cell layers. All tumor cells residing in a distance of more than three cell layers enter the resting phase GO because of the lack of oxygen and nutrient supply.

  (2) If there is no free position around the dividing tumor cell, it divides into the direction which has the shortest distance between the tumor cell and the nutrient medium. If there are equal minimum distances in various directions, a pseudo-random number generator determines the direction in which the tumor cell will divide.

- Computergraphics software packages for representation of 2-D and 3-D simulation results.

After transforming these statements, rules and equation into algorithms computer program were written in FORTRAN IV. The input data to the simulation model are the cell-cycle phase durations (see Table 1) of a specific tumor cell. In comparison to Figure 1 the simulation result of a spheroidal tumor growth is demonstrated in Figure 3. A good agreement between the simulation (Figure 3) and the results obtained from experiments (Figure 1) has been achieved. The number of tumor cells as a function of time is represented in Figure 4. The study of the simulated tumor spheroid at T = 300 units of time will be chosen to be the starting point for computer experiments performed to clarify the influence of standard and non-standard irradiation.

Modelling and simulation of different irradiation schedules

In addition to our simulation model of tumor growth developed so far, the simulation of irradiation treatment schedules (7, 8, 9, 10) requires numerous supplement algorithms and programs.

(1) To construct a model describing radiation treatment it is necessary to know the number of tumor cells hit by radiation. In this case we have made use of the survival function $S(D)$ via the "Linear Quadratic Model" (11)

$$S(D) = (exp - \alpha D) \times (exp - \beta D^2).$$

D stands for doses and α and β are parameters depending on the kind of radiation and the kind of cells. Thus, it is possible to calculate the number of the hit proliferating and hypoxic tumor cells as a function of the dose (see Table 2).

(2) A cell is able to repair cell injuries within a limited scope. In this paper the assumption is made that 30will be repaired in a mean time of 15 hours.

(3) Furthermore, it is assumed that a lethally hit tumor cell which is not repairable needs about 5 days for lysis. Then the cell space is free again for being filled with proliferating tumor cells.

(4) After lysis of the lethally hit tumor cells in the outmost margin of the spheroid there is a better nutrient supply of the hypoxic cells which can now be recruited into the cell cycle.

The input data of the computer (VAX 730 machine) are: cell-cycle phase durations, irradiation parameters and treatment schedules. The time needed to simulate a clinical irradiation scheme of 40 days takes about 40 hours.

While Figure 5 shows a 2-D cross-sectional image through an irradiated tumor spheroid in the Figures 6 and 7 clinical treatment schedules were applied to in-vitro tumor spheroids under different assumptions to answer the question: "Standard or non-standard irradiation?"

It is surprising that in both cases (Figure 6 and Figure 7) with nearly the same overall dose after 5 weeks the number of tumor cells has decreased to about the same level. Thus, it is

tempting to speculate that the choice of a multifractionated irradiation or of an irradiation with a high single dose will depend on the radiation response of normal cells including side-effects.

From this we may conclude that much simulation work remains to be done (variation of the cell cycle time, changing of the dose rates and of the breaks between treatment sessions etc.) for finding the optimal treatment schemes.
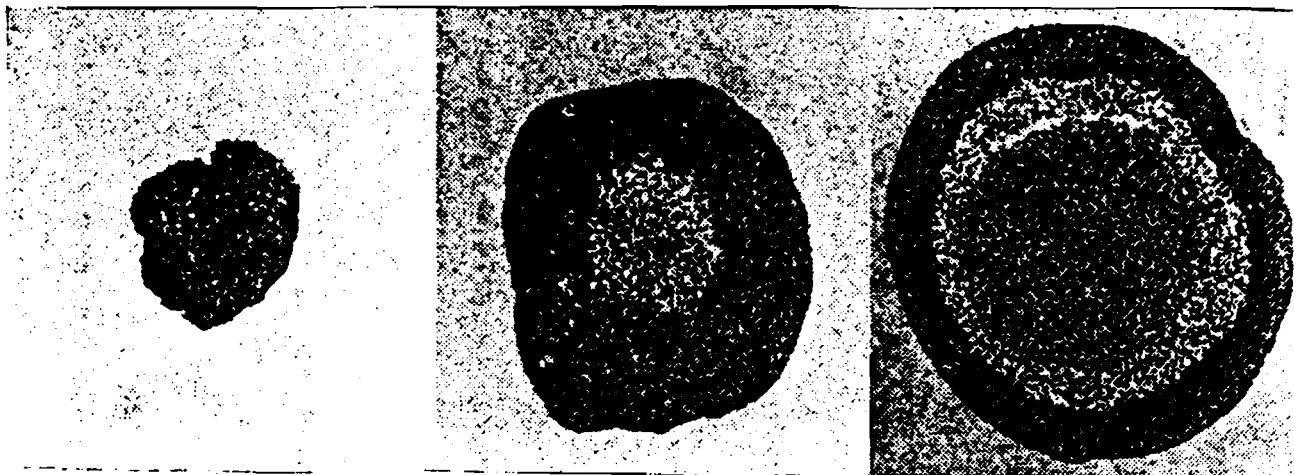
Figure 1. Real growth of a MGH-U1 tumor spheroid from (5).
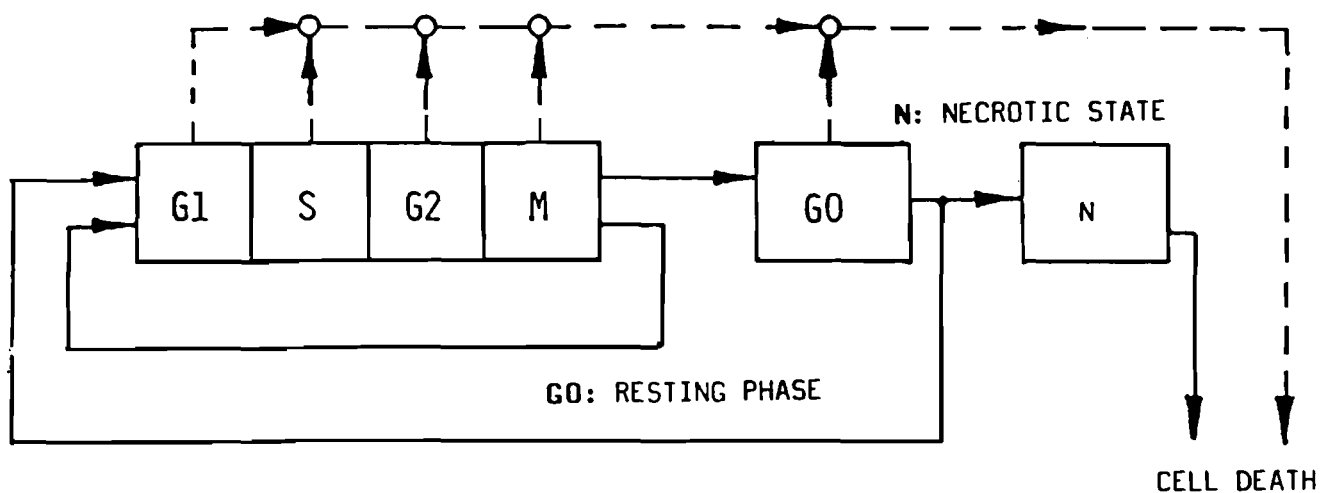
Figure 2. Simplified cytokinetic model of a tumor cell (6).

Nomenclature of phase duration	T_{G1}	T_S	T_{G2}	T_M	T_{G0}	T_N
Phase duration in hours	6	5	2	2	25	60
Deviation σ in hours	1	1	1	0	5	3

Table 1. Cell cycle phase durations of the adenocarcinoma of the mouse (cell cycle time $T_C = T_{G1} + T_S + T_{G2} + T_M = 15$ h).
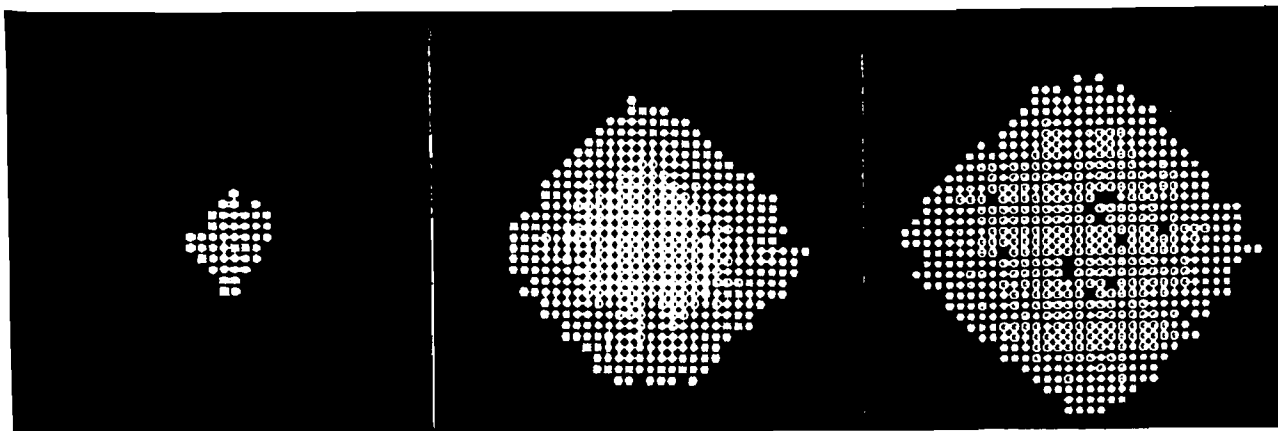
Figure 3. Simulation of spatial
tumor growth in vitro (6).

SYMBOLS:

Ⓞ   N-PHASE

◈   GO-PHASE

✳   M -PHASE

✿   G1-, S- AND G2-PHASE

NUMBER OF TUMOR CELLS

10000

OVERALL

8000

6000

P-SHARE

4000

2000

GO-SHARE

0

0   48   96   144   192   240   288   336

TIME/h
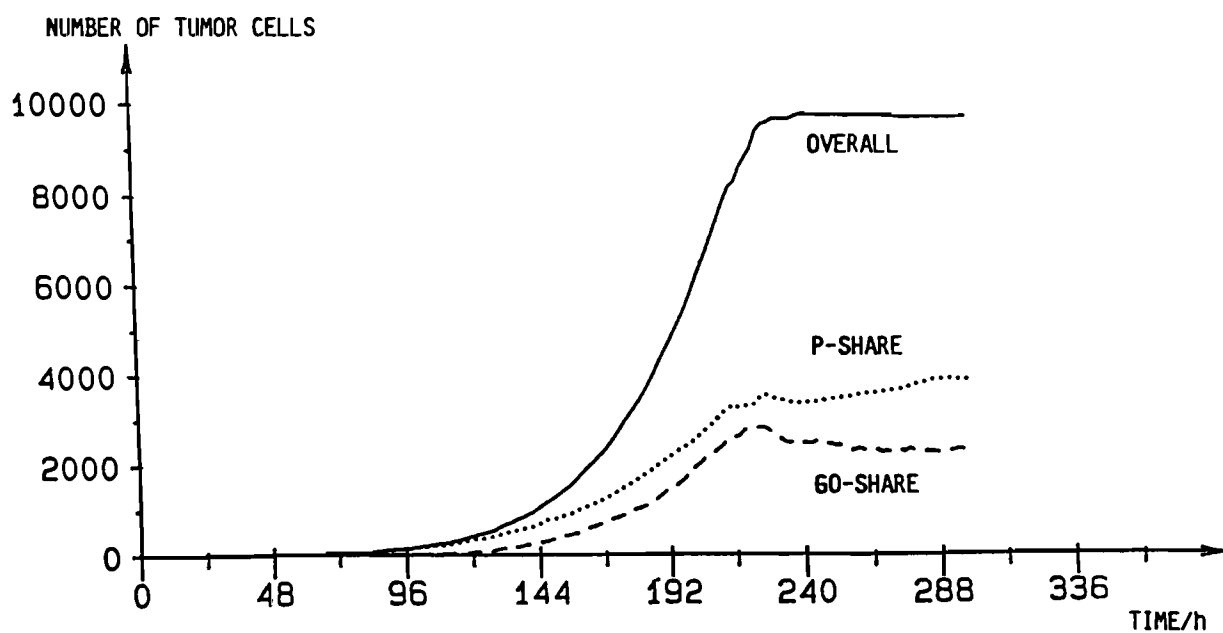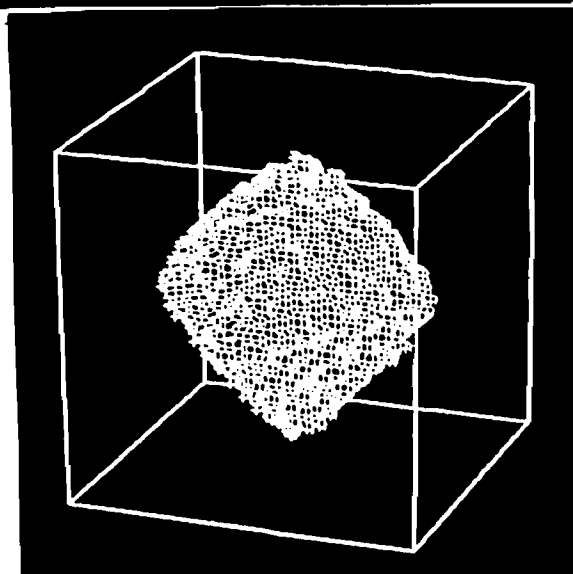
Figure 4. Number of tumor cells as a function of time (Simulation result).

Dose D in Gy	0,7	1,0	2,0	6,0
Percentage number of the hit P-cells: $(1-S(D))$ in x^1	21	28	48	85
Percentage number of the hit G_0-cells: $(1-S(D))$ in x^2	8	10	20	49

Table 2. Percentage of number of specific tumor cells hit by X-rays as a function of dose. In this case α and β are parameters of the adenocarcinoma of the mouse.

$^1\alpha = 0.25$ 1/Gy; $\beta = 0.07$ $(1/Gy)^2$

$^2\alpha = 0.1$ 1/Gy; $\beta = 0.01$ $(1/Gy)^2$

NUTRIENT MEDIUM

SYMBOLS:

🕛 N-PHASE

◈ GO-PHASE

✳ M -PHASE

✡ G1-, S- AND G2-PHASE

TIME= 375.
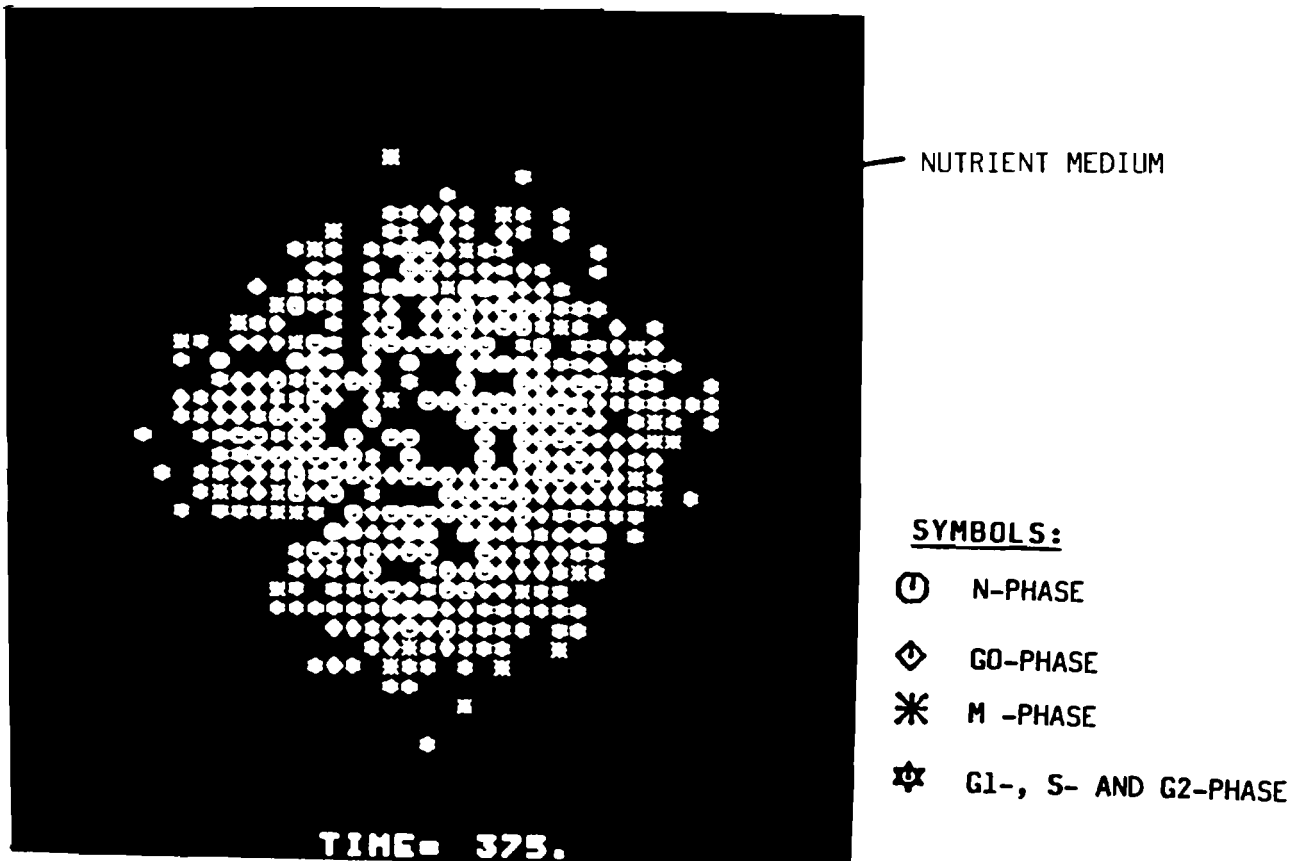
Figure 5. 2-D cross-section image through an irradiated tumor spheroid (simulation result).
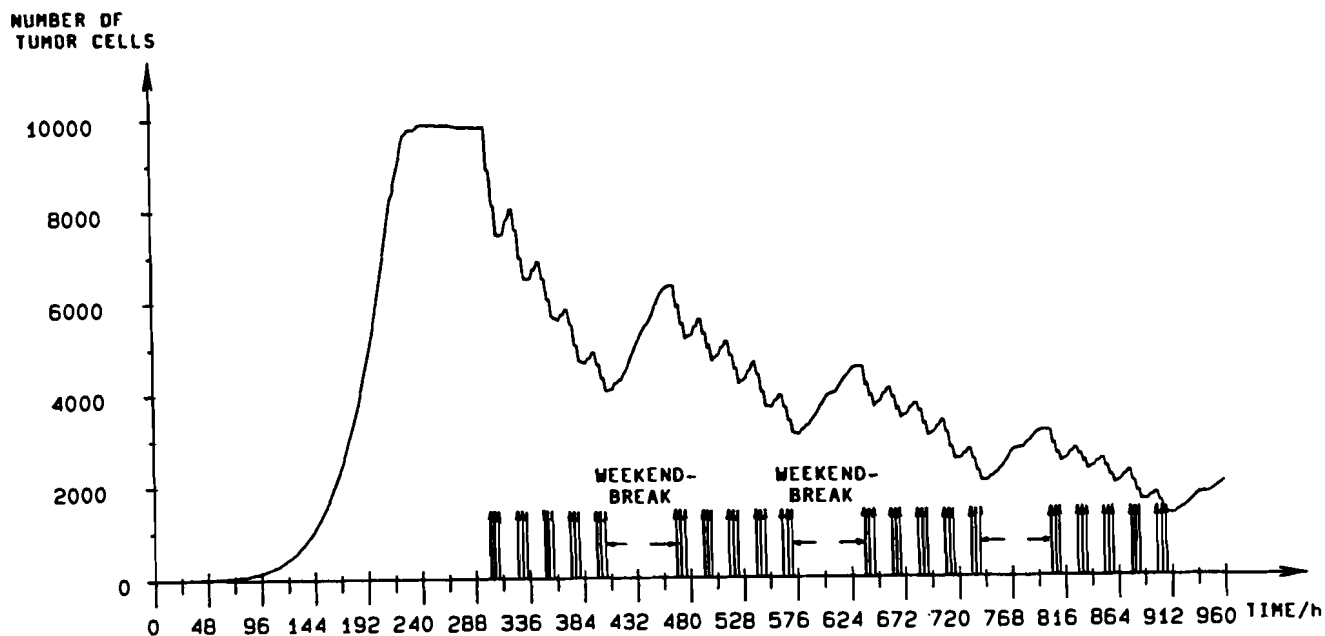
Figure 6. Simulation of a multifractionated irradiation of a tumor spheroid: 5x3x0.7 Gy per week; overall dose: 63 Gy; 30% of the hit cells will be repaired after 15 h; lysis duration of the lethally hit cells: 5 days; cell-cycle phase durations see Table 1; irradiation parameters see Table 2.
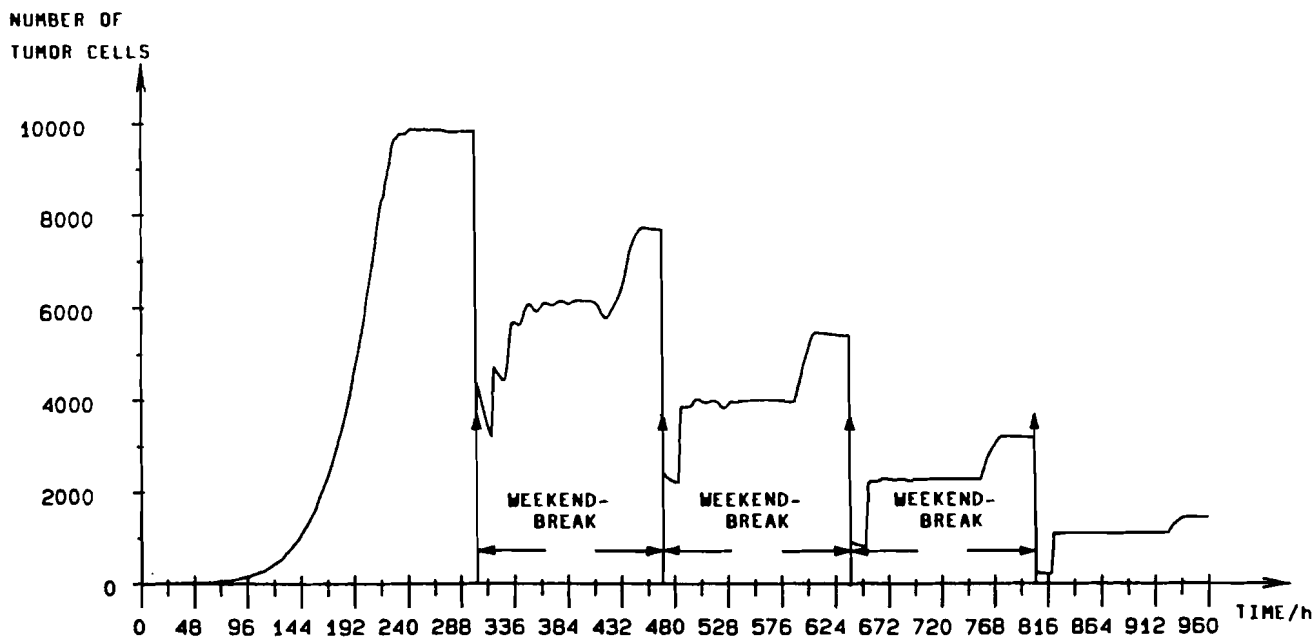
Figure 7. Simulation of an irradiation of a tumor spheroid with a high single dose: 1x6 Gy per week; overall dose: 60 Gy; 30% of the hit cells will be repaired after 15 h; lysis durations of the lethally hit cells: 5 days; cell-cycle phase durations see Table 1; irradiation parameters see Table 2.

Bibliography

[1] Cherruault, Y. "Mathematical Modelling in Biomedicine" D. Reidel Publishing Company, Dordrecht, 1986

[2] Düchting, W. "Krebs ein instabiler Regelkreis, Versuch einer Systemanalyse" Kybernetik, 1968, 5. Band, 2. Heft, pp. 70-77

[3] Düchting, W. and Vogelsaenger, T. "Aspects of Modelling and Simulating Tumor Growth and Treatment" J. Cancer Res. Clin. Oncol., 1983, 105, pp. 1-12

[4] Müller-Klieser, W. "Multicellular Spheroids" J. Cancer Res. Clin. Oncol., 1987, 113, pp. 101-122

[5] Sherar, M.D., Noss, M.B. and Foster, F.S. "Ultrasound backscatter microscopy images the internal structure of living tumor spheroids" Nature, 1987, Vol. 330, pp. 493-495

[6] Düchting, W., Vogelsaenger, T. "Three-dimensional pattern generation applied to spheroidal tumor growth in a nutrient medium" Int. J. Bio-Med. Comp. 1981, 12, pp. 377-392

[7] Cohen, L. "Biophysical Models in Radiation Oncology" CRC Press, Boca Raton, Florida, 1983

[8] Ivanov, V.K. "Optimization of Radiation Therapy in a Model for a Heterogeneous Population of Tumor Cells" Automatika in Telemekhanika, 1986, 5 pp. 102-107

[9] Yakovlev, A. Yu. and Zorin, A.V. "Computer Simulation in Cell Radiobiology" Springer Verlag, Berlin, 1988

[10] Swan, G.W. "Optimization of Human Cancer Radio-therapy" Springer Verlag, Berlin, 1981

[11] Ulmer, W. "Some aspects of the chronological dose distribution in the radiobiology and radiotherapy" Strahlentherapie und Onkologie, 1986, 162, pp. 374-386

Chapter 7

Models and Data Analysis of Cancer Patients

A.L. Asachenkov
International Institute for Applied Systems Analysis
2361 Laxenburg, Austria

B.G. Sobolev
Research Centre of Radiological Medicine
Medical Academy of the USSR, Kiev, USSR

7.1 Introduction

Let us suggest that the state of the organism is characterized by vector $X = (x_1, \ldots, x_n)$ each component of which is an indicator measured in the clinic. The disorders in normal functioning of main homeostatic systems of the organism, caused by the disease, lead to a deviation of these indicators from the values corresponding to a healthy organism. Values and a character of these deviations are an important source of information on the disease [4]. We shall consider the dynamics of immunological indicators after the radical surgery of patients with a solid tumor. Let at time t_H a tumor cell arise in the organism. Denote a number of cancer cells $z(t) \in R^1$. According to the clinical practice a detected tumor is removed by surgery. Let us denote the operation time as $t_0 = 0$. After surgery the treatment of patients will continue and if necessary the additional one can be used (chemotherapy, immune stimulation, etc.) As known, in response on tumor growth the immune system reacts by the production of specific cells and molecules, which can distinguish and destroy cancer cells. Denote $x(t) \in R^n$ as a vector of immunological tests measured in the clinic. The tumor growth leads to deviations of these indicators from their homeostatic values. After successful surgery the convergency of immunological indicators to their homeostatic values is observed (Fig. 1).

Formally the model describing a relationship between tumor cells number $z(t)$ and immune system indicators $x(t)$ could be expressed as follows

$$dz(t)/dt = g(z, x),$$

$$dx(t)/dt = f(z, x), \tag{7.1}$$

$$z(t_H) = z_H > 0, \quad x(t_H) = x_H > 0, \quad t \in [t_H, t_0).$$

The radical surgery can be simulated through changing the initial values at $t = t_0, z(t_0) = z_0 > 0, x(t_0) = x_0 > 0$. If $z_0 = 0$, then dynamics of immunological indicators after surgery might be described as a solution of the following equation

$$dx(t)/dt = f(0, x), \tag{7.2}$$
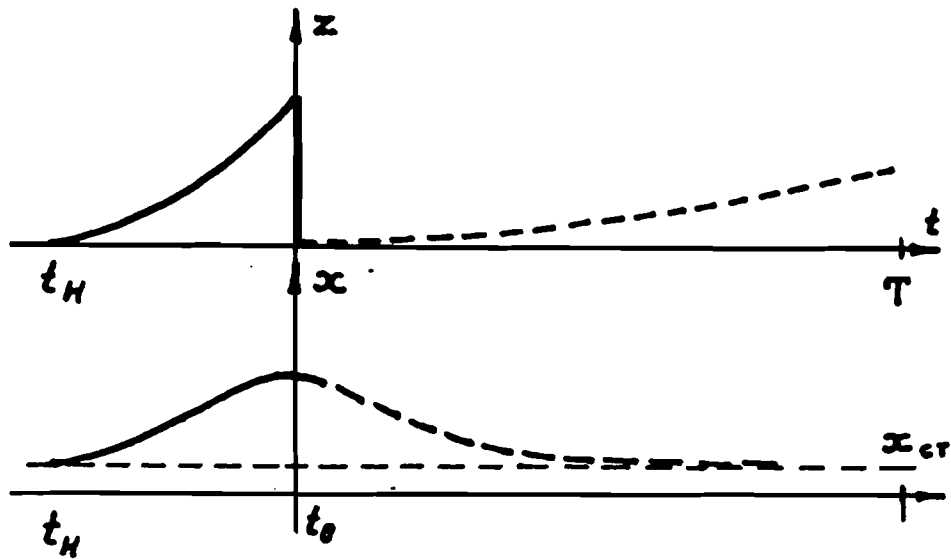
Figure 7.1.
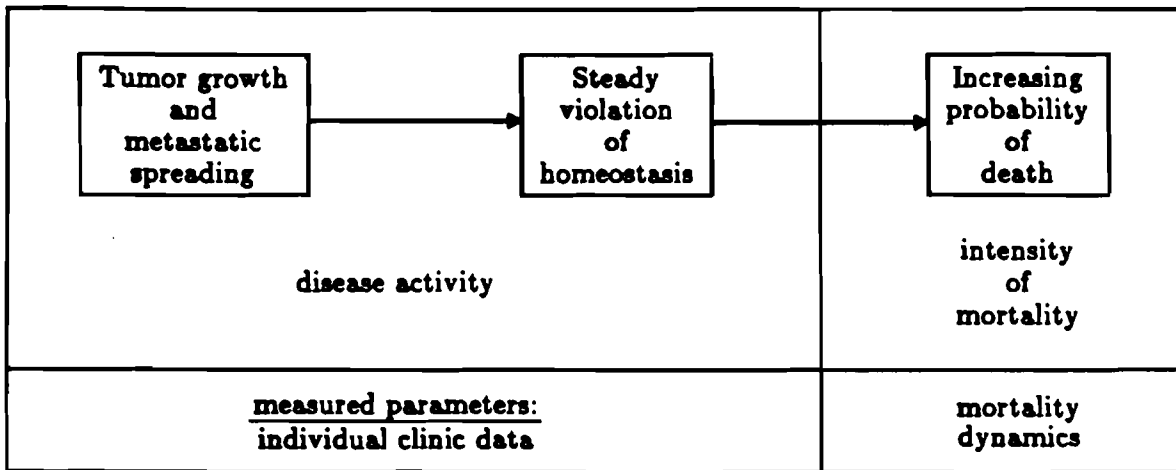
Figure 7.2. Principal characteristics of the oncological disease

$$x(t_0) = x_0 > 0, \quad t \in [t_0, T].$$

Unfortunately the remaining tumor mass can increase and give metastatic spreading. Moreover, if we consider the trajectory of $x(t)$ in a group of patients we observe the broken tendencies. The instants of such breaks have some stable distribution depending on the stage of illness, method of treatment etc. That is why we have an additional population characteristic of cancer as a survival function $s(t)$.

The connection between the basic characteristics of cancer could be formally presented by the following graph (Fig. 2).

In this paper we investigate the interrelationships between the dynamics of the observed variables and mortality dynamics which is a fundamental characteristic of a tumor. In [1,2,3] such an approach was used for the analysis of immunological data for the stomach cancer.
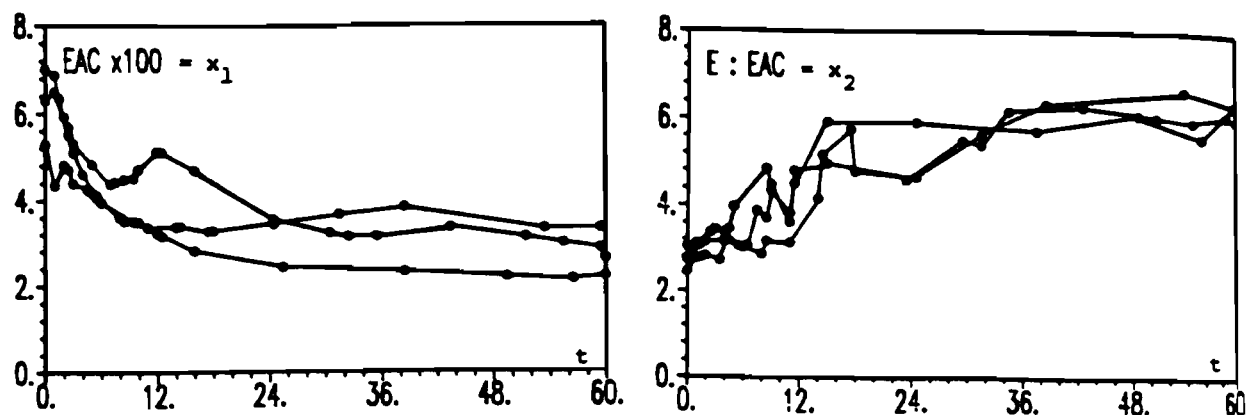
Figure 7.3. Examples of individual trajectories of the immunological data dynamics from the group of patients with the best clinical form of disease

7.2 Individual Characteristic of Cancer

As known, it is difficult to separate a group of cancer patients who have complete functional recovery systems and organs. Nevertheless, we can separate a group of patients with the favorable clinical history when the life span after the beginning of treatment is not shorter than 5 years.

Reference trajectory

Let the average dynamics of immunological indicators for a group of patients with favorable clinical history be described by the equation

$$dx_t/dt = f(x_t, \alpha), \tag{7.3}$$

$$x_0 > 0, \quad t \in [t_0, T],$$

where $x_t \in R^n, \alpha \in R^l$—is a vector of unknown coefficients.

Definition The solution of equation (3) $x(t, \alpha_0)$ for the average dynamics of immunological indicators in the group of patients with favorable clinical history we will define as a support solution or a reference trajectory. The vector $\alpha = \alpha_0$—a reference or support vector.

Denote $X_1 = \{\hat{x}_t^j; \quad t \in \theta_t, j = 1, \ldots, m_1\}$— trajectories set of indicators measured at the time $\theta^j = \{t_1^j, t_2^j, \ldots, t_K^j\}$, where m_1 is a number of patients in a group. If the values of indicators at $t \in \theta^j, j = 1, \ldots, m_1$ are connected by straight line, then we will have trajectories bunch. (A Typical situation is given in Fig. 3.) It is clear that $\hat{x}_t^j$ doesn't belong to a solution set of the equation (3).

Tra⁄jectory deviations of the observed data from $x(t, \alpha_0)$ are explained by influence on the process of uncontrollable factors. The main role belongs to a remainder tumor growth process. From the medical point of view it is not necesary to make distinctions between these trajectories because all these ones belong to a group of patients with favorable clinical history. The mathematical model for describing such deviations will consist of O.D.E. with random perturbance in the coefficients by some stochastic processes which reflect nonregular diffusion influence of different factors on the organism. Assume that for each trajectory $\{x_t(\omega), \quad \omega \in \Omega, \quad t \in [0, T]\}$ a function $\alpha_t(\omega) = \alpha_0 + \xi_t(\omega)$ exists, where $\xi_t(\omega)$ is a fast non-regular perturbation. In this case, the individual trajectories of immunological indicators may be considered as realizations

of a stochastic process which satisfies the equation

$$dx_t^\varepsilon/dt = f(x_t^\varepsilon, \alpha_0 + \sqrt{\varepsilon}\, d\omega_t^\varepsilon/dt) \tag{7.4}$$

$$x_0 > 0, \quad t \in [t_0, T], \quad \varepsilon > 0 \quad \text{is a small parameter,}$$

$$\omega_t^\varepsilon = (\sqrt{\varepsilon})^{-1} \int_0^t \xi_{s/\varepsilon}\, ds.$$

Deviation Model

The solution of the equation (4) can be written as

$$x_t^\varepsilon = x_t^{(0)} + \sqrt{\varepsilon}\, x_t^{(1)} + \ldots, \tag{7.5}$$

where $x_t^{(1)}$ satisfies the stochastic differential

$$dx_t^{(1)} = \frac{\partial}{\partial x} f(x_t^{(0)}, \ \alpha_0) x_t^{(1)} dt + \frac{\partial}{\partial \alpha} f(x_t^{(0)}, \alpha_0) d\omega_t^\varepsilon$$

and $y_t^\varepsilon = x_t^\varepsilon - x_t^{(0)} \approx \sqrt{\varepsilon}\, x_t^{(1)}$, may be approximated by

$$dy_t^\varepsilon = \frac{\partial}{\partial x} f(x_t^{(0)}, \alpha_0) y_t^\varepsilon dt + \frac{\partial}{\partial \alpha} f(x_t^{(0)}, \alpha_0) d\omega_t^\varepsilon.$$

When $\varepsilon \to 0$ the process ω_t^ε weakly converges to a Gaussian process ω_t on the interval $[0, T]$ with $E\omega_t = 0$ and covariance matrix Gt [3,7],

$$\text{where} \quad \|G^{ij}\|_{l \times l}, \quad G^{ij} = \lim_{T \to \infty} \int_0^T \int_0^T E\{\xi_s^i \xi_t^j\}\, dt\, ds.$$

Therefore, the dynamic of the deviations $y_t = x_t - x_t(\alpha_0)$ is approximated by the linear stochastic differential

$$dy_t = a(t) y_t dt + \Gamma_1 b(t) d\omega_t, \tag{7.6}$$

$$y_0 = 0, \quad t \in [0, T], \quad \Gamma_1 = \varepsilon G,$$

$$a(t) = \frac{\partial}{\partial x} f(x_t^{(0)}, \alpha_0), \quad b(t) = \frac{\partial}{\partial \alpha} f(x_t^{(0)}, \alpha_0).$$

7.3   Population Characteristic of Cancer

Denote $T > 0$ a random variable having a continuous distribution function $F(t) = P\{T \leq t\}$, $t > 0$. Let T be a patient termination time. Group mortality dynamics is described by the survival function

$$s(t) = \int_t^\infty f(u)\, du, \tag{7.7}$$

where $f(t)$ is a probability density function. The hazard function $\lambda(t)$ is

$$\lambda(t) = \frac{1}{s(t)} ds(t)/dt = -d\log s(t)/dt. \tag{7.8}$$

Integral intensity for the interval $[0, t]$ is

$$\Lambda(t) = \int_0^t \lambda(u)\, du = -\log s(t), \quad \Lambda(0) = 0. \tag{7.9}$$

We will interpret $\Lambda(t)$ as a load on the organism due to disease.

As a rule available experimental data are the sample from a heterogeneous group of patients. Heterogeneity is manifested in the individual dynamic of measured variables. Let $y(t,\omega) \in R^n$ denote a vector of indicators for the individual with index $\omega \in \Omega$, where Ω is a set of indicators. The ω characterizes homogeneity with respect to the life span group of patients. The individual evolution in the time $\{y(t,\omega)\}$ can be considered as a realization of a stochastic process $\{y(t,\omega), \quad t \in [0,T], \quad \omega \in \Omega\}$. In this case [5], if the conditional survival function $s(t,\omega)$ may be represented in the form

$$s(t,\omega) = exp\{-\int_0^t \mu(u,\omega)du\},\qquad(7.10)$$

then the individual hazard function $\mu(t,\omega)$ will be given by

$$\mu(t,\omega) = P\{t \le T \le t + dt \mid T > t, \quad (y(u,\omega), 0 \le u \le t)\}.\qquad(7.11)$$

Therefore [5] the group mortality dynamics in terms of observation can be written as

$$P\{T > t\} = E\{exp\{-\int_0^t \mu(u,\omega)du\}\},\qquad(7.12)$$

and a convenient hazard function for a group is given by [5]

$$\lambda(t) = E\{\mu(y(t,\omega),t) \mid T > t\}.\qquad(7.13)$$

Parameterization of the individual hazard function

Analysis of the clinical data for the patients with stomach cancer [1,2] shows that the character of deviations $y(t)$ has a close correlation with life span. Taking this into account, we can parameterize an individual hazard function in the form

$$\mu(y,Q) = y_t^T Q y_t + \lambda_0(t),\qquad(7.14)$$

where Q is an unknown symmetrical, nonnegative definite matrix, $\lambda_0(t)$ is a hazard function which is not related to the tumor growth process (it may be the function of sex, age, etc.)

Relationships Between Individual and Population Characteristics of Cancer

Assume that the deviations are approximated by the equation (6) and the hazard function has the form (14). Now we can define a system of O.D.E. which relates individual and population characteristics of cancer.

Proposition [6] Let a stochastic process $\{y(t,\omega), t \ge, \omega \in \Omega\}$ satisfy the equation (6) and the conditional survival function has the form (14). Then the mortality dynamics for a group of patients is described by O.D.E.

$$dA_t/dt = m_t^T Q m_t + Sp(Q\gamma_t), \quad A_0 = 0$$

$$dm_t/dt = a(t)m_t - 2\gamma_t Q m_t, \quad m_0 = m^0 \qquad(7.15)$$

$$d\gamma_t/dt = a(t)\gamma_t + \gamma_t a^T(t) + (\Gamma_1 b(t))^T b(t)\Gamma_1 - 2\gamma_t Q\gamma_t, \quad \gamma_0 = \gamma^0,$$

where

$$A_t = -log s(t), \quad m_t = E\{y_t \mid > t\}, \quad \gamma_t = E\{(y_t - m_t)(y_t - m_t)^T \mid T > t\}.$$
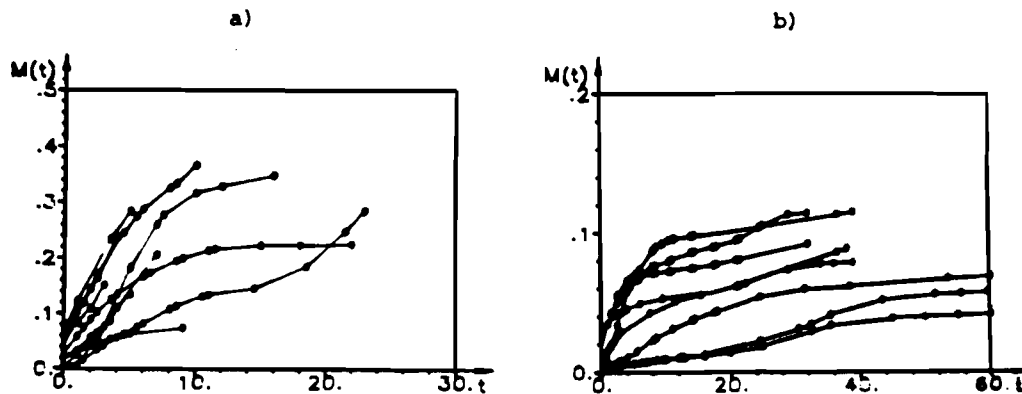
Figure 7.4. Individual estimations $\hat{M}$ for two groups of patients: a) $T \geq 40$ months, b) $T < 40$ months

7.4 Individual Estimation for Intensity of the Tumor Growth Process

Let the functions $a(t)$ and $b(t)$ be known. We may estimate matrices Q, Γ_1 by individual dynamics of immunological indicators and observable function $\lambda(t)$. In [2,7] methods for the estimation of coefficients of the O.D.E. system and some results for patients with stomach cancer are discussed.

Now for the individual estimation of the remaining tumor growth process we can use the index

$$\hat{M}_t = \int_0^t (y_u^T Q y_u + \lambda(u)) du. \tag{7.16}$$

In Figure 4 we can see $\hat{M}_t^j, j = 1, \ldots, m_1$ for two groups of patients differing in life span after surgery. The dynamics of the estimation $\hat{M}_t$ differ in the groups with different life span. Using (16), we can watch the individual intensity of the tumor growth process and formulate the optimal treatment problem.

7.5 Optimal Treatment Problem

Let $A_1, A_2, A_1 \cap A_2 = \emptyset$ be groups of patients with different methods of treatment. The patients from group A_1 have only had a surgery, and those from group A_2 have had a surgery and a treatment (chemotherapy, immune stimulation) additionally. Each group is characterized by

$$X_1 = \{\hat{x}^j(t): \quad t \in \theta^j, \quad j = 1, \ldots, m_1\},$$

$$X_2 = \{\hat{x}^j(t): t \in \theta^j, \quad j = 1, \ldots, m_2\}$$

trajectories sets of indicators measured at the time $\theta^j = \{t_1^j, t_2^j, \ldots, t_{k_j}^j\}$, and $s_1(t), s_2(t), s_1(t) \neq s_2(t)$ survival functions. The reference trajectory is described by the equation (3) with $\alpha = \alpha_0$. For the second group the control set $U = \{u(\tau), \tau_1 < \tau_2 < \ldots < \tau_N, \quad 0 \leq u(\tau) \leq u_{max}\}$ is known. First of all we have to estimate the influence of the treatment on the dynamics of the observe indicators.

The Equations with Control

The trajectories of immunological indicators with control may be described in the following form

$$dx_t/dt = f(x_t, \alpha_0 + \beta u(t)), \tag{7.17}$$

$$t \in [0, T], \quad x_0 = x^0,$$

where the function $u(t)$ is known and β is an unknown vector. In this case the dynamics of the deviations $y_t = x_t - x_t(\alpha_0)$ are approximated by the linear S.D.E.

$$dy_t = a(t, u)y_t dt + \Gamma_u b(t, u)d\omega_t, \quad t \in [0, T], \tag{7.18}$$

Now we rewrite (15) using (18)

$$d\Lambda_t/dt = m_t^T Q m_t + Sp(Q\gamma_t), \quad \Lambda_0 = 0$$

$$dm_t/dt = a(t, u)m_t - 2\gamma_t Q m_t, \quad m_t = m^0 \tag{7.19}$$

$$d\gamma_t/dt = a(t, u)\gamma_t + \gamma_t a^T(t, u) + \Gamma_u^T b(t, u))^T b(t, u)\Gamma_u - 2\gamma_t, Q\gamma_t, \gamma_0 = \gamma^0,$$

where $\Lambda_t = -logs(t), m_t = E\{y_t | T > t\}, \gamma_t = E\{y_t - m_t)(y_t - m_t)^T | T > t\}$.
Let $Q = \hat{Q}$. We can estimate Γ_u, β by $U, s_2(t), X_2$.

Statement of the Optimal Treatment Problem

Let $u(t)$ be a known function, for example,

$$u(t) = \begin{cases} u_k = const & \text{for } t \in [\tau_k, \tau_k + \Delta], \quad k = 1, 2, \ldots, N. \\ 0 & \text{for } t \notin [\tau_k, \tau_k + \Delta] \end{cases}$$

$$\tau_1 \geq \Delta, \quad \tau_1 + (N + 1)\Delta \leq T, \quad \Delta = const, \quad u \in U.$$

The optimal treatment problem may be formulated in the following form

$$J(u) = E\left\{ \int_0^T (y_v^T Q y_v + \lambda(v))dv \right\} \Rightarrow \min_{u,\tau,N} \tag{7.20}$$

under the conditions

$$dy_t = a(t, u)y_t dt + \Gamma_u b(t, u)d\omega_t, \quad t \in [0, T]. \tag{7.21}$$

In other words we are going to choose dose, time τ_k and number of injections N to minimize $J(u)$.

If $u(t)$ is an unknown function, we deal with the linear quadratic regulator problem. This statement of the optimal treatment problem has some defects. First, the individual characteristics of patients are not considered. The second one is related to the toxicity problem.

Individual Treatment. Stochastic Problem.

Consider the scalar case $n = 1$ and $\lambda(t) = 0$. Divide the interval $[0, T]$ on two $[0.t_0), [t_0, T]$ and rewrite (7.20)

$$J(u, T) = E\left\{ \int_0^{t_0} Qy^2(s, u)ds + \int_{t_0}^T Qy^2(s, u)ds \right\}. \tag{7.22}$$

Let $y_i(u, t)$ be a known individual realization on $[0, t_0)$.
Consequently, we can calculate

$$J^i(u, t_0) = E \int_0^{t_0} Q y_i^2(u, s) ds \quad \text{and} \quad y_i(t_0).$$

In this case we can consider the following optimal treatment problem

$$J^i(u, T - t_0) = E \left\{ \int_{t_0}^T Q y^2(u, s) ds \right\} \Rightarrow \min_u \tag{7.23}$$

under

$$dy(t, u) = a(t, u) y(t, u) dt + \Gamma_u b(t, u) dw_t, \tag{7.24}$$

$$y(u, t_0) = y_i(t_0), \quad t \in [t_0 T], \quad u \in [0, 1].$$

Here, the individual disease history is taken into consideration by means of the initial condition in (7.24).

Deterministic Problem. Notice, that

$$E y^2(u, t) = \gamma(u, t).$$

Using this fact we can consider the following deterministic problem

$$J^i(u, T - t_0) = \int_{t_0}^T Q \gamma_i(t, u) dt \Rightarrow \min_u \tag{7.25}$$

under

$$\frac{d}{dt} \gamma_i(t, u) = -2a(t, u) \gamma_i(t, u) + (\Gamma_u b(t, u))^2, \tag{7.26}$$

$$\gamma_i(t_0, \cdot) = \gamma_i(t_0) \geq 0, \quad t \in [t_0, T], \quad u \in [0, 1]$$

Toxicity problem. Toxicity is a major problem with anticancer drugs. A number of clinicians suggest that toxic effects may be characterized by

$$\text{toxicity} \propto \int_0^T R(u(s)) ds, \tag{7.27}$$

where $R(\cdot)$ is a known function.

Taking into consideration (7.27) we can write the performance index for the problem (7.25) in the following form

$$J(u, T - t_0) = \int_{t_0}^T [Q \gamma_i(s, u) + R(u(s))] ds. \tag{7.28}$$

References

[1] Marchuk, G.I., A.L. Asachenkov, B.G. Sobolev, E.S. Smolianinov, *On the problem to analyze clinical data from oncological patients*, Sov. J. Numer. Anal. Math. Modelling, 1989, Vol. 4, No. 5, pp. 381-356.

[2] Asachenkov, A.L., B.G. Sobolev, E.S. Smolianinov, *Mathematical Modelling and Analysis of Data from Immunological Tests for Oncological Patients*, IIASA Working Paper WP-89-032, 1989.

[3] Asachenkov, A.L., Nonlinear models and data analysis of cancer patients, *Proc. IEEE Int'l Symp. Circuits & Systems*, Portland, OR, May 1989.

[4] Marchuk, G.I., Mathematical Models in Immunology, Optimization Software, Inc., Publications Division, New York, 1983.

[5] Yashin, A.I., K.G. Manton, E. Stallard, *Evaluating the effects of observed and unobserved diffusion processes in survival analysis of longitudinal data.* Mathematical Modelling, Vol. 7, 1986, pp. 1353-1363.

[6] Zuev, S.M., Mathematical Models of Diseases and Data Analysis, Nauka, Moscow, 1988 (in Russian).

Chapter 8

On Tumor Modeling and Control

K.S. Lee, R.R. Mohler
Department of Electrical Engineering
Oregon State University, Corvallis, OR, 97331

8.1 Introduction

The aim of all forms of cancer therapy is to remove or to destroy the tumor without seriously damaging the host. Often, this can be achieved by surgery, radiotherapy, chemotherapy, or immunotherapy, or by its combination. Compared to chemotherapy, radiotherapy, and surgery, immunotherapy is the most efficient therapy because immune effector cells kill the target cells without destroying normal neighborhood cells.

The potential methods of tumor immunotherapy can be classified into two broad categories: active, those that attempt to induce in the host a state of immune responsiveness to tumor; and passsive (adoptive), those that transfer directly to the host immunologically active reagents that mediate an antitumor response themselves [1].

Since late 70's, some mathematical models for the interaction between tumor cells and the immune system are proposed. Rescigno and Delisi [2], Grossman and Berke [3], presented a simple model for the interaction of tumor cells and cytotoxic (killer) T-lymphocytes. Lefever and Garay [4] analyzed the cell-mediated cytotoxic reactions against transformed cells and its negative regulation by blocking factors. Merrill [5] proposed and analyzed a model of immune surveillance mediated by NK cells. It is well known that the immune response to a tumor involves several effector cells, e.g., T-lymphocytes, B-lymphocytes, Macrophages, etc.. Simple kinetic model of the anti-tumor immune response describes only one aspect of the complex phenomena. Therefore, the model proposed above are not sufficient to explain the very complex immune response against a tumor.

Recently, DeBoer, Hogeweg, and their associates [6,7] presented a model of the macrophage T lymphocyte interactions that generate an antitumor immune response. However, they didn't mention tumor escape mechanisms and natural killer activity. Therefore, that model is not sufficient to explain the complex immune system.

In this paper, we present a mathematical model of the effector mechanism in which the immune system attacks tumor cells—called cell-mediated immunity (CMI). We formulate a detailed, knowledge-based mathematical model of the immune system. We also consider control the dynamics of immune surveillance, which is a final goal of tumor immunology.

8.2 Mathematical Model

A. Model Description

The concept of immunity against established tumors and the related concept of "immunologic surveillance" against emerging new clones of malignant cells are based on two important hypotheses, namely that

(i) tumor cells differ antigenically from normal cells.
(ii) host defense mechanisms are capable of recognizing and exploiting these differences.

In order to be successful for immunotherapy, it appears that a tumor must be antigenic. This means that it can stimulate an immune response inferred to be relevant for tumor rejection. If the antigenicity of the tumor is low, immunotherapy will have less effect. A weakly antigenic tumor evokes a weak immune response, and the tumor load has become too large to control by the time a sufficient number of effector cells are generated.

The debris of these tumor cells is phagocytosed by antigen presenting cells (APC), that subsequently present antigens in an Ia-restricted fashion to T cells to initiate cell mediated immunity.

Although several types of phagocytic cells may be instrumental in the degradation of antigens, only cells of the mononuclear system can be considered antigen-presenting cells (APC) but only macrophages with the I-A or I-E protein on their surface can cooperate with T_h cells in the immune response. The dendritic cell is also capable of antigen presentation. The stimulation of T lymphocytes by antigen has often described as requiring at least two signals:

a. **First signal:** binding by the compound receptor of a T-cell to the Ia-antigen complex on the accessory cell constitutes the first signal for the activation of T cell,
b. **Second signal:** to complete this process of activation, the accessory cell must deliver a second signal in the form of the lymphokine interleukin 1 (IL-1).

Although macrophages and dendritic cells are important sources of IL-1, keratinocytes and other cells may produce IL-1 [10].

After triggering, and concomitant with with proliferation, T_h cells release an array of lymphokines with a variety of functions.

a. Macrophage Chemotactic Factor (MCF);
b. Migration Inhibition Factor (MIF);
c. Macrophage Activating Factor (MAF) [11];
d. Lymphotoxin (LT) [12];
e. Interleukin-2 (IL-2).

A major function of IL-2 is as follows [13], [15]

(1) induces the lymphokine production by T cells,
(2) induces the growth of activated T cells, thymocytes,
(3) induces cytotoxic T lymphocyte activity,
(4) increases natural killer cell activity,
(5) increases lymphokine-activated killer cell activity,
(6) increases monocyte cytotoxicity.

Effector cells on tumor immunity

Humoral and cellular immune effector mechanisms capable of destroying tumor cells are summarized in Table 1 [14].

   a. Large Granular Lymphocytes (LGL) cell

Table 8.1. Humoral and Cellular Effector Immune Mechanisms in Tumor Destruction.

- Humoral Mechanisms

    (1) Lysis by Ab and Complement
    (2) Ab and/or Complement-mediated opsonization
    (3) Ab-mediated loss of tumor cell adhesion

- Cellular Mechanisms

    (1) Destruction by cytotoxic T cells
    (2) Ab-dependent, Cell-mediated Cytotoxcity (ADCC)
    (3) Destruction by activated macrophages
    (4) Destruction by NK cells

Figure 8.1. Schematic representation of CMI response

$LGL's$ probably include cells formerly known as NK cells.

b. Antibody Dependent Cell-mediated Cytotoxicity (ADCC)

ADCC involves the binding of tumor-specific Ab to the surface of tumor. The Ab is usually an IgG and may be of any subclass. The effector cell must have surface receptors for the Fc portion of IgG;

(i) M_ϕ granulocytes (especially neutrophils) have these receptors
(ii) Platelets and B cells do not participate even though they have Fc receptors.
(iii) Null cells ($= K$ cells).

The importance of this mechanism in the destruction of tumor cells in vivo is still not clear.

c. Macrophage ($M_p hi$)

Macrophages are indirectly derived from bone marrow promonocytes. After differentiation of the promonocytes to blood monocytes they settle in the tissues and mature into macrophages. Here they constitute the reticulo-endothelial system. Macrophages may become highly cytotoxic when they become activated by MAF [16].

d. Cytotoxic T cell (T$_c$)

The T-cells can be divided into 3 different subsets: T_c, T_h, and T_s. A viral infection can stimulate a population of killer T-cells (T_c) which are specifically cytotoxic for virus infected host cells that bear viral antigen. Regulation of CMI response is a complex biological process governed by a series of positive and negative signals. T-helper cells (T_h) are capable of providing necessary signals which enhance T-cytotoxic cell proliferation. T-suppressor cells are characterized by an ability to inhibit the helper function. The network of T_s cells is involved in the regulation of the T_h cell. Suppressor T cells produce soluble factors that mediate suppressive activity. Each T_s subset produces its own type of suppressive factor [17], [18].

B. Mathematical Equation

The humoral responses to tumor in vivo are still unknown. We assume that humoral mechanisms have no role in the tumor destruction. Therefore, we exclude antibody (Ab) from the model. The block diagram of the whole CMI mechanisms is shown in Fig. 1.

Based on our knowledge of tumor immunology, we can make a mathematical model of the anti-tumor immune response due to cell kinetics. These cellular kinetics are quite well defined from conservation equations and chemical mass-action principles [19-20]. In general, the cellular population (or concentration), x_i, of the ith class may be described by:

$$dx_i/dt = v_i(t) - x_i/\tau_i + p_i(\cdot)x_i \\ + \sum_{j \neq i} 2p_j(\cdot)p_{ji}(\cdot)x_j - \sum_{k \neq i} 2p_k(\cdot)p_{ik}(\cdot)x_k, \tag{2.1}$$

where $v_i(t)$: source term (from bone marrow via blood), τ_i: death time constant, $p_i(\cdot), p_{ji}(\cdot)p_{ik}(\cdot)$: appropriate growth coefficients (including, probabilities of stimulation and differentiation, from one class to the other).

These coefficients or probabilities represent parametric feedback control in the immune system of a very complex nature. Indeed, it is these terms upon which much of immunological research is currently focused, i.e., what manner is cell production activated and controlled by mainly molecular regulated substances. Consequently, $p_i(\cdot), p_{ji}(\cdot), p_{ik}(\cdot)$ are functions of primarily molecular concentrations. They may be deterministic functions or random processes depending on the approximations used.

1. Cell-mediated Immune (CMI) Response Model

A widely used general deterministic tumor growth model is of the form (Gompertz growth law) [21]

$$\frac{dN}{dt} = bN ln(\frac{k}{N}) \tag{2.2}$$

where $N(t)$: the measure of tumor size, i.e., the number of tumor cells, k: the maximum tumor size, $1/b$: the length of time required for the specific growth rate, to decrease by a factor of $1/e$ the e-folding time.

Similar to cellular concentration model, a perturbed tumor cell population takes a following form:

$$dN_{dt} = bN\ln(\frac{k}{N}) - \text{kill}\,(\cdot)N \tag{2.3}$$

where kill $(\cdot)$, the parametric control, is a function of concentrations of T_c, M_a, and LGL, etc.

The typical cytotoxicity against TNF/LT concentration takes the form of sigmoidal dose-response curves [12]. We assume that the TNF/LT concentration is proportional to the population of each cell. Then, the sigmoidal relation takes the following equation [22]:

$$CTX = CTX_0 + \alpha_x \tanh[\beta_x(x - x_0)] \tag{2.4}$$

where CTX: Cytotoxicity, CTX_0: $(CTX_h + CTX_1)/2, CTX_h$: max. cytotoxicity, CTX_1 : min. cytotoxicity, α_x: $(CTX_h - CTX_1)/2$, x: cytotoxin concentration, $\alpha_x\beta_x$: slope at x_0, x_0: x value corresponding to CTX_0,

Tumor debris of concentration x_d might be generated to enhance tumor recognition by the immune mechanisms. This would be modelled by the latter term in Eq. (2-3) with removal time constant τ_d so that

$$\frac{dx_d}{dt} = \text{kill}\,(\cdot)N - \frac{x_d}{\tau_d}.$$

The antigen presentation by activated macrophages against antigen concentration follows Michaelis-Menten dynamics [23]. It might be approximated by

$$Z = \frac{z_s \cdot x_d}{x_{d0} + x_d}x_a \tag{2.6}$$

where x_a: concentration of M_a, z_s: APC saturation, x_{d0}: antigen value corresponding to $z_s/2$.

One of the major activities of interleukin-1 is to induce the synthesis and secretion of the T cell-derived mitogenic lymphokine, interleukin-2 (IL-2). This link between IL-1 and IL-2 is an essential element in the T cell activation sequence because it involves the conversion of a primary macrophage-derived maturational signal into a secondary T-cell derived proliferative signal that results in the amplification of specific immune reponse.

As mentioned earlier, IL-2 production by T_h cells requires two signals i.e., antigen and IL-1. Mizel [24] examined that the production of IL-2 is dependent on IL-1 and IL-2 is not produced in response to antigen only. The experimental data show the IL-2 synthesis when stimulated with IL-1 and mitogen. It takes the form of sigmoidal relation. We can formulate the relations between IL-1 and IL-2 as follows:

$$F(\cdot) = \{d_F + (a_F - d_F)/[1 + (z/c_F)^k F]\}FTH \tag{2.7}$$

$$FTH = \frac{T_h}{T_h\text{sat} + T_h}$$

where $F(\cdot)$: IL-2 concentration, z: concentration of IL-1, a_F: min. IL-2 concentration, d_F: max. IL-2 concentration, k_F: slope parameter, c_F: concentration of IL-1 giving 50maximal response, $T_h sat$: T-helper cell saturation.

Activated T lymphocytes proliferate in response to interleukin 2 (IL-2) produced by T helper cells. When an activated T cell divides, it may remain activated or it may return to the resting state. It may depend on the IL-2 receptor expression on the daughter cells. Milanese [25] suggests that it remain activated state and in the absence of additional antigenic stimulation, it returns to the resting state. The growth response of T lymphocytes to IL-2 is accurately described by a four-parameter logistic function [26].

$$y_T = d_T + \frac{[a_T - d_T]}{1 + (x/c_T)k_T} \tag{2.8}$$

where y_T: proliferative response, x: concentration of IL-2, a_T: min. response, d_T: max. response, k_T: slope parameter, c_T: concentration of IL-2 giving 50

In healthy state (normal steady state), a constant number of lymphocyte precursors cells are produced each day. However, the influx of precursors is increased due to inflammatory reaction in cancerous state. Consequently, cell influx is described by:

$$v_i(t) = v_i(1 + p_{0i}) \tag{2.9}$$

where v_i: cell birth rate at normal state, p_{0i}: inflammation rate.

The differentiation of cytotoxic T cell precursors depends on the contact with tumors and IL-2. T suppressor effector cells may inhibit the generation of each precursor cells.

The activity of LGL cells can be augmented by lymphokines such as interferons (IFN) and interleukin-2 (IL-2). Macrophages (M_ϕ) may become activated by γ-interferon (= MAF, Macrophage Activating Factor). Several recent studies have suggested that interleukin-2 regulates the generation of γ-interferon (γ-IFN) [13, 27-28]. The kinetics of γ-IFN production by T_h cells stimulated with IL-2 take the same form of sigmoidal relations. Therefore, the relationships between γ-IFN and IL-2 can be expressed by a four-parameter logistic function.

$$\gamma - IFN = D_{IFN} + a_{IFN} - d_{IFN})/[1 + (F/c_{IFN})^k IFN] \tag{2.10}$$

The differential equations of the model which are considered above are given in Table 2.

Table 2: Differential Equations of the Model

$$dx_1/dt = v_1(t) - x_1/\tau_1 - p_{16}x_1 - p_{81}x_1$$
$$dx_2/dt = v_2(t) - x_2/\tau_2 - p_{27}x_2 - p'_{27}x_2x_1 1 - p_{82}x_2$$
$$dx_3/dt = v_3(t) - x_3/\tau_3 - p_{38}x_3 - p_{83}x_3$$
$$dx_4/dt = v_4(t) - x_4/\tau_4 - p_{49}x_4 - p'_{49}x_4$$
$$dx_5/dt = v_5(t) - x_5/\tau_5 - p_{5,10}x_5$$
$$dx_6/dt = p_{16}x_1 - x_6/\tau_6 + p_6x_6$$
$$dx_7/dt = p_{27}x_2 + p'_{27}x_2x_1 1 - x_7/\tau_7 + p_7x_7$$
$$dx_8/dt = p_{38}x_3 - x_8/\tau_8 + p_8x_8$$
$$dx_9/dt = p_{49}x_4 + p'_{49}x_4 - x_9/\tau_9$$
$$dx_{10}/dt = p_{5,10}x_5 - x_{10}/\tau_{10}$$
$$dx_{11}/dt = p_{11}x_{11} - x_{11}/\tau_{11} - p_{7,11}x_1 1 - p_{10,11}x_1 1$$
$$dx_{12}/dt = x_{11}/\tau_{11} + p_{7,11}x_{11} + p_{9,11}x_{11} + p_{10,11}x_1 1 - x_{12}/\tau_{12}$$

a. x_i ; State of each cell at a certain time instant. The subscripts are as follows:

1. T_h^p 6. T_h
2. T_c^p 7. T_c
3. T_s^p 8. T_s
4. LGL^p 9. LGL
5. M 10. M_a
11. Tu 12. Tu debris

b. $v_i(t) = v_i(1 + P_{0i})$, $i = 1, ...5$: Cell influx

$P_{0i} = P_{id} + (P_{ia} - P_{id})/(1 + (F/c_i)^k i)$: Inflammation rate

$F(\cdot) = (d_F + (a_F - d_F)/(1 + z/c_F)) * (x_6/T_h sat + x_6))$: Differentiation rate

$z = F_D(\cdot)x_{10}$

$F_D(\cdot) = (z_s \cdot x_{12}/(x_{d0} + x_{12}$

$\gamma - IFN = d_{IFN} + (a_{IFN} - d_{IFN}/[1 + (F/c_{IFN})^k IFN]$: $\gamma - IFN$

$p_{16} = \mu_1$: Differentiation rate

$p_{27} = \mu_2$: Differentiation rate

$p'_{27} = \mu_2 F(\cdot)$: Differentiation rate

$p_{38} = \mu_3(1 + F(\cdot))$: Differentiation rate

$p_{49} = \mu_4(1 + F(\cdot))$: Differentiation rate

$p'_{49} = \mu_4^* \gamma - IFN$: Differentiation rate

$p_{5,10} = \mu_5^* \gamma - IFN$: Differentiation rate

$p_{81} = p_{82} = p_{83} = T_s F =$: Differentiation rate

$d_{TSF} + (a_{TSF} - d_{TSF})/(1 + (x_8/c_{TSF})^k TSF)$

$p_6 = p_7 = p_8 =$

$d_T + (a_T - d_T)/(1 + (x/c_T))_T^k$: Proliferation rate

$p_6 = b ln(k/x_{11})$: Tumor growth rate

$p_{7,11} = p_{9,11} = p_{10,11} = CTX$: Killing rate

$CTX = CTX_0 + \alpha_x tanh[\beta_x(x - x_0)]$: Cytotoxity

c. I assume that the inflammation rates for all immune effector cells are identically the same.

d. Initial conditions:

$x_1(0) = 1.05 \times 10^8$, $x_2(0) = 2.2 \times 10^7$, $x_3(0) = 2.2 \times 10^7$, $x_4(0) = 1.3 \times 10^7$, $x_5(0) = 1.3 \times 10^7$,
$x_6(0) = 5.25 \times 10^6$, $x_7(0) = 1.1 \times 10^6$, $x_8(0) = 1.1 \times 10^6$, $x_9(0) = 1.56 \times 10^6$, $x_{10} = 6.5 \times 10^4$,
$x_{11} = 1$, $x_{12} = 0.001$

2. Parameter values

The data which fit the model behavior should have been obtained from the same conditions, e.g., same material and same tumor, etc. It is very difficult to obtain consistent data. Here, the parameter values are obtained from many literatures, which is often not so consistent among different experiments. Several parameters are, however, still unknown. Therefore, the parameter values were chosen somewhat arbitrary.

A typical thymus contains about 200 millions cells. The thymic cortex is producing about 50 million cells each day, most of which will disappear within three days, i.e., $\tau_i = 3(i = 1, 2, 3)$ [day]. It is assumed that 30% of these cells to be Tc/s and 70% to be T_h [29]. Activated T lymphocytes are considered to be long living cells. The turn over time of T cells is assumed to be 50 days [3].

It is shown that bone marrow is required for proliferation/differentiation of natural killer (NK) cells and that NK cells have a life span of a few weeks. In human peripheral blood, cells with NK cell phenotype represent an average of 15variations [30]. The total number of T cells in the blood is of the order of 10^8 cells. The influx of NK cells is, therefore, 750.000 cells per day.

Blood monocytes originate in the bone marrow from dividing precursor cells. They then enter the peripheral blood, in which they circulate until they leave it to become macrophages in the tissues. The normal macrophages in the tissues consist of 1.5×10^7 cells [31]. This is almost consistent with the macrophage concentrations of one per 10 or 100 T cells in vitro [32]. The calculated mean turnover time of macrophages is about 20 days. The influx of macrophages is, therefore, 750.000 cells per day. The turnover time of activated macrophages is assumed to be short, 1 day [6],

During the inflammatory reaction, the influx of immune effector cells is assumed to increase 10 times.

The parameter values for the simulation are shown in Table 3.

Table 3: Parameter values of the model.

$\tau_i = 3$ $(i = 1, 2, 3)$	[day]	: Lymphocyte death time constant
$\tau_4 = 20$	[day]	: LGL^p death time constant
$\tau_5 = 20$	[day]	: macrophage death time constant
$\tau_i = 50$ $(i = 6, 7, 8)$	[day]	: T cell death time constant
$\tau_9 = 20$	[day]	: LGL death time constant
$\tau_10 = 1$	[day]	: Angry macrophage death time constant
$\tau_11 = 1000$	[day]	: Tumor death time constant
$\tau_12 = 0.5$	[day]	: Tumor debris removal time constant
$\mu_i = 0.001$	[cell/day]	: Activation rate $(i = 1, ..., 5)$
$v_1 = 3.5 \times 10^7$	[cell/day]	: Lymphocyte birth rate
$v_2 = 7.5 \times 10^6$	[cell/day]	: Lymphocyte birth rate
$v_3 = 7.5 \times 10^6$	[cell/day]	: Lymphocyte birth rate
$v_4 = 750,000$	[cell/day]	: LGL birth rate
$v_5 = 750,000$	[cell/day]	: Macrophage birth rate
$1/b = 9.35$		: e-folding time
$k = 2.93 \times 10^{10}$	[cells]	: Max. tumor size
$CTX_h = 10$		: Max. cytotoxicity
$CTX_h = 0$		: Min. cytotoxicity
$\beta_x = 0.2$		: Slope at x_0
$z_s = 1$		: APC saturation constant
$x_{70} = 7 \times 10^8$		: T_c corresponding to CTX_0
$x_{90} = 3 \times 10^7$		: LGL corresponding to CTX_0

$x_{100} = 1 \times 10^6$: M_a corresponding to CTX_0

$x_{d0} = 5 \times 10^5$: Antigen value corresponding to $z_s/2$

$d_F = 1,000$: Max. IL-2 concentration

$a_F = 0.01$: Min. IL-2 concentration

$k_F = 1$: slope parameter

$c_F =$: It varies according to antigenicity

$d_{IFN} = 40$: Max. IFN concentration

$a_{IFN} = 5$: Min. IFN concentration

$c_{IFN} = 10$: Concentration of IL-2 giving
                                 : 50% of the maximal response

$k_{IFN} = 1$: slope parameter

$p_{id} = 10$: Max. response ($i = 1, ..., 5, 13$)

$p_{ia} = 0$: Min. response ($i = 1, ..., 5, 13$)

$k_i = 1$: slope factor ($i = 1, ..., 5, 13$)

$c_i = 10$: Concentration of IL-2 giving
                                 : 50% of the maximal response

$a_T = 0$: min. response

$d_T = 1$: max. response

$k_T = 1$: slope parameter

$c_T = 10$: concentration of IL-2 giving
                                 : 50% of the maximal response

$d_{TSF} = 9$: min. response

$a_{TSF} = 0$: max. response

$k_{TSF} = 1$: slope parameter

$c_{TSF} = 10^7$: concentration of T_s giving
                                 : 50% of the maximal response

$T_h sat = 5 \times 10^8$: T_h cell saturation

8.3 Simulation and Results

Experimentation shows the multiplicative (or parametric) control of the tumor by means of individual immune mechanisms results in the death rate of the tumor being increased by immune effector cells. The slope of the tumor death rate is so steep that we can't solve effectively a differential equation of this immune model using conventional numerical integration methods (e.g., explicit Runge-Kutta method). It is called a 'stiff' differential equation and the general solution has an exponential term such as $c_1 e^{bx}, b > 0$.

Numerous methods have been developed for the solution of initial value ordinary differential equations. The model is stiff and this infers an excessively small step size requiring enormous computing time to solve the system equations. Thus one must choose a reliable model solver. As a means of solving general stiff systems, the most commonly used methods are semi-implicit Runge-Kutta and Gear method [33]. In the present paper the IMSL routine DGEAR it used to integrate the ODE's.

At first, I have investigated the effects of antigenicity of tumors. As mentioned earlier, higher antigenic tumors stimulate the T_h cells, that produce enough IL-2 to make necessary effector cells to remove target cells. Fig. 2a shows that a tumor which has one cell at initial time grows exponentially until sufficient effector cells appear and regress rapidly. Then, immune effector cells do not have any reason to retain so many cells. They, therefore, decrease according to the decrease of the size of tumors. In case of lower antigenicity, there is not sufficient IL-2 and the concentrations of effector cells are the same as the healthy state. The tumors could no longer be rejected and Fig. 2b shows a breakthrough phenomenon. IFN is also very important in
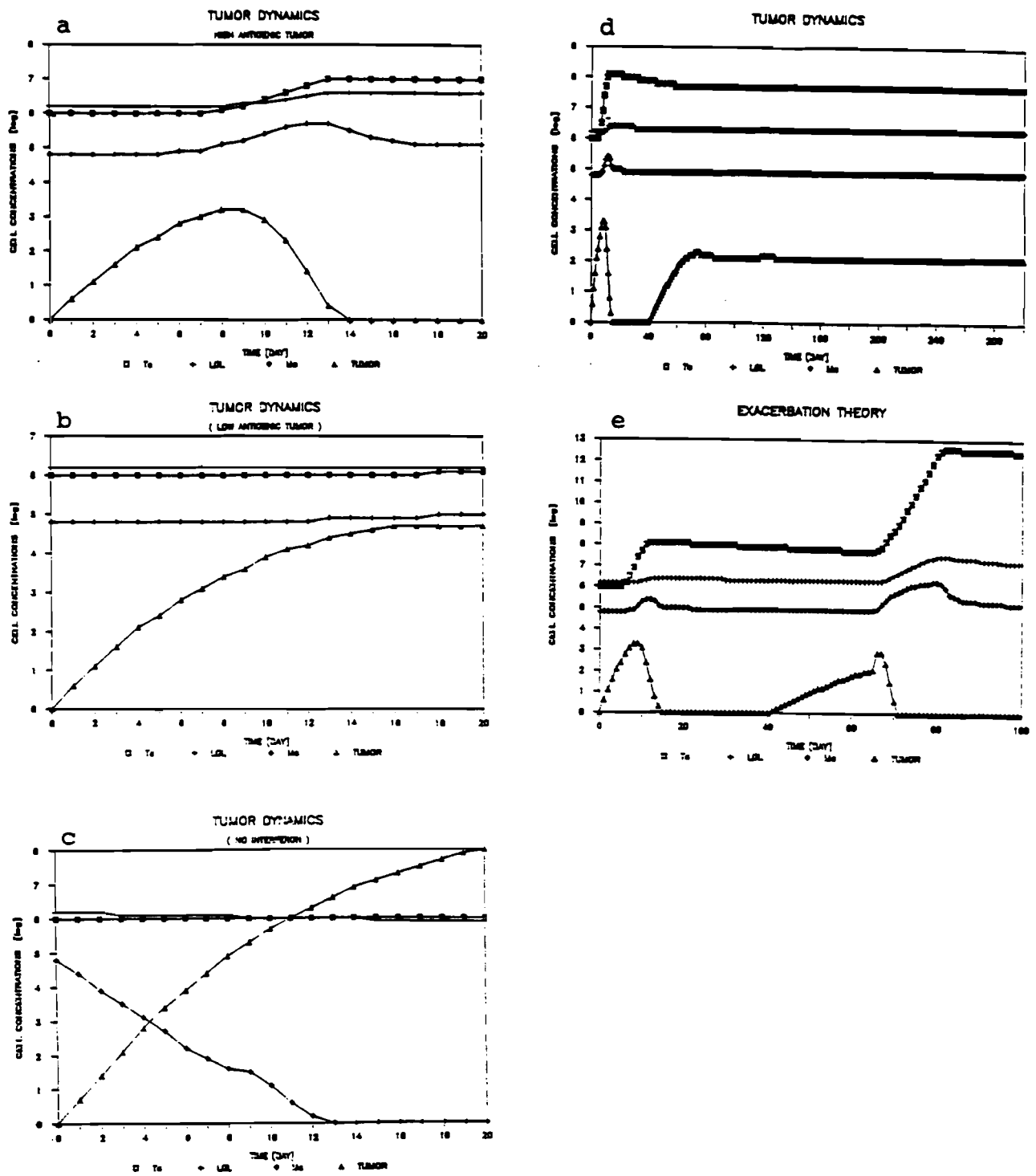
Fig.2 Tumor dynamics and control.
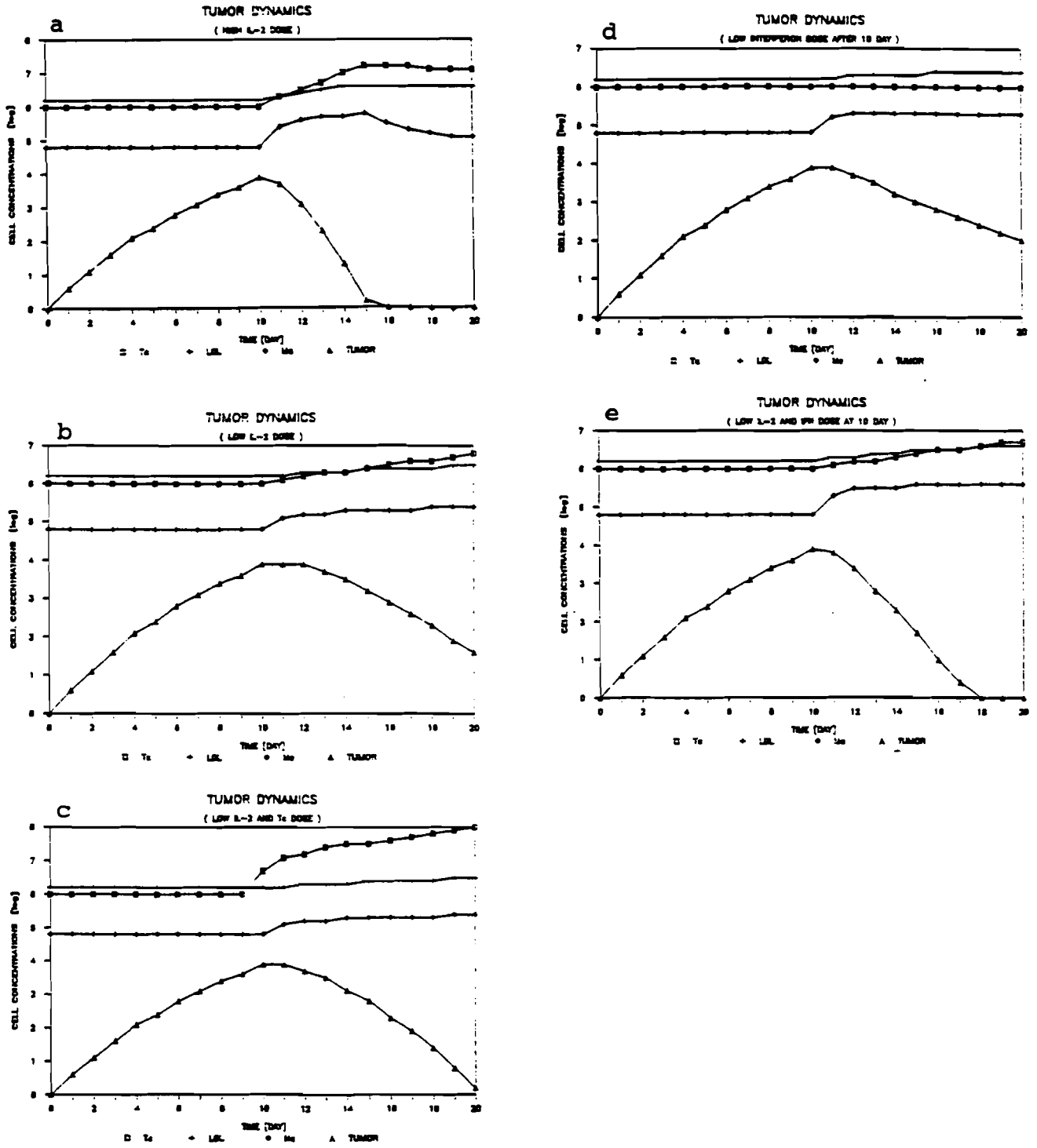
Fig.3   Adoptive immunotherapy.

removing the tumor cells. Fig. 2c shows that the tumor grows progressively when no IFN is produced. The population of M_a decreases exponentially in this case.

In tumor immunology, the final goal is a control of tumor. Among several methods of immunotherapy, exacerbation theory is good for treating tumor. Fig. 2d shows the tumor regression due to increase of effector cells at first. During the decrease of effector cells, the tumor was reoccurred and reached the equilibrium state. At 66 days, 10^3 tumor cells are injected for 2 weeks. This higher tumor concentration evokes the stimulation of effector cells and tumor is destroyed completely (Fig. 2e).

Recent reports have demonstrated that the antitumor activity was observed on treatment with either a high dose of IL-2 alone or a lower dose of IL-2, due to the toxicity of the IL-2, in combination with lymphokine (IL-2) - activated killer (LAK) cells [34, 35]. They have also shown that administration of IL-2 and IFN produces a substantial synergistic therapeutic effect and that their effect is synergistic with that of tumor-infiltrating lymphocytes (TIL).

Fig. 3a shows that the administration of a high dose of IL-2 against weakly antigenic tumor at 10-15 day can mediate tumor regression.

The antitumor activity of combination therapy with low dose IL-2 and antitumor effector cells such as lymphokine - activate killer cells or tumor infiltrating lymphocytes is simulated against weakly antigenic tumor. Fig. 3c demonstrates the synergistic antitumor effects of combination therapy with IL-2 and T_c cells after 10 days (compare with Fig. 3b).

Likewise, the combined administration of IL-2 and IFN can be designed to increase therapeutic potency (Fig. 3e, compare with Fig. 3d).

Satisfactory demonstration runs of the model indicate that it could represent a useful tool in verifying the results of experimental and clinical immunotherapy courses and planning treatment strategies.

References

[1] M. Lotze and S. Rosenberg, The Immunologic Treatment of Cancer, A Cancer J. for Clinicians, vol. 38, 2, pp. 68-94, 1988.

[2] A. Rescigno and C. DeLisi, Immune Surveillance and Neoplasia - II : A Two stage Mathematical Model, Bulletin of Math. Biol., vol. 39, pp. 487-497, 1977.

[3] Z. Grossman and G. Berke, Tumor Escape from Immune Elimination, J. Theor. Biol., Vol. 83, pp. 267-296, 1980.

[4] R. Lefever and R. Garay, A. Mathematical Model of the Immune Surveillance Against Cancer, Theoretical Immunology (Ed. G.I. Bell, et al.), pp. 481-518, Marcel Dekker, New York, 1978.

[5] S.J. Merrill, A Model of the Role of Natural Killer Cells in Immune Surveillance- II, J. Math. Biology, vol. 17, pp. 153-162, 1983.

[6] R.J. De Boer, P. Hogeweg, H.F. Dullens, R. De Weger, and W. Den Otter, Macrophage T Lymphocyte Interactions in the Anti-Tumor Immune Response: A Mathematical Model, J. Immunology, v. 134, no. 4, pp. 2748-2758, 1985.

[7] R.J. De Boer and P. Hogeweg, Interactions between Macrophages, and T-Lymphocytes: Tumor Sneaking through Intrinsic to Helper T Cell Dynamics, J. Theor. Biol., vol. 120, pp. 331-351, 1986.

[8] J.T. Barrett, Textbook of Immunology: An Introduction to Immunochemistry and Immunobiology, 5th ed., The C.V. Mosby Co., 1988.

[9] P. Erb, G. Ramila, et al., Role of Macrophages in T Cell activation, in Recent Advances in Immunology, Plenum Press, N.Y., pp. 17-22, 1984.

[10] S.K. Durum, et al., Interleukin-1,: An Immunological Perspective, Ann. Rev. Immunol., v. 3, pp. 263-287, 1985.

[11] A. Gronberg, et al., Interferon is able to Reduce Tumor Cell Susceptibility to Human Lymphokine-Activated Killer (LAK) Cells, Cellular-Immunology, v. 118, pp. 10-21, 1989.

[12] A. Meager, H. Leung and J. Woolley, Assays for Tumor Necrosis Factor and Related Cytokines, J. Immunological Methods, vol. 11 6, pp. 1-17, 1989.

[13] A. O'Garra, et al., B-cell Factors are Pleiotropic, Immunology Today, vol. 9, no. 2, pp. 45-57, 1988.

[14] E. Benjamini and S. Leskowitz, Immunology: A Short Course, Alan R. Liss, Inc., N.Y., 1988.

[15] R.B. Herberman, Activation of Natural Killer (NK) Cells and Mechanism of their Cytotoxic Effects, in Mechanisms of Lymphocyte Activation and Immune Regulation (eds. S. Gupta, et al.), pp. 275-283, Plenum Press, N.Y. 1987.

[16] W.D. Otter, The Effect of Activated Macrophages on Tumor Growth in Vitro and in Vivo, Lymphokines, vol. 3, pp. 389-422, 1986.

[17] G.L. Asherson, et al., An Overview of T-Suppresor Cell Circuits, Ann. Rev. Immunol., vol. 4, pp. 37-68, 1986.

[18] E. Klein and F. Vanky, Natural and Activated Cytotoxic Lymphocytes which act on Autologous and Allogeneic Tumor Cells, Cancer Immunol. Immunother., vol. 11, pp. 183-188, 1981.

[19] R.R. Mohler, Foundations of Immune Control and Cancer, in Recent Advances in Communication and Control Theory (Ed. A.V. Balakrishnan), pp. 475-489, Optimization Software, Inc., New York, 1987.

[20] R.R. Mohler and Z.H. Farooqi, On Immune Process Stochastic Structure, in Theoretical Immunology (Ed. A.S. Perelson), vol. II, pt. 1., pp. 327-345, Addison-Wesley Publ. Co., Inc., 1988.

[21] F. Hanson and C. Tier, A Stochastic Model of Tumor Growth, Math. Bios., vol. 61, pp. 73-100, 1982.

[22] E.R. Carson, et al., The Mathematical Modeling of Metabolic and Endocrine Systems: Model Formulation, Identification, and Validation, John Wiley & Sons, N.Y. 1983.

[23] J.A. Berzofsky, et al., Antigen Processing for Presentation to T Lymphocytes: Function, Mechanisms, and Implications for the T-cell Repertoire, Immunological Reviews, vol. 106, pp. 5-31, 1988.

[24] S.B. Mizel, Interleukin 1 and T Cell Activation, Immunological Rev., vol. 63, pp. 51-72, 1982.

[25] C. Milanese et al., Human T Lymphocyte Activation, in Mechanisms of Lymphocyte Activation and Immune Regulation (S. Gupta et al., eds.) pp. 59-67, Plenum Press, New York, 1987.

[26] J.W.L. Hooton, et al., Interaction of Interleukin 2 with Cells: Quantitative Analysis of Effects, J. Immunology, vol. 135, no. 4, pp. 2464-2473, 1985.

[27] M. Dohlsen, et al., Proliferation of Human $CD4^+45R^+$ and $CD4^+45R$ T Helper Cells is Promoted by both IL-2 and IL-4 while Interferon - Gamma Production is Restricted to IL-2 Activated $CD4^+45R$ T Cells, Immun. Letters, vol. 20, pp. 29-34, 1989.

[28] J. Vilcek, et al., Interleukin-2 as the Inducing Signal for Interferon - Gamma in Peripheral Blood Leukocytes Stimulated with Mitogen or Antigen, in The Biology of the Interferon System 1984 (Ed., H. Kichner, et al.), pp. 385-396, 1985.

[29] R. Scollay and K. Shortman, Cell Traffic in Adult Thymus: Cell Entry and Exit, Cell Birth and Death, in Recognition and Regulation in Cell-Mediated Immunity (Eds. J.D. Watson, et al.), pp. 3-30, Marcel Dekker, Inc., N.Y., 1985.

[30] G. Trinchieri, et al., Regulation of Activation and Proliferation of Human Natural Killer Cells, in Mechanisms of Lymphocyte Activation and Immune Regulation (eds. S. Gupta, et al.), pp. 285-298, Plenum Press, N.Y. 1987.

[31] R. Van Furth, et al., The Current View on the Origin of Pulmonary Macrophages, Path. Res. Prac., vol. 175, pp. 38-49, 1982.

[32] I.G. Kevrekidis, et al., Modeling Dynamical Aspects of the Immune Response: I. T Cell Proliferation and the Effect of IL-2, in Theoretical Immunology (Ed. A.S. Perelson), vol. II, pt. 1, pp. 167-197, Addison-Wesley Publ. Co., Inc., 1988.

[33] B. Carnahan and J. Wilkes, Numerical Solution of Differential Equations—An Overview, in Foundations of Computer-Aided Chemical Process Design (R. Mah, ed.), vol. 1, pp. 225-340, Engineering Foundation, N.Y., 1981.

[34] R. Cameron, et al., Synergistic Antitumor Effects of Combination Immunotherapy with Recombinant Interleukin-2 and a Recombinant Hybrid α-Interferon in the Treatment of Established Murine Hepatic Metastases, Cancer Research, vol. 48, pp. 5810-5817, 1988.

[35] S. Rosenberg, et al., Combination Immunotherapy for Cancer: Synergistic Antitumor Interactions of Interleukin-2, Alfa Interferon, and Tumor-Infiltrating Lymphocytes, J. of the National Cancer Institute, vol. 80, no. 17, pp. 1393-1397, 1988.

Part III

Clonal Affinity Distributions and Immunogenetics
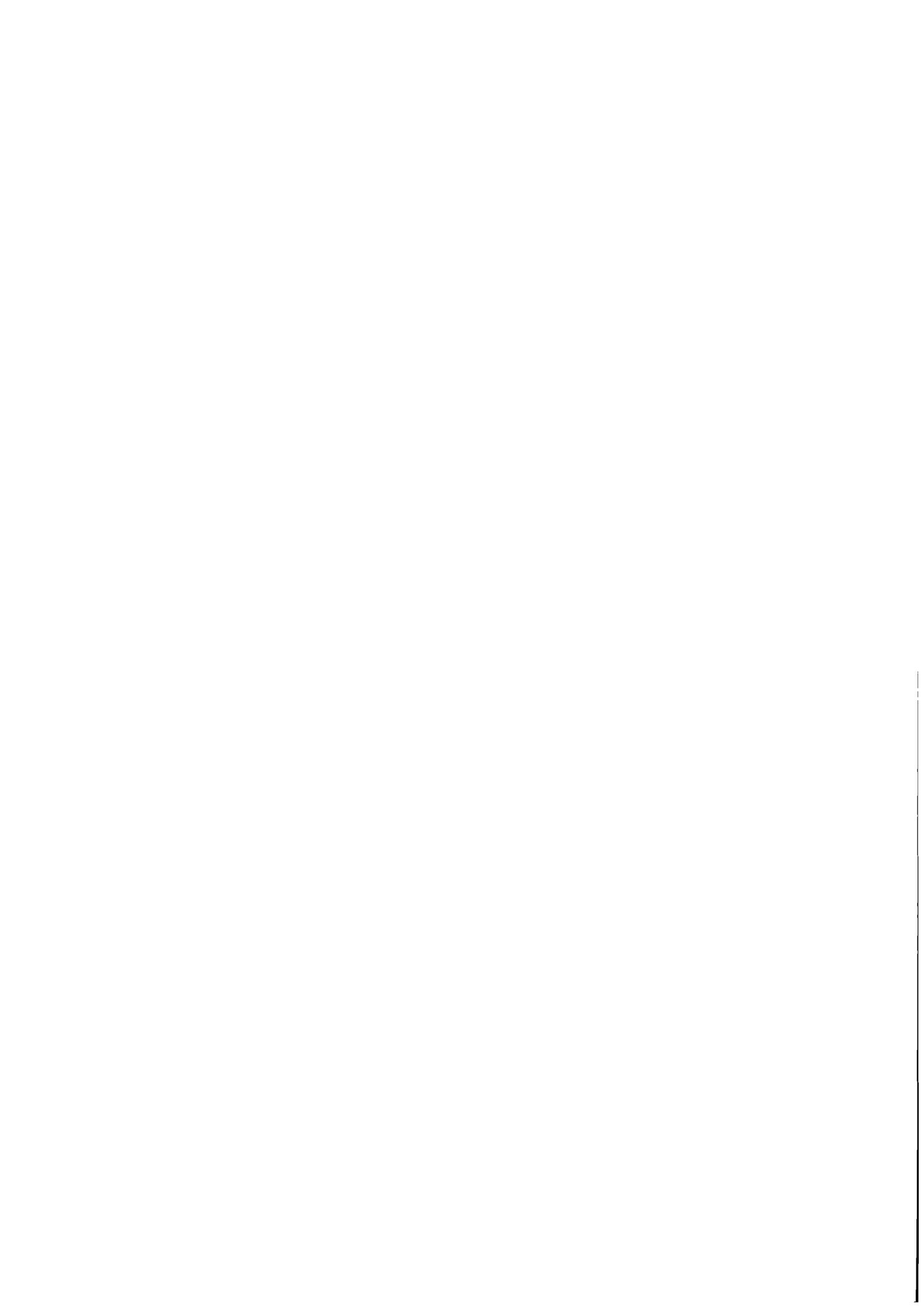
Chapter 9

Models for Antibody and Immunoassay Dynamics Based on Clonal Affinity Distributions

Peter J. Hingley
Tokyo Securities Co. (Europe) Ltd.,
London Wall Buildings
London EC2M 5PP, England

9.1 Introduction

Simple timecourse models can be developed for the response of the immune system to killed vaccines. If relatively few parameters are specified, in a model that can still adequately describe measurable responses to vaccination, useful predictions can be made for routine animal experiments. In a previous report [1] I presented a model based on a partial differential equation for the evolution of antibody concentration with a particular affinity, to be used in conjunction with an initially specified distribution of affinities (affinity density). The model allows for prediction over time of various quantities like total antibody concentration and mean affinity. Immunoassay measures that can themselves be modelled in terms of such quantities, such as ELISA, can also be predicted over time.

In this paper I consider the implications of various ways that a class of models of this type can be specified. I have previously considered data from Foot and Mouth Disease immunoassays on sera from vaccinated cattle, but it is possible that many experimental systems could be analyzed with an appropriate choice of conditions. The main variations to be considered include the metric of affinity on which the model is to be specified, the functional form of the initial affinity density, the functional form of the subsidiary immunoassay model, and the initial values taken by the various parameters.

The timecourse model can be written in the form of the following partial differential equation.

$$\frac{\partial y(t, K)}{\partial t} = Ay(t_0, K) + cKx(t)y(t, K) - Ay(t, K) \qquad (1)$$

$$c > 0, \ A > 0, \ K > 0.$$

where $y(t, K)$ is the concentration of antibody produced from the single clone with affinity K at time t, c is a constant of proportionality, A is a constant background production/excretion rate, and also is the removal rate of antigen from the animal.

$x(t)$ is the concentration of antigen in the animal at time t, usually assumed to decline exponentially with rate λ.

In this form the metric to be used is that of the thermodynamic equilibrium constant K for the binding of antibody to antigen [2]. Thus, in an idealized system at equilibrium, assuming monovalent antibody and antigen, we have

$$K = \frac{x, y(t, K)}{x(t) y(t, K)} \tag{2}$$

Where $x, y(t, K)$ is the concentration of antibody-antigen complex.

The affinity density at time t in this metric is given by

$$P(t, K) = \frac{y(t, K)}{\int_0^\infty y(t, K) dK} = \frac{y(t, K)}{y(t)} \tag{3}$$

Where $y(t)$ is the total concentration of antibody in the animal at time t.

Equation 1 defines a timecourse model in which the affinity metric (i.e. metric of K) is bounded at $K = 0$. Models can be defined on other metrics by replacing K in equation 1 with appropriate alternative measures. Two such possibilities will be considered below. Solution of equation 1 gives the following expression for $y(t, K)$

$$y(t, K) = \left[\left(A \int_{t_0}^t \exp\left[\int_{t_0}^r (A - Kcx(s)) ds\right] dr\right) + 1\right]. \tag{4}$$

$$y(t_0, K) \exp\left[\int_{t_0}^t (Kcx(s) - A) ds\right]$$

where t_0 is the time of vaccination.

This equation can be used to obtain the affinity density $P(t, K)$, and total antibody concentration $y(t)$, at any time t. If the "affinity density" is set up as a discontinuous distribution at a small number of K values, then $P(t, K)$ can be completely determined [3]. If the density is continuous the process can be sampled at various representative values of K, and the form of $P(t, K)$ can then be determined to any desired degree of accuracy by averaging over regions of K [4]. The average affinity at time t, $\mu(t, K)$, is an important quantity which can be obtained from the affinity density. In models of this sort the mean affinity $\mu(t, K)$ remains at high levels longer than the total antibody concentration $y(t)$. The persistence of $\mu(t, K)$ suggests that it might be used to represent immune memory for antigen [5].

The immunoassay model forms the important link between the timecourse model and measured data. Assume that an immunoassay is used in which measured response represents the saturation of serum antibody with various concentrations of applied antigen (e.g. ELISA [6] or radioimmunoassay [7]). The data are most usefully represented in the form of of a sigmoid saturation curve (Figure 1), so that they are amenable to statistical analysis without the estimation bias that commonly occurs with linearizing transformations like the Scatchard plot [8]. When immunoassay data are collected, a direct attempt can be made to delineate the underlying affinity density [9]. However, for practical application it is often more useful if a predefined function can be fitted to the data.

Assuming monovalent interaction of antigen and antibody, and following Sips [10] and Bruni et al. [11], the saturation data can be modelled as follows (assuming a continuous affinity density for convenience).

$$w(t, z) = v(t) \int_0^\infty \frac{Ke^z}{1 + Ke^z} P(t, K) dK = v(t) E_t\left[\frac{Ke^z}{1 + Ke^z}\right] \tag{5}$$

where $w(t, z)$ is the immunoassay response at time t, $P(t, K)$ is the affinity density at time t, z is the log antigen concentration applied in the test, $v(t)$ is a constant of proportionality, showing the maximum value of $w(t, z)$ obtained if serum antibody is fully saturated at time t.

$E_t[\ldots]$ indicates expectation over the affinity density at time t.
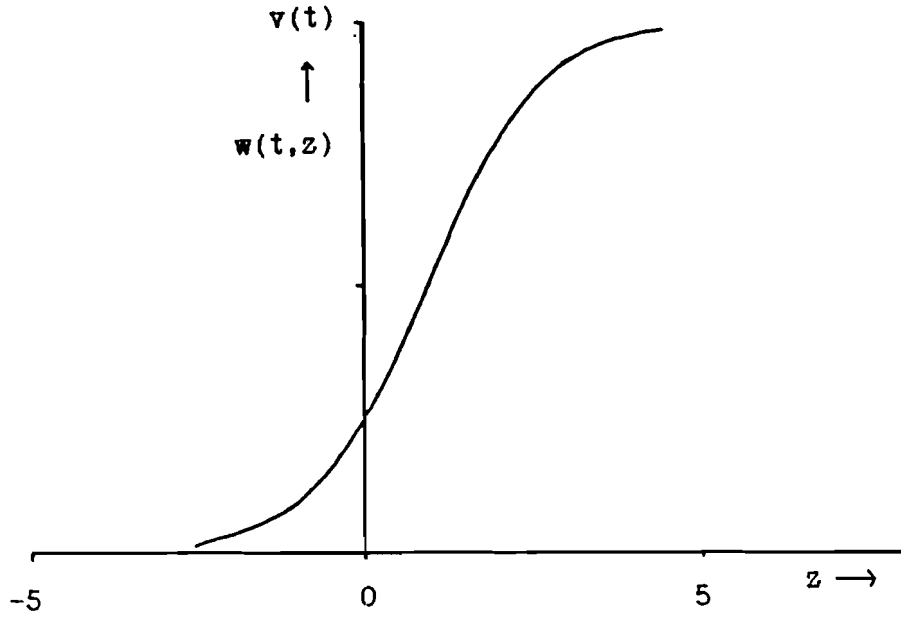
Figure 9.1. Logistic saturation curve $w(t,z)$ generated by Sips density. $\gamma(t) = -1$, $a(t) = 0.5$ (Equation 17).

Equivalents to Equation 5 can be obtained when affinity is expressed on some other metric, but the resulting quantity $w(t,z)$ should be the same whichever metric is chosen (see Equations 14 and 15). It can be seen that the form of the function $w(t,z)$ depends upon $P(t,K)$, which itself is modified through time under the influence of the timecourse model.

9.2 Continuous Models and Thresholds

An initial negative exponential density can be written

$$y(t_0, K) = \frac{y(t_0)}{\mu(t_0, K)} \cdot \exp\left[\frac{-K}{\mu(t_0, K)}\right] \tag{6}$$

With this kind of unbounded initial affinity density, problems can arise if excessive antigenic stimulation leads to infinite total antibody concentration $y(t)$. This causes degeneration of the affinity density $P(t, K)$ because of the unboundedness of the integral in Equation 3. In reality the clonal distribution of affinity must be bounded at some maximum value $K = K_{max}$. Other authors [4] have developed models with censored affinity densities and, although it is difficult to define K_{max} in the absence of experimental data, the problems of boundedness disappear with censoring at any finite level.

As the immune response develops it is of interest to consider the existence of turning points in the profile to $y(t, K)$ vs. K. From Equation 4 it can be shown [5] that a turning point will exist at $K = K_d$ if

$$\int_{t_0}^{t} cx(s)ds = \Lambda(K_d) - \Phi(t, K_d) \tag{7}$$

where

$$\Lambda(K_d) = \frac{-1}{y(t_0, K_d)} \left[\frac{\partial y(t_0, K)}{\partial K}\bigg|_{K=K_d}\right] \tag{8}$$

A>0

y(t,k) ↑   y(t,k) ↑   y(t,k) ↑

k → k_a k →   k →

A=0

y(t,k) ↑   y(t,k) ↑   y(t,k) ↑

k →   k →   k →

Stage 1   Stage 2   Stage 3
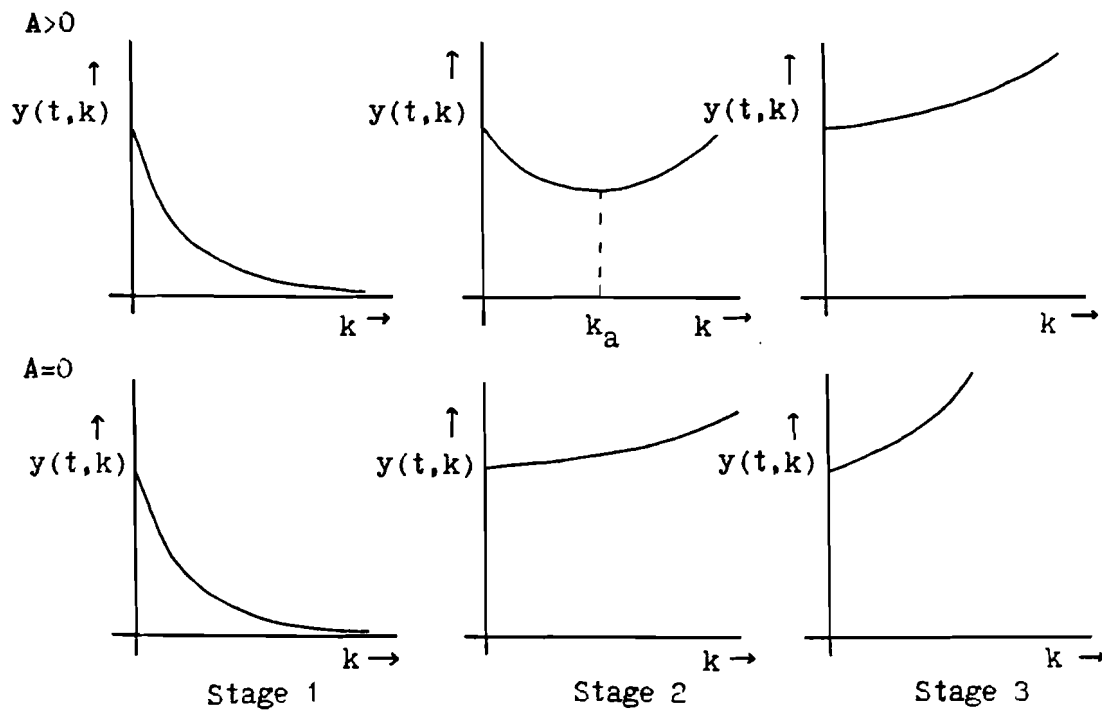
Figure 9.2. Evolution of the antibody profile $y(t, K)$ vs. K, when the initial affinity density is a negative exponential. **Stage 1:** No turning points before $t = t_*$ (Equation 11). **Stage 2:** Turning point exists if Equation 12 is satisfied and $A > 0$. **Stage 3:** No turning points when t is too large.

and

$$\Phi(t, K_d) = \frac{A\left[\int_{t_0}^{t}\left(\int_{t_0}^{r} -cx(s)ds\right)\exp\left[\int_{t_0}^{r}\left(A - K_dcx(s)\right)ds\right]dr\right]}{\left[\left(A\int_{t_0}^{t}\exp\int_{t_0}^{r}\left(A - K_dcx(s)\right)ds\right) + 1\right]}. \tag{9}$$

$\Phi(t, K_d)$ is independent of $y(t_0, K)$ but depends on the timecourse parameters $(t, x(t_0)$, λ, A, $c)$. $\Lambda(K_d)$ depends on $y(t_0, K)$ but is independent of the timecourse parameters. When the timecourse parameters are fixed, $\Phi(t, K_d)$ is a negative function of K_d, which increases monotonically from some negative value towards 0 as $K_d \to \infty$. Equation 7 shows that the condition for a turning point depends upon one factor specified by the form of the initial affinity density, and another factor specified by the timecourse parameters.

In the case of the initial negative exponential function, Equation 8 gives

$$\Lambda(K_d) = \frac{1}{\mu(t_0, k)} \tag{10}$$

No turning points exist initially, but a single minimum exists when a threshold, at time $t = t_*$, is crossed and $y(t, K)$ becomes unbounded.

$$\frac{1}{\mu(t_0, K)} = \int_{t_0}^{t_*} cx(s)ds \tag{11}$$

When $t > t_*$, a minimum is defined by Equation 7.

$$\int_{t_0}^{t} cx(s)ds = \frac{1}{\mu(t_0, K)} - \Phi(t, K_d) \tag{12}$$

As t increases further the turning point disappears. Figure 2 shows various shapes that $y(t, K)$ can take as time progresses. When $A = 0$ no turning points ever exist and $y(t, K)$ remains exponential in form. The system only passes from one stage to another if $x(t_0)$ is big enough for a particular set of model parameters. Although $P(t, K)$ is degenerate in all stages beyond $t = t_*$, the methodology could be used to investigate the shapes of $y(t, K)$ and $P(t, K)$ for initially censored exponential distributions. The general form of Equation 7 can be used for any initially specified continuous distribution.

9.3 The Affinity Metric

The timecourse model (Equation 1) and the immunoassay model (Equation 5) have both been specified in the metric of K. In this section two other affinity metrics will be presented. The affinity density for a new metric can be obtained from the original density (on the K metric) by use of a suitable determinant [12]. The metric of $Q = \text{Log}K$ is useful because there is a symmetry between affinity densities and saturation curves, and from the thermodynamic perspective the free energy of interaction between antigen and antibody is proportional to $\text{Log } K$ (see Ref. [2]).

Another metric with useful properties is that of a variable $R(z_\infty)$, conditional on a fixed value $z = z_\infty$.

$$R(z_\infty) = \frac{Ke^{z_\infty}}{1 + Ke^{z_\infty}} \tag{13}$$

Equation 5 for the saturation curve $w(t, z)$ can be recast as an expected value on the metrics of Q or $R(z_\infty)$.

$$w(t, z) = v(t) \int_{-\infty}^{\infty} \frac{e^{Q+z}}{1 + e^{Q+z}} P(t, Q)dQ = v(t)E_t \left[\frac{e^{Q+z}}{1 + e^{Q+z}} \right] \tag{14}$$

$$w(t, z_\infty) = v(t) \int_{0}^{1} R(z_\infty) P(t, R(z_\infty))dR(z_\infty) = v(t)E_t[R(z_\infty)] \tag{15}$$

THE Q METRIC:

The kernel of Equation 14 is a simplified form of the Langmuir Equation for localised absorption at a constant temperature [10]. Shifts in the location of the affinity density $P(t, Q)$ result in equivalent shifts in the location of the saturation curve $w(t, z)$. Equivalently, if $P(t, Q)$ can be presented in such a way that one of the parameters measures location and has no effect on the shape of the density, then this parameter will also measure location of the corresponding saturation curve $w(t, z)$. It is also possible to show that a symmetric density $P(t, Q)$ will generate a rotationally symmetric curve $w(t, z)$ [5].

A commonly used expression for the saturation curve is the logistic [6].

$$w(t, z) = v(t) \frac{(\bar{K}(t)e^z)^{a(t)}}{1 + (\bar{K}(t)e^z)^{a(t)}} \tag{16}$$

Although $\bar{K}(t)$ is a measure of average affinity, it is not the expected value of affinity on the K metric. It is more useful to parameterise the logistic on the Q metric as

$$w(t, z) = v(t) \frac{e^{(\gamma(t)+z)a(t)}}{1 + e^{(\gamma(t)+z)a(t)}} \tag{17}$$

where $\gamma(t) = \text{Log } \bar{K}(t)$.

The equivalent affinity density is known as the "Sips density" [10].

P(t,Q)

1.2

0.8

0.4

-3   -2   -1   0   Q →   1

a(t)=1.0

a(t)=0.8

a(t)=0.5
a(t)=0.2
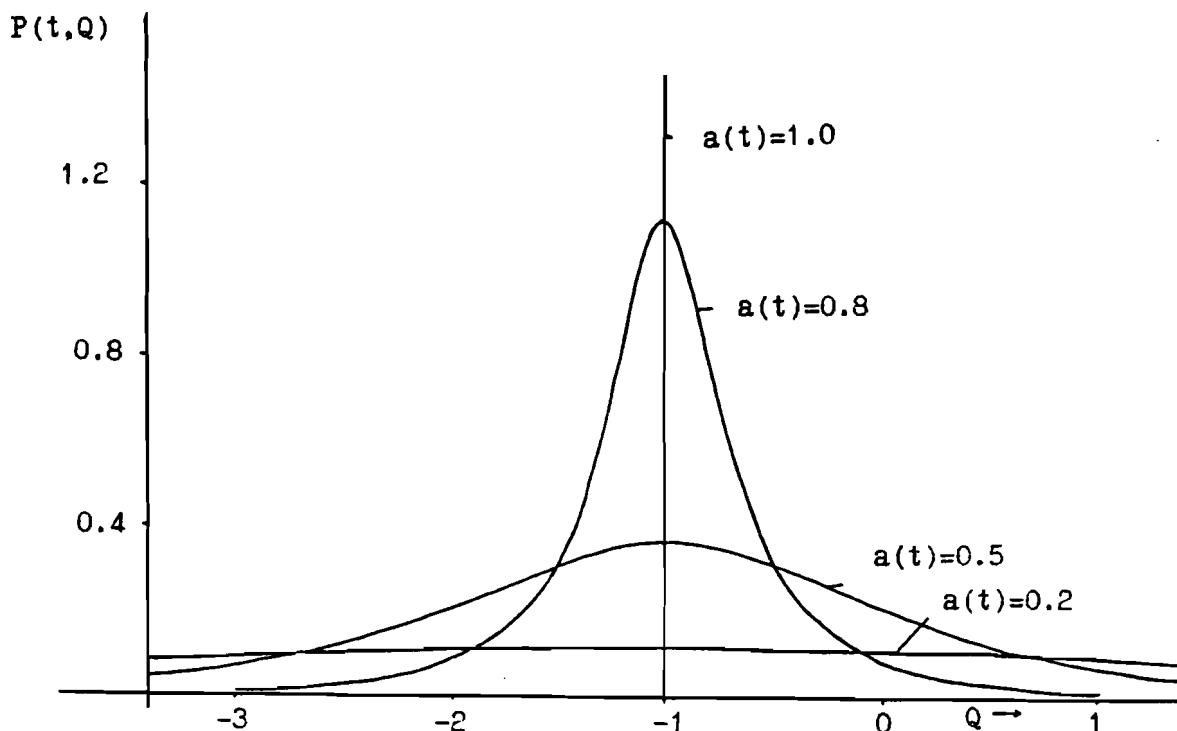
Figure 9.3. Sips affinity densities $P(t,Q)$, $\gamma(t) = -1$. Various values of $a(t)$ (Equation 18).

$$P(t,Q) = \frac{1}{\Pi} \frac{\exp\left[a(t)(\gamma(t) - Q)\right]\sin\left(\pi a(t)\right)}{1 + 2\exp\left[a(t)(\gamma(t) - Q)\right]\cos\left(\pi a(t)\right) + \exp[2a(t)(\gamma(t) - Q)]} \tag{18}$$

This density is continuous, symmetric and unimodal when $0 < a(t) \leq 1$. The mean and model are located at $E_t[Q] = \gamma(t)$.

The parameter $a(t)$ indicates the spread of the of the density. When $a(t) = 1$ the density degenerates to a discontinuous spike with infinite value at the mean. As the value of $a(t)$ decreases towards 0 the density becomes more spread; until at $a(t) = 0$ it becomes infinitely spread, with vanishingly low probability density at all values of Q (Figure 3). As the degree of dispersion in the distribution is described by $a(t)$, the value of this parameter is often used as an index of antibody heterogeneity [13]. The variance of the Sips density is given [10] by

$$\mathrm{Var}_t[Q] = \frac{\Pi^2(1 - a(t)^2)}{3a(t)^2} \tag{19}$$

THE $R(z_\infty)$ METRIC:

Consider the transformed variable $R(z_\infty)$ defined in Equation 13. $P(t, R(z_\infty))$ is the affinity density for $R(z_\infty)$. The effect of the transformation to the new metric is to produce an affinity density that is bounded between 0 and 1. The density function depends upon K and z_∞. This seems inconvenient but Equation 15 establishes that the value of the saturation curve $w(t, z_\infty)$ at a given applied log antigen concentration z_∞ is equal simply to the expected value of the affinity density. The variance at $z = z_\infty$ is given [5] by

$$\mathrm{Var}_t[R(z_\infty)] = \left[\frac{w(t, z_\infty)}{v(t)} \frac{(1 - w(t, z_\infty))}{v(t)}\right] - \frac{1}{v(t)}\left[\frac{\delta w(t, z)}{\delta z}|_{z=z_\infty}\right]. \tag{20}$$

It is only necessary to measure $v(t)$, and the value and slope of the saturation curve $w(t, z_\infty)$ at a particular z_∞ value, to obtain the mean and variance of $P(t, R(z_\infty))$. This can be done even
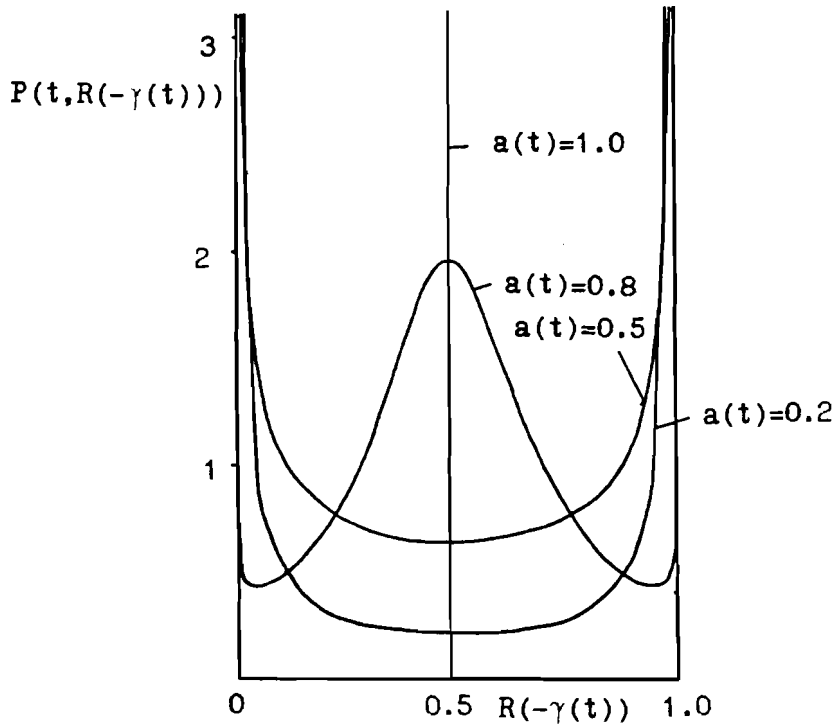
Figure 9.4. Sips affinity densities $P(t, R(z_\infty))$, with $z_\infty = -\gamma(t)$. Various values of $a(t)$ (Equation 21).

if the parametric form of the affinity density is not known. It is possible to show that a location shift in $w(t, z_\infty)$ makes no change to $P(t, R(z_\infty))$, provided that the value of z_∞ is shifted by the same amount.

The formula for the Sips density is, (writing $z = z_\infty$, $R = R(z_\infty)$ and ignoring t),

$$P(R) = \frac{1}{TR(1-R)} \frac{\left[e^{\gamma+z} \cdot \frac{1-R}{R}\right]^a \cdot \sin(\Pi a)}{1 + 2\left[e^{\gamma+z} \cdot \frac{1-R}{R}\right]^a \cdot \cos(\Pi a) + \left[e^{\gamma+z} \cdot \frac{1-R}{R}\right]^{2a}} \tag{21}$$

When $z_\infty = -\gamma$, this density is symmetric. Figure 4 shows the effect of the parameter $a(t)$ on the shape of such a density. This figure is comparable to Figure 3, which showed the same densities for $P(t, Q)$. As before $a(t) = 1$ gives a discontinuous spike indicating total homogeneity. As $a(t)$ decreases towards 0 the central peak becomes reduced and disappears. The density becomes more and more trough like until, at $a(t) = 0$, it becomes vanishingly small at all values of $R(z_\infty)$ except 0 and 1, at which it is undefined.

The variance is

$$\mathrm{Var}_t[R(z_\infty)] = (1 - a(t)) \left[\frac{w(t, z_\infty)}{v(t)} \frac{1 - w(t, z_\infty)}{v(t)}\right] \tag{22}$$

OTHER AFFINITY DENSITIES:

Other affinity densities can be expressed on the metrics K, Q or $R(z_\infty)$. For example consider the negative exponential density on the K metric, defined above at Equation 6. The equivalent density on the Q metric is

$$P(t_0, Q) = \frac{e^{Q-d}}{\exp[e^{Q-d}]}$$ (23)

where $d = \text{Log } \mu(t_0, K)$.

The equivalent density on the $R(z_\infty)$ metric is (using the same conventions as in Equation 21)

$$P(R) = \frac{1}{e^{\gamma+z}(1-R)^2} \cdot \exp\left[\frac{-1}{e^{\gamma+z}} \cdot \frac{R}{(1-R)}\right]$$ (24)

9.4   Alterations to the Timecourse Model

The timecourse model, defined at Equation 1, operates on the assumption of antibody increasing at a rate essentially proportional to the affinity of interaction K, antigen concentration $x(t)$, and clonal antibody concentration $y(t, K)$. However, the model could be respecified on other metrics like those described in the previous section. Counterparts to Equation 1 exist, and the useful effect of persistence of the mean affinity will hold on other metrics also.

As an example, consider respecification on the metric $Q = \text{Log } K$

$$\frac{\partial y(t, Q)}{\partial t} = Ay(t_0, Q) + cQx(t)y(t, Q) - Ay(t, Q)$$ (25)

where $y(t, Q)$ is concentration of clonal antibody with affinity Q.

Other terms are defined as in Equation 1.

As Q can in theory take negative values, Equation 25 suggests tha tthe introduction of antigen would lead to the destruction of antibody with negative affinity. This seems to be against the spirit of the clonal selection theory, and raises the possibility of the absurdity of negative values of $y(t, Q)$ evolving over time. In order to avoid this, constraints on Q, $y(t, K)$ or $P(t, Q)$ would need to be introduced.

Respecification of the model in Equation 1 on the metric $R(z_\infty)$ gives

$$\frac{\partial y(t, R(z_\infty))}{\partial t} = Ay(t_0, R(z_\infty)) + cR(z_\infty)x(t)y(t, R(z_\infty)) - Ay(t, R(z_\infty))$$ (26)

where $y(t, R(z_\infty))$ is the concentration of antibody with affinity $R(z_\infty)$ at time t.

$R(z_\infty)$ is bounded in the range $(0, 1)$ but, since this encapsulates the whole spectrum of Q, it does not cause a practical problem. No negative values of $y(t, R(z_\infty))$ can evolve under Equation 26.

Consider the case where the initial saturation curve $w(t_0, z)$ is of the logistic form (Equation 17) with $\gamma(t) = \gamma(t_0)$. In the special case of Equation 26 with $A = 0$, it can be shown that the saturation curve remains logistic for all t.

$$w(t, z) = v(t)\frac{e^{a(\gamma(t)+z)}}{1 + e^{a(\gamma(t)+z)}}$$ (27)

The parameter a remains constant for all t, while $\gamma(t)$ is given by

$$\gamma(t) = \gamma(t_0)\left[c\left(\frac{1}{a} - 1\right) \int_{t_0}^{t} x(s)ds\right]$$ (28)

This model shows that the behaviour of an affinity density defined on the Q metric can sometimes be predicted from a timecourse model specified on the $R(z_\infty)$ metric.

Figure 5 shows an example of the evolution of $\gamma(t)$ for various possible values of a. The fact that a logistic saturation curve can be maintained under the timecourse model, albeit in the special case $A = 0$, gives some theoretical foundation to the empirical use of logistics. The model may be of practical use in delineating the early phase of an immune response, before antibody
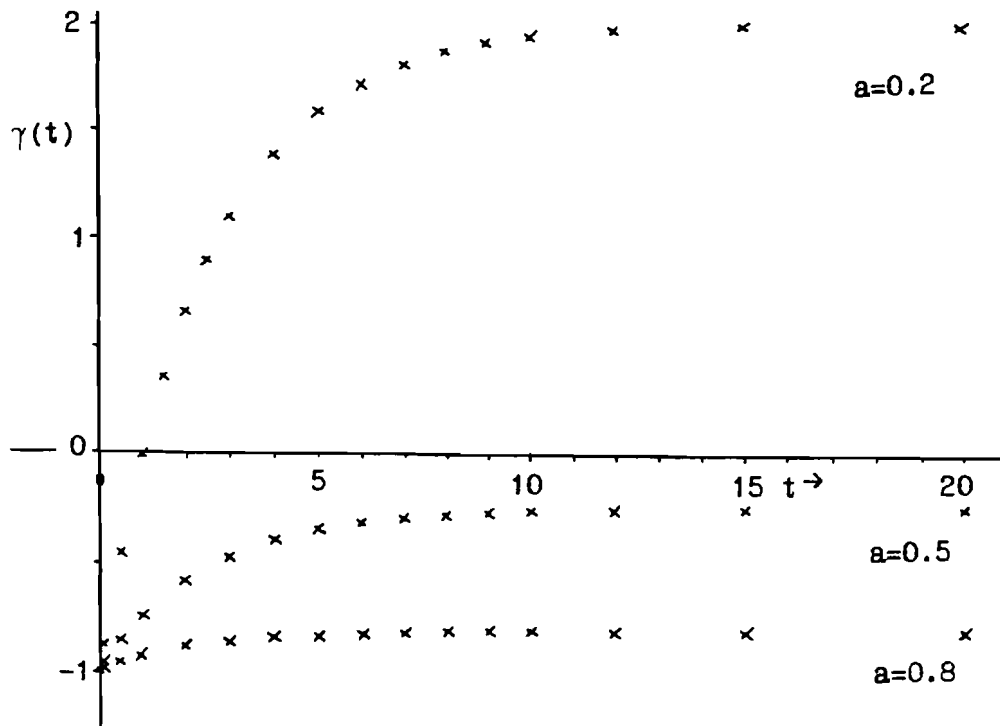
Figure 9.5. Evolution of mean affinity $\gamma(t)$ under the invariant logistic model (Equations 27, and 28). Vaccination at 0 days. $\lambda = 0.4$, $a = 0.2, 0.5$ and 0.8. $A = 0$. $\gamma(t_0) = -1$. $c = 0.01$. $x(0) = 30$.

levels start to decline from their peaks. It would be interesting to see whether this result could be generalised in some way to the case $A > 0$.

9.5 Conclusions

The $R(z_\infty)$ metric described above could be very useful for experimenters, because parameters of an underlying affinity density can be estimated directly from saturation curve data without specification of the functional form of the density. The argument leading to Equation 28 has also shown that timecourse models specified on this metric may have intersting properties.

It has been shown that the basic model described in Equation 1 can be modified to give classes of models that might be applicable to many kinds of immune timecourse data. The chief attraction of such models is the simplicity of the formulation, and hence the relative ease with which definitive results can be obtained. The true immune system is of course more complicated than the system I have described, but the approach could be used to provide Null Hypotheses against which data could be tested statistically. Such test would establish whether or not more complicated models were necessary.

The assumption of monovalent interaction between antibody and antigen is clearly an over-simplification, but the methods can be modified to take this into account [5]. Another practical problem arises where saturation data are available only at applied antigen concentrations, rather than free antigen concentrations at equilibrium. Again modifications to the methods can be suggested (e.g. see Meinert and McHugh [14]).

9.6   Acknowledgements

9.7   References

[1] Hingley, P.J. (1988) *Antibody affinity distribution based models for vaccine potency assessment.* In: *Theoretical Immunology.* A.S. Perelson (Ed.). Addison Wesley, Reading, Massachusetts. Part 1, p. 311.

[2] Yudkin, M. and R. Offord. (1973) *Comprehensible biochemistry.* Longman, London.

[3] Bell, G. (1970) *Mathematical model of clonal selection and antibody protection.* Journal of theoretical biology. **29**, p. 191.

[4] Bruni, C., et al. (1975) *A dynamical model of humoral immune response.* Mathematical Biosciences. **27**, p. 191.

[5] Hingley, P.J. (1985) *Problems in modelling the responses of animals to foot and mouth disease vaccines.* PhD Thesis, Univeristy of Reading.

[6] Hingley, P.J. and E.J. Ouldridge. (1985) *The use of a logistical model for the quantitative interpretation of indirect sandwich enzyme labeled immunosorbent assays (ELISA) for antibodies and antigens in foot and mouth disease.* Computers in Biology and Medicine. **15**, p. 137.

[7] Robard, D. (1974) *Statistical quality control and routine data processing for radioimmunoassays and immunordiometric assays.* Clinical chemistry. **20**, p. 1255.

[8] Ruppert, D., et al. (1989) *A transformation / weighting model for estimating Michaelis-Menten parameters.* Biometrics. **45**, p. 637.

[9] Hsu, C.S. (1988) *Estimation of antibody affinity via reduced order modelling.* In: *Theoretical Immunology.* A.S. Perelson (Ed.), Addison Wesley, Reading, Massachusetts. Part 2, p. 135.

[10] Sips, R. (1948) *On the structure of a catalyst surface.* Journal of Chemical Physics. **16**, p. 490.

[11] Bruni, C., et al. (1976) *Derivation of antibody distribution from experimental binding data.* Journal of theoretical biology. **61**, p. 143.

[12] DeGroot, M.H. (1986) *Probability and Statistics.* Second Edition. Addison Wesley, Reading, Massachusetts.

[13] Eisen, H.N. and G.W. Siskind. (1964) *Variations in affinities of antibodies during the immune response.* Biochemistry. **3**, p. 966.

[14] Meinert, C.L. and R.B. McHugh. (1968) *The biometry of isotope displacement immunologic microassay.* Mathematical biosciences. **2**, p. 319.

Chapter 10

Specific Antibodies and Antibody-Producing Cells Upon Experimental Influenza

B.L. Voitsechovsky, I.I. Agafonova, L.F. Meringova
I. Dukhin, I.V. Yakovleva
Institute of Experimental Medicine
AMS USSR, Leningrad

Introduction

In order to base the principles of immunopathological state prognosis and methods for their correction it is necessary to model the state of immune net nodes and their interaction [1, 2, 3]. One of the serious problems on the way of elaborating such a system is the inability of direct experimental studying of the humoral specific immunity. The mathematical model which allows to derive the antibody affinity distribution that is a quantitative characteristic of specific immunoglobulins functional activity [4].

The present study is an attempt to describe in terms of experimental-mathematical modelling the specific humoral immune response upon viral infection.

Methods of anti-influenza antibodies experimental analysis

The virological part of this work containing the infection of mice F1 (CBA x C57/B1) by sublethal influenza virus doses and control of influenza virus A/PR8 (H1N1) reproduction was performed in accordance with [5]. The rate of specific immunoglobulins IgG in sera was assayed by second antibody method ELISA in accordance with [6]. Experimental data for binding plots were obtained by ELISA method of successive saturation in accordance with [7]. Modifications of above mentioned methods for the case of use of native viral particles as antigens are reported in [8].

Conditions of each experiment (initial concentrations of antigens and antibodies) were chosen in such a way that by the known method sensitiveness the maximal number of significant points on binding plot was provided.

Methods of experimental verification of mathematical modelling results

The physical separation of serum immunoglobulin compounds was carried out by method of high-effective gel-penetrating fluid chromatography in accordance with [9]. Analysis of influenza virus specific antibodies being synthesized directly by antibody-producing cells (APC) was performed by ELISPOT method in accordance with [10]. Nitrocellulose filters after ELISPOT were filtered by two-probes method [11] to obtain the experimental function of parameter distribution that correlates with affinity of antibodies being investigated. Then APC frequently distributions vs. concentration and affinity of produced antibodies were derived by commonly used statistical methods.

Mathematical model

The affinity distribution of antibodies was carried out on the basis of experimental binding plots. The model of the one-stage binding reaction of pseudo-first order between N-valent antigen and heterogeneous antibody receptor population was chosen [12]. The ratio of filled antibody receptors sites Sb to their total amount St can be expressed in accordance with this model as follows:

$$R = \frac{Sb}{St} = \int_0^\infty \frac{KH}{1 + KH} p(K) dK \qquad (10.1)$$

where H is the free antigen concentration, $p(K)$ - the probability density distribution of receptors vs. affinity K (i.e. fraction of receptors with affinities between K1 and K2 is $\int_{K1}^{K2} p(K) dK$).

The model of one-stage binding reaction between bivalent antibody IgG and N-valent antigent was chosen because for the influenza virus the bivalent binding of antibody is little probable [13]. In this case we may assume all N virus antigenic receptors being independent and take N^*H in equation (1).

Experimental binding plots reflect the dependence of R on H. So the needed distribution $p(K)$ can be obtained by conversion of integral equation (1) that is Stieltjes transform of $p(k)$ with parameter $1/H$. Then if the analytical form of $R(H)$ is present the distribution $p(K)$ can be calculated by well-known conversion formula. However we cannot define the function $R(H)$ analytically from experimental data. The form of $R(H)$ proposed in [12, 14] as a generalization of Sips formula [15] and used there for calculations in hapten-univalent antibody system proved to be unsuccessful for the case of virus-specific IgG reaction. Therefore we used the numerical techniques to solve eq. (1) as in [16, 17]. The distribution $p(K)$ was written as a weighed sum of special functions with following determination of weights by general curve-fitting methods.

As a base function for development of $p(K)$ in series the Gaussian log-normal distribution has been chosen:

$$f(lnK) = \frac{1}{\sqrt{2\pi}\sigma} \exp\{-\frac{(lnK - lnK\sigma)^2}{2\sigma^2}\} \qquad (10.2)$$

The available experimental data show that the antibody affinity distribution is a multimodel [18]. Then the distribution $p(K)$ can be defined by the following sum

$$p(K) = \sum_{i=1}^{L} A_i f(K; lnK\sigma_i),$$

moreover from the $\int_0^\infty p(K) dK = 1$ follows $\sum_{i=1}^{L} A_i = 1$.

Parameters A_i in $K^{oi}, i = 1, \ldots, L$ were estimated by minimization of the function Φ:

$$\Phi = \sum_{j=1}^{M} (\hat{R}_j - \int_0^\infty \frac{KH}{1 + KH_j} \cdot p(K) dK)^2 / d_j^2, \qquad (10.3)$$

where M is experimental points number, R_j-experimental values of antibody bound receptor fraction for antigen concentration H_j, d_j-experimental error for R_j. Search of minimum of (3) was realized by the Nelder-Mead method (nonlinear simplex).

The stochastic variable $Z = (\hat{R} - R \bmod)/d$ will be normally distributed with zero mean and dispersion $= 1$. Then function $\Phi = \sum_{j=1}^{M} Z_j^2$ will be distributed as χ^2. Therefore the coincidence of Φ-value with χ^2-value for given freedom degrees number and significance level can serve as a validity criterium for the chosen model. Modes number L and antigen valence N were selected also from the condition of minimum χ^2.

The reliability, reproductability and sensitivity of the proposed method on the set of generated ideal data was examined. Details of these computational simulations will be published. All computations were performed on IBM-PC-AT using program package "Immunoassay Software Library" written on Turbo-Pascal 5.0.

Mathematical modelling results and their experimental verification

Affinity distribution in noninfected animals sera.

The choice of this investigation object was caused by well-known fact about the existence of natural antibodies to influenza virus in sera of noninfected animals. Affinity distribution analysis has shown that such sera contains two antibody subpopulations with mean binding constants Kb near 10^4 and 10^6 1/mol related one to another as 2:1 (Figure 1).

It should be emphasized that in all these the value χ^2 was abnormally large (> 100) what points to unsufficiency of accepted model to real binding data. It practically did not decrease after change of any initial conditions (modes number, initial values of Kb, valence). This fact can be considered as evidence of nonspecific character of binding. To find out the nature of these proteins the physical separation of sera being investigated was executed. The experimental results allowed to determine that noninfected animal sera contain 2 fractions of immunoglobulin-like proteins able to bind the influenza virus: (A) proteins with molecular mass (MM) of 40-80 KDa and with Kb near 10^4 1/mol and B) proteins with MM of 100-200 KDa and Kb 10^6 1/mol. A-fraction proteins did not react with protein A St. Aureus and could not be totally eliminated from IgG-containing B-fraction by gel-penetrating chromatography. This way the results of physical separation of material being studied have confirmed those obtained using mathematical modeling, and namely that noninfected animal sera contain 2 subpopulation of proteins related immunochemically to IgG and capable to unspecific low-affinity binding with influenza virus surface antigens. The structure and origin of these "natural" antiviral antibodies will be investigated further, however basing on data reported here one can suggest that these substances differ from IgG appearing during immune response upon infection. They could be both immuno-competent cell products (antigen-recognizing receptors of IgG-restricted T- or B-cells [19]) and products of nonlimphoid-type cells like R-proteins [20].

IgG affinity distribution in sera of infected animals

Our mathematical model was used to describe the virions binding by specific IgG during infection process. Minimal values of consistency criterium ($\chi^2 < 10$) were achieved for antigen valence of 5 and mode number $L = 1, \ldots, 3$. During the observation period (21 days) three antibody subpopulations different by their binding constant were discovered in sera of infected animals. Their mean values were in intervals of (A) $10^4 - 10^5$, (B) $10^6 - 10^7$ and (C) $10^{10} - 10^{12}$ 1/mol. An example of three-model affinity distribution of serum IgG, registered on 9th day after infection is shown in Figure 2. These data were verified by the results of experimental determination of subpopulational structure of antibodies produced by APC during the first 2 hours after their extraction from animal spleen.

The method being used here consists of multiparameter estimation of each spot formed by individual APC and following determination of appearance frequency distribution vs. parameters that correlate with antibody affinity. (The details are described in [21].)

APC frequency distribution vs. affinity is given in Figure 3. Comparison of Figures 2 and 3 shows that discovered in this experiment serum antibody subpopulations were formed by nearly 10 APC clons which could be combined in 3 groups. Consideration of analogous data being obtained on other days after infection has delivered comparable results: unimodel antibody distribution corresponds to 1-2 clon groups in APC preparations, bimodel one - to 2-4 groups. The total number of active clons never exceeded 20, and one group consisted of 1-5 clons.

These results have confirmed the efficiency of the used method for describing affinity distributions in heterogeneous populations of virus-specific IgG.

Serum antibody affinity distribution in the course of infection process

The analysis of serum antibody distribution (tests were picked daily for 21 days from the infection) has shown that during the infection period successive substitution of initial antibody subpopulations by subpopulations with higher affinity occurs. The total dynamics of this process was as follows (Figure 4): beginning on 6-7th day after infection (first reliable registration of specific IgG) the increase of subpopulation B and decrease of subpopulation A (immunoglobulin-like proteins with MM near 60 KDa) occurred. On 9-10th day after infection appeared for the first time on the 13th day became statistically significant a new subpopulation of high-affinity antibodies (C). Maximal amount of these antibodies was registered on 14-15th day, from the 17th day their reliable decrease was observed.

This way it was determined that in mice sera in the course of 21 days after infection with influenza virus 3 subpopulations of antigen-binding proteins belonging by their immunochemical properties to superfamily of immunoglobulins [22] can be distinguished. Proteins that belong to the first of these populations seem not to be the "true" immunoglobulins, they have low affinities and MM in the range of 40-80 KDa and are present also in sera of noninfected animals. The second subpopulation belongs to the true IgG fraction, it has moderate affinity values and occurs in different amounts both in noninfected and in infected animals during the period of observation. The third one appears on the top of humoral immune response and contains proteins with Kb near the maximum possible value. Antibodies similar by their affinity properties to those from the third subpopulation were found in sera of rabbits which were immunized by washed splenocytes from infected mice. This fact can serve as an indirect indication of antibody specificy to the viral antigens related to the immunocompetent cell membranes [5].

Discussion

Dynamics of humoral immunity upon viral infection is a complex cyclic process [23] including both synthesis of different by affinity antibody subpopulations and their elimination during interaction with antigens [8]. In this situation the standard statistical approach seems to be unsufficient to obtain the objective immune state evaluations. To solve this problem the study of functional structure of heterogeneous population of humoral effectors is needed. The mathematical modelling of affinity distribution using experimental binding plots is a real possibility to obtain the solution because the direct experimental measure of affinity runs into great difficulties. The proposed method was adapted specially to the influenza virus - antiviral antibodies system. Data obtained on each stage of the investigation were verified by means of alternative physiochemical and immunochemical methods. Results of this study allowed to reveal the new important features of the humoral immune response upon influenza infection.

The humoral immune response phenomena upon viral infection found out in this investigation can be explained in terms of recent clonal selection and immune network theories [21]. So, for example, two "natural antibody" subpopulations in noninfected animals can be considered as initial antigen-recognizing immune net components determining the "virgin state of the immune system" (by Hofmann, [24]). We can propose here the following mechanism of replacing of active subpopulations. Antibody affinity to viral antigens is an activity regulator for APC clons group, which synthesize these antibodies [25]. After increase of affinity level (in consequence of clons selection inside the group) up to some maximal value being a physiological limit for the given group it stops its production according to clonal-deletional tolerence model [26]. A new APC clon with significantly higher initial affinity level to stimulus antigens becomes involved into immune reponse. "Step" of affinity value by such a replace of active groups was according to our data near 10^2 1/mol. Thus the results being presented in this work can be regarded as an evidence of humoral immunity with discrete structure. Bernett considered clon as an elementary unit of immune system, however, taking into account the modern ideas about clonal activation mechanism one can assume that such an elementary unit will be a family of clons carrying the regulative idiotops [27]. Data about antibody subpopulations structure being presented on Figures 3 and 4 confirm this assumption. It should be noted that in immune response caused by such a complex antigen with $MM > 100MDa$ (influenza virus) only a small number of APC clon work. Virus itself demonstrates a rather low valence value $N = 5$. However these data were experimentally confirmed in [28, 13, 29] having shown that independently of antigen structure complexity (hapten, protein, bacterium) the number of specific to the given antigen antibody subpopulations is in vivo always not large and doesn't exceed some units or some tens. As a mechanism providing such a minimization of antibody spectrum one can consider the well-known phenomenon of supression of idiotype selection by mature APC [30].

The assumptions being presented here need of course the additional experimental control, but already now they can serve as a base for system analysis of humoral immune response under viral infection.

Fig. 1.

Fig. 2.

APC Affinity Distribution at 9 Day of Infection

X – Lg(Ks/H) ; Y – Clone's Weights

Fig. 3.

Lg of Dissotiation Constant

Days of Influenza Infection
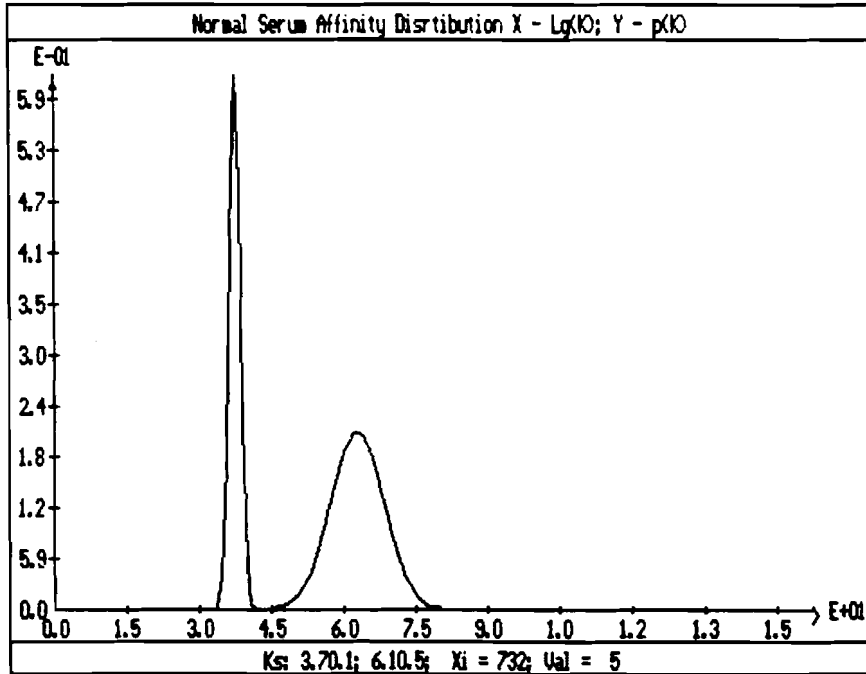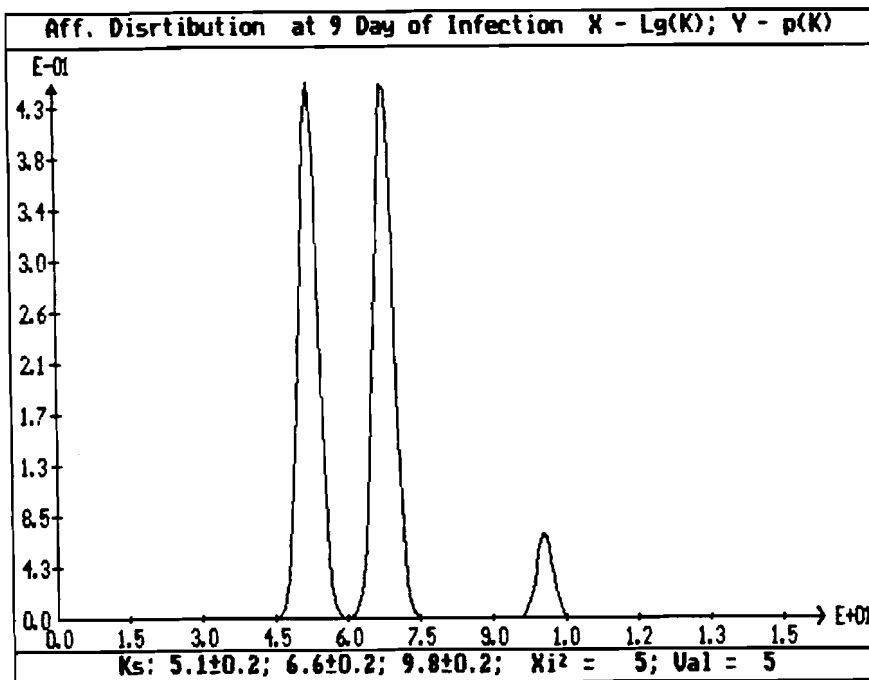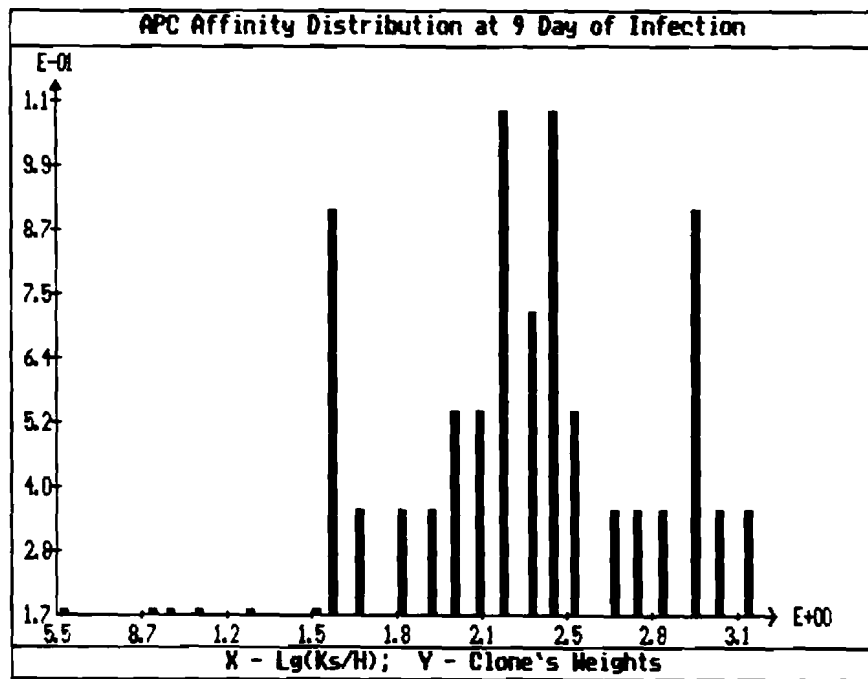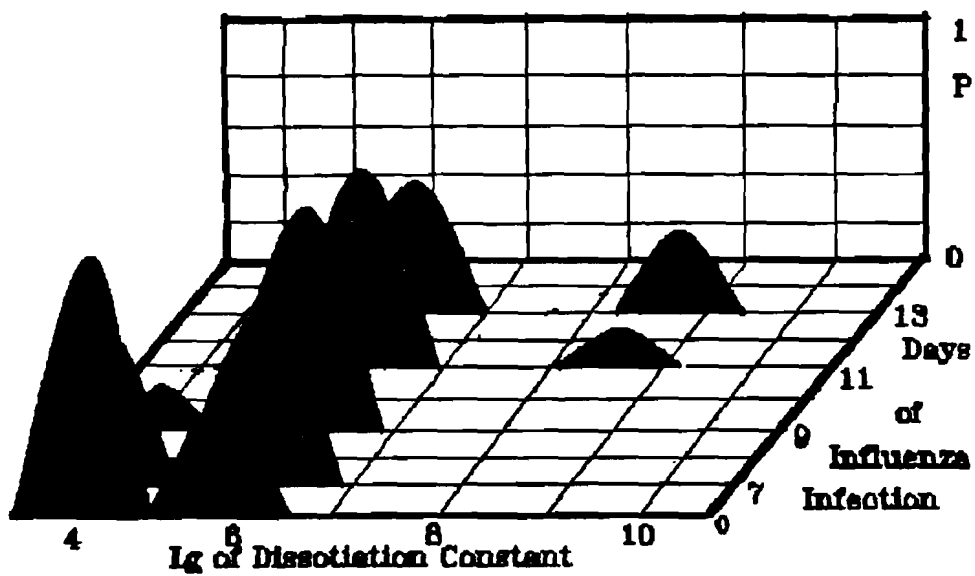
Fig.4

Bibliography

[1] Mohler, R.R. Bruni, K. et al. IEEE Trans. 1980, Vol. 68, Nr. 8, pp. 36-26

[2] Poljak, R.Y., Dubrovina, T.Y. et al. "Mathematical models in immunology and medicine" M., 1986, 235 pp.

[3] Marchuk, G.I., Petrov, R.W. "Wychislitelnye prozessy i systemy" M., 1983 pp. 5 -19

[4] Brown, S.E., Howard, C.R., et al. J. Immunol. Meth. 1984, Vol. 42, pp. 41-48

[5] Poljak, R.Y., Belykh, L.N., et al. "Strategia wosbuditelja w organisme chosiaina" 1987, pp. 10-24

[6] Voitsechovsky, B.L. "Twerdophasny immunofermentny analis" L., 1988, pp. 42-58

[7] Friguet, B. et al. J. Immunol. Meth. 1985, No. 77, pp.305-319

[8] Meringiva, L.F., Voitsechovsky, B.L., et al. "Immunology", 1989, No. 6, pp. ooo

[9] Thorell, L., Blomback, B. Thombosis Res. 1984, Vol. 35, pp. 431-450

[10] Jones, D.D., Ada, G.L. Virology, 1986, Vol. 60, pp. 64-70

[11] Verhoturov, W.N., Rubin, A.B. "Awtomatizatia biophisicheskich issledovaniy" M., 1988, pp. 100-200

[12] Bruni, K., Gandolfi, A., et al. "Mathematical models in immunology and medicine" MM., 1986, pp. 56-70

[13] Karulin, A.Y., Egorov, A.M., et al. Biochimia, 1986, Vol. 5, No. 5, pp. 746-754

[14] Thakur, A.K., Munson, P.J., et al. Analyt. Biochem. 1980, Vol. 103, pp. 240-254

[15] Sips, R. J. Chem. Phys. 1948, Vol. 16, pp. 490-497

[16] Mukkur, T.K.S., Szewezuv, M.R., et al. Immunochemistry, 1974, Vol. 11, pp. 9-13

[17] Evwin, P.M., Aladjem, E., Immunochemistry, 1976, Vol. 13, pp. 873-883

[18] Scuitto, E., Garat, B. et al. Mol. Immunol. 1987, Vol. 24, pp. 577-585

[19] Fathman, C.G., et al. J. Exp. Med. 1982, Vol. 156, pp. 361-370

[20] Kulberg, A.Y., Elistratova, I.A., et al. Immunology, 1986, No. 2, pp. 14-18

[21] Voitsechovsky, B.L., Meringova, L.F., et al. Westnik AMN, SSSR, 1989, No. 11, pp. 57-64

[22] Manko, W.M., Haitow, R.M., Uspechi nauki i techniki, Ser. Immunology, M. 1987, Vol. 18, 238 pp.

[23] Jones, P.D., Ada, G.L., "Cell Immunol." 1987, Vol. 109, pp. 53-64

[24] Hoffman, G.W., Boca Raton: CRC Press, 1982, pp. 137-162

[25] Gerson, R.K., Paul, W.E. J. Immunol. 1971, Vol. 106, pp. 872-874

[26] Kohler, H. et al. Eur. J. Immunol. 1980, Vol. 10, pp. 810-815

[27] Paul, W.E., Bona, C. Immunol. Today 1982, Vol. 3, pp. 230-234

[28] Herman, N.E., Siskind, G.W. Biochemistry 1974, Vol. 3, No. 7, pp. 996-1008

[29] Lewy, M.M. Immunology, 1984, No. 1, pp. 18-22

[30] Goild, E.A., et al. Eur. J. Immunol. 1980, Vol. 10, pp. 810-818

Chapter 11

Analysis of Antibody Binding To Conformation-Dependent Epitopes

A. Gandolfi
Istituto di Analisi dei Sistemi ed Informatica del CNR
Viale Manzoni 30, 00185 Roma, Italy

Roberto Strom
Dipartimento di Biopatologia Umana, Universita di Roma
Viale Regina Elena 324, 00161 Roma, Italy

11.1 Introduction

It is well known, that, in native proteins, some antigenic determinants depend critically on the tertiary and/or quaternary structure, rather than on the primary protein sequence (see, for instance, the studies on lysozyme [1,2], myoglobin [3,4], β-galactosidase [5]). These "conformation-dependent" epitopes appear to consist of adjacent in space aminoacid residues which are far in linear sequence, or belong to distinct protomers in a multimeric complex.

The possible reversibility of the processes (intramolecular rearrangement or bimolecular association) which lead to the existence of a conformation- dependent epitope, and the affinity (low, though often still measurable) of the antibody binding site toward the isolated constituents of such a complex antigenic determinant, introduce other thermodynamic and kinetic parameters in the usual description of the interaction between paratope and epitope. This interaction, on the other hand, can be expected to influence the structure of the antigen, by inducing or increasing the stability of the conformation which carries the epitope with the highest reactivity.

Since the factors controlling the existence of a given conformation in a single polypeptide chain would require a rather detailed model, in this paper we restricted our attention to the interaction of antibodies (or receptors) with complex epitopes arising upon association of two protomers into a dimeric structure. The general description that we devised can adequately be adapted to a variety of cases. In particular, we considered: a) the control exerted by specific antibodies on the association of dimeric, enzymatically inactive, β-galactosidase into active tetramers; b) the binding to T-cell receptors of immunogenic peptides that combine, on the surface of Antigen-Presenting cells, with major histocompatibility complex (MHC) type II molecules.

11.2 General model

Let us consider a system of two associating protomers X and H, in which association generates a new epitope bringing a certain region on the X molecule adjacent to another one on the H

molecule. We want to investigate the interaction of this conformational epitope with the binding of a specific antibody (or receptor) R (see Fig. 1a). We will distinguish, within the binding site, two distinct subsites specific for the two constituents of the conformational epitope, and we will assume that the interactions of isolated protomers with the corresponding subsites cannot be disregarded. We will assume, moreover, reversibility and, for simplicity, independency of bond formation. As the only exception to independency, there will be, anyhow, steric impairment to the full association between protomers which are both bound to separate binding sites. Fig. 1b summarizes the reactions taking place in the system. In this scheme the different complexes are represented by vectors, and the presence or absence, within a given complex, of bonds between X and H, X and R, or H and R, is indicated by symbols 1 or 0, respectively, in the first, second or third component of the vector.

Let K_1 be the imolecular association constant between protomers X and H; K_2 and K_3 be the bimolecular association constants of X and H with their respective subsites on the binding site; K'_1, K'_2 and K'_3 be the dimensionless equilibrium constants regulating, within the ternary $X - H - R$ complex, the monomolecular bond formation between X and H, X and R, and H and R respectively. From mass action law, at equilibrium, we have:

$$C_{100} = K_1 X H \tag{11.1}$$

$$C_{010} = K_2 X R \tag{11.2}$$

$$C_{001} = K_3 H R \tag{11.3}$$

$$C_{110} = K_1 K_2 X H R \tag{11.4}$$

$$C_{011} = K_2 K_3 X H R \tag{11.5}$$

$$C_{101} = K_1 K_3 X H R \tag{11.6}$$

$$C_{111} = K'_3 K_1 K_2 X H R = K'_2 K K_1 K_3 X H R, \tag{11.7}$$

where C_{ijk} denotes the concentration of complex (ijk), and X, H and R denote the concentrations of free X molecules, free H molecules and free binding sites, respectively. As it is apparent from (7), detailed equilibrium implies some relations among parameters, so that only 4 parameters are independent. We introduce the parameter K^*, which represents the association constant of the conformational epitope with the binding site, defined by

$$K^* = K'_3 K_2 = K'_2 K_3 = K'_1 \frac{K_2 K_3}{K_1}.$$

Thus we will write

$$C_{111} = K^* K_1 X H R, \tag{11.8}$$

and the parameters of the system will be, therefore, K_1, K_2, K_3 and K^*.

Let us denote by X_t, H_t and R_t the total concentrations of X protomers, H protomers and binding sites, respectively. From mass conservation, it follows that

$$(1 + K_1 H)X + [K_2 X + K_2 K_3 X H + (K_2 + K_3 + K^*)K_1 X H]R = X_t \tag{11.9}$$

$$(1 + K_1 X)H + [K_3 H + K_2 K_3 X H + (K_2 + K_3 + K^*)K_1 X H]R = H_t \tag{11.10}$$

$$R + [K_2 X + K_3 H + K_2 K_3 X H + (K_2 + K_3 + K^*)K_1 X H]R = R_t. \tag{11.11}$$

By solving eqs. (8-10) in the variables X, H and R, and taking into account eqs. (1-7), a complete description of the system can be achieved. Without solving eqs. (8-10), however, some properties of the system can be established.

An increase, starting from zero, in the concentration of binding sites is obvious paralleled by a decrease in the concentration of free conformational epitopes, and by an increase in the concentration of bound epitopes. There is however, if the value of K^* is sufficiently large,

also an *increase* in the concentration of associated protomers (i.e. in the total concentration of conformational epitopes), since the combining site can cross-link the protomers and thus stabilize the $X - H$ complex. Formally, by defining $C^* = C_{100} + C_{110} + C_{101} + C_{111}$, and taking into account that, from eq. (10), $dR/dR_t > 0$, it can be shown, by computing $(dXH/dR)_{R=0}$ from eqs. (8) and (9), that

$$\frac{dC^*}{dR_t}dR_{t|R_t=0} > 0 \qquad (11.12)$$

if and only if

$$K^* > K_2K_3\frac{-1 + \sqrt{\alpha^2 - 4K_1^2X_tH_t}}{K_1} \qquad (11.13)$$

where

$$\alpha = 1 + K_1(X_t + H_t). \qquad (11.14)$$

When instead $R_t \to \infty$, since from eqs. (8) and (9) it follows that X and H are both $O(1/R)$ s $R \to \infty$, we have

$$lim_{R_t \to \infty}C^* = 0. \qquad (11.15)$$

In a large excess of binding sites, indeed, isolated protomers will be bound and the association between protomers will then be prevented. Note that, if the steric impairment on the association of bound protomers was not complete, we would have $lim_{R_t \to \infty}C^* > 0$.

We can also analyze how, at fixed concentrations of the protomers, the level of occupancy of binding sites depends on the overall site concentration. Let us consider the ratio R_b/R, where $R_b = R_t - R$ denotes the concentration of occupied binding sites. From eqs. (8-10) it can be easily derived that for $R_t \to 0$ it is

$$lim_{R_t \to 0}\frac{K_2K_3}{K_1} + K^*)\frac{\alpha - \sqrt{\alpha^2 - 4K_1^2X_tH_t}}{2K_1} + K_2X_t + K_3H_t \qquad (11.16)$$

where α is given by (13). Focussing our attention on the dependence of this limit value, nu_0, on the value of K_1 in the simple case of $X_t = H_t = n_t$, we can see that

$$lim_{K_1 \to 0}\nu_0 = (K_2 + K_3)n_t + K_2K_3n_t^2$$

and

$$lim_{K_1 \to 0}\nu_0 = (K_2 + K_3 + K^*)n_t.$$

Thus $lim_{K_1 \to \infty}nu_0 > lim_{K_1 \to 0}nu_0 > lim_{K_1 \to 0}nu_0$ if and only if $K^* > K_2K_3n_t$. Only under this condition, therefore, higher K_1 values favor occupancy of binding sites in the zone of protomers excess (see Fig. 2, where R_b/R is plotted vs. $R_b/2n_t$). For $R_t \to \infty$, instead, R_b tends to $X_t + H_t$ and the ratio R_b/R tends, obviously, to zero.

11.3   Antibody-mediated activation of a defective β-galactosidase

It has been shown in 1968, by Rotman and Celada [6], that antibodies directed against bacterial-galactosidase are able to induce a striking recovery of the enzymatic activity of defective (quasi-inactive) enzyme produced by mutant bacterial strains. While the active enzyme is a tetramer consisting of four identical protomers, the defective macromolecule is unstable at room temperature and tends to dissociate into dimers [7]. Monoclonal antibodies endowed with activating capacity have also been described [8,9] and their affinity for the tetramer, when measured, has been found substantially higher than for the dimer [9]. The activating effect exerted by the antibody could therefore be mediated by an association of the dimeric species into tetramers, occurring presumably through the binding of a specific antibody site to an epitope depending on

the tetrameric conformation [10]—actual cross-linking of dimers by divalent antibodies excluded by the activating effect of monovalent Fab fragments [11].

According to this working hypothesis, the activation phenomenon can be analyzed by a suitable adaptation of the previously described model, assuming that: i) two dimeric *beta*-galactosidase molecules can (weakly) associate and, upon association, generate a complex epitope constitued of two identical protomers, the defective macromolecule is undstable at room temperature and tends to dissociate into dimers [7]. Monoclonal antibodies endowed with activating capacity have also been described [8,9] and their affinity for the tetramer, when measured, has been found substantially higher than for the dimer [9]. The activating effect exerted by the antibody could therefore be mediated by an association of the dimeric species into tetramers, occurring presumably through the binding of a specific antibody site to an epitope depending on the tetrameric conformation [10]—actual cross-linking of dimers by divalent antibodies being excluded by the activating effect of monovalent Fab fragments [11].

According to this working hypothesis, the activation phenomenon can be analyzed by a suitable adaptation of the previously described model, assuming that: i) two dimeric *beta*-galactosidase molecules can (weakly) associate, upon association, generate a complex epitope constitued of two identical subepitopes; ii) the binding sites of the activating antibodies carry two identical subsites, each capable of binding a subepitope; iii) the level of enzyme activity is proportional to the actual concentration of tetrameric molecules. Let K_1 be the association constant between dimers; K be the intrinsic association constant between subepitopes and subsites; K^* be the equilibrium constant among free tetramers, free binding sites and tetramers bound to both the subsites of a binding site. Still assuming the hypothesis of independency of bond formation as stated in Section 2, the concentration C^* of tetramers, at equilibrium, will be given by

$$C^* = [1 + (4K + K^*)R]K_1X^2, \tag{11.17}$$

where X and R denote now the concentrations of free dimers and of free activating binding sites, respectively. These concentrations satisfy the following conservations equations:

$$X + 2K_1X^2 + [2KX + 2K^2X^2 + 2(4K + K^*)K_1X^2]R = X_t \tag{11.18}$$

$$R + [2KX + K^2X^2 + (4K + K^*)K_1X^2]R = R_t, \tag{11.19}$$

where X_t and R_t are the total concentrations of dimers and of activating binding sites, respectively.

As expected from properties (11) and (14) of the general model, C^* first will increase with R_t, provided that K^* have suitable values, and then, for increasing large values of R_t, will tend to zero. Fig. 3 shows how the ratio between tetramer and total dimer concentrations varies as a function of the overall concentration of antibody sites. The curves were computed according to eqs. (16-18), with values of parameters reasonably chosen with respect to the experimental knowledge. A several-fold activation of the enzyme can therefore be accounted for, followed by an inhibiting effect of antibody excess. Note that the shape of the activation curve depends also on the concentration of defective enzyme: such a dependence could be useful for an experimental validation of this model. For a qualitative comparison, in Fig. 3 are reported two experimental activation curves obtained using different antisera. It is possible to observe in one case (mouse antiserum) an activity decrease at high antibody concentrations, as predicted by the model; in the other case (rabbit antiserum), such a decrease cannot be excluded at antibody concentrations higher than the maximal value used in the experiment.

11.4   Recognition of peptide-MHC molecule complex by *T*-cell receptors

Several studies indicate that, in *T*-cell-mediated humoral immune response, the antigen is not capable by itself of triggering *T*-helper cells: relatively small peptides must be generated by

intracellular processing of the antigen [12, 13], and can stimulate T-cells upon presentation on the surface of Antigen-Presenting cells (AP-cells) in association with type II MHC molecules [14, 15]. The role of the MHC molecule is not that of a mere presentation of the peptide, specific MHC baminoacid residues being actively involved in the interaction with the T-cell receptors [16]. The receptor sites on the surface of a given T-cell subset recognize indeed a complex epitope, resulting from an adequate spatial arrangement of some residues of the peptide and some other residues of the MHC molecule [17, 18].

The binding of T-cell receptors to this new epitope, if the association between peptides and MHC molecules occurs on the AP-cell surface, could therefore be analyzed by our model of a ternary interacting system. Since however such a binding occurs in the contact region between T-cells and AP-cells, and the resulting bonds lead to links between the cells, our model must be inserted in a description of cell-to cell adhesion. Bell et al. [19] have studied, by a thermodynamic approach, how formation of reversible bonds between one pair of complementary molecules compete with repulsion between cells, assuming that free and bound species behave as ideal solutes on the membrane, and that the repulsive force is due to compenetration and compression of cellular glycocalices. We will refer to this simple model; we therefore have not considered the possible lateral mobility of the molecules responsible for the repulsive forces [20], nor have we taken into account the mechanical work that must be done to deform the cells [21, 22].

Let X be an immunogenic peptide, H the MHC molecule able to associate with X, and R the T-cell receptor; X and H be mobile on the AP-cell surface and R be mobile on the T-cell surface. When a T-cell is in contact with an AP-cell, the interactions among X, H and R can be described according to the scheme of Fig. 1b, taking into account that formation of the peptide-MHC molecule complex takes places on the whole AP-cell surface, while the interactions with T-cell receptors occur in the (two dimensional) contact region. Let us assume that all complexes involving R be effective links between T and AP-cells and that only these molecular bridges cause cell adhesion. Since bridges must be stretched to exert the adhesion forces, and since different types of molecular bridges can be present, with possibly different elastic properties and different unstressed lengths, a general description of the equilibrium state is rather complicated. As a first though rather crude approximation, let us suppose that all bridges have the same elastic constant κ and unstressed length L. Let us assume that, in the unstressed state, there still be independency of bond formation. The free energy function for the closed system containing two adhering cells, taking into account the energy of molecular stress and the energy of cell repulsion, can then be written as in [19]. Since the free energy at equilibrium attains a local minimum, the following equation can be derived for the equilibrium state:

$$A_1(1 + K_1 H)X + A[R_b - \nu(S)K_3 H R] = N_x \tag{11.20}$$

$$A_1(1 + K_1 X)H + A[R_b - \nu(S)K_2 X R] = N_H \tag{11.21}$$

$$A_2 R + AR_b = N_R \tag{11.22}$$

$$\frac{\Gamma(S)}{kT} = R_b \tag{11.23}$$

$$-\frac{d\Gamma}{dS} = \kappa(S - L)R_b \tag{11.24}$$

where

$$R_b = \nu(S)[K_2 X + K_3 H + K_2 K_3 X H + (K_2 + K_3 + K^*)K_1 X H]R \tag{11.25}$$

$$\nu(S) = exp\left[-\frac{1}{2}\frac{\kappa}{kT}(S - L)^2\right]. \tag{11.26}$$

In the above equations, κ is the Boltzmann constant and T the absolute temperature; N_X and N_H are the total numbers of X and H molecules on the AP-cell surface; N_R is the total number of receptor on the T-cell surface; X, H and R are the surface concentrations of free X, H and

R molecules; A_1 and A_2 are the areas of the AP-cell and T-cell surface, respectively; A is the area of the contact region; S is the separation distance between cells; K_1, K_2, K_3 and K^* are the equilibrium constants, as defined in Sect. 2, for bond formation in the unstressed state (i.e. when $S = L$). $\Gamma(S)$ denotes the potential energy (*per* unit area of contact) of cell repulsion, at a separation distance S. A suitable expression for Γ, depending on glycocalix parameters, is given in [19]. Equations (19-21) express maxx conservation; equation (22) represents the balance between the pressures, on the boundary of the contact region, due to cell repulsion and to the concentration of bridging bonds; equation (23) expresses the balance of forces. The factor $\nu(S)$ takes into account the decrease of bond stability due to the stretching of the complexes.

The above equations, in the variables, S, A, X, H and R, describe the interaction between T-cell and AP-cell when no constraint is imposed on the size of the contact region. The separation distance can be computed from eqs. (22) and (23) and its value, denoted by S, depends only on κ, L and on the parameters of Γ. (19-22), instead, can lack in some cases any solution with $A > 0$. From eqs. (19-21) and (24) it follows that, when $A > 0$, $R_b < lim_{A\to 0}R_b$, so that there is an admissible solution if and only if

$$\frac{\Gamma(\hat{S})}{kT\nu(\hat{S})} < lim_{A\to 0}R_b.$$

Denoting by X_t, H_t and R_t, now, the $N_X/A_1, N_H/A_1$ and N_R/A_2 ratios respectively, adhesion between T-cells and AP-cells can occur if and only if

$$\frac{\Gamma(\hat{S})}{kT\nu(\hat{S})} < y, \tag{11.27}$$

where

$$y = \left[(\frac{K_2K_3}{K_1} + K^*)\frac{\alpha - \sqrt{\alpha^2 - 4K_1^2X_tH_t}}{2K_1} + K_2X_t + K_3H_t \right] R_t, \tag{11.28}$$

and

$$\alpha = 1 + K_1(X_t + H_t). \tag{11.29}$$

It can be noted that, when cell adhesion occurs, eq. (22) causes the local concentration of bound T receptors to be independent of X_t, H_t and R_t, and of the values of the association constants.

Focussing our attention on the dependence of the threshold value y on X_t, it can be seen from eq. (27) that, for $X_t \to 0, y \to K_3H_tR_t$ and

$$lim_{X_t\to 0}\frac{dy}{dX_t} = \left[(\frac{K_2K_3}{K_1} + K^*)\frac{K_1H_t}{1 + K_1H_t} + K_2 \right] R_t, \tag{11.30}$$

whereas, for $X_t \to \infty$,

$$lim_{X_t\to\infty}\frac{dy}{dX_t} = K_2R_t. \tag{11.31}$$

The initial slope of y vs. X_t thus increases as K_1 increases if $K^* > K_2K_3H_t$, and it decreases if $K^* < K_2K_3H_t$. We have moreover:

$$lim_{K_1\to 0}y(X_t) = [(K_2K_3H_t + K_2)X_t + K_3H_t]R_t \tag{11.32}$$

and

$$lim_{K_1\to\infty}y(X_t) = \begin{cases} [(K^* + K_2)X_t + K_3H_t]R_t & \text{if} X_t < H_t \\ [K_2X_t + (K^* + K_3)H_t]R_t & \text{if} X_t \geq . \end{cases} \tag{11.33}$$

Therefore, as illustrated in Fig. 4, if $K^* > K_2K_3H_t$ an increase of the peptide-MHC molecule association constant K_1 will enhance the value of Y, and thus *favor* cell adhesion, only if X_t is relatively small (the upper value of X_t being approximately given by K^*/K_2K_3). If instead K^* is smaller than $K_2K_3H_t$, the peptide-MHC association will have, irrespectively of the peptide concentration, an unfavorable effect on the interaction between the T-cell and the AP-cell.

11.5 Concluding Remarks

The model presented in this paper appears to be useful in the assessment of a variety of situations in which antibodies, or more in general receptors, interact with complex epitopes. Its application to the antibody-mediated activation of defective β-galactosidase was successful in predicting the qualitative aspects of the phenomenon. A more rigorous validation of the model should, however, involve curve-fitting of experimental activation curves obtained at different values of enzyme concentration. Our study of the binding between T-cell receptors and peptide-MHC molecule complexes, allows to visualize how the surface concentrations of peptides, MHC molecules and T-cell receptors, and the association constants between the various molecular species, modulate the T-cell-AP-cell interaction. By the present approach, a rather simple description of a very complex system was achieved. It should however be noted that, in addition to the stated simplifying assumptions about the mechanical properties of cell membrane and of molecular bridges as well as about cell repulsion, the possibility of a shedding of the antigenic peptide from the cell surface was neglected. Moreover, our treatment does not take into consideration the kinetics of the various processes. The consequences of these limitations are yet to be evaluated.

References

[1] Atassi, M.Z. (1978). The precise and entire antigenic structure of lysozyme: Implications of surface-simulation synthesis and the molecular features of protein antigenic sites. *Adv. Exp. Med. Biol.* 98, 41-99.

[2] Smith-Gill, S.J., Wilson, A.C., Potter, M., Prager, E.M., Feldmann, R.J., and Meinhart, C.R. (1982). Mapping the antigenic epitope for a monoclonal antibody against lysozyme. *J. Immunol.* 128, 314-322.

[3] Berzofsky, J.A., Buckenmeyer, G.K., Hicks, G., Gurd, F.R.N., Feldman, R.J., and Minna, J. (1982). Topographic antigenic determinants recognized y monoclonal antibodies to sperm whale myoglobin. *J. Biol. Chem.* 257, 3189-3198.

[4] East, I.J., Hurrell, J.G.R., Todd, P.E.E., and Leach, S.J. (1982). Antigenic specificity of monoclonal antibodies o human myoglobin. *J. Biol. Chem.* 257, 3199-3202.

[5] Celada, F., Fowler, A.V., and Zabin, I. (1978). Probes of *beta*- galactosidase structure with antibodies. Reaction of anti-peptide antibodies against native enzyme. *Biochemistry* 17, 5156-5160.

[6] Rotman, M.B., and Celada, F. (1968). Antibody-mediated activation of a defective *beta*-galactosidase extracted from an *Escherichia Coli* mutant. Proc. Natl. Acad. Sci. USA 60, 660-667.

[7] Conway de Macario, E., Ellis, J., Guzman, R., and Rotman, M.B. (1978). Antibody-mediated activation of a defective *beta*-galactosidase: dimeric form of the activable mutant enzyme. *Proc. Natl. Acad. Sci. USA* 75, 720-724.

[8] Frackelton, A.R., and Rotman, M.B. (1980). Functional diversity of antibodies elicited by bacterial β − D-galactosidase; monoclonal activating, inactivating, protecting and null antibodies to normal enzyme. J. Biol. Chem. 255, 5286-5290.

[9] Accola, R.S., Cinà, R., Montesoro, E., and Celada, F. (1981). Antibody-mediated activation of genetically defective *E. Coli beta*- galactosidases by monocloncal antibodies produced by somatic cell hybrids. Proc. Natl. Acad. Sci. USA 78, 2478-2482.

[10] Celada, F., and Strom, R. (1983). β-Galactosidase: Immune recognition of conformation and mechanism of antibody-induced catalytic activation. *Biopolymers* 22, 465-473.

[11] Celada, F., Strom, R., and Bodlund, K. (1970). Antibody mediated activation of a defective β-galactosidase (AMEF). Characteristics of binding and activation processes. In *The Lactose Operon* (J.R. Backwith and D. Zipser, eds.), Cold Spring Harbor Laboratory, pp. 291-298.

[12] Shimonkevitz, R., Kappler, J., Marrack, P., and Grey, H. (1983). Antigen recognition by H-2 restricted T cells. I. Cell-free antigen processing. *J. Exp. Med.* 158, 303-316.

[13] Allen, P.M., and Unanue, E.R. (1984). Differential requirements for antigen processing y macrophages for lysozyme-specific *T* cell hybridomas. *J. Immunol.* 132, 1077-1079.

[14] Babbit, B.P., Allen, P.M., Matsueda, G., Haber, E., and Unanue, E.R. (1985). Binding of immunogenic peptides to Ia histocompatibility molecules. *Nature* 317, 359-361.

[15] Buus, S., Sette, A., Colon, S., Jenis, D., and Grey, H. (1987). The relationship between major histocompatibility complex (MHC) restriction and the capacity of Ia to bind immunogenic peptides. *Science* 235, 1353-1358.

[16] Ronchese, F., Schwartz, R.H., and Germain, R.N. (1987). Functionally distinct subsites on a class II major histocompatibility complex molecule. *Nature* 329, 254-256.

[17] Sette, A., Buus, S., Colon, S., Smith, J.A., Miles, K., and Grey, H.M. (1987). Structural characteristics of an antigen required for its interaction with *Ia* and recognition by *T*-cells. *Nature* 328, 395-399.

[18] Komissarenko, S.V., Skok, M.V., Kavoon, E.M., Chudnovets, V.S., and Evstigneeva, R.P. (1988). Immune recognition of cytochrome c.I. Molecular requirements for antibody recognition and immune response stimulation studied *in vitro* with synthetic peptides. *A.. Inst. Pasteur/Immunol.* 139, 517-530.

[19] Bell, G.I., Dembo, M., and Bongrand, P. (1984). Cell adhesion. Competition between nonspecific repulsion and specific bonding. *Biophys. J.* 45, 1051-1064.

[20] Torney, D.C., Dembo, M., and Bell, G.I. (1986). Therodynamics of cell adhesion II. Freely mobile repellers. *Biophys. J.* 49, 501-507.

[21] Evans, E.A. (1985). Detailed mechanics of membrane-membrane adhesion and separation. zii. Discrete kinetically trapped molecular crossbridges. *Biophys. J.* 48, 185-192.

[22] Kuznetsov, V.A., Borisova, L.R., and Skalko, Ju.I. (1989). Analysis of kinetics and thermodynamics of cell-to-cell adhesion in the cytotoxic reaction of immune lymphocytes. International Workshop on *Mathematical Modeling in Immunology and Medicine*, Kiev, 28 August - 7 September, 1989.
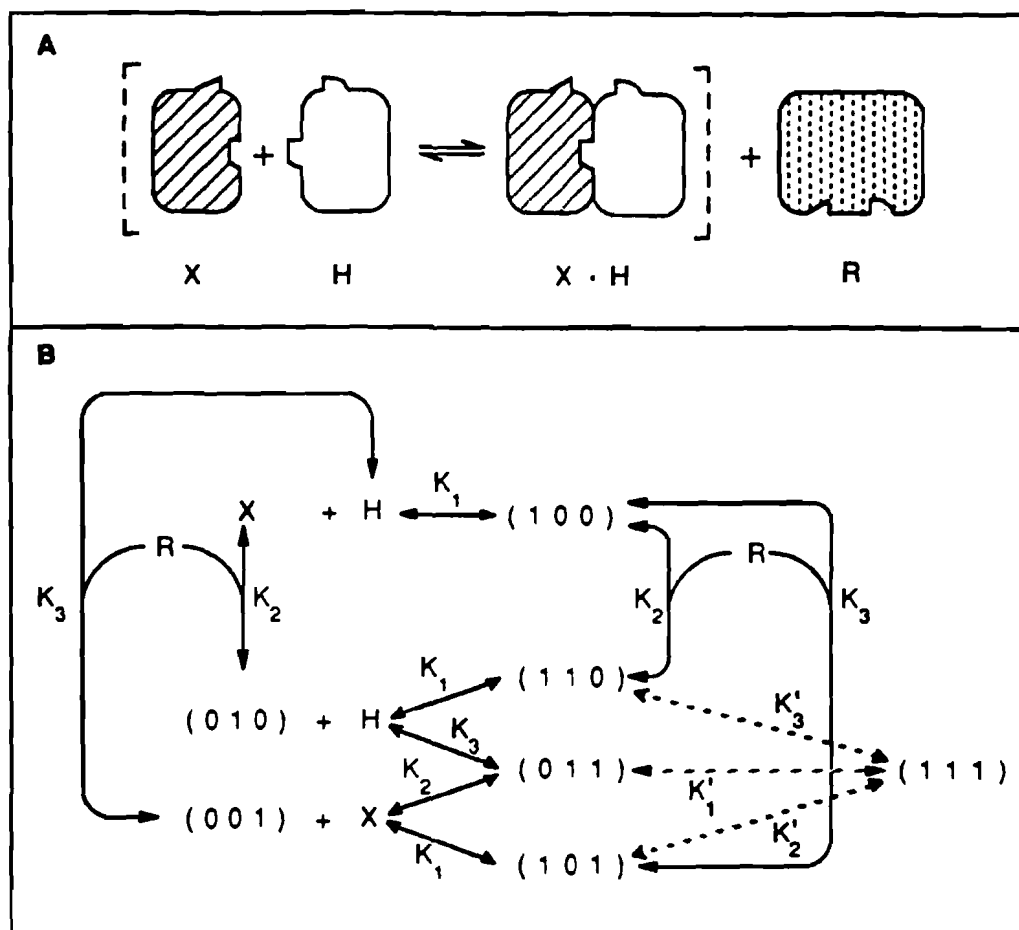
Fig. 1 A) Association of X and H protomers to form a complex interacting with a receptor binding site R. B) Scheme of the reactions occurring in the system. Bimolecular and monomolecular reversible reactions are represented, respectively, by continuous and dotted arrows. Symbols are defined in the text.
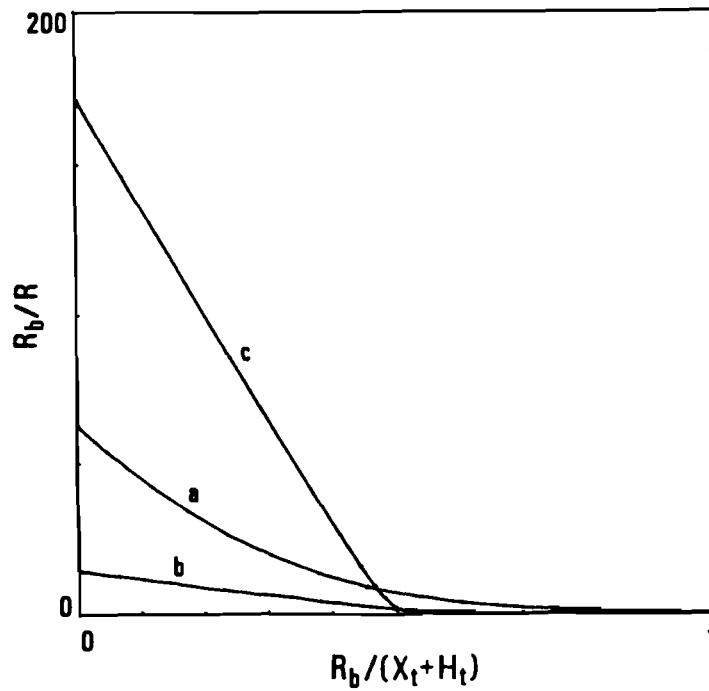
Fig. 2 Plot of R_b/R vs. $R_b/(X_t + H_t)$, for different values of K_1 and K^*: $K_1 = 0$ (K^* is not defined), curve (a); $K_1 = 10^8$ M^{-1} and $K^* = 0$, curve (b); $K_1 = 10^8$ M^{-1} and $K^* = 1.75 \times 10^8$ M^{-1}, curve (c). The other parameter values are: $K_2 = K_3 = 7 \times 10^6$ M^{-1}, $X_t = H_t = 10^{-6}$ M.
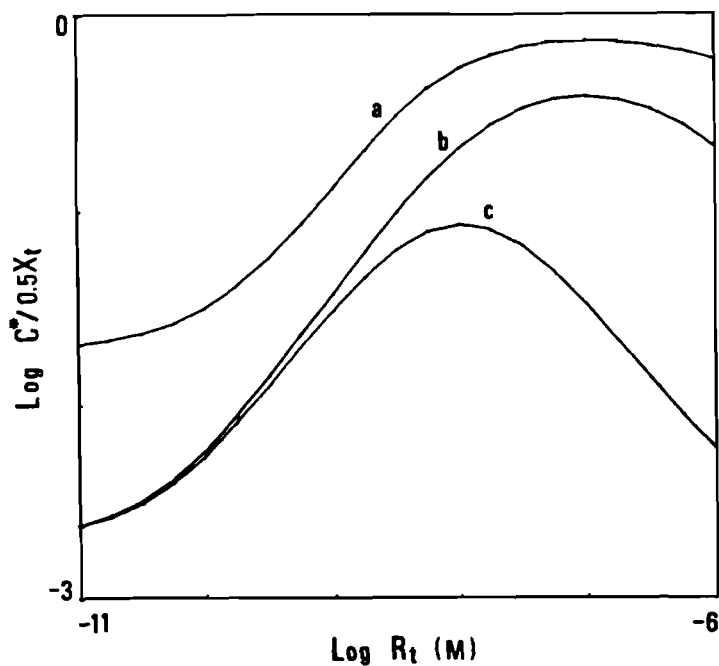
Fig. 3 Computed normalized concentration of the tetrameric form of defective β-galactosidase as a function of the total concentration of activating antibody sites. In curves (a) and (b), $X_t = 10^{-8}$ M and $X_t = 10^{-9}$ M, respectively; in both curves, $K = 5 \times 10^6$ M^{-1}, $K^* = 2 \times 10^{10}$ M^{-1}. In curve (c), $X_t = 10^{-9}$ M, $K = 5 \times 10^7$ M^{-1} and $K^* = 2 \times 10^{10}$ M^{-1}. In all curves, $K_1 = 10^6$ M^{-1}.
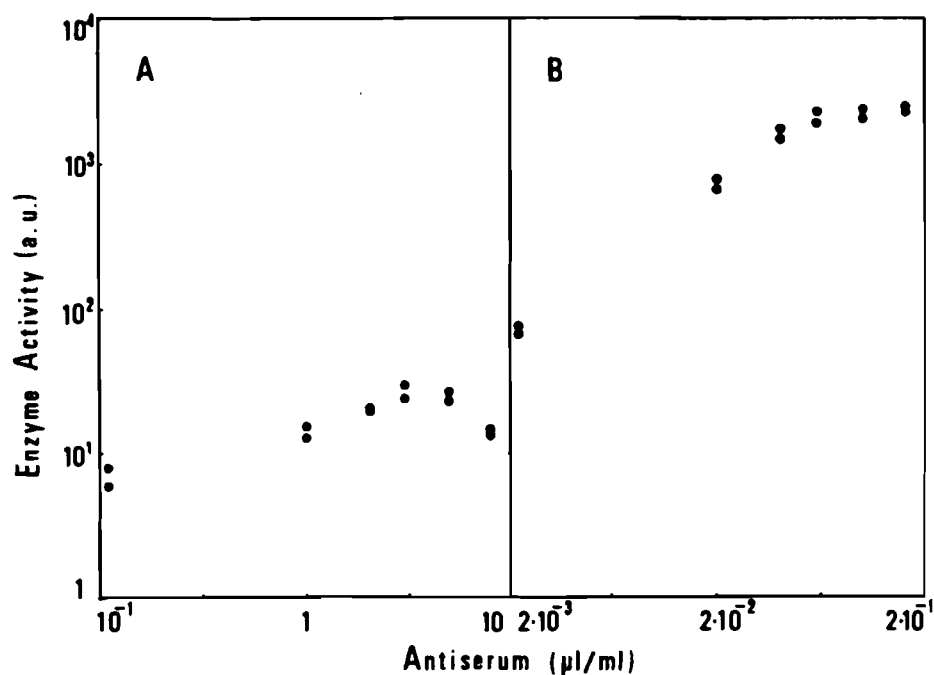
Fig. 4 Dependence of the activity of a defective β-galactosidase (extracted from *E. Coli* strain W6101) on the concentration of mouse (A) or rabbit (B) antisera elicited against the fully active, tetrameric enzyme. Unpublished experimental data by Strom and Celada.
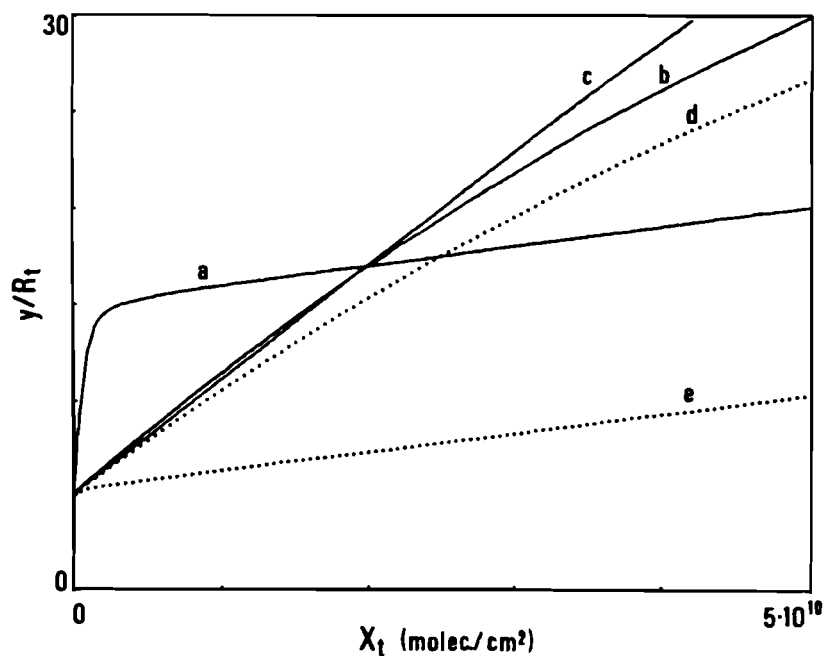
Fig. 5 Upper bound of the values of $\Gamma(\hat{S})/(kTR_t)$ that allow adhesion of T-cells to AP-cells, as a function of the overall surface concentration of an immunogenic peptide. In curves (a), (b) and (c), K_1 equal to 10^{-8}, 10^{-11} and 10^{-12} cm^2/molecule, respectively; $K^* = 10^{-8}$ cm^2/molecule. In curves (d) and (e), K_1 equal to 10^{-11} and 10^{-8} cm^2/molecule, respectively; $K^* = 2 \times 10^{-10}$ cm^2/molecule. In all curves, $K_2 = 10^{-10}$ cm^2/molecule, $K_3 = 5 \times 10^{-9}$ cm^2/molecule and $H_t = 10^9$ molecules/cm^2.

Chapter 12

Somatic Mutation and the Antibody Repertoire: A Computer Model

Richard G. Weinand
Department of Computer Science
Wayne State University
Detroit, Michigan 48802, U.S.A.

12.1 Introduction

The diversity of the pre-immune antibody repertoire, as expressed by the surface immunoglobulin (sIg) on mature, unstimulated B cells, arises from (1) combinatorial rearrangements of the germ-line variable (V), diversity (D) and joining (J) segments, (2) variations in joining at the $V - D - J$ junctions, and (3) combinatorial associations of the variable light (V_L) and heavy (V_H) chains. Preferential selection from the repertoire of those B cells with the highest affinity for the antigen has long been recognized at the cornerstone of the humoral immune response (Siskind and Benacerraf, 1969). Although the initial repertoire that confronts an antigen is quite large, it can be expanded after exposure to antigen by the process of somatic mutation (Weigert et al., 1970; Bernard et al., 1978). These mutations are generally focused in the region of the antibody that forms the antigen-binding site (the V region), and can often result in a radical change (increase or decrease) in the binding characteristics of the antibody (Allen et al., 1988; Griffiths et al., 1984; Rudikoff et al., 1982). Thus, it has been suggested that somatic mutation provides a basis for generating additional antibody specificities which can interact with the antigen. Preferential selection of those variants with a high affinity for the antigen can then lead to a progressive increase in average affinity over time, as well as provide the basis for a heightened secondary response.

Informal models of the humoral immune response that include somatic mutation have been presented by several authors, among them Berek et al. (1987), Manser et al. (1987) and Rajewsky et al. (1987). Their models are descriptive in nature, and are derived from an analysis of nucleotide sequencing data obtained from experiments with immunized mice. These models are particularly important in that they clearly illustrate and emphasize the dynamic and stochastic nature of a continuously expanding and contracting repertoire of antibody specificities. Many important questions remain to be answered however. The rate of somatic mutation has been estimated to be on the order of 10^{-3} per V region base pair per generation (Clark et al., 1985; McKean et al., 1984; Sablitzky et al., 1985). Based on a V region of about 700 base pairs, this translates roughly into one point mutation per cell division. How are antibodies able to withstand such an onslaught of random mutations and improve their affinity for the antigen? Also, random mutations clearly create the possibility of generating antibodies that are harmful to self. How is this risk controlled or minimized?

Our overall objective is to provide answers to these and other important questions through the use of a computer model. A fundamental requirement for such a model is that it must represent individual antibody specificities at a level that permits us to randomly mutate an antibody and calculate the affinity of the mutant antibody for the antigen. This requirement poses a number of difficult problems. Antibodies are proteins made up of a linear sequence of amino acids that take on a three-dimensional conformation as a result of the process of protein folding. The antigen-binding properties of the antibody, in turn, are determined in a large part by the resulting conformation as well as the nature of the specific residues that constitute the binding site. Our knowledge of the specific mechanisms, processes and forces involved in protein folding and antibody-antigen binding is still quite limited, however. Although a great deal of progress has been made in recent years, we are not yet able to accurately predict how the substitution of a single amino acid in an antibody will affect its affinity for an antigen. Equally restrictive from a modeling standpoint is that the computational resources required for even a modestly realistic representation of these processes is well beyond the capacity of currently available equipment.

On the other hand, a great deal of information is available regarding: (a) the general mechanisms by which diversity is generated in the antibody repertoire, and (b) the general characteristics of antigens, antibodies and their interactions. Our approach, then is to devise discrete artificial antibody and antigen repertoires that utilize these mechanisms, exhibit these known characteristics, permit us to make the required calculations of affinity changes resulting from mutations, and remain within the bounds of computational feasibility. We implement this approach in the following steps:

(1) Define a set of behavioral characteristics that capture the essential nature of the interactions between antigen and antibodies.
(2) Devise a simplified three-dimensional representation of antibody-antigen binding that permits the calculation of affinity changes resulting from mutations.
(3) Using the above representation, create a number of artificial antibody/antigen repertoires and test their performance against the required behavioral characteristics.
(4) Imbed the artificial repertoires in a dynamical system model of the humoral immune response.

Step 4 is beyond the scope of this paper and will be pursued in a future work. We do, however, include here an analysis of some of the behavioral characteristics of the model repertoires when subjected to random somatic mutation.

12.2   Design of the Model Repertoire

12.2.1   Behavioral Characteristics of Antibody/Antigen Interactions

We assume that the following set of behavioral characteristics are representative of the major interactions between antibodies and antigens, and consider them to be essential requirements of the model repertoires:

(1) Most antigens react with B cells of more than one specifity, thereby initiating a response that is heterogeneous with regard to the affinity of antibodies produced.
(2) There are more B cell specificities that have a low affinity for an antigen than there are those that have a high affinity for the antigen.
(3) The substitution of a single base pair in the DNA sequence that codes for the antigen-binding site can have a wide range of effects on the binding properties of the antibody. The affinity can be either increased or decreased greatly, minimally or not at all (Griffiths et al., 1984; Rudikoff et al., 1982).
(4) The binding strength and specificity of an antibody generally exhibit an inverse relationship, i.e., antibodies with high average binding strengths are generally less specific than antibodies with low average binding strengths (Karush, 1978; Ninio, 1986).
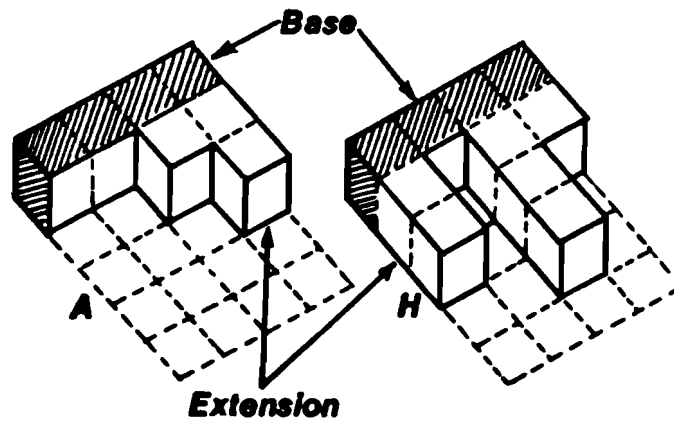
Figure 12.1. Configuration of amino acids *A* and *H*.

12.2.2 Representation of Model Antibody/Antigen Repertoires

The primary assumption behind our model repertoire is that the binding strength between an antibody and an antigen is a function of the complementarity of their molecular surfaces in terms of (a) size, (b) shape, and (c) functionality. Molecular size and shape determine the proximity of the functional sites, and their functional complementarity determines the magnitude of the bond (Amit et al., 1986; Chothia and Janin, 1975; Geysen et al., 1987; Rebek, 1987; Sela, 1969). This structural assumption is incorporated directly into our representation of the antibody and antigen repertoires.

2.2.1 Physical Representation. The basic units of our model antibodies are amino acids, which are translated from nucleotide triplets (codons) according to a genetic code. We use a slightly modified version of the genetic code that maps the 64 possible codons onto 16 amino acids instead of 20 (Appendix I). Each amino acid is composed of a number of 3-dimensional units arranged in a variety of shapes. Two examples of such amino acids are shown in Figure 1.

Each amino acid shape has a common base four units in length. Attached to each of the base units are side extensions, each of which can vary in length from 0 to 3 units. This construction permits the formation of 256 (4^4) possible amino acid configurations, any 16 of which define an antibody repertoire (Appendix II).

The antigen-binding site of an antibody is represented as a 3-dimensional cavity one unit deep formed by the apposition of 4 amino acids (Figure 2).

The four amino acids are oriented on an 8 × 10 unit grid, with their bases aligned at the outer edges. This representation defines an antibody repertoire of size 65,536 (16^4). We will refer to a particular antibody in the repertoire by an ordered list of four letters, taken from the model genetic code, that identifies its amino acid constituents. The antibody in Figure 2, for example, will be referred to as antibody [AHLR].

Antigenic epitopes are constructed of units similar to those of the antibodies, and are represented as projections from the surface of the antigen. Since there are many more possible antigens than antibodies (Inman, 1978, has estimated that there are at least 10^{16} distinguishable families of antigen structures) we allow an antigen to consist of any possible combination of units within an 8-unit by 8-unit shape. The number of possible antigens that can be represented in this fashion is on the order of 10^{20}.

2.2.2 Calculation of Binding Strength. The bond between an antigenic epitope and an antibody (expressed as an affinity constant) is the result of complex interactions between chemical functional groups on the surface of the antigen and amino acid side groups in the binding site of the antibody. The types of forces involved include hydrogen bonds, electrostatic interactions, van der Waals interactions and hydrophobic associations, and complementarity of size, shape and functional groups is critical in forming and determining the strength of the bond. We
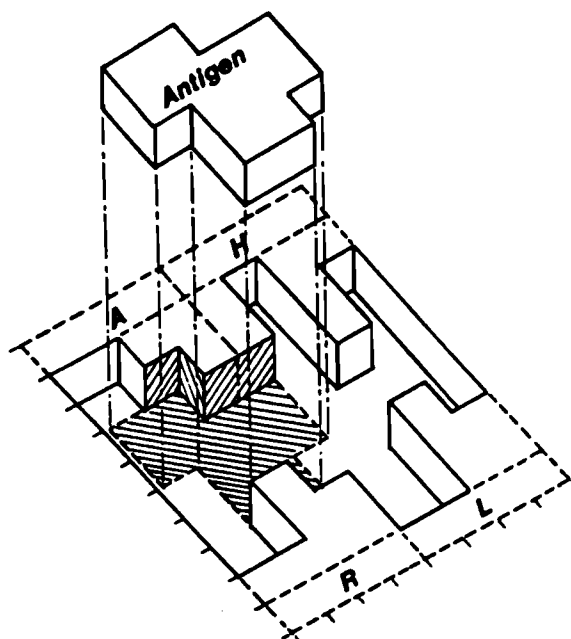
Figure 12.2. Antigen-binding site formed by amino acids, A, H, L, and R.

make no attempt to mimic the real structures and forces involved in antigen-antibody binding, but utilize a much simplified representation that we think captures the essential features of the process. We also assume that for the purpose of calculating an affinity constant, antibody and antigen configurations can e treated as though they are rigid and do not undergo conformational change upon binding (Alzari et al., 1988; Rebek, 1987).

Each unit surface that forms a portion of the floor or walls of the cavity is an accessible contact surface for an antigen, and is assigned one of five functional types. These functional types are somewhat arbitrary in the sense that they do not correspond directly with real functional types, but they provide a means for representing molecular functionaality as an important parameter in antibody-antigen interactions. The binding strength between an antibody and an antigen is calculated as a function of the number and type of functional surfaces that make contact with each other, according to the following rules:

(1) An epitope must 'fit' completely within the cavity to form a bond.

(2) A force is exerted only where two unit surfaces come into full contact.

(3) The force exerted at each contact location is determined by the functional types of the two contacting surfaces.

(4) The total bond between an antigen and an antibody is defined by some function of the individual forces.

(5) The binding force is considered to the 'best fit' force, considering all possible unit translations and 90° rotations of the two shapes.

The binding force between any two types of functional units that make contact is defined by a matrix, an example, of which is shown in Table 1. Each value in the body of Table 1 represents the units of binding force exerted between a pair of functional types on the antibody and antigen surfaces that make contact. For example, if a unit surface of functional type c on an antibody makes contact with a unit surface of functional type b on an antigen, the strength of that particular bond would be 6. A major feature of this representation is that it permits us to easily vary the relative importance of the three major binding strength parameters; size, shape and functionality. The binding characteristics of the repertoire can be varied by assigning different functional types to each of the units that make up the amino acid and antigenic surfaces, and by assigning various values to the weights in the function matrix.

Table 12.1. Binding Force Matrix

Functional type of contacting surface					
antibody	antigen				
	a	*b*	*c*	*d*	*e*
a	1.0	1.0	1.0	1.0	1.0
b	1.0	-4.0	6.0	1.0	1.0
c	1.0	6.0	-4.0	1.0	1.0
d	1.0	1.0	1.0	4.0	1.0
e	1.0	1.0	1.0	1.0	11.0

The affinity constant for an antibody-antigen combination is calculated by first summing the individual bonds for each of the unit surfaces making contact. This produces a total bond expressed as a number of arbitrary bond units, generally falling in the range from 0 to 100. The total bond units are then mapped onto a physiologically relevant range of affinity constants by the function given in Equation 1.

$$K_{ij} = c_1 c_2^{B_{ij}}, \tag{1}$$

where K_{ij} = affinity constant for antibody i, antigen j; B_{ij} = total bond units for antibody i, antigen j; c_1 = scaling factor, and c_2 = slope factor.

This function permits us to control the number and distribution of antibody affinities that will be triggered by an antigen by varying the threshold affinity and the values of c_1 and c_2. Throughout the remainder of this paper we will use the terms 'affinity' and 'bond strength' interchangeably.

12.3 Performance of the Model Repertoires

Four complete antibody repertoires of 65,536 antibodies each (Repertoires A, B, C and D), were generated along with a random sample of 100 antigen configurations. In this section we analyze the binding characteristics of these repertoires and compare them with the requirements formulated previously in Section 2.1.

12.3.1 Repertoire A

The characteristics of the generated antibody/antigen repertoires with regard to the requirements for (1) heterogeneity of affinity, and (2) distribution of affinities can be seen in Figure 3. Figure 3 is a binding distribution for antigen # 84, an 'average' antigen from the sample of 100. Antigen # 84 has a bond strength > 0 for 4,098 (6.25%) of the antibody configurations in the repertoire. The distribution of bond strengths is approximately normal, ranging from a low of 2 to a high of 82. If we consider a bond strength of 65 ($K_a \approx 1.0 \times 10^5 M^{-1}$) to be the minimum required for triggering an immunogenic response, then 90 of the antibodies (0.137 % of the complete repertoire) would be *triggerable*. The proportion of triggerable antibodies is also seen to be a generally decreasing function of affinity, i.e., there are many more antibodies of low affinity than high affinity. These characteristics satisfy the first two requirements.

The third requirement of the model repertoire is that the substitution of a single amino acid should be capable of producing a wide range of effects on the affinity of the antibody. We evaluated this property of the model repertoire by deriving the set of all possible antibodies that could be generated by the substitution of a single amino acid for each of the 90 triggerable antibodies. As an example, antibody [EPIH] can generate 27 other antibodies as shown in Table 2.
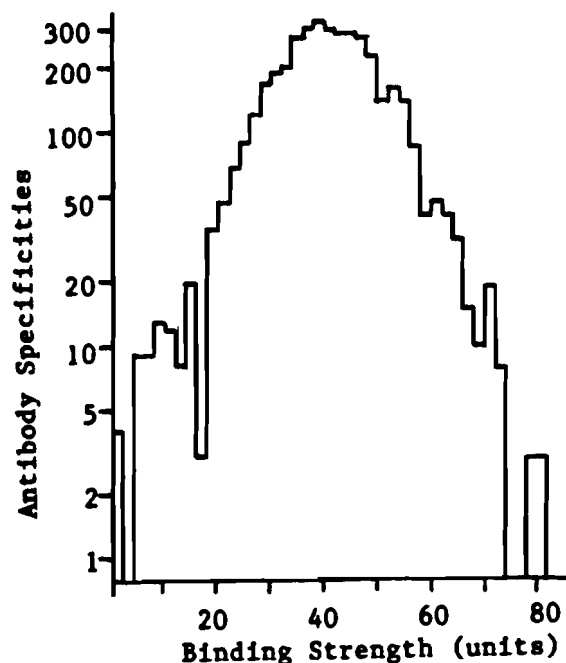
Figure 12.3. Histogram showing the distribution of binding strengths of antibody repertoire *A* vs. antigen # 84. The number of antibody specificities (ordinate) is plotted against binding strength units (abcissa).

Table 12.2. Possible mutations of antibody [EPIH]

	Position 1		Position 2		Position 3		Position 4	
	Antibody	Bond	Antibody	Bond	Antibody	Bond	Antibody	Bond
	[A – – –]	54	[– A – –]	0	[– – V –]	0	[– – – L]	57
	[V – – –]*	65	[– L – –]	51	[– – L –]	0	[– – – P]*	71
	[G – – –]	0	[– S – –]	0	[– – M –]	0	[– – – N]	0
	[N – – –]	0	[– T – –]	0	[– – S –]	0	[– – – C]	0
	[D – – –]*	79	[– N – –]	0	[– – T –]	0	[– – – D]	0
	[K – – –]*	70	[– R – –]	0	[– – C –]	33	[– – – R]	0
			[– H – –]	41	[– – K –]	0		
					[– – R –]	0		

Unchanged amino acids are indicated by a '-' Productive mutations are indicated by an '*'.

There are 6 permitted substitutions for amino acid E in position 1, 7 for amino acid P in position 2, 8 for amino acid I in position 3, and 6 for amino acid H in position 4. Four of these mutant antibodies are productive, i.e., they have a bond strength at least as great as the triggering threshold of 65 bond units. Antibody [KPIH] has the same bond strength of 70 as antibody [EPIH], antibodies [EPIP] and [DPIH] have higher bond strengths of 71 and 79 respectively, and antibody [VPIH] has a lower bond strength of 65. We also note that amino acids P and I in positions 2 and 3 respectively are absolutely essential to the formation of a productive bond. All substitutions of either of these amino acids are non-productive. At the other extreme, amino acid E in position 1 is productively replaceable 50% of the time.

Many of the other triggerable antibodies are similar to antibody [EPIH] in that they can tolerate many mutations, some which have a higher affinity and some of which have the same or lower affinity. There are also several other antibodies, such as [IIPD], that cannot tolerate even a single amino acid substitution without losing their ability to be triggered by antigen #84.

Binding Strength vs. Specificity
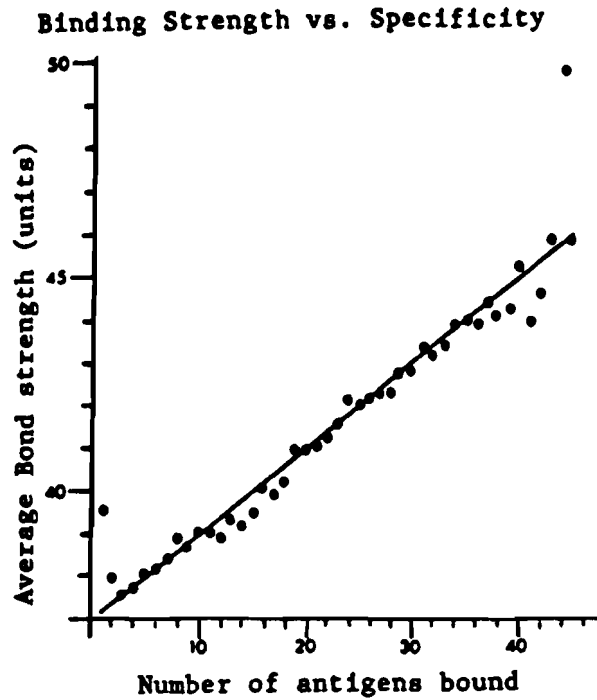
Figure 12.4. Plot of the relation between affinity and specificity. Each data point represents the average bond strength (ordinate) of all antibody specificities that bind a specific number (abcissa) of different antigens.

Maser et al. (1985) discusses this property of an antibody to withstand mutations. The authors refer to this as the 'adaptability' component of 'fitness', and discuss its importance relative to clonal expansion. This is a critical concept, and one which we will return to later on when we analyze the dynamics of clonal development in more detail.

The fourth requirement concerns the relationship between specificity and affinity. Antibodies vary greatly in the number of antigens that they can bind as well as in the strengths of their bonds. Using a random sample of 61 antigens, we calculated the average binding strength of each antibody in the repertoire to each of the antigens. These average binding strengths were grouped into categories based on the number of antigens bound, and the results are displayed in Figure 4. These data clearly exhibit the inverse relationship between specificity and affinity. Antibodies with a high average bond strength (affinity) are seen to be generally less specific (bind more different antigens) than antibodies with a low average affinity. It must be pointed out, however, that this is a general relationship. Exceptions where an antibody has both high affinity and high specificity do occasionally occur in the model repertoire.

12.3.2 Repertoires B, C and D

Repertoires (B, C and D) were evaluated to test the generality of the results presented above. Repertoire B was created by randomly selecting a different set of amino acids as its base, leaving the values in the function matrix unchanged. Repertoires C and D were then created by using the amino acids of Repertoires A and B, and modifying the values in the function matrix to give less weight to the functionality parameter. The behavioral characteristics of Repertoires B, C and D are found to be essentially the same as those of Repertoire A. The major differences in the four repertoires are in the range and variability of their binding strength distributions. Repertoires A and B, which have high values assigned to functionality, generate distributions that cover a wide range of affinities and have a modest degree of variability within that range. Repertoires C and D, on the other hand, produce binding strength distributions that are much narrower and less variable than that of Repertoire A.

12.3.3 Limitations of the Model Antibody Repertoire

X-ray crystallographic studies have shown that the binding site of an antibody appears as an irregularly shaped cavity or pocket formed by the amino acids that constitute the complementarity-determining regions (CDRs) of the variable heavy (V_H) and light (V_L) chains (Alzari et al., 1988; Amit et al., 1986). Although the CDRs consist of about 60 amino acids, the limited size of the binding site (Kabat, 1976) permits only a portion of them to make direct contact with the antigen. One example of the number of amino acids that participate directly in an antibody-antigen bond is given in the study by Alzari et al. (1988), where seventeen amino acids from the antibody are shown to make contact with the antigenic epitope. Fifteen of the amino acids are in the CDRs and two are in the framework regions. This type of structure permits gradual as well as drastic changes in shape and function to result from the substitution of a single amino acid. Substitutions of amino acids that form the surface of the binding site are most likely to produce large increases or decreases in affinity, whereas substitutions of other amino acids are more likely to produce more subtle effects by inducing slight conformational changes in the binding sites. Our model antibodies do not have this important property of gradualism that is essential in evolutionary systems (Conrad, 1983). They consist of V regions that have only four amino acids (all of which directly form the antigen binding site), and no framework or constant regions. All amino acid substitutions, therefore, are likely to produce significant changes in the binding strength because one-fourth of the binding surface is changed. Including the gradualism feature would vastly expand the computational requirements of the model since it requires the inclusion of many additional amino acids in the representation of an antibody. We will see later, however, that experiments with the model make it possible to form conclusions about the likely significance of such additional amino acids.

12.3.4 Suitability of the Repertoires

The results presented in this section do not represent a complete and systematic exploration of all the characteristics of the model repertoires. Our primary objective is to investigate somatic mutation, and our intention here is simply to ensure that the model repertoires are suitable for that purpose. Based on the information presented above we conclude that the behavioral characteristics of each of the four model repertoires satisfy the established requirements.

12.4 The Effect of Somatic Mutation on the Antibody Repertoire

We mentioned earlier that it is beyond the scope of this initial investigation to test the antibody repertoire model in a dynamical system model of the immune response. We do, however, extend our analysis of the model antibody repertoire by considering some behavioral aspects of the effects of somatic mutation.

The process by which somatic mutation generates antibodies with increased affinity for an antigen has been demonstrated to occur in a step-wise fashion (Clarke et al., 1985; Sablitzky et al., 1985). New antibody specificities are generated primarily by single point mutations, and those mutants with a sufficiently high affinity for the antigen are selected for continued proliferation and mutation. Mutant antibodies with low affinity for the antigen, on the other hand, are excluded from further participation. An important consequence of this process is that high-affinity antibodies can be generated only by mutations of other high-affinity antibodies already present in the system. If the sequential mutation path from one high-affinity antibody to another includes one or more low affinity antibodies, that path is effectively blocked. Cells with low-affinity sIg are excluded from the proliferating pool and therefore do not generate additional mutations.
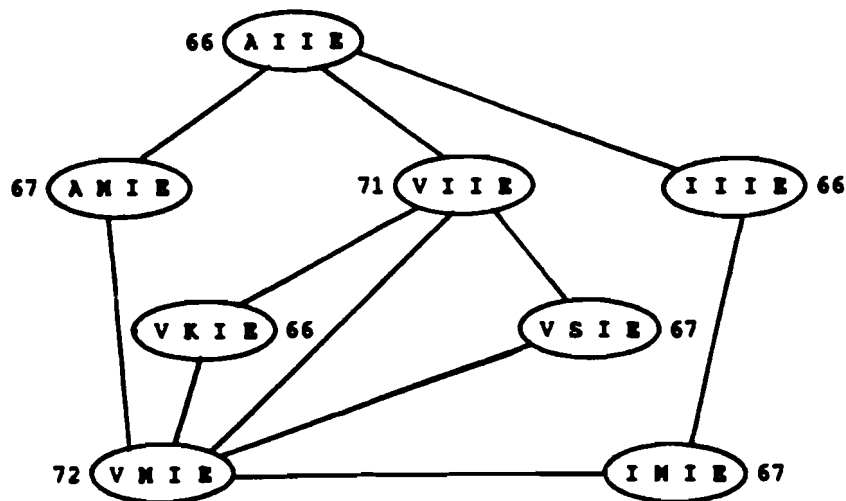
Figure 12.5. Diagram of the set of antibody specificities derivable from antibody [VIIE] by a step-wise sequence of single amino acid substitutions permitted by the genetic code.

We explored this characteristic of the antibody repertoire further by deriving and analyzing the set of all possible antibodies that could arise from antibody [VIIE] as the result of sequential single base mutations (Figure 5). Antibody [VIIE] is seen to be a member of a connected set of eight antibodies. Any antibody in the set can be reached from any other antibody in the set by either a single mutation or a sequence of mutations because each of the antibodies in the set has a sufficiently high affinity for the antigen. Mutations to antibodies not contained in this set do occur, but lead to an immediate dead end because they are not of sufficiently high affinity to remain in the proliferating pool. By direct interference, then, we can conclude that (a) none of the other 82 high-affinity antibodies in the repertoire can be reached from any of the antibodies in this set, and (b) mutations *into* this set from antibodies outside the set are not possible.

By definition, antibodies that are directly mutable into each other can only differ by one amino acid. From this it naturally follows that the antibodies in a mutation set are likely to have a great deal of structural similarity. In principle, though, two antibodies that are separated by four mutations could have completely different amino acids and be very different structurally. This has not occurred in this mutation set, however, as evidenced by each antibody having the same amino acids *I* and *E* in positions 3 and 4. The amino acids in these two positions are therefore essential. Any change in either of them reduces the affinity of the antibody below the triggering threshold.

The mutation set of another triggerable antibody [VPIH] is depicted in Figure 10. This mutation set has 19 antibodies, and has characteristics similar to those of the set previously described. The antibodies in this set also have a great deal of structural similarity. Each antibody has the same amino acids (P and I) in positions 2 and 3, 11 of the antibodies have amino acid P in position 4, and the other 8 have amino acid H in that position.

The complete set of 90 high-affinity antibodies were analyzed in the same fashion, and is summarized in Appendix III.

12.5   Findings, Conclusions and Summary

12.5.1   The Concept of Mutation Sets

An important finding of our investigation of the characteristics of the model antibody repertoire is that somatic mutation, although random, provides a controlled mechanism for expanding the pre-immune repertoire into a *limited* segment of the potential repertoire as follows:

(a) The genetic code and the structure of the antibody repertoire, in combination with threshold affinity-based selection by antigen, dynamically partitions all triggerable clones in the potential repertoire into a number of mutation sets.

(b) A limited number of mutation sets are *activated* when the system is challenged by an antigen, i.e., those mutation sets containing one or more antibodies that are *present* and *triggerable* by the antigen.

(c) The complete set of antibody specifications in the potential repertoire that are triggerable by the antigen and that can be reached by somatic mutation is defined by and limited to those antibodies belonging to the activated mutation sets.

Although this conclusion was derived from the analysis of data produced by experiments with an artificial antibody repertoire, we believe it can be generalized to the real system as well. The concept of mutation sets can be logically derived for the real system from a few basic assumptions, independent of our simulation model. The size of mutation sets in the real system may very well be much larger (or even smaller) than in our model system, but we expect that even very large size differences would not change the nature of the results obtained. Their significance, however, may be altered.

12.5.2   Implications for Autoimmune Disease

We can summarize the findings of our model by examining its implications for autoimmune disease. The first point to note is that from the practical point of view, a mutation set structure is valuable for *maintaining* tolerance. Suppose that the commonly made assumption that self-tolerance arises through clonal deletion is basically correct. If the mutation sets were identical to the potential repertoire, the delected clones would inevitably reappear in response to a wide variety of antigen challenges. If the mutation sets are like isolated pools with respect to a wide variety of antigens (as in the model repertoire), the likelihood of reappearance is greatly reduced. The likelihood of reappearance is also less if the mutation sets are smaller. But in this case the organism's ability to mount a defense against a wide variety of antigens is reduced. Thus, two pressures act on mutation sets. Large size is an advantage relative to external antigens, whereas small size is an advantage from the point of view of self-tolerance.

The second point is that the available mutation sets will in practice vary from individual to individual. The exact structure depends in part on the antigenic challenge and other milieu factors that affect affinity, and that therefore determine which sequences can be reached in a single step fashion. Factors intrinsic to the immunoglobulin molecule also play a role. In our model we have only mutated variable regions. The mutation set that can arise through a series of single step mutations will be influenced by the sequence of amino acids in the constant region as well. This may vary from individual to individual. It is reasonable to expect the mutation set structures to be broadly similar over all individuals in a given species, but to show slight variations depending of differences in the constant regions. This is important, since it explains why certain patterns of autoimmunity are commonplace, but not universal. If the mutation sets were a universal feature of a species it is clear that all individuals would be equally susceptible to the same antigens, which is clearly not the case.

The third point is that if the mutation sets are too small they would be ineffective for surveillance of malignant cells, whereas (as pointed out above) they would be dangerous from the point of view of autoimmunity if they are too large. This is another pressure which undoubtedly

influences the size of the mutation sets. We hasten to add that we cannot claim that the size of mutation sets is fine tuned by phylogenetic evolution to optimize the balance among all of these factors. Evolutionary selection undoubtedly acts here, since organisms must have working immune systems. But whether the evolved immune system is near or far from achieving an optimum balance is an open question at this time.

The above conclusions make it possible to make some projections about what would happen if we increased the number of amino acids in the representation of an antibody. If the addition of amino acids increased the gradualism of affinity changes resulting from single mutations in the variable region, the mutation sets would become larger. This would increase the fraction of productive mutations and would therefore increase the overall rate of expansion of the proliferating pool. It would also increase the ability of the organism to deal with a large repertoire of antigens. Since most of the variant antibodies produced would be very similar, it would not adversely affect tolerance and the possibility of autoimmune problems as long as it does not open up new pathways to undesireable antibodies. The frequency of such pathway openings would depend on the detailed structure of the antibodies, and would therefore be difficult to project in a specific way without actually enlarging the model.

12.6   References

[1] Allen, D., et al. (1988) *Antibody engineering for the analysis of affinity maturation of an anti-hapten response.* EMBO J. 7:1995 - 2001.

[2] Alzari, P.M., et al. (1988) *Three-Dimensional Structure of Antibodies.* Ann. Rev. Immunol. 6:555 - 80.

[3] Amit, A.G., et al. (1986) *Three-Dimensional Structure of an Antigen-Antibody Complex at 2.8 A Resolution.* Science. 233:747 - 53.

[4] Berek, C. and C. Milstein (1987) *Mutation Drift and Repertoire Shift in the Maturation of the Immune Response.* Immunol. Rev. 96:23 - 41.

[5] Bernard, O., et al. (1978) *Sequences of Mouse Immunoglobulin Light Chain Genes Before and After Somatic Changes.* Cell. 15:1133 - 1144.

[6] Chothia, C. and J. Janin (1975) *Principles of Protein-Protein Recognition.* Nature. 256:705 - 708.

[7] Clarke, S.H., et al. (1985) *Inter- and Intraclonal Diversity in the Antibody Response to Influenza Hemmagglutinin.* J. Exp. Med. 161:687 - 704.

[8] Conrad, M. (1983) *Adaptability: The Significance of Variability from Molecule to Ecosystem.* Plenum Press, New York. 191 - 197.

[9] Geysen, H.M., et al. (1987) *Chemistry of Antibody Binding to a Protein.* Science. 235:1184 - 1190.

[10] Griffiths, G.M., et al. (1984) *Somatic Mutation and the Maturation of Immune Response to 2-Phenyl Oxazolone.* Nature. 312:271 - 275.

[11] Inman, J.K. (1978) *The Antibody Combining Region: Speculations on the Hypothesis of General Multispecificity.* In: *Theoretical Immunology.* G.I. Bell and A.S. Perelson (Eds). Dekker, New York. 243 - 278.

[12] Kabat, E.A. (1976) *Structural Concepts in Immunology and Immunnochemistry.* Second Edition. Holt, Rinehart & Winston, New York.

[13] Karush, F. (1978) *The Affinity of Antibody: Range, Variability and the Role of Multivalence, in Comprehensive Immunology.* Vol. 5, Immunoglobulins. G.W. Litman and R.A. Good (Eds). Plenum, New York. 85 - 116.

[14] Manser, T., et al. (1985) *The Molecular Evolution of the Immune Response.* Immunol. Today. 6:94 - 101.

[15] Manser, T., et al. (1987) *Evolution of Antibody Variable Region Structure During the Immune Response.* Immunol. Rev. 96:142 - 162.

[16] McKean, D., et al. (1984) *Generation of antibody diversity in the immune response of BALB/c mice to influenze virus hemagglutinin.* Proc. Natl. Acad. Sci. USA. 81:3180 - 3184.

[16] Ninio, J. (1986) *Adaptation and Evolution in the Immune System.* In: *Evolutionary Processes and Theory.* S. Karlin and E. Nevo (Eds). Academic Press, New York. 143 - 165.

[17] Rajewsky, K., et al. (1987) *Evolutionary and Somatic Selection of the Antibody Repertoire in the Mouse.* Science. 238:1088 - 1094.

[18] Rebek Jr., J. (1987) *Model Studies in Molecular Recognition.* Science. 235:1478 - 1484.

[19] Rudikoff, S., et al. (1982) *Single Amino Acid Substitution Altering Antigen-Binding Specificity.* Proc. Natl. Cad. Sci. USA. 1979 - 83.

[20] Sablitzky, F., et al. (1985) *Somatic Mutation and Clonal Expansion of B Cells in an Antigen-Driven Immune Response.* EMBO J. 4:345 - 350.

[21] Sela, M. (1969) *Antigenicity: Some Molecular Aspects.* Science. 166:1365 - 1374.

[22] Siskind, G.W. and B. Benacerraf (1969) *Cell Selection by Antigen in the Immune Response.* Adv. Immunol. 10:1 - 50.

[23] Weigert, M.G., et al. (1970) *Variability in the Lambda Light Chain Sequences of Mouse Antibody.* Nature. 228:1045 - 1047.

12.7 Appendix

I. Model Genetic Code (16 amino acids)

	Standard Codes		Model Codes	Nucleotide Triplets	No. of Triplets
(Hydrophobic)					
1	A	ala	A	GC*	4
2	V	val	V	GU*	4
3	L	leu	L	CU*, UU {A, G}	6
4	I	ile	I	AU {U, C, A}	3
5	P	pro	P	CC*	4
6	M	met	M	AUG	1
7	F	phe	M	UU {U, C}	2
8	W	trp	M	UGG	1
(Hydrophilic)					
9	G	gly	G	GG*	4
10	S	ser	S	UC*, AG {U, C}	6
11	T	thr	T	AC*	4
12	N	asn	N	AA {U, C}	2
13	C	cys	C	UG {U, C}	2
14	Y	try	C	UA {U, C}	2
15	Q	gln	C	CA {A, G}	2
(Negatively Charged)					
16	D	asp	D	GA {U, C}	2
17	E	glu	E	GA {A, G}	2
(Positively Charged)					
18	K	lys	K	AA {A, G}	2
19	R	arg	R	CG*, AG {A, G}	6
20	H	his	H	CA {U, C}	2
	Terminal			UA {A, G}, UGA	3
				Total	64

II. Amino Acid Shapes

(Repertoire A)

```
    A           V           L           I           P           M           G           S
# # # - -   # # - - -   # - - - -   # # - - -   # - - - -   # - - - -   # - - - -   # # # # -
# # - - -   # # # - -   # - - - -   # - - - -   # # # - -   # # # - -   # # - - -   # - - - -
# - - - -   # - - - -   # # # # -   # # - - -   # # # - -   # # - - -   # # # # -   # - - - -
# - - - -   # # - - -   # # # - -   # # # # -   # # - - - -  # # # # -   # # - - -   # # # - -

    T           N           C           D           E           K           R           H
# - - - -   # # # # -   # - - - -   # # # - -   # # # - -   # # # # -   # # - - -   # # - - -
# # # # -   # # - - -   # # # - - -  # # # - -   # # # # -   # # # - -   # # - - -   # # # # -
# # # - -   # # # # -   # # # - -   # # # - -   # # # # -   # # # - -   # # # # -   # - - - -
# # - - -   # - - - -   # # - - -   # # # - -   # # - - -   # # - - -   # # # - -   # # # - -
```

III. List of All Triggerable Clones in Repertoire A

(by Mutation Set)

Set No.	No. of Clones in set	List of Clones
1	4	[RLPL]-66, [RIPL]-66, [RDPL]-69, [RHPL]-66
2	1	[ADPL]-65,
3	3	[IPPI]-71, [SPII]-70, [KPII]-71
4	4	[IIIP]-67, [SIIP]-68, [KIIP]-67, [SIIH]-65
5	19	[IPIP]-82, [PPIP]-74, [GPIP]-72, [SPIP]-81, [TPIP]-72, [NPIP]-72, [DPIP]-73, [EPIP]-71, [KPIP]-82, [RPIP]-72, [HPIP]-72, [VPIH]-65, [SPIH]-XX, [TPIH]-72, [CPIH]-70, [DPIH]-79, [EPIH]-70, [KPIH]-70, [HPIH]-71
6	7	[VMIP]-72, [AMIH]-69, [VMIH]-80, [LMIH]-70, [IMIH]-70, [MMIH]-70, [VKIH]-72
7	7	[ ]-65, [ ]-65, [ ]-74, [ ]-66, [ ]-73, [ ]-74, [ ]-72
8	2	[DEIP]-65, [DEIM]-71
9	9	[IPDP]-67, [SPDP]-66, [KPDP]-67, [IPEP]-74, [PPEP]-73, [SPEP]-73, [KPEP]-74, [SPDH]-65, [SPEH]-72
10	2	[DPEP]-62, [DPEH]-71
11	3	[IEEP]-66, [SEEP]-65, [KEEP]-66
12	1	[IIPD]-67
13	1	[IPPD]-67
14	1	[MDPD]-66
15	1	[IEPD]-70
16	1	[IAMD]-67
17	14	[MPIE]-67, [GPIE]-65, [TPIE]-65, [NPIE]-66, [DPIE]-66, [KPIE]-68, [RPIE]-66, [HPIE]-67, [MLIE]-66, [NLIE]-65, [DLIE]-66, [KLIE]-67, [RLIE]-65, [HLIE]-66
18	8	[AIIE]-66, [VIIE]-71, [IIIE]-66, [AMIE]-67, [VMIE]-72, [IMIE]-67, [VSIE]-67, [VKIE]-66
19	1	[VMDH]-65
20	1	[VMLH]-72
Total	90	

Chapter 13

Mathematically Defined Complex Affinities - Corrobation at the DNA Level

A. Wohlgemuth
Department of Mathematics, University of Maine
Orono, Maine 04469, USA

D.P. Dubey
Dana-Farber Cancer Institute
Boston, Massachusetts 02115, USA

The imagined structure of immunogenetic systems is influenced by the convention of using the same symbol, for example $A1$, to denote both a genetic factor and the serological reagent, called therefore anti-$A1$, used to identify the factor. This convention forces a conceptual one-t-one correspondence between genetic factors and the antibodies of reagents used to recognize them. In systems where cross-reactivity cannot be ruled out, this notational convention may bias descriptions of the system. The notation oversimplifies things immunologically, and, when the notation is used to describe a whole system, the complexity of nature, not to be denied, may appear as a false, or artifactual, genetic complexity. We will later cite several examples of what we consider to be instances of such artifactual genetic complexity. These examples motivated a new look at the HLA class I system in terms of a general symbolism that assumed neither knowledge of chromosomal loci nor a one-t-one correspondence between genetic factors and reagents.

In [11] a description of HLA class I was sought in terms of general symbols which would not smuggle in the biases mentioned above. The standard symbols $A1 - A32, B7 - B62, Cw1 - Cw8$ were used to identify reagents only. Genetic factors were to be symbolized by a neutral set of numbers. The correspondence between reagents $A1 - Cw8$ and genetic factors was to be determined by the symbolic investigation, done by computer [9], and not prejudged to be one-to-one. Nor were there any assumptions made about chromosomal loci for these factors. The results showed that there existed a natural alternate symbolic description of the HLA class I system. The correspondence between reagents (identified by the standard notation) and genetic factors (identified by the numbers 171-254) did *not* turn out to be one-to-one. This correspondence is given in Table 1—taken from Table 8 of [11]. The genetic factors 171 - 254 were forced, by the symbolic description, into two distinct sets which we feel will ultimately be shown to correspond to genetic loci. Genetic factors assigned to each of the two hypothetical loci are listed with the set of *all* reagents which recognize them.

Table 13.1. Reagents, in standard notation that recognize the antigens in the alternate class I HLA genetic model.

"locus 1"		"locus 2"	
genetic factors	recognizing reagents	genetic factors	recognizing reagents
171	B44	174	A2
206	B18	176	A32
177	B7, Cw7	181	A31
178	B51	173	A25
193	B35, Cw4	213	A24
175	B7	185	A3
186	B15	172	A1
205	Cw3	254	A24, Cw4
219	B8	241	A2, Cw2
223	B62, Cw3		
192	B35		
218	B17		
226	B39		
221	B49		

From the list of reagents reacting with the genetic factors listed at each locus, it is clear that the computer program has rediscovered the *A* and *B* loci. These results have been confirmed with a larger data set [2]. The rediscovery of the *A* and *B* loci is, however, now done in a way that makes the *C* locus unnecesary—at least for the data available. The locus assignments were made without regard for recombination (family) data. However, in [12] it was shown that all recombination (family) data affecting these factors is consistent with the alternate two-locus model.

This new model predicts that when the HLA genome is unequivocally mapped by molecular means, there will be an ultimate cross-reactivity between genetic factors and the reagents customarily used to define alleles in standard notation. That is, it will be clearly seen that these two sets are not in a one-to-one correspondence. This will contradict the serologically determined notation in which HLA class I is described.

In fact, molecular studies have recently corroborated one of the predictions in Table 1: We note that according to the table, there is a single genetic factor, denoted by 193, which is recognized by the two reagents, anti-B35 and anti-Cw4. Recent work by Chertkoff and coworkers [1] corroborates his specific prediction. Using DNA from donors typed for HLA B35, Cw4 and hybridization with HLA class I supposedly locus specific probes, it was reported that DNA digested with EcoRV enzyme gave a 4.6kb band in donors with HLA B35+, Cw4+ typing whereas HLA B35+, Cw4- and B35-, Cw4+ donors yielded a different RFLP pattern without the band. The band was therefore present for exactly those donors that would have antigen 193 in our model. Chertkoff and coworkers conclude that: "The results suggest that the 4.6 kb fragment contains the B35 gene". Since there is a 100of the band with gene 193 but not with B35+, it appears much more apt to conclude that the fragment contains the gene 193.

Table 2 reproduces Table 10 of [11] which compares the two models.

In Table 2, cells identified by a phenotype number are assigned genetic factors A1-A32, B7-Bw63, Cw2-Cw7 according to positive reactions with antibody reagents labeled with a single such identifier, e.g. anti-A1, anti-B7, etc. Cells and reagents are also assigned numerical labels

Table 13.2. A comparison of the standard three-locus serologically defined genetic model for the Class I HLA system with a computer suggested two-locus model based on alternate serological interpretation.

phenotype identity number	phenotype labelling: standard 3-locus				phenotype labelling: suggested 2-locus			
	locus A		locus B		locus C	locus 2		locus 1	
220	A1	A25	B44	B8		172	173	171	219
289	A2	A32	B7	B51	Cw7	174	176	177	178
26	A3	A24	B15		Cw3 Cw4	185	254	186	205
23	A31	A3	B18	B8		181	185	206	219
170	A2		B44	B8		174		171	219
264	A1	A31	B8	B39		172	181	219	226
206	A25	A31	B44	B51		173	181	171	178
167	A1		B8			172		219	
100	A1		B18	B8		172		206	219
132	A31	A3	B18	B49		181	185	206	221
195	A32	A31	B51	B35	Cw4	176	181	178	193
19	A3		B7			185		175	
259	A31	A3	B35	Bw62	Cw3	181	185	192	223
223	A25	A2	B7	B18		173	174	175	206
127	A32	A2	B44	B39	Cw2	176	241	171	226
6	A2		B7			174		175	
625	A2	A3	B18	B17		174	185	200	218
174	A32	A3	B7	B35	Cw4	176	185	175	193

by the computer program. The labeling of reagents with both standard and computer-generated labels is given in Figure 3 (Table 9 from [11]).

Note that in Table 3 each reagent is given a single label in standard notation but either one or two labels in the alternate notation.

The cross-reactivity seen in Table 1 might be explained in terms of multiple epitopes on the proteins coded for by each gene. Thus each reagent might recognize a single epitope (and therefore be truly monospecific) and each genetic factor (gene) code for a protein with those epitopes indicated by Table 1. It is consistent with this model that each class I protein has two or more regions that act as epitopes. For certain of these proteins, antibodies have been found for only one of the epitopes—for others, antibodies have been found for more than one. This creates confusion in interpreting the nucleotide sequence information on a given gene in relation to its functional or serological identification, and consequently may prevent us from understanding the underlying biological mechanism.

There is currently no absolute proof for either of the two models suggested in Table 2. Parham et al. [7] report that "The serologic definition of HLA-C alleles is poor, due to low expression levels on lymphocyte cell surfaces, and the number of HLA-C alleles is still small, so that molecular definition cannot yet compensate for the inadequate serology." At this time there appears to be some evidence on each side. Analysis of HLA Class I genes at the molecular level is complicated by the approximate and sometimes faulty nature of serologically defined antigenic and genetic systems. This is further confounded by the high degree of polymorphism between the coventionally defined HLA-A, B, and C genes and the high degree of nucleotide sequence homology.

Table 13.3. Labeling of reagents in the standard class I HLA model and in the alternate computer suggested model.

Standard	Alternate
anti-A1	anti-172
anti-A2	anti-174/241
anti-A3	anti-185
anti-A24	anti-213/254
anti-A25	anti-173
anti-A31	anti-181
anti-A32	anti-176
anti-B7	anti-175/177
anti-B8	anti-219
anti-B15	anti-186
anti-B17	anti-218
anti-B18	anti-206
anti-B35	anti-192/193
anti-B39	anti-226
anti-B49	anti-221
anti-B51	anti-178
anti-B44	anti-171
anti-Bw62	anti-223
anti-Cw2	anti-241
anti-Cw3	anti-205/223
anti-Cw4	anti-193/254
anti-Cw7	anti-177

In general, molecular biologists have assumed serological definitions and have attempted to find a molecular basis for these. For example, Parham and coworkers report identification of locus specific sequences for the HLA A, B, and C loci. These locus specific sequences have been determined, however, from cloned genes which have been identified by their serological definition. The relative nature of this identification can be seen, in general, from the following example.

Consider the set of all permutations of the letters A, B, and C:

Grouping this set into loci as in Table 4 gives the indicated "locus specific" part of the sequence:

Claims have been made for the existence of highly locus-specific HLA-A, B, and C sequences ([6] and [7] with references). The elementary shuffling of locus assignments seen in Tables 4 and 5 is meant to illustrate that identifying specific sequences that correlate with an assumed serological definition does not necessarily confirm the serological definition. The situation with respect to the two HLA models is not as simple, however, since one model is not obtained from the other by merely shuffling locus assignments. From Table 1 we see that cloning the gene supposedly responsible for Cw4 might result in actually cloning either of the genes 193 or 254. Since gene 193 is also recognized by anti-B35 we would expect to see some sort of "cross-reactivity". In fact studies have also revealed a significant cross-reactivity and hybridization between the HLA-C locus DNA and the HLA-B locus specific probes [3]. The question remains whether the cross-reactivity seen is due to an inadequate symbolic representation of the genes defined by serological methods.

The nucleotide distribution in the exons of cloned HLA Class I genes based on the conventional serological definitions from [7] is given in Table 6.

Table 13.4. Number of nucleotides in each of the serologically defined loci.

loci	Exon 1	Exon 2	Exon 3	Exon 4	Exon 5	Exon 6	Exon 7	Exon 8
HLA-A	73	270	276	276	117*	33	48	5
HLA-B	73	270	276	276	117*	33	44	–
HLA-C	73	270	276	276	120*	33	48	5

* In order to maximize homology there are supposed to be 9 gaps in HLA-A and B, and 6 gaps (in another place in the sequence) for HLA-C. In determining the number of nucleotides per exon, if we include gaps also, then the total number of base pairs in Exon 5 will be 126 at all loci.

It is clear that gene counting arguments will give very different results when counting, on the one hand, (traditional) factors believed to correspond in a one-to-one fashion with reagents, and, on the other hand, the factors 171 through 254. [10] shows that at least some of the linkage disequilibrium found in HLA, may be accounted for by the redefinition of genetic factors according to the new model. That is, some of the linkage disequilibrium may be an artifact of inappropriate notation. Linkage disequilibrium describes the correlation of the genetic factors with each other. Clearly the correlation of genetic factors with disease also depends on the definitions of the factors. Correct definitions are needed for correct correlations.

Hirschfeld and Wohlgemuth [4] showed that *all* linkage disequilibrium in the common human *Ag* bloodgroups disappeared when an alternate symbolization, which allowed for cross-reactivity, was used. In [8] it was shown that the cis-trans effect seen in the Rh blood group system with standard notation, did not appear when the system was symbolized with a new notation which allowed for cross-reactivity. The new notation described a straightforward system with codominant alleles. Our results on HLA suggest that the C locus may itself be only a symbolic artifact—an apparent genetic complexity produced by the immunological oversimplification involved with standard symbolism [2]. Hoover and Wohlgemuth [5] show, by an example, that what might appear as serological (e.g. blocking) evidence favorable to a standard labeling scheme, can, infact, be the result of the tacit assumption of a one-t-one correspondence between *alleles* and *antigens* implicit in the notation.

There is no reason to expect that when molecular studies reveal factors which are not in one-t-one correspondence with traditional reagents, it will then be possible to find new reagents that are in such a correspondence, and which will therefore salvage the traditional symbolic methodology. (Indeed, monoclonal antibodies do exhibit cross-reactivity.) But this is not necessary. Genetic factors can be unequivocally defined by a certain kind of panel of cross-reacting sera. In the past there has been no attempt to develop such a panel, since it was believed to be possible to always identify a genetic factor with "its corresponding" antibody.

The problem of deciding between alternate models is made more difficult by the following human tendency observed by Tolstoi: "I know that most men including those at ease with problems of the greatest complexity, can seldom accept even the simplest and most obvious truth if it be such as would oblige them to admit the falsity of conclusions which they have delighted in explaining to colleagues, which they have proudly taught to others, and which they have woven, thread by thread, into the fabric of their lives.

References

(1) Chertkoff, L.P., Herrera, M., Mota, A.H., Palavecino, E., Fainboim, L., Satz, M.L., DNA polymorphism of the HLA-B35 gene associated to different HLA-C locus alleles. *Human Immunology*, 1988, v. 23, p. 241-253.

(2) Dubey, D.P., Wohlgemuth A. Is the HLA-C locus artifactual? Abstracted in Proc. ASHI, 1988.

(3) Gussow, D., Rein, R.S., Meijer I., deHoog W., Seemann G.H.A., Hochstenbach, F.M., Ploegh, H.L. Isolation, expression, and the primary structure of HLA-Cw1 and HLA-Cw2 genes: evolutionary aspects. *Immunogenetics*, 1987, v. 25, p. 313-322.

(4) Hirschfeld, J., Wohlgemuth, A. Conceptual framework shifts in immunogenetics. Progress in Theoretical Biology, 1978, 1978, V. 5, p. 129-182.

(5) Hoover, D.N., Wohlgemuth, A. Serological interpretation - theoretical limits to information from blocking. Submitted 1989.

(6) Koller, B.H., Sidwell, B., DeMars, R., Orr, H.T. Isolation of HLA locus-specific DNA probes from the 3'-untranslated region. *Proc. Natl. Acad. Sci, USA*, 1984, v. 81, p. 5175.

(7) Parham, P., Lawlor, D.A., Lomen, C.E., Enis, P.D. Diversity and diversification of HLA-A, B, C alleles. *J. Immunology*, 1989, v. 11, p. 3937-3950.

(8) Wohlgemuth, A. Abstract immunogenetic systems. *J. Theor. Biol.*, 1978, v. 73, pp. 469-508.

(9) Wohlgemuth, A. An interactive program for determining tentative gene assignments from immunological data. *Comput. Biomed. Res.*, 1987, v. 20, pp. 76-84.

(10) Wohlgemuth, A. Symbolic interpretation of data and the definition of factors in immunogenetics. *Theoretical Immunology*, Part Two, Santa Fe Institute Studies in the Science of Complexity, Ed. A.S. Perelson, Addison-Wesley, 1988.

(11) Wohlgemuth, A., Dubey, D.P. The impact of symbolism on immunogenetics: an application to HLA. *J. Theor. Biol.*, 1987, v. 126, pp. 149-165.

(12) Wohlgemuth, A., Dubey, D.P. Symbolic interpretation of HLA gene products—impact on interpretation of HLA data at the molecular level. CABIOS, 1987, v. 3, N. 3, pp. 233-238.

Part IV

System Analysis and Medical Decision Making
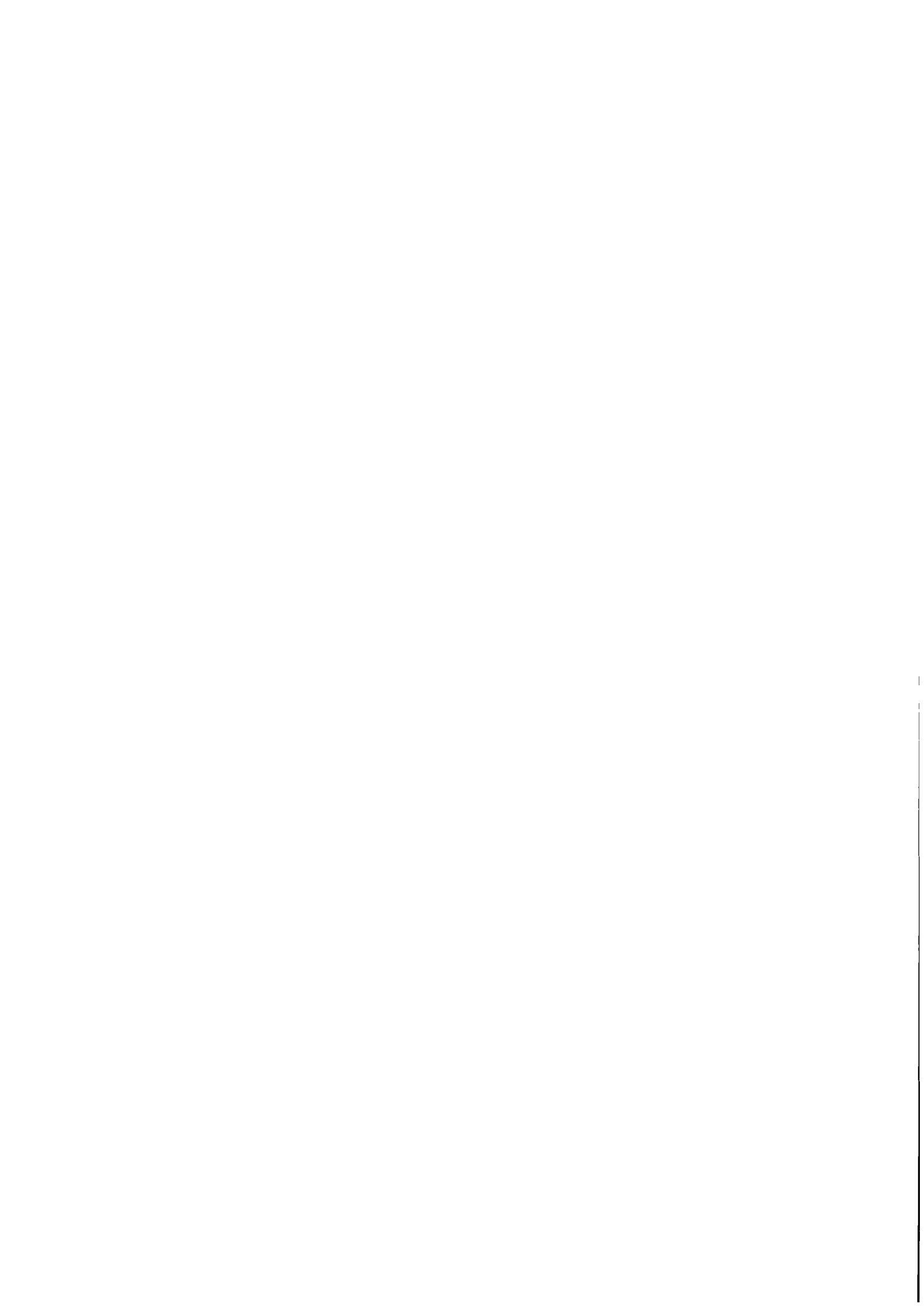
Chapter 14

Unifying Dynamical System Models and Phenomenological Algorithms for Medical Decision Making

Nicholas DeClaris
School of Medicine
University of Maryland
at Baltimore, MD 21201 U.S.A.

Scientific and technological advances in the last decade have brought dramatic changes in the way medical decisions are made. The speed of automated information processing makes possible a "war-on-disease" viewpoint which uses C^3 (communication-control-command) methodologies for strategic planning and the tactical deployment wide range of available resources. It can be employed at all levels; at the bedside [1] when dealing with the pathophysiological conditions of a single critically-ill patient, when testing medical scientific hypotheses [2], or when deciding on the efficacy of medical treatments on the basis of epidemiological studies.

Such a setting for medical decision making is very complex indeed, Figure 1. It requires acquisition and efficient processing of data from many sources and depends heavily on the use of models. The dominant modelling concepts are based traditionally a) on "homeostasis" and, b) on "mathematical dynamics" - such as those encountered in pharmacology, quantitative pathophysiology, and more recently in "immunology" [3]. The qualitative reasoning of homeostasis accommodates clinical intuition and empirical associations, which is of great practical importance among humans, but very difficult to systematize and/or automate. The analytical reasoning of mathematical dynamics on the other hand brings to bear well defined conceptual representations (such as differential equations, stochastic process and numerical techniques) but it also creates substantial practical difficulties when applied to concrete cases involving humans. Numerical techniques and the use of likelihood functions offer the potential of overcoming some of these difficulties - they are very well presented in a recent concise article [4]. The last two decades however brought about also numerous algorithmic representations of "phenomenological" homeostatic models for computer implementations purposes. Algorithmic representations in general tend to be conceptually very simple, as outlined in Figures 2 and 3. However in order for computer implementations of artificial intelligence in medicine [5], to be problem-specific useful, require massive software development efforts involving strong collaborations between groups of specialists (in this case between clinicians and computer specialists). Two such efforts, the MYCIN and CADUCEUS expert systems for modeling the diagnosis and management of certain illnesses, produced very impressive results. Nevertyheless they have had limited success because these implementations require extensive computer and "knowledge engineering" skills. A major

difficulty is that there is a dichotomy in mathematical methodology when dealing with these two representation classes (dynamic systems-analytical, artificial intelligence-algorithmic). The dichotomy disappears as soon as computer methodology takes over to implement these models into machine executable programs.

Here we introduce a novel conceptual scheme based on "Disease-Therapeutic Dynamics" which involves computer-aided reasoning from the outset. There are five essential medical elements in this conceptualization:

- Pathophysiological Dynamics
- Immunological and Allergic Dynamics
- Pharmacokinetics
- Observations and Measurements
- Iatrogenics

They are conceptualized by means of analytical (differential equations, random processes, etc.) and algorithmic techniques (datastructures, etc.) as well as phenomenological associations involving skill and specialized knowledge based on training and experience. These techniques and the techniques afforded by automated information processing create connectivity constraints between the elements, resulting into the system shown in Figure 4. Intense research and development efforts in intelligent instruments, biosensors, immunogenetics, humoral and cellular events make the conceptualization of some of the components subjects to rapid change. Provisions have been made in this scheme to accommodate them. The key is the introduction of a conceptual framework which unifies the representation of the system elements as well as the connectivity constraints, Figure 5. That is, the framework addresses from the outset the unification of analytical and algorithmic methodologies for efficient computer-based implementation. Thus unification is achieved through the notions [6] of two unifying vectors partitioned respectfully into:

- state, control and feature variables,
- measurements, database and classification parameters.

These notions permit characterizations for modeling 1) dynamics in the form of differential or difference equations, 2) statics by means of algebraic equations and 3) production rules by means of algorithms. Transitions from one characterization modality to another as well as finding solutions or terminating algorithms involve still another characterization modality: cognitive "associations".

Cognitive associations afford computer implementations in the form of symbolic processing that go beyond numerical techniques. There are several "cognitive processing" schemes. Prominent among them are the Artificial Neural Network models, also implementable by means of commercial digital computer programs [7]. Mathematically cognitive associations, are ordered-pairs and more generally, n-tupples, Figure 6. They are central to database design as well as to phenomenological "classification" and "pattern recognition". Often used in algorithm-based artificial intelligence schemes, (to create knowledge-bases in expert systems for example) and in machine-learning to automate useful acquired-experience not amiable to scientific theory. The usual computer implementation mechanism for these schemes are searches and decision trees, which in the context of medical setting have not proved very successful for the reasons mentioned earlier. However the notion of discriminant, Figure 6, which is in the heart of the approach discussed here, is subject to rigorous mathematical analysis and at the same time it accommodates very well phenomoenological associations. It forms the cornerstone of our methodology by providing needed links among the different models embedded in the system (dynamical systems, clustering, classification and pattern recognition techniques and learning algorithms) and their input/output data. Moreover discriminants provide a mathematical approach to feature generalization. The mathematical aspects of discriminants are beyond the scope of this presentation.

They fall well within the mathematics of nonlinear operator theory and appear to offer exciting applications including non-supervised machine learning.

The unified model sketched above, makes possible a computer implementation in the form of a microprocessor-based LAN (Local Area Network) that incorporates the communication-control-command setting diagrammatically depicted in Figure 1. Its hallmarks are 1) Adaptive medical workstations [9] that provide very friendly computer environments to the healthcare practitioners and researchers (by means of interactive graphics and with voice-interactions when they become commercially available) and 2) highly reliable network communication paths needed in critical medicine [10]. The LAN contains a large number of microcomputers operating under a software system architecture that access all databases through shells integrating information processing from all data acquisitions sources, dynamic system models, cognitive models, production rule models with database management. The friendly computer interaction with the models and the data is imperative for medical intuition and empirical knowledge are very important in medicine. The semistate vector and the parameter vector employed in the Unified Model create a global computer environment that accommodates symbolic asnd numerical equations and algorithms. Coefficients appearing in equations and algorithms are a mixture of symbols and numbers, which are sorted out through the use of the "feature" variables, "classification" parameters and cognitive "associations" (model-based or phenomenological). These coefficients play key roles in the interactive environment and in the automatic selection of an applicable conceptualization modality. The result is a hierarchical medical decision making scheme that is appropriate to the modeling sophistication needed to support it. For example non-life threatening medical problems which do not require dynamic system cosiderations and which can be diagnosed and treated on the basis of "physical findings" and "proved drug therapies" are dealt with only simple database management operations. However critical-care cases requiring heart-beat to heart-beat monitoring, and for which vital systems (circulatory, respiratory, etc.) and immunological dynamics as well as pharmacokinetics are very important, involve several distinct mathematical models. These models interact continuously with many monitoring and iatrogenic algorithms, feature extraction and pattern recognition schemes thereby automatically recognizing and setting parameters to fit the data, to activate alarms and therapeutics and to carry out interactive communication with the attending clinical personnel.

The databases required for and internally generated by the automated hierarchical medical decision scheme discussed in this paper are massive and throughout of the order of two to four hundred of MIPS (million instructions per second) and of MFLOPS (millions of floating point calculations per second) is needed. Such throughput is only economically feasible by means of a Distributed Processing environment that uses the large number of the microcomputers and workstations contained in the LAN to operate with a high degree of parallelism when needed, achieving remarkable performance, Figure 7. Until now the computer power needed to implement the unified conceptual model presented here would have required the dedicated use of supercomputers making development and operational cost prohibitive.

References

[1] De Claris N., Cowley R.A., Trump B.F., *Systems Approach to Intensive Care Medicine*, American Surgeon, 1979.

[2] DeClaris N., Qualitative Dynamics of Cell Response to Injury, Chapter 2, *Pathophysiology of Shock, Anoxia and Ischemia*, R.A. Cowley and B.F. Trump (eds.), William and Wilkins, Baltimore and London, 1982.

[3] Marchuk, G.I. MATHEMATICAL MODELS IN IMMUNOLOGY, Optimization Software, Inc. Publications Division, New York, 1987.

[4] Marchuk G.I., Belykh L.N., Zuev S.M., *Mathematical Models in Immunology*, RECENT ADVANCES IN COMMUNICATION AND CONTROL THEORY R.E. Kalman, G.I. Marchuk,

A.E. Ruberti and A.J. Viterbi (eds.), Optimization Software, Inc. Publications Division, New York, 1987.

[5] Szolovits P., (ed.) Artificial Intelligence in Medicine, Westview Press, Inc. Colorado 1989.

[6] DeClaris N. and Rindos A., *Semistate Analysis of Aplysia California*, Proc. 1984 IEEE Midwestern Symposium on Circuits and Systems, August 1984.

[7] DeClaris N., *Neural Networks*, Chapter in *Yearbook of Science and Technology*, McGraw-Hill Book Co., New York, (in press).

[8] DeClaris N., *On Neural-Model Based Cognitive Theory and Engineering* Proc. 1986 IEEE International Conference on Systems, Man and Cybernetics, pp. 1-5, 1986.

[9] DeClaris N., *An Adaptive Medical Information System* Proc. IEEE International Conference on Systems, Man and Cybernetics, pp. 286-92, 1986.

[10] DeClaris N. and Paratore B., *A Universal Communication Infrastructure for Intensive Care Microcomputer Networks*, Computers in Cardiology, M.I.T., 1986.
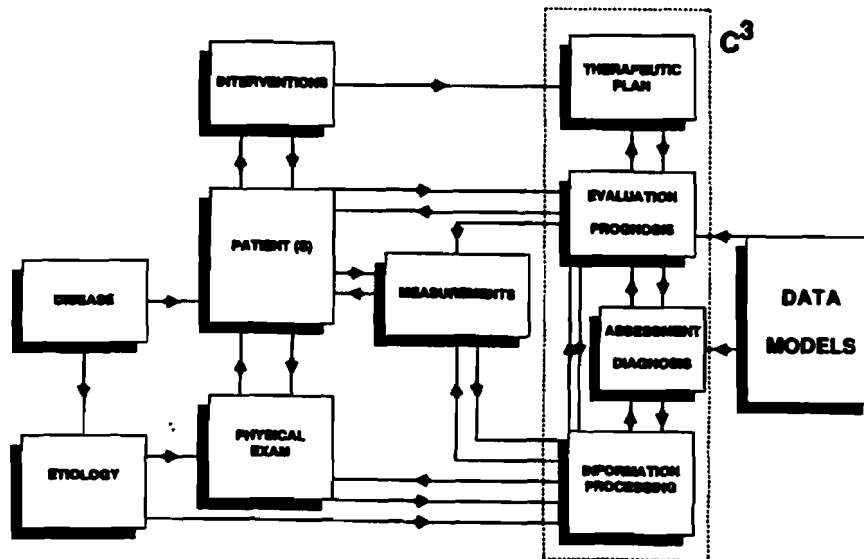
Figure 1 MEDICAL DECISION-MAKING ARCHITECTURE

MODELING
(Problem Representation for Computer Implementation)

I. ALGORITHMIC (phenomenological)

Framework:

Datastructure: $D_k = \{d_{kl} \in \Re\} \quad k = 1, 2, ...M$

Global Database: $D = \{d_j \in \cup D_k\}$

Production Rules: $P = \{P_1, P_2 ...P_n \text{ s.t. } P_l d_r = d_j\}$

Algorithm: L (do $P_l d_j$, next, goal)

Approach (Production System):

Set-up: $D_k, \quad P_j$

Create: Control Scheme (strategy) for L

1) choose one d_r

2) apply one P_j so that: $d_{kl} \leftarrow P_j d_r$

3) repeat 1) & 2) until

4) goal is achieved, terminate.

Control Scheme Models:

Predicate Calculus

Associative Nets

Figure 2

Basic Concepts:

Computational Formalism Involving
String replacement (Post)

Replacement Rule order (A. Markov)

Current Methodology:

Forward, Backward, Bidirectional Productions

- Graph Search Systems
- Pattern-Directed Inference Systems

Abduction

- Evidence
- Probability (Bayes Rule)

Examples:

MYCIN

CADUCEUS (INTERNIST)

Figure 3

DISEASE-THERAPEUTIC DYNAMICS: COMPUTER-AIDED REASONING

> Intelligent Instruments
> Biosensors

@ Automation

OBSERVATIONS
AND
MEASUREMENTS

● Datastructures
● Taxonomy
● Cause-effect Associations
● Pattern Recognition

@

@ > Morphology

PHARMACO-
KINETICS

★ ●

PATHO
PHYSIOLOGICAL
DYNAMICS

★ ●

IATROGENICS

●   ○

IMMUNOLOGICAL
AND
ALLERGENIC
DYNAMICS

★ ●

○ Skills
○ Knowledge

★ Differential Equations
★ Random Processes
★ Numerical Techniques

> Immunogenetics
> Humoral & Cellular Events
> Antigen-Antibody Interactions

Figure 4

UNIFIED MODEL
(Sketch)

Framework:

Semistate: $\quad X_t = \begin{bmatrix} \lambda \\ \upsilon \\ \omega \end{bmatrix} = \begin{bmatrix} \text{state} \\ \text{control} \\ \text{feature} \end{bmatrix}$

Measurements: $\quad \mu$

Databases: $\quad d$

Classification: $\quad \rho$

Approach:

Dynamics: $\quad X_t = f\,(X_t,\, \alpha,\, \rho;\, t)$

Statics: $\quad g\,(x,\, \beta,\, \rho;\, t) = 0$

Associations: $\quad \{\omega,\, \mu,\, d,\, \rho,\, \alpha,\, \beta\}$

Production Rules

Discriminants ⎫
                ⎬ **Artificial Neural Networks**
Generalization ⎭

Figure 5

COGITIVE
(Classification & Pattern Recognition)

Framework:

Associations: Known Ordered Pairs
$$\{\, x_j,\ q_j\, \}$$
where:
$$x_I \in X^m \supset \Re^m \quad q \in Q^n \supset \Re^n$$

Classification: Given x_i, find q_j

Feature Space: $\Omega \supset \Re^s$

Discriminant: For a known association there
exist a $W \in \Omega$ such that:
$$F[\, x_i, W, \phi\,(x_i\ w_i)] = q_j$$
where:
$$\phi\,(\ ) \in \Re \text{ and } F[\ ] \in \Re^n$$

Approach: (Learning Algorithms)

Set-up: F and ϕ

Choose Initial: $W_o = W + \varepsilon_o$

Compute: $F\,(x_i, W_o, \phi) = q_i + \varepsilon_o$

Choose: $W_{k+1} = W_k + \Delta_k\,(\varepsilon_k)$

So that: $F\,(x_i, W_{k+1}, \phi) = q_i + \varepsilon_{k+1}$

And: $|\ \varepsilon_{k+1}\ | < |\ \varepsilon_k\ |$

Figure 6

DISTRIBUTED COMPUTING
BENCHMARK PERFORMANCE

CLOSED-COUPLED MULTIPROCESSORS | <$100K

PROCESSORS

LOCAL AREA NETWORK <$1M

NODES
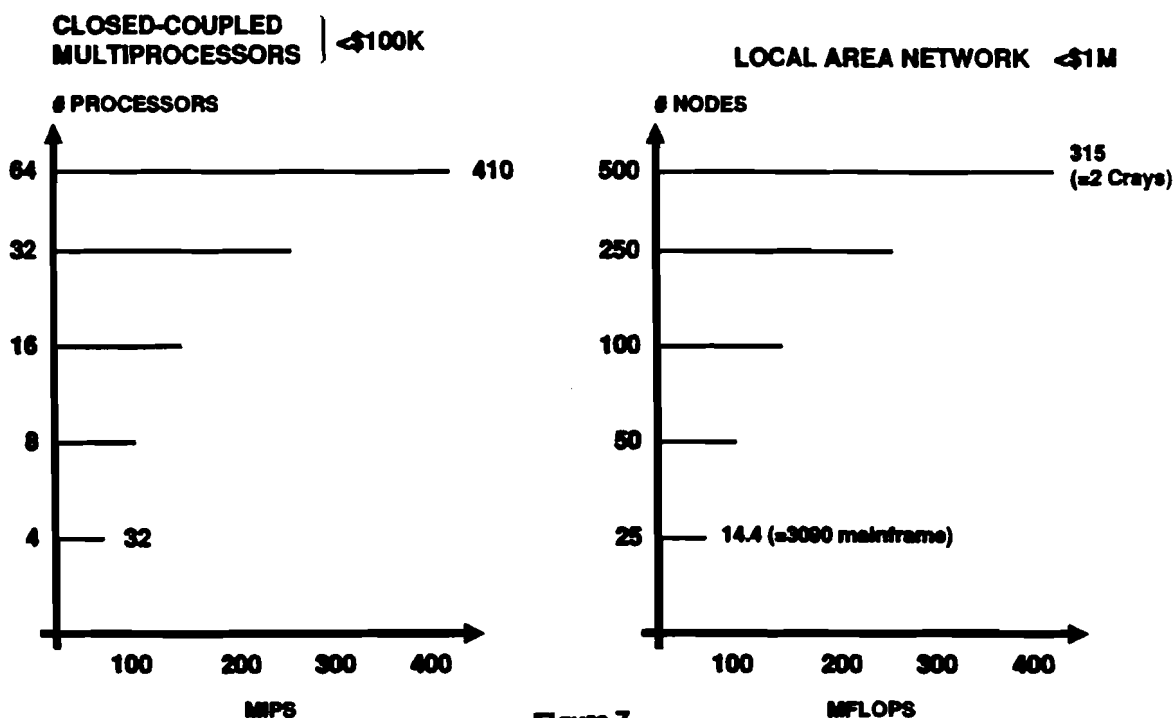
Figure 7

Chapter 15

System Analysis of Mechanisms of Organism's Defensive Functions Regulation (MODFR)

V.S. Mikhalevich, V.M. Janenko, and K.L. Atoev
V.M. Glushkov Institute of Cybernetics,
Academy of Sciences of the Ukrainian SSR,
252207 Kiev, U.S.S.R.

15.1   Introduction

This paper treats the problem of mathematical simulation of the immune response control at various levels of biosystem organization and represents the further development of the ideas stated in [1-3]. Hierarchic MODFR models are constructed including the parameters of subcellular, cellular and tissue levels. A number of questions are discussed which until recently have been outside the scope of "mathematical immunology". In particular, the mechanisms considered involved in immune response regulation by metabolic factors (Ca^{++} , cyclic nucleotides (CN), energetic substrates (ES), biologically active substances (BAS)), adaptive redistribution and restorative cells accumulation, restriction of energy consumption for the immune system's cells protection from energetic exhaustion and death. Proceeding from the system analysis of MODFR, a formalization of the immune status of an organism (ISO) is carried out, and a group of parameters which allow for evaluating the balance of separate links of the immune system and the efficient influence on the immune response is defined. The results of the system investigation make it possible to set forth a hypothesis on the existence of several alternative mechanisms participating in ISO correction:

(1) synchronization of effector and suppressor lymphocytes populations due to their simultaneous inhibition, i.e., transfer of the immune system into a state where there exists a synergism between effectors and suppressors;

(2) transfer of the immune system into a state with low level of energy expenditure which reduces adaptation possibilities of a system but protects from high amplitudes of an ES level drop and high amplitudes of an immune response intensity drop;

(3) regulation of differentiation and proliferation phases realized by BAS and CN.

The action of some therapeutic preparations used in clinical practice is analyzed in the context of the investigated mechanisms.

15.2 MODFR Model

The main MODFR mechanisms are presented in Figure 1. The following designations are given here: $M(c_1), L_{TB}(c_2)$ are cells of erythro-, mielo- and lymphopiesis; $N(c_3)$ is a nervous system; $E(c_4)$ is an endocrine system; $Ag(c_5)$ is an antigen; $S(m_1)$ is a polypotent hemopoietic truncal cell (HTC); $P_M(m_3), P_L(m_4)$ are cells-predecessors of erythro-, mielo- and lymphopoiesis; $E_p(m_5)$ are erythropoietinsensitive cells; $Eb(m_6)$ is erythroblast; $Thrb(m_7)$ is thrombopoietin-sensitive cells; $Er(c_6)$ is erythrocyte; $Thrp(m_8)$ is thromobopoietin-sensitive cells; $Thr(c_7)$ is thrombocyte; $Mb(m_9)$ is mieloblast; $pMc(m_{10})$ is promielocyte; $Bss(c_8), N_s s(c_9), E_s s(c_{10})$ are relating to stable neutrophile and segment nuclear basophils, neutrophils and eosinophils; $Mb(c_{11})$ is monoblast; $pM(m_{12})$ is promonocyte; $Mn(m_{13})$ is monocyte; $Mp(c_{11})$ is macrophage; $pB(m_{14})$, $PT(m_{15})$ are predecessors of B and T lymphocytes-blasts; $Bb(m_{16})$, $Tb(m_{17})$ are B and T lymphocyte-blasts; $B_L(m_{18})$, $B_2(m_{19})$ are B-lympnocytes stimulated and non-stimulated by T-helpers; $P(m_{20})$ are antibody generating cells; $I_9 E, G, \dots$; (c_{12}) are immunoglobulins $E, G, \dots$; $TB(c_{13})$are tissue basophils; $BAS(c_{14})$ are biologically active substances; $G(c_{15})$ are hystaminase; $OM(c_{16})$ are tissue cells of an organ-target; $pL_T(m_{21})$, $L_T(c_{17})$ are cortisone-sensitive and cortisone-nonsensitive (or mature) thymocytes; $pT_k(m'_{21})$, $pT_x(m''_{21})$, $pT_c(m'''_{21})$, $pT_e(m''''_{21})$ are predecessors of T-lymphocytes of $T_k(c_{17})$ killers, $T_x(c''_{17})$ helpers, $T_c(c'''_{17})$ suppressors, $T_e(c''''_{17})$ hypersensitivity effectors of retarded type; $Lk(c_{22})$ are lymphokines; $u(c'_4)$, $v(c'_4)$ are poietines and kinetines; $st(c'''_4)$ are stressors; $P_{mm}(c''_5)$, $P_{BB}(c'''_5)$, $P_{TT}(c''''_5)$ are Ag leukosis cells; $\sum(c_{18})$ are cells of stroma; $AId - L_{TB} - Ig(c_{19})$ are antiidiotypic AId cells of L_{TB} and Ig immune network; $M_{IN}(m_{22})$, $C(c_{20})$ are internal and external factors of an organism; BM is bone marrow; PLO, SLO are primary and secondary lymphoid organs; $IL - 1, IL - 2$ are interleukines 1 and 2; $FSE(c'_{13})$ is a factor stimulating eosinophils; $CSF(c'_{11})$ is a colony stimulating factor; $TRF(c''''_{17})$ is a factor stimulating differentiation of B_1-lymphocytes; $BCGF(c''''_{17})$ is a factor stimulating B_1-lymphocytes proliferation.

Each of the aforesaid i-th sprouts contains a contour for regulating the processes of cells reproduction from the respective subpopulations where cells proliferation mainly occurs. Transition of cells from the higher level into the lower one is regulated by mechanisms of their differentiation. The relative share of cells participating in proliferation amounts to Y_{ij}, and in differentiation - to $1 - Y_{ij}$; where i is the number of a sprout. The specific rate of cells proliferation is α_{ii}, and the rate of differentiation and interaction is α_{ij}. The principal moments occurring during HRS cells interaction are as follows: when Ag enters an organism, mechanisms of its recognition, detection, formation and failure of defensive reactions are activated.

Defensive reactions formation can take place in several directions: a) immune response with subsequent Ag destruction and/or its elimination from an organism; b) non-response (tolerance); c) allergic reaction manifested by the elements of an injury.

Cessation of immune reaction is realized by: a) suppression of idiotypic IDL_TB and Ig reactions with the help of $AIdL_TB$ and $AIdIg$; b) suppressive action of factors of a cell's micro environment.

From the analysis of connections represented in Figure 1, it follows that the efficiency of functioning of defensive reactions of an organism substantially depends on the state of proliferation (m) and differentiation regulation system (c).

For quantitative a MODFR description we accept the statements formulated in [2] and resulting in an integrofunctional dynamic model endowed with a number of important regularities. Interaction between m_i and c_i is determined on the basis of the models [1, 2].

$$m_i(t) = \int_{a_i(t)}^{t} \alpha_{ij}(\tau, t, M_i, C_j) y_{ij}(\tau) m_i(\tau) d\tau, \; i = \overline{1, r}, \; m = M'$$

$$c_j(t) = \int_{b_j(t)}^{t} \beta_{ij}(\tau, t, M_i, C_j)[I - y_{ij}(\tau)] m_i(\tau) d\tau, \; j = \overline{i, p}, \; c = C', \qquad (1)$$

$$P_i(t) = \int_{a_i(t)}^{t} y_{ij}(\tau)d\tau + \int_{b_j(t)}^{t} [1 - y_{ij}(\tau)]m_i(\tau)d\tau, \ 0 \leq y_{ij}(\tau) \leq 1,$$

$$G_i(t) = \int_{t^*}^{a_i(t)} y_{ij}(\tau)m_i(\tau)d\tau + \sum_{t^*}^{b_j(t)} [1 - y_{ij}(\tau)]m_i(\tau)d\tau, \ t \geq t_0.$$

Here α_{ij}, β_{ij} are the indices of functioning efficiency along the channels $m_i - m_i$, $m_i - c_i$, respectively; y_{ij} is a relative share of a resource/or the cells of the type m_i : $a_i(t), b_j(t)$ are temporal limits of obsolete cells elimination; P_i is the general quantity of the cells functioning in i-th organ; G_i are non-functioning cells in i-th organ; t^* is the starting point of functioning; t_0 is the beginning of simulation. As shown in [1, 2], the system (1) has the unique by $m(c)$ solution for the assigned α_{ij}, β_{ij}, y_{ij}, $G(P)$, $C(M)$ and rather general assumptions, and it can be found with the aid of the efficient numerical methods. To find Y, we use the optimization problem

$$I_1 = \sum_{t_0}^{T} c(t)dt \longrightarrow \max_y$$

The study of this problem showed that in the case of sufficiently small $[t_0, T][2]$, the desired maximum is attained when y is minimally possible; and with sufficiently great $[t_0, T]$ - when y differs substantially from the minimally possible value at the initial, greater part of interval $[t_0, T]$, and is minimally possible at the end of this interval. Hence, the biological consequence is such that over a short time interval the maximal value of the external function is attained with the maximal utilization of the available resources, and over a large period of remission - through restorative accumulation of resources spent on the interval demands. This phenomenon is termed as the effect of adaptive redistribution and restorative cells accumulation differentiating in the organ [2] and is considered using an example of thymus gland.

Depending on the intensity of hydrocortisone action, proliferation and differentiation efficiency of processes occurring in thymus gland, variation of population composition of thymocytes in the cortex and medulla of thymus gland lobules take place at least in two stages of various duration: a) a stage of adaptive redistribution of thymocytes and products of their destruction, and here, intensive destruction, differentiation and thymocytes migration, mainly into a spleen, occurs; b) a stage of restorative thymocytes accumulation characterized by an advance restorative thymocytes reproduction in a cortex of thymus gland lobules due to the increased share of cells entering proliferation and shortening of their mitotic cycle $[t - A_{pL_T}(t)]$; alongside with it, the rate of cells differentiation and migration in a spleen and lymphatic nodes (C_{L_T}) slows down. The immunomodulating effect of levamisole consists, in particular, in its influence on the process of thymus gland lobule's thymocytes proliferation which ensures the more efficient pL_T restoration, and hydrocortisone enhances the efficiency of the immune system functioning due to dose-independent acceleration of T-lymphocytes differentiation.

A more complex picture is observed when investigating the structural properties of solutions of minimax problem arising in the process of studying the interaction of two and more systems of the type (I), which is formulated as:

$$I_3 = \int_{t_0^c}^{T} c_{j_0}(t)dt - \sum_{\substack{j=1 \\ j \neq j_0}} \gamma_j \int_{t_0}^{T} c_j(t)dt = \min_{\{y_{ij}, a_j, b_j, u_j, v_j\}} \max_{\{y_{ij_0}, a_{j_0}, u_{j_0}, v_{j_0}\}} \quad (3)$$

with limitations on the functions connected by the model of the type (I), and $m_i' \leq m_i \leq m_i^+$, $c_j^- \leq c_j \leq c_j^+$, $\alpha_{ij}^- \leq \alpha_{ij} \leq \alpha_{ij}^+$, $\beta_{ij}^- \leq \beta_{ij} \leq \beta_{ij}^+$, $t \in [t_0, T]$, y where in the framework of hemopoiesis regulation system HRS, y_{ij_0}, y_{ij} is the relative share of c_{j_0} antigen reproduction, respectively, of different j-th hemopoietic sprouts of the $HRS(j \neq j_0)$, $n_{j_0}^{\pm}$, $c_{j_0}^{\pm}$, $m_j^{\pm}$, $c_j^{\pm}$, $\alpha_{ij_0}^{\pm}$, $\alpha_{ij}^{\pm}$, $\beta_{ij_0}^{\pm}$, $\beta_{ij}^{\pm}$ are the assigned limits of variation of the model functions; $[t - a_i(t)]$ is an average age of reproduction of the i-th sprout of the HRS.

From the properties of the type (I) models, there follows still one more substantially new understanding of possibilities of APVN effect utilization. For example, with infectious process of bacterial nature, it is possible to attain the increase in IS functioning activity be way of an interaction of an adequate dose immunocorrectors - levamisole, into a productive phase of the immune response. In the given case it allows, perhaps to liquidate a contradiction of the type "to accumulate-to issue", as soon as the secondary immune defficiency state (IDS) arising in an organism after stresses at the expense of glucocorticoids and *Ag* of bacterial nature, is sufficiently corrected by the respective levamisole doses and its derivatives.

15.3 Immune status and the ways of its correction

Clinic observations show that despite the single-type course of disease, the immunological indices have significant variations. Considerable parameters variation in the immune system with patients as well as healthy persons, and also availability of different alternative regulation mechanisms bring about the thought that *ISO* estimation should be realized not by a level of separate parameters but by the degree of their balancing.

ISO formalization with the aid of a mathematical model was carried out in [3]. The main regulation mechanisms considered in this model include mainly the parameters which can be attributed to tissue level of regulation; X - antigen, Z - pool of cells-predecessors, Y_1 - pool of cells effectors, Y_2-IL-2, Y_3 - pool of cells-suppressors, H - herapin level, G - histamine level, C_1, C_2, C_3, are Ca^{2+} levels in obese cells, effectors and contractile system, respectively; F_1 and F_2 - are the respective shares of activated histamine reservoirs and connected tropomyosin by which spasm intensity is evaluated; P - proliferation level, O - a degree of edema, C - cortisole, Vl - vilosen, T - thymalin. The principal regulation mechanisms are shown in Figure 2b.

Mathematical problem statement is formulated as follows: to determine the domains of the model $\{k\}$ parameters, corresponding to various MODFRs, d_j, (where j is an index of investigated classes of diseases).

The performed investigation showed that a model appears to be connected with one caspoidal catastrophes. And ther, one of the stationary states is associated with a norm, and the rest are characterizing MODFRs corresponding to various types of pathology.

The results of system investigation were used for nowadays. Within the framework of hypotheses [3], the facts can be explained connected with possible immunocorrecting action of cortisone, vilosen and tymalin, showing positive results with a number of IDS cases. Along with inhibition of activity of suppressor and effector cells, they display anti-proliferation and anti-epidemic action. Proceeding from the results of simulation, it is possible to suppose that one of the possible mechanisms for ISO correlation by cortisone is the synchronization of effector and suppressor populations due to their simultaneous inhibition. On the contrary, vilosen and tymalin enhance proliferative potential, so their immunocorrecting effect can be combined with some other mechanism. This mechanism can be related to suppression of activity of obese cells which eject G and H through Ag-antibody reaction. A decrease in G level prevents edema formation and also an increase in blood supply of inflammatory focus. A decrease in the heparin level must weaken angiogenesis.

The paper [3] also suggests the formula for ISO estimation

$$S_k(I,t) = \frac{P_{Ef_K}}{[T_{\max} - t_0]_K [Ag][Ik] + c_0} \qquad (4)$$

where S is ISO, P_{Ef} is a summarized area restricted by the curve of Ef concentration, by an abscissa axis, by the limits of commencement t_0 of Ag penetration and moment $T_{\max}$ of maximal concentration Ef occurrence; Ag is concrete concentration of Ag admitted to an organism; Ik is immunocorrector concentration, admitted into a body; $k = \overline{I,K_0}$ is a serial number of a patient; Ef - the summary effector function of MODFR; c_0 - const.

Define ΔS values scattering for a group of patients with the similar ISO conditions in the following way:

$$\sigma^2[\Delta S(I,t)] = \frac{1}{K_0 - 1} \sum_{K=1}^{K_0-1} \{|\overline{S_K^2(I,t)} - [\overline{S_K(I,t)}]^2|\} \tag{5}$$

Here σ^2 is ΔS value disersion.

On the one hand the functional $\sigma^2[\Delta S(I,t)]$ allows for compact representation of ISO states of organisms falling into one of classes of states, since ISO parameters standardization is realized: for the more mobile MODFR the values of time of attaining Ef max and P_{Ef} maximum are less than the respective intervals and areas characterizing the more inert MODFR. In a number cases these variations may appear to be proportional. On the other hand, for the given group of patients f_k $k = (I, K_0)$ or for the given patient, in a case of various doses of Ag action, the following scattering of $\sigma^2[\Delta S]$ values is observed; the higher $\sigma^2[\Delta S]$, the greater the compensation limit, and vice versa.

15.4 Immunocorrecting action of therapeutic substances on cellar and sub cellar levels

In the previous section we considered the mechanisms being realized at the tissue level. Now consider rapid processes that preceed the proliferation onset after a mitogen was injected, i.e., the processes taking place during the first minutes and hours following a mitogen injection. The flow-chart of these processes is shown in Figure 2a. And here: C is Ca level, F is the level of protein phosphorylation, L is the level of phosphatidylcholine, Ak is the level of archidonic acid, Pr is the level of prostaglandine, cA - $cAMP$, P is a level of proliferation, cG - $cGMP$.

The following assumptions are accepted for a model construction: 1) a mitogen activity results in capping of surface Ig that brings along the intensified Ca flow into a cell; 2) Ca^{++} intake results in phospholipase activation and protein phosphorylation; 3) phosphorylation results in activation of synthesis of phosphadylcholine and archidonic acid, which in turn serves as a substrate for prostaglandines; phosphatidylcholine activated $cGMP$ synthesis and inhibits $cAMP$ synthesis; 4) $cAMP$, $cGMP$ and the products of their decomposition from a closed pool; 5) phosphodiesterase cA and cC are activated by calcium, besides, cC activates phosphodiesterase cA; 6) cG retards Ca intake, when cA activates it. Within the framework of the above-mentioned assumptions, the mathematical model has the form:

$$\frac{dF}{dt} = \frac{k_1(1 - F)C}{k_2 + cA} - k_3 F, \quad \frac{dL}{dt} = \frac{k_1 F}{1 + F} - k_5 L, \quad \frac{dAk}{dt} = \frac{k_6 F}{1 + F} - k_7 Ak, \tag{6}$$

$$\frac{dPr}{dt} = k_8 Ak - k_9 Pr, \frac{dC}{dt} = \frac{k_{10}\nu cA}{k_{11} + cG} - \frac{k_{12}C}{k_{13} + C}, \frac{dcA}{dt} = \frac{k_{14}Pr(1 - cA - cG)}{k_{15} + L} - k_{16}cA(\alpha+c)(\beta+cG)$$

$$\frac{dcG}{dt} = k_{17}L(1 - cA - cG) - k_{18}cG(1 + C), \frac{dP}{dt} = \frac{k_{19}(cG + 1)}{k_{20} + cA} - k_{21}P,$$

where α , k_i , β are the model's parameters, and $\nu = (1 - e^{-k_{22}t})e^{-k_{23}t}$, $(i = \overline{1,23})$.

As it is indicated by the results of the model's investigations, cA and cG are changing in an antiphase. First of all, cG growth and cA drop takes place, which leads to proliferation activation, and then as Ca accumulation proceeds, prostaglandines are accumulated and they activate cA synthesis, that leads finally to reduction of the proliferative potential. Immunocorrecting action of thymalin and vilosen is accompanied by enhancement of cA and cG levels and the increased proliferation potential [7]. The model (6) reproduces a number of experimental dependencies and can be used as a tool of investigation of intracellular targets to which the action of the efficient immunocorrectors is directed.

15.5   System MODFR Analysis During the Aging Process

Along with CN system, the important role in intracellular mechanisms regulation is also attached to the intensity of synthesis and energy consumption processes in the cells of immune system, processes of anaerobicmetabolism activation [4], as well as to mechanisms preventing the cells from energetic exhaustion [5]. Interrelation between Ca and the processes of energy synthesis and consumption in a cell is not restricted to a monodirectional conjugation scheme understood as subsequent energy transformation from one form to another. There are feedback connections through which the energetics can regulate Ca flows into the cell and the intensity of ATP hydrolysis. The essence of this regulation resides in the following. The cell is capable of limiting the energy consumption before energodeficiency onset, i.e., during still rather a high level of ATPase activity. It was shown that under stress conditions, accompanied by variation of a cell's energetic status, inhibition of processes connected with the high level of energy consumption takes place. It is possible to realize the activity control of the mechanism preventing energetic exhaustion of a cell by regulation of differentiation and proliferation phases, and vice versa, affecting the metabolism, it is possible to regulate the differentiation and proliferation phases. On the basis of the study carried out in [5], an assumption was set forth that the strategy of biochemical adaptation in ontogenesis is directed towards creation of such metabolic conditions which would preserve the cell from high amplitudes of ES and external function levels drop. At the same time, realization of the given protective mechanism reduces the range of cell's possibilities and makes it vulnerable in the cases when mobilization of adaptational mechanisms is needed. Proceeding from these concepts, MODFR analysis was carried out during the processes of aging. Two main generalized regulation systems were distinguished. The first one is the system of an organism's functional reactions, and the second one is the system of an organism's defensive immunologic functions regulation (SODIFR) ensuring control of genetic constancy [6]. The simulating influence of energetic link on both SOFIR and SODIFR was investigated by the use of the mathematical model. It is shown that the drop of efficiency of energy consumption during aging results in transition to the more favourable, for an organism under these conditions, low level of metabolism. In this connection, the course of energy-dependent processes, for example, proliferation of cells-predecessors, is retarded, the effector function is weakened, etc. Moreover, accumulation of various failures leads to autoimmune reactions, to the subsequent idiotype-antiidiotypic interactions of the immune system which at the end reduce the immune network efficiency.

During the solution of problems of minimax SOFIR and SODIFR interaction with Ag it was shown that breaking of the uniqueness of the solution is related to occurrence of conflicting situation in an organism, i.e., the preservation of functional integrity due to weakening of genetic stability.

15.6   Conclusion

The realized system analysis of MODFR made it possible to consider the immune response regulation at different levels of structural organization of biosystems as well as at various levels of temporal hierarchy inherent to the immune system. High-speed processes were studied which proceeded at the first minutes and hours after the immune response had started and which determine the level of proliferation to which the cell-predecessors, effectors and suppressors amount later on and which substantially influence the balance between separate links of immune system at the later phases of the immune response.

The processes were treated which can be termed as medium with respect to continuation, since they were developing during dozens of days - several years, embracing the interaction of various lymphocytes populations and various links of the immune system, i.e., these processes were proceeding at tissue and system levels.

Finally, slow processes were considered, i.e., the dynamics of the immune response and the state of the immune system in ontogenesis were investigated.

Allowances made for such factors as CN, ES, BAS, Ca^{++} metabolism permitted to examine the laws of MODFR functioning and its interrelation with other systems and to reveal the new axiomatics based on the strategy of an organism's biochemical adaptation in ontogenesis.

15.7 References

[1] Atoev, K.L. (1985) *Mathematical Model of Regulation of Myocardium Contraction by a System of Energy Transport.* Kibernetika i vychislitel'naja teknika. vyp. 66, p. 86-90.

[2] Atoev, K.L. and V.M. Janenko. (1988) *Immune Status of Organism: Synergism and Antagonism of Effector and Suppressor Lymphocytes Populations. Mathematical Investigation.* Kibernetika. N4, p. 115-125.

[3] Glushkov, V.M., et.al. (1982) *Simulation of Principal Mechanisms for Systems Development Control.* 2nd All-Union Conference on Problems of Systems Development Control. "Course II". Abstracts of papers. Tallin, U.S.S.R. April, 1982. M.: Nauch. Soviet Kibernetika. AN SSR. p. 12-13.

[4] *Immunology: In 3 volumes.* (1987) U. Pole (Ed) M.: Mir, p. 476.

[5] Janenko, V.M. and K.L. Atoev. (1988) *System Analysis of Mechanisms of Organism's Defensive Function Regulation During Aging.* Y All-Union Congress of Gerontologists and Geriatrists: Abstracts of papers. Tiblisi, U.S.S.R. November, 1988. Kiev: Nauk Dumka. p. 752.

[6] Janenko, V.M., K.L. Atoev and V.A. Berezovskij. (NO DATE) *Mathematical Model of Interaction of Aerobic and Anaerobic Oxidation in Hypothetic Myocardium Cell During Hypoxia. Special and Clinical Physiology of Hypoxic States.* Kiev: Nauk Dumka. p. 2.

[7] Mikhalevich, V.S, et.al. (1986) *Integrofunctional Model of Hemopoiesis Regulation System.* Kibernetika. N3 p. 69-74, 86.

Figure 1: Flow-chart of the MODFR model.

Figure 2: Immunocorrecting influence of therapeutic drugs at the cellular and subcellular levels (a) and at the level of the entire immune system (b).

a

б
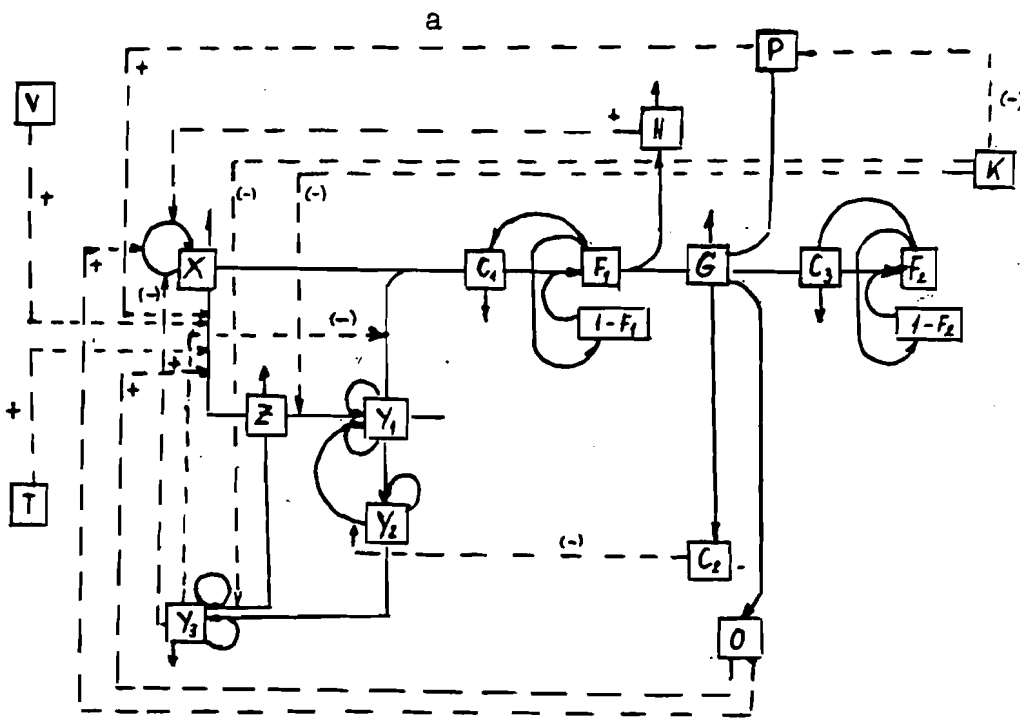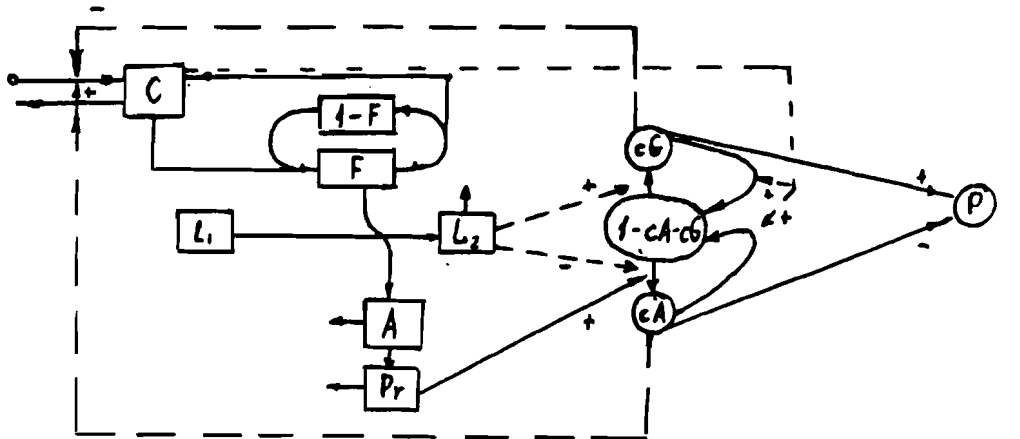
Chapter 16

Uniqueness of Limit Cycles in a Predator-Prey Model Simulating an Immune Response

Xun-Cheng Huang
Department of Mathematics
New Jersey Institute of Technology
Newark, New Jersey 07102 U.S.A

16.1 Introduction

Since the paper of May (1972 [10]), determining conditions which guarantee uniqueness of limit cycles in predator-prey models has become an outstanding problem in mathematical ecology. Recently, Kuang and Freedman (1988 [9]), Huang (1987 [5]), Huang and Merrill (1989 [7]) provided some criteria for uniqueness of limit cycles in predator-prey models. The idea of their criteria is based on a uniqueness theorem of limit cycles for a general Lienard equation by Zhang [16, 17]. Huang also proposed a general Kolmogorov-type model which consists of the above two and many other models (Cheng, 1981 [2], for example) as special cases. Huang also discussed the existence and uniqueness of limit cycles and the proof of the uniqueness theorem does not depend on Zhang's theorem (see Huang, 1989 [8]).

The general model is

$$\frac{dx}{dt} = \phi(x)(F(x) - \pi(y)) \tag{1.1}$$

$$\frac{dy}{dt} = \varrho(y)(\psi(x) + \xi)),$$

where x is the prey density, y is the predator density, $\phi(x)$, $\psi(x)$ are predator response functions, $\pi(y)$, $\varrho(y)$, $\xi(y)$ are predator density functions $\frac{\phi(x)F(y)}{x}$ is the "relative" or "per capita" growth function which governs the growth of the prey in the absence of predators, $\frac{\phi(x)\pi(y)}{x}$ is the death rate of the prey due to the predator, $\frac{\varrho(y)\psi(0)\xi(y)}{y}$ is the death rate of the predator in the absence of prey.

The fundamental assumptions on the model (1.1) are

(H_1): $\phi, \psi, \pi, \varrho, \xi, \ C^1[0, \infty)$, $F \in C^1(0, \infty)$, $F(0) \in (0, \infty]$; $\phi(0) = \pi(0) = \varrho(0) = \xi(0) = 0$, $\phi' > 0$ for $x \geq 0$, $\pi > 0$, $\varrho' > 0$, $\xi' \leq 0$ for $y \geq 0$; there exist $\bar{x}$ such that $\psi(\bar{x}) = 0$, $\psi'(\bar{x}) > 0$ for $x \neq \bar{x}$, and $K > \bar{x}$ such that $F(K) = 0$, $F'(K) < 0$, $F(x) > 0$, for all $0 < x < K$. Moreover, $\phi(x) \leq mx$ for some $m > 0$ and $0 \leq x \leq K$.

(H_2): The curves $F(x) - \pi(y) = 0$ and $\psi(x) + \xi(y) = 0$ are defined on $0 < x \leq K$.

147

(*H*3): There exist positive M and ϵ_M such that $\pi(y) \geq M\varrho(y)$ for $y \geq \epsilon_M$, and also N and ϵ_N such that $\varrho(y) \geq Ny$ for $y \geq \epsilon_N$.

It has been shown that many predator-prey models satisfy these assumptions, and also it is possible to have $F(0) = \infty$ in most cases presented here. In such cases $(0,0)$ is no longer an equilibrium point. Also, it is easy to extend domains of ϕ, ψ, π, ϱ and ξ to the whole real axis.

The first predator-prey model in immunology was proposed by Bell in 1973 [1]. In the model, Bell considered the invading replicating antigens such as virus, bacteria, or foreign cells as the "food" of antibodies which are molecules manufactured by the organism to fight the antigen invasion. The antibodies specifically bind to the antigen and hasten its destruction and elimination from the organism. This model has been thoroughly discussed by Bell [1] and Pimbley [12, 13].

In 1974, Bell proposed another predator-prey model (see Pimbley, [14, 15]), that added one differential equation governing the growth of the B-cell population to the previous model. This equation acts to change the "environment" in which the antibody-antigen intersections are occurring. The qualitative study of this model can be found in Pimbley [14, 15], and Hü and Kazarinnoff [4].

The model constructed here is different from the above ones. We assume that the replication of antigens requires some kind of nutrient [3], and that antibodies have two states: hungry state and saturated state. The hungry state antibody represents the free antibody and the saturated antibody the bound antibody (to antigen). Furthermore, we consider the process of destruction of bound antibody and production of new antibody as saturated predator returning to the hungry state, because the "food" has been assimilated and digested. In addition, for simplicity, we assume that each unit of antigen has only a single site for binding antibody and similarly that each antibody can bind at only a single antigen site. (Merrill, [11]).

16.2   The Model

Let Ag be the concentration of antigen and Ab the concentration of antibody. We construct a mo #ßNßdlows:

The rate of capture can be considered as a linear function of both the concentration of antigen and the concentration of hungry antibody Ab_1:

$$\text{rate}\,1 = \nu_1 Ag Ab_1 \tag{2.1}$$

The rate of assimilation or the rate of new antibody production, is a linear function of the concentration of saturated antibody:

$$\text{rate}\,2 = \mu_2 Ab_2 \tag{2.2}$$

ν_1 and μ_2 in (2.1) and (2.2) are constants rates for the capture and assimilation processes, respectively. One can assume that the two processes will be maintained in a dynamic equilibrium and the growth rate of the antibody or the consumption rate of the prey will be equal, i.e. at equilibrium

$$\text{rate}\,1 = \text{rate}\,2 = \text{predation rate}.$$

Since the total concentration of antibodies

$$Ab = Ab_1 + Ab_2,$$

we have

$$\mu_2 Ab_2 = \nu_1 Ag Ab_1 = \nu_1 Ag(Ab - Ab_2).$$

Thus,

$$\frac{Ab_2}{Ab} = \frac{Ag}{K + Ag}, \tag{2.3}$$

$$\frac{Ab_1}{Ab} = \frac{K}{K + Ag}, \tag{2.4}$$

where $K = \frac{\mu_2}{\nu_1}$.

The value of K expresses the relationship between an antibody's capture of food and the elimination of bound antibody or the production of "new" antibody. For example, a small ν_1 (low binding rate) and a large μ_2 (high elimination rate) will result in a large K. From the view point of the predator's functional response, the parameter K can be considered "efficiency" and is expressed in units of antigen concentration.

The changes in antigen concentration due to antibody predation can be represented as

$$\frac{dAg_2}{dt} = \nu_1 Ag Ab_1 = \frac{\mu_2 Ag Ab}{K + Ag}. \tag{2.5}$$

The change in the antigen concentration due to growth is described by (Cui et al. [3])

$$\frac{dAg_1}{dt} = \mu_1 Ag \frac{1 - Ag/\theta}{1 - Ag/\theta'}, \tag{2.6}$$

where μ_1 is a velocity parameter for the antigen population increment, θ the maximum antigen concentration allowed by a limiting nutrient supply; θ' a parameter, in units of antigen concentration,

$$\theta' = \frac{(K + S_\theta)}{\alpha} = \frac{K}{\alpha} + \theta. \tag{2.7}$$

The parameter K in (2.7) is the Michaelis-Menten constant, the concentration of nutrient necessary for half-maximum concentration of nutrient supply, and α a "transfer" coefficient translating nutrient concentration to antigen population concentration, that is,

$$S_\theta = \alpha\theta, \quad S = \alpha Ag$$

Combining equations (2.5) and (2.6) will result in an equation that expresses net change in antigen concentration

$$\frac{dAg}{dt} = \mu_1 Ag \frac{1 - Ag/\theta}{1 - Ag/\theta'} - \mu_2 \frac{Ag Ab}{K + Ag}. \tag{2.8a}$$

Similarly,

$$\frac{dAb}{dt} = -\mu_3 Ab + \mu_2' \frac{Ag Ab}{K + Ag}, \tag{2.8b}$$

where μ_3 is decay rate of antibody concentration in the absence of antigen (Bell, [1]) and μ_2 the rate of production of antibody stimulated by the binding of antigen to antibody.

The equation (2.8) constitutes the fundamental model that describes the behavior of antibody-antigen systems based on nutrient kinetics.

16.3 Main Theorems

For the general predator-prey model (1.1), we have

Theorem 3.1. Let (x^*, y^*) be an equilibrium point in the interior of the first quadrant Ω. Then (x^*, y^*) is stable if $H(x^*, y^*) < 0$ and unstable if $H(x^*, y^*) > 0$, where

$$H(x, y) = \phi(x)F'(x) + \varrho(y)\xi'(y).$$

Theorem 3.2. The system (1.1) always has a stable equilibrium or limit cycle which is stable from the outside, or both.

Theorem 3.3. In addition to assumptions (H_1) - (H_3), if

$H(x, y) > 0$, $\xi'(y) \equiv 0$ or $\xi'(y) \neq 0$ a.e. on $\{(x, y) | \psi(x) + \xi(y) = 0\}$,

and $(\phi F')'(\xi + \psi) - \psi' H \leq 0$ for $0 < x < K, y > 0$,

then the system (1.1) has at most one limit cycle surrounding (x^*, y^*), and if it exists it is stable.

The proofs of Theorems 3.1 - 3.3 can be found in Huang (1989, [8]).

Now let $x = Ag$, $y = Ab$, and rewrite model (2.8) as

$$\frac{dx}{dt} = \mu_1 x \frac{1 - x/\theta}{1 - x/\theta'} - \mu_2 \frac{xy}{K + x} \qquad (3.3)$$

$$\frac{dy}{dt} = -\mu_3 y + \mu_2' \frac{xy}{K + x},$$

where the parameters μ_1, μ_2, μ_2', μ_3, θ, θ' and K are all positive and K is the predation "efficiency" parameter.

It is easy to see that if $\theta < \theta'$, then $\frac{1-x/\theta}{1-x/\theta'} > 0$, for all $x > \theta'$. That is, the prey isocline remains in the interior of the first quadrant for the density of prey is sufficiently large. Therefore, the first assumption $g(x) < 0$ for all $x > K$ in [9] does not satisfy. Hence (3.3) does not belong to Kuang-Freedman's model.

Setting $\frac{dx}{dt} = \frac{dy}{dt} = 0$, we find the equilibrium points $(0,0), (\theta, 0)$ and (x_e, y_e), where

$$x_e = \frac{\mu_3 K}{\mu_2' - \mu_3}$$

$$y_e = \frac{\mu_1 \mu_2' K}{\mu_2(\mu_2' - \mu_3)} \frac{1 - \frac{\mu_3 K}{\theta(\mu_2' - \mu_3)}}{1 - \frac{\mu_3 K}{\theta'(\mu_2' - \mu_3)}}. \qquad (3.4)$$

To ensure that (x_e, y_e) is in the interior of the first quadrant, we must assume that

$$\theta' \geq \theta \text{ and } \frac{\theta}{K} \frac{\mu_2' - \mu_3}{\mu_3} > 1. \qquad (3.5)$$

Clearly, in this case, $x_e < \theta$.
Rewriting the system (3.3) as

$$\frac{dx}{dt} = \frac{\mu_2 x}{K + x} \left(\frac{\mu_1(K + x)}{\mu_2} \frac{1 - x/\theta}{1 - x/\theta'} - y \right)$$

$$\frac{dy}{dt} = y(-\mu_3 + \mu_2' \frac{x}{K + x}), \qquad (3.6)$$

and letting

$$\phi(x) = \frac{\mu_2 x}{K + x}, \psi(x) = -\mu_3 + \mu_2' \frac{x}{K + x},$$

$$F(x) = \frac{\mu_1}{\mu_2}(K + x)\frac{1 - x/\theta}{1 - x/\theta'}, \pi(y) = \varrho(y) = y, \xi(y) = 0,$$

we can see that assumptions $(H_1) - (H_3)$ are satisfied.
Furthermore,

$$F'(x) = \frac{\mu_1}{\mu_2}\frac{\theta'}{\theta}\frac{1}{(\theta' - x)^2}(\theta\theta' - K(\theta' - \theta) - 2\theta'x + x^2).$$ (3.7)

Let

$$w(x) = \theta\theta' - K(\theta' - \theta) - 2\theta'x + x^2.$$

If $H(x_e) < 0$, then by Theorem 3.1, the equilibrium point (x_e, y_e) is stable if $H(x_e) > 0$, it is unstable. We note that

$$w(x_e) = \theta'\theta - K(\theta' - \theta) - 2\theta'\frac{\mu_3 K}{\mu_2' - \mu_3} + \frac{\mu_3^2 K^2}{(\mu_2' - \mu_3)^2}$$

$$= \frac{1}{(\mu_2' - \mu_3)^2}(\theta\theta'(\mu_2' - \mu_3)^2 - K(\mu_2' - \mu_3)(\theta'(\mu_2' + \mu_3)$$

$$-\theta(\mu_2' - \mu_3)) + \mu_3^2 K^2),$$

whose sign is determined by the quadratic form

$$\theta\theta'(\mu_2' - \mu_3)^2 - K(\mu_2' - \mu_3)(\theta'(\mu_2' + \mu_3) - \theta(\mu_2' - \mu_3)) + \mu_3^2 K^2$$

with roots

$$K_1 = \frac{1}{2\mu_3^2}((\mu_2' - \mu_3)(\theta'(\mu_2' + \mu_3) - \theta(\mu_2' - \mu_3))$$

$$-(\mu_2' - \mu_3)\sqrt{(\theta'(\mu_2' + \mu_3) - \theta(\mu_2' - \mu_3))^2 - 4\mu_3^2\theta\theta'}),$$ (3.8)

$$K_2 = \frac{1}{2\mu_3^2}((\mu_2' - \mu_3)(\theta'(\mu_2' + \mu_3) - \theta(\mu_2' - \mu_3))$$

$$-(\mu_2' - \mu_3)\sqrt{(\theta'(\mu_2' + \mu_3) - \theta(\mu_2' - \mu_3))^2 - 4\mu_3^2\theta\theta'}).$$

Let

$$K_0 = \frac{\theta(\mu_2' - \mu_3)}{\mu_3}.$$ (3.9)

It is not difficult to show that

(i) if $\theta = \theta'$, $\mu_2' > \mu_3$, $K_1 = K_2 = K_0$;
(ii) if $\theta = \theta'$, $\mu_2' > \mu_3$, $K_1 < K_0 < K_2$.

We now have, by Theorems 3.2 and 3.3,
Theorem 3.4. If $\theta < \theta'$, $\mu_2' > \mu_3$, and $K_1 < K_0 < K_2$, then (x_e, y_e) is stable; if $\theta < \theta'$, $\mu_2' > \mu_3$. and $0 < K < K_1$, (or, $K > K_2$), then (x_e, y_e) is unstable and the system (3.3) has at least one limit cycle which is stable from the outside around (x_e, y_e).

Note: The global stability cannot be guaranteed by this theorem. In fact, some solutions of the system (3.3) are unbounded. For example, solutions that begin with initial condition in the region $\{(x,y) : 0 \le x \le \theta, 0 < y\}$ stay in that region, and solutions beginning with $x > \theta$ stay in that region, too. Thus if $\mu_2'\frac{\theta}{K+\theta} - \mu_3 > 0, y(t)$ grows without bound.
Now, compute

$$G(x) \equiv \frac{-\phi(x)F'(x)}{\psi(x)}$$ (3.10)

$$= \frac{-\mu_1 \theta' x(\theta\theta' - K(\theta' - \theta) - 2\theta' x + x^2)}{\theta(\theta' - x)^2(-\mu_3 K + x(\mu_2' - \mu_3))}.$$

It is easy to see that the condition in Theorem 3.3 is equivalent to that $G(x)$ is nondecreasing for $0 < x < \theta$. Thus the system (3.3) has a unique stable limit cycle around the unstable equilibrium point (x_e, y_e). For simplicity, we consider only the case where the prey are not affected very much by nutrient supply, i.e. $\theta < \theta'$ but almost equal.

Since

$$G(x)|_{\theta=\theta'} = \frac{-\mu_1 x}{-\mu_3 K + x(\mu_2' - \mu_3)},$$

$$G'(x)|_{\theta=\theta'} = \frac{\mu_1 \mu_3 K}{(-\mu_3 K + x(\mu_2' - \mu_3))^2} > 0.$$

If we consider $G(x)$ as a function of θ, then it is continuous for $\theta > 0$. We, thus, can choose an $\epsilon > 0$ such that, for $\theta \in (\theta' - \epsilon, \theta')$,

$$G(x) > 0$$

Therefore, we have

Theorem 3.5. If $\theta \in (\theta' - \epsilon, \theta')$, where ϵ is some small positive number, and $0 < K < \frac{\theta(\mu_2' - \mu_3)}{\mu_3}$, then the system (3.3) has a unique limit cycle around (x_e, y_e).

Acknowledgement. The author wishes to thank Professor S.J. Merrill for his useful comments.

16.4   References

[1] Bell, G.I. (1973) *Predator-prey equations simulating an immune response.* Math. Biosci. **16**, p. 291 - 314.

[2] Cheng, K.S. (1981) *Uniqueness of a limit cycle for a predator-prey system.* SIAM J. Math. Anal. **12:4**, p. 541 - 548.

[3] Cui, Q. and G.J. Lawson. (1982) *Study on models of single populations: an expansion of the logistic and exponential equations.* J. Theor. Biol. **98**, p. 645 - 659.

[4] Hsü, I.D. and N.D. Kazarinnoff. (1977) *Existence and stability of periodic solutions of a third order nonlinear autonomous system simulating immune response in animals.* Proc. Roy. Soc. Edin. **A 77**, p. 163 - 175.

[5] Huang, X.C. (1987) *A predator-prey model simulating an immune response.* Seminar Report, Marquette University, Milwaukee.

[6] Huang, X.C. *Stability of a general predator-prey model.* To appear.

[7] Huang, X.C. and S.J. Merrill. (1989) *Conditions for uniqueness of limit cycles in general predator-prey systems.* Math. Biosci.

[8] Huang, X.C. *Limit cycles in a Kolomogorov-type model.* Preprint.

[9] Kuang, Y. and H.I. Freedman. (1988) *Uniqueness of limit cycle in Gause-type models of predator-prey system.* Math. Biosci. **88**, p. 67 - 84.

[10] May, R.M. (1972) *Limit cycles in predator-prey communities.* Science **177**, p. 900 - 902.

[11] Merrill, S.J. *Mathematical models of humeral immune response,* in Modeling and Differential Equations in Biology. T.A. Burton (Ed). Marcel Dekker, New York.

[12] Pimbley Jr., G.H. (1974a) *Periodic solutions of predator-prey equations simulating an immune response I.* Math. Biosci. **20**, p. 27 - 51.

[13] Pimbley Jr., G.H. (1974b) *Periodic solutions of predator-prey equations simulating an immune response II.* Math. Biosci. **21**, p. 251 - 277.

[14] Pimbley Jr., G.H. (1976a) *Periodic solutions of third order predator-prey equations simulating an immune response.* Arch. Rat. Mech. Anal. **64**, p. 169 - 192.

[15] Pimbley Jr., G.H. (1976b) *Bifurcation behavior of periodic solutions of the third order simulated immune response problem.* Arch. Rat. Mech. Anal. **64**, p. 169 - 192.

[16] Zhang, Zhifen. (1958) Dokl Akad Nauk USSR **119**, p. 659 - 662. (in Russian).

[17] Zhang, Zhifen. (1986) *Proof of the uniqueness theorem of limit cycles of generalized Lienard equations.* Appl. Anal. p. 67 - 76.

Chapter 17

Similarity Correlations in Analysis of Immunophysiological Process

I.B. Pogozhev
Department of Numerical Mathematics
USSR Academy of Sciences, Moscow, USSR

Parameters which describe the interaction intensity of various particles in liquid media of an organism are often used in mathematical modelling of immunophysiological processes [1]. T- and B-lymphocytes, macrophages, viral particles, antibody molecules, bacteria, some organic molecules, etc., which can interact between each other as well as with cells of a subject's organs and tissues could act here as interacting particles. In statistical evaluation of values of those parameters according to observation data [3] one often faces a well-known difficulty due to practical impossibility of getting enough measurements for each subject to identify properly all its parameters.

Let

$$\dot{x}_t = f(x_t, \alpha), \ x_t, \ \dot{x}_t \in R^n, \ \alpha \in R^l, \ t > 0 \tag{17.1}$$

as it is in [3], i.e., these are equations which describe changes of phase variables $x_t = x_t^1, \ldots, x_t^n$ of a process in question in fixed parameters $\alpha = \{\alpha^1, \alpha^2, \ldots, \alpha^n\}$ which are to be evaluated according to observation data for each subject. We would show that the difficulty could be sometimes substantially diminished if parameters $\alpha \in R^l$ are considered as functionals of interacting particles trajectories and similarity correlations proposed here are used for their micromovements. In this context it is possible to link parameters $\alpha \in R^l$ of every subject in question with the corresponding parameters $\alpha \in R^l$ of a specially chosen basal organism by means of a single personal parameter HL, which characterizes relative intensity of micro-movements of interacting particles in liquid media of a subject in question being compared with a basal organism.

17.1 Assumption of Micromovement Similarity

From thorough analysis out in [5] it follows that the general vital functions are approximately similar not only in different human organisms but in many mammals as well. According to [5] animal's organisms are much alike: they consist of the cells of approximately equal size, however their total number defines an organism's size. The sizes of inter-cellular space, blood capillaries, erythrocytes, lymphocytes, macrophages and other particles interacting in immunophysiological processes are also almost the same as well as volume fraction of an organism's liquid media like blood plasma, lymph, intra-tissue fluid, their temperature and viscosity, concentration of lymphocytes, macrophages, proteins, glucose and other interacting particles. Vital lung volume

and heart mass vary with body mass, and about five systoles fall on one breathing cycle in humans and many other mammals.

Analysis of these and modern physiological data allows to adopt the following *assumption of similarity of interacting particle micromovements in liquid media of the organisms to be compared*:

$$q(t) \doteq \frac{V_b}{\underline{V}_b} \cdot \underline{q}(t \cdot \frac{\tau_c}{\underline{\tau}_c}),$$ (17.2)

where

$$q(t) = \{q^1(t), \ldots, q^n(t)\}, \quad \underline{q}(t) = \{\underline{q}^1(t), \ldots, \underline{q}^n(t)\}$$

are generalized coordinates;

$$\dot{q}(t) = \{\dot{q}^1(t), \ldots, \dot{q}^n(t)\}, \quad \underline{\dot{q}}(t) = \{\underline{\dot{q}}^1(t), \ldots, \underline{\dot{q}}^n(t)\}$$

are generalized velocities of interacting particles in liquid media of an organism in question and basal one respectively; $V_b, \underline{V}_b$–are specific velocities of blood flows (calculated per mass unit); $\tau_c, \underline{\tau}_c$–are average duration of cardiac cycle of an organism in question and basal one respectively; S–is a number of degrees of freedom in the system of interacting particles in question.

Here we consider $q(t)$ and $\dot{q}(t) \in R^S$ as S-dimensional random stationary and ergodic processes, which satisfy the condition of intensive mixing when the organisms a preserve certain physiological state [6]. Symbol $\doteq$ in (2) and below is interpreted as stochastic equivalence of corresponding random processes [7].

According to [2] changes of statistical properties of micromovements of interacting particles in liquid media of an organism are defined mainly by a change of specific velocity of blood flow and average duration of the cardiac cycle. In this context the characteristic time during which an organism preserves its physiological state (about an hour) is assumed to be much longer than that one of mixing (about a minute), during which a marked link between positions of interacting particles exists.

17.2   Similarity correlation for intensity matrices

Let us consider intensity matrices of micromovements B, $\underline{B}$ for an organism in question and basal one respectively:

$$B = \{B_{ij} = \int_{-\infty}^{+\infty} E[q^i(t+z) - Eq^i(t)(q^j(t) - Eq^j(t)] \, dz, \}$$ (17.3)

$$\underline{B} = \{\underline{B}_{ij} = \int_{-\infty}^{+\infty} E[\underline{q}^i(t+z) - E\underline{q}(t)(\underline{q}^j(t) - Eq^j(t)] \, dz, \}$$ (17.4)

$$i, j = 1, S.$$

Integrals in (4) are finite and independent of moment of time $t > 0$ since the processes $q(t)$ and $\underline{q}(t)$ are ergodic and stationary. Having used (2) we obtain the following similarity correlation for matrices (3) and (4):

$$B = \underline{B}HL,$$ (17.5)

where

$$HL = -\frac{V_b^2 \cdot \tau_c}{\underline{V}_b^2 \cdot \underline{\tau}_c}$$ (17.6)

characterizes relative intensity of micromovements of interacting particles in an organism in question being compared with the basal one and is personal parameter of the former; $V_b, \underline{V}_b, \tau_c, \underline{\tau}_c$ are defined in (2).

17.3 Similarity correlations for a number of particles

Let

$$\nu^{\varepsilon}_{t_1 t_2} \doteq \Phi[u^{\varepsilon}(z), t_1 < z < t_2], \quad \underline{\nu}^{\varepsilon}_{t_1 t_2} = \Phi[\underline{u}^{\varepsilon}(z), t_1 < z < t_2], \tag{17.7}$$

are the numbers of contacts of active zones of interacting particles of specified types in time interval (t_1, t_2) in liquid media of an organism in question and basal one respectively;

$$u^{\varepsilon}(z) = \frac{\int_0^z \dot{q}(t/\varepsilon)dt - zE\dot{q}(t/\varepsilon)}{\sqrt{\varepsilon}}, \quad \underline{u}^{\varepsilon}(z) = \frac{\int_0^z \dot{\underline{q}}(t/\varepsilon)dt - zE\dot{\underline{q}}(t/\varepsilon)}{\sqrt{\varepsilon}} \tag{17.8}$$

are centered S-dimensional random processes of micromovements of interacting particles in an organism in question and basal one respectively; $\varepsilon = \tau_1/\tau_2$ is a small parameter equal to the ratio of the characteristic pulsation time, i.e., ratio of time in which a particle collides with the organism's cells and other particles thus changing its trajectory to the characteristic time of fixing location of particles (the latter could not be less than the characteristic duration of interaction: for a man $\tau_1 \sim 1$ sec., $\tau_2 \sim 10$ min, $\varepsilon \sim 10^{-3}$). It is easy to check that matrices of intensities of random processes (8) are independent of parameter ε and agree with the corresponding matrices $B, \underline{B}$. Let us assume that processes (8) and functional Φ (7) provide passing to a limit, invariance conditions [7] as well as the following properties of processes $\nu^{\varepsilon}_t, \underline{\nu}^{\varepsilon}_t$ [8]:

17.3.1 A. Stationarity

For any $t_2 > t_1 \geq 0$, $t = t_2 - t_1$.

$$\nu^{\varepsilon}_{t_1 t_2} \doteq \nu^{\varepsilon}_{t_2 - t_1, 0} \doteq \nu^{\varepsilon}_t,$$

$$\underline{\nu}^{\varepsilon}_{t_2 t_1} \doteq \underline{\nu}^{\varepsilon}_{t_2 - t_1, 0} \doteq \underline{\nu}^{\varepsilon}_t$$

17.3.2 B. Ordinarity

For small $\Delta t > 0$:

$$P\{\nu^{\varepsilon}_{t+\Delta t} - \nu^{\varepsilon}_t = 1\} = \lambda \cdot t + 0(\Delta t), P\{\underline{\nu}^{\varepsilon}_{t+\Delta t} - \nu^{\varepsilon}_t = 1\} = \underline{\lambda} \cdot \Delta t + 0(\Delta t), \tag{17.9}$$

$$P\{\nu^{\varepsilon}_{t+\Delta t} - \nu^{\varepsilon}_t = K\} = 0(\Delta t), P\{\underline{\nu}^{\varepsilon}_{t+\Delta t} - \nu^{\varepsilon}_t = K\} = 0(\Delta t), \quad K = 2, 3, \ldots$$

where $\lambda, \underline{\lambda} > 0$ are intensities of contact number of specified type particles in an organism in question and basal one.

For these assumptions the main *statement* is valid: Processes $\nu^{\varepsilon}_t, \underline{\nu}^{\varepsilon}_t$ (6) provided $\varepsilon \to 0$ converge weakly to Poisson processes $\nu^0_t, \underline{\nu}^0_t$ which satisfy similarity correlation:

$$\nu^0_t \doteq \underline{\nu}^0_t \cdot HL, \tag{17.10}$$

where HL is relative intensity of micromovements (5) for an organism in question which is equal for all types of interacting particles.

In this context for all $t > \tau_2 > 0$ the following equalities are valid:

$$P\{\nu^0_t = K\} = \frac{[\lambda \cdot t]^K}{K!} e^{-\lambda t}, \tag{17.11}$$

$$P\{\underline{\nu}^0_t = K\} = \frac{[\underline{\lambda} \cdot t]^K}{K!} e^{-\underline{\lambda} t},$$

$$\lambda = \underline{\lambda} \cdot HL, \tag{17.12}$$

where $\lambda, \underline{\lambda} > 0$ are intensities of particle contacts of concerned types in an organism in question and basal one respectively.

Let us prove this main statement in three stages.

First, let us adjust weak convergence of centered processes of micromovements (8) to diffusion processes $u^0(z), \underline{u}^0(z) \in R^S$ which have zero mathematical expectances and diffusion matrices $B, \underline{B}$ respectively when $\varepsilon \to 0$. This statement is a particular case of a more general statement proved in [6] which is used effectively in [3] in grounding methods of statistical asessment of parameters of disease models.

Then, using (5) let us show that limited diffusion processes $u^0(z), \underline{u}^0(z)$ thus determined are connected by similarity correlation:

$$u^0(z) \doteq \underline{u}^0(z \cdot HL). \tag{17.13}$$

And finally let us assume that processes of contacts of interacting particles

$$\nu_t^0 = \Phi[u^0(z), 0 < z < t], \quad \underline{\nu}_t^0 = \Phi[\underline{u}^0(z), 0 < z < t] \tag{17.14}$$

determined by diffusion processes $u^0(z), \underline{u}^0(z)$ are the processes without consequences [8], and with account for (9)—Poisson processes. Correlations (10) and (12) which fix similarity of these processes in the organisms to be compared follow from (13). It is allowed for processes (7) and functional Φ to satisfy general invariance conditions [7] therefore pass to limited processes is assumed in (14).

Thus each physiological state of an organism corresponds to stationary Poisson processes of contacts of interacting particles, relative intensities of which being compared with basal organism are determined by personal parameter HL (6). It allows to consider all coefficients $\alpha \in R^l$ of the model (1) whose values are determined by interaction of corresponding particles as functions of HL parameter. In the more simple and typical case when these coefficients correspond to average intensities of particle interactions in unit concentrations, the following similarity correlation is valid:

$$\alpha = \underline{\alpha} \cdot HL \tag{17.15}$$

where $\alpha, \underline{\alpha} \in R^l$ are parameters of an organism in question and basal one respectively.

During a disease which may last for several days an organism changes its states many times. It leads to uncontrollable changes of HL parameter and coefficients of model (1) which can be considered as fast random variations as compared with "slow" change of phase variables of model (1). This statement corresponds to a scheme accepted in [3] in statistical assessment of parameters of model (1) according to observation data.

17.4   Comparison with Observation Data

The similarity correlations (10)-(15) were used in [4] in analysis of various well-known to the specialists data of physiological, medical and immunological observations. Below are the main results of this analysis where the following groups of data were used:

A. Depedence of metabolism intensity, blood flow velocity, body mass and average duration of cardiac cycle on age [5, 9]. Analysis of these data has shown validity of the following dependence for the HL parameter (6):

$$HL \approx \exp[-0.008(T - 25)] \tag{17.16}$$

where T–man's age in years. This correlation corresponds to the known in physiology Claiber equation [9]. It is assumed that a case when $HL = 1$ corresponds to a group of healthy people of 20-30 years old.

B. Change of an organism's reaction to a standard glucose load (Kohn, 1940) with the years according to [9]. These data ("sugar curves") are shown in Fig. 1, while Figs. 2-5 represent the results of their analysis with the aid of similarity correlations.

C. Change of insulin concentration 1 hour later standard glucose load (Wellborn, 1969) with the years according to [9]. These data and results of their analysis are given in Fig. 4

D. Rise of probability of death of cancer within a year, Fig. 7. These data were calculated using average values of mortality rate of cancer for a group of 8 countries in 1967 [12].

While analyzing a group of data related to carbohydrate metabolism (Figs. 1-5) we have transformed Bolier model [4] which describes this process, using similarity correlations to a form:

$$\dot{x}_t = f(x_t, HL), \quad x_t, \dot{x}_t \in R^3, \tag{17.17}$$

$$\underline{\alpha} \in R^7, \; HL \in R^8$$

$$x_0 = x_0(HL)$$

HL parameters were assessed here for every age group, while model parameters $\underline{\alpha}, x_0$ using data on all age groups. The estimates were best derived with regard to least-squares technique, and we were able to transform all results of observations to the conditions of general "sugar curve" (Fig. 2). Agreement of computational results with observation data is shown in Figs. 3, 4, and correspondence of obtained estimates of HL parameter to Claiber equation (16) - Fig. 5. According to these results our conclusions made with the aid of similarity correlations (15) do not contradict observation data. With regard for data represented in Fig. 5 values of HL parameter corresponding to age groups of examined subjects (Fig. 4, 6, 7) are determined from (16).

While analyzing data given in Fig. 6 we used the following correlation [4]:

$$R = 1 - (1 - \underline{R})^{P^{HL-1}} \tag{17.18}$$

where $R, \underline{R}$ are probabilities of detecting autoantibodies in an organism in question and basal one respectively; $\underline{P}$ - probability of transformation of B-lymphocyte into plasma cell due to contact with organism's cells.

While deriving (18) we used similarity of distributions of contact number (10-12) as well as results of [10]. The latter allow to assume when number of contacts with receptors of an organism's cells is insufficient, B-lymphocyte may turn out unactivated and become plasma cell producing autoantibodies.

According to Fig. 6 agreement of dependence (18) with observation data is not too bad when $\underline{P} \approx 10^{-5}, \underline{R} \approx 0,0005$.

When analyzing data represented in Fig. 7 it appeared possible to use correlation (18) according to [4] interpreting its values as follows: $R, \underline{R}$—probability to die of cancer within a year for an organism in question and basal one respectively; P—probability of that oncogenes shall be activated in a cell of basal organism, and that this cell shall not be destroyed by immune system or nonspecific defence. According to Fig. 7 $P \approx 10^{-7}, \underline{R} \approx 10^{-5}$.

Results concerned above show that the proposed similarity correlations (10)-(12), (15) do not contradict data of various observations.

17.5 HL and "vital heat of organism"

Properties of HL parameter outlined when analyzing observation data (Figs. 1-7) are very important. It is difficult to assume that such properties could remain unnoticed in those fields of medicine which have a centuries-old experience. Thus, eastern medicine have been using an idea of "vital heat of organism" for long, and the physician determines its level by pulse and uses it in treatment. It is considered that a man can remain healthy for a long time if "vital heat of organism" is at a certain level corresponding to certain place and season. Subject with normal level of "vital heat" seldom catches cold, easily endures weather variations, has great working capacity. When "vital heat" decreases systematically, there are created conditions for the development of diseases of "chilled blood": virus infection, rheumatism, diabetes mellitus,

autoimmune diseases, cancer, blood system diseases. On the contrary, when it increases excessively there is a jeopardy of "hot" diseases like malaria, dysentery, typhoid, schizophrenia, etc.

The above mentioned properties of HL parameter do not contradict these statements if we assume its possible interpretation as "vital heat of organism". It is essential that eastern medicine possesses wide experience of regulating the level of "vital heat of organism" with the aid of diet, drugs and medical procedures. That can be used after thorough investigations.

References

[1] Marchuk, G.I. Mathematical Models in Immunology. 2nd edition. Moscow: Nauka, 1985, 240 pp.

[2] Belykh, L.N. Analysis of Mathematical Models in Immunology. Moscow: Nauka, 1988, 196 pp.

[3] Zuev, S.M. Statistical Assessment of Parameters of Disease Mathematical Models. Moscow: Nauka, 1988, 192 pp.

[4] Pogozhev, I.B. Intensity of Interactions in Liquid Media of an Organism. Moscow: OVM AN SSSR, 1989, 152 pp.

[5] Schmidt-Nielson, K. Sizes of Animals: Why are they so important? Moscow: Mir, 1987, 259 pp.

[6] Ventsel, A.D., Freidlin, M.I. Fluctuations in Dynamic Systems in Small Random Disturbances. Moscow: Nauka, 1979, 424 pp.

[7] Kovalenko, I.N., Kuznetsov, N.Yu., Shurenkov, V.M. Random Processes: Guide-book, Kiev: Naukova Dumka, 1983, 365 pp.

[8] Gnedenko, B.V., Kovalenko, I.N., Introduction to Theory of Mass Service. 2nd edition. Moscow: Nauka, 1987, 336 pp.

[9] Handbook in Physiology. Age Physiology. Leningrad: Nauka, 1975, 691 pp.

[10] Dozmorov, I.M. Functional reversibility in interaction of lymphocytes with allogenic truncal cells: Dr. Sci. Thesis. Moscow, 1986, 240 pp.

[11] Walford, R.L. The Immunologic Theory of Aging. Copenhagen: Munkegaard, 1969.

[12] World Sanitary Statistics Annual, 1967. Demographic statistics and causes of death. Geneve: World Health Organization, 1973. Vol. 1
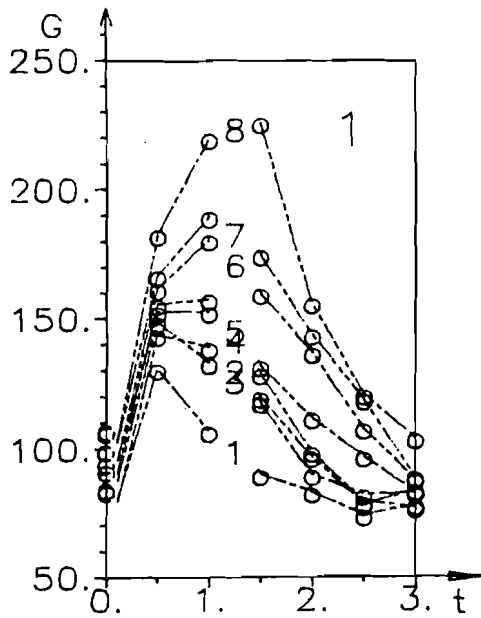
Figure 1: Sugar curves for subjects of different age (observation data). G - blood sugar (mg%) t hours after glucose load. Age groups (years): 1 - up to 10; 2 - 10+20; 3 - 20+30; 4 - 30+40; 5 - 40+50; 6 - 50+60; 7 - 60+70; 8 - more than 70.
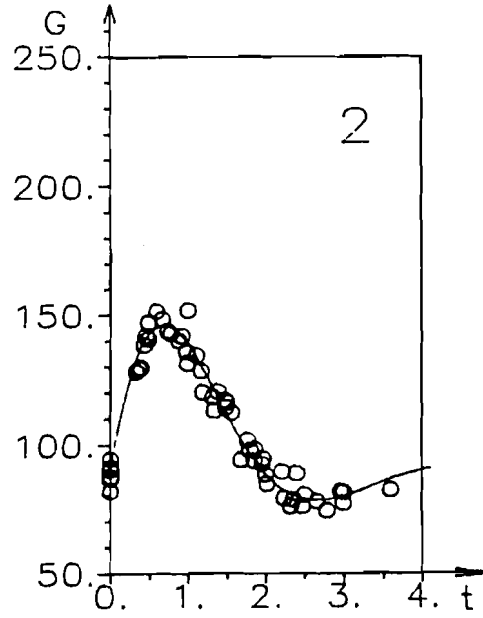
Figure 2: Determination of "norm" with the aid of similarity relations from the sugar curves in Figure 1.
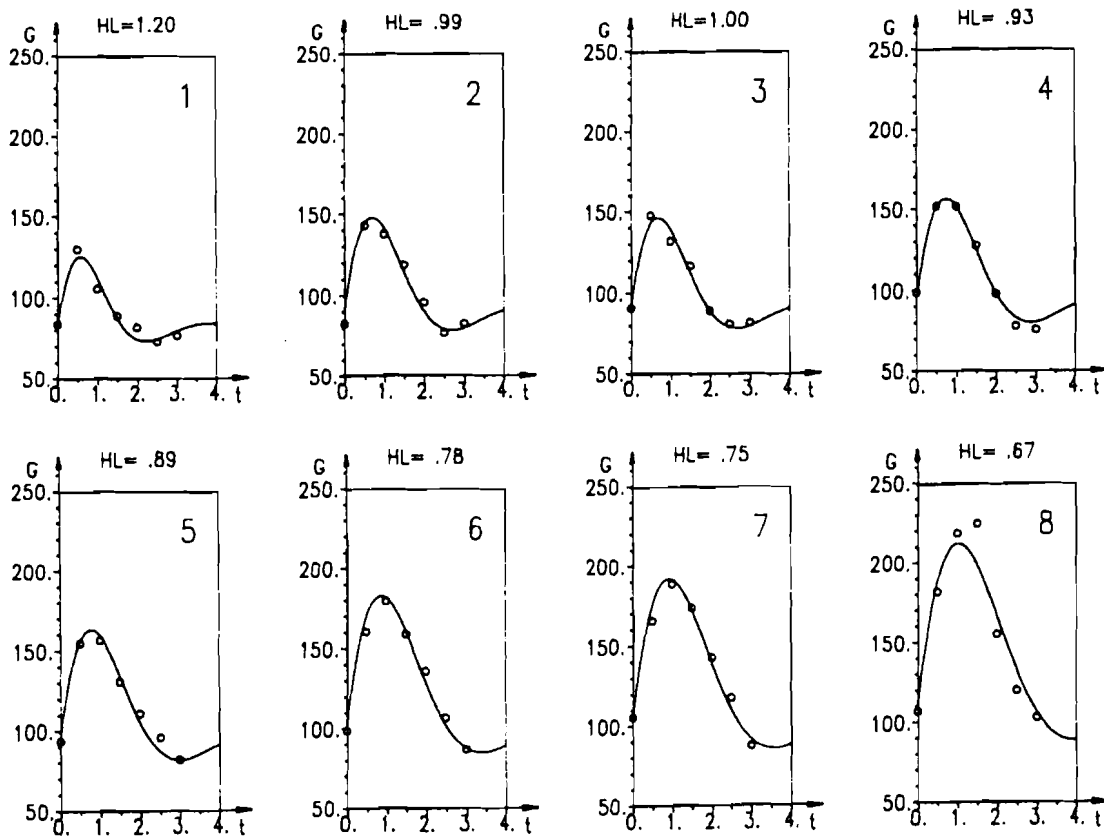
Figure 3: Comparison of sugar curves plotted with the aid of similarity relations with respect to "norm" (Fig. 2) with the observation data (Fig. 1). Number of charts and values of HL parameter corresponds to age groups in Fig. 1.
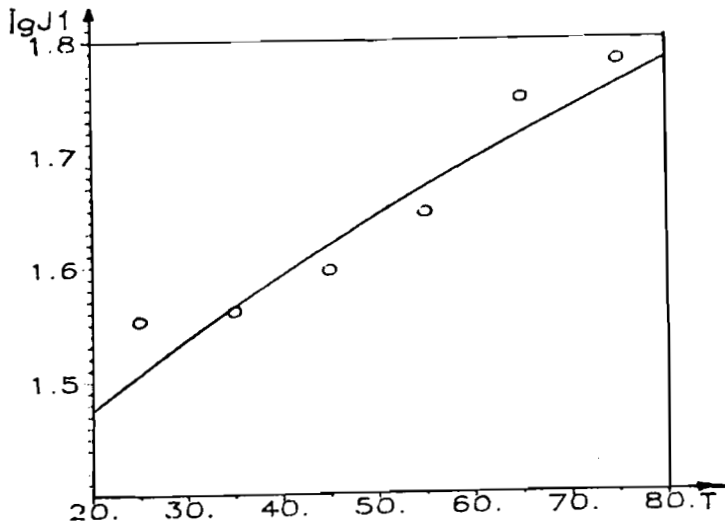
Figure 4: Blood insulin (lgI) an hour after standard glucose load subject to age T (years). Circles correspond to observation data.
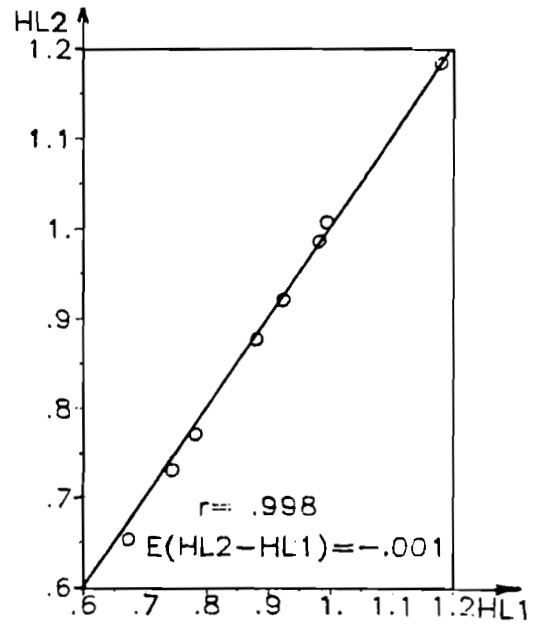

Figure 4a. Correlation between values of HL parameter obtained by different methods. HL1 - "Boliet" version, HL2 - "Polynomial".
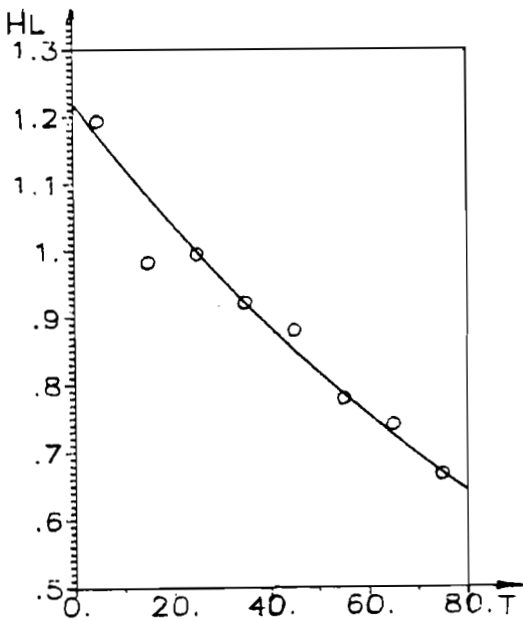

Figure 5: HL parameter as a function of age T (years). Circles correspond to sugar curves in Fig. 3, continuous curve - to Claiber equation.
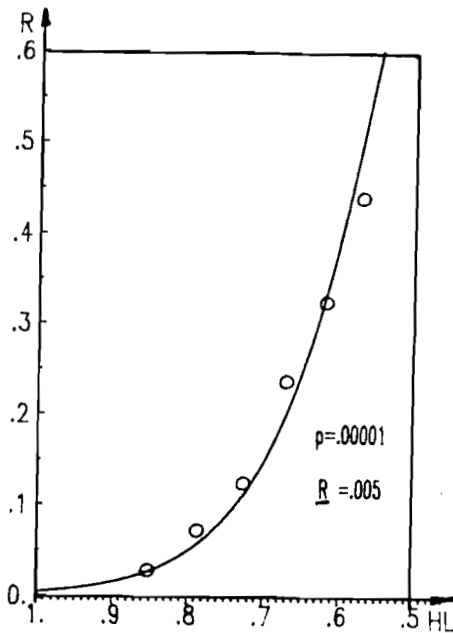

Figure 6: Probability of revealing autoantibodies (R) subject to HL parameter. Circles correspond to observation data for different age groups.
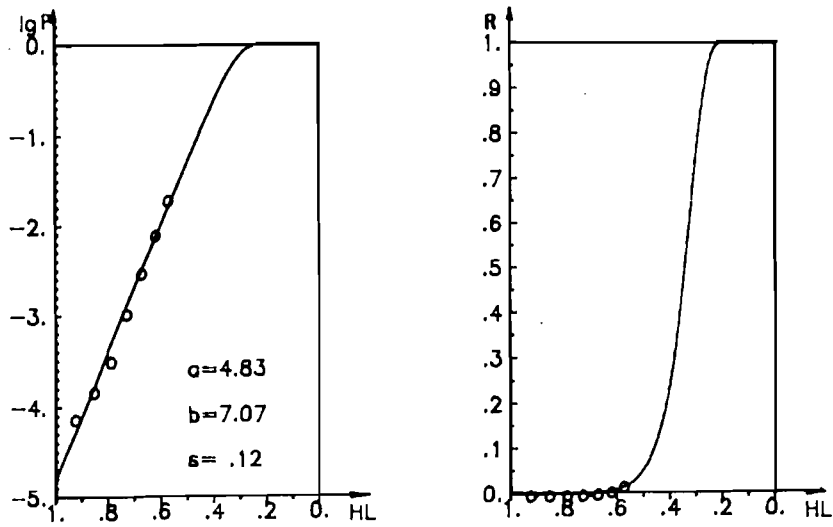
Figure 7: Mean over group of countries probability to die of cancer and circulatory system disturbances within a year subject to HL parameter. Circles correspond to observation data. For comparison the same data are shown in two charts at different scales: logarithmic (lgP) and ordinary (R).